# Investigation of $CO_2$ Tracer Gas-Based Calibration of Multi-Zone Airflow Models

by

Steven Christopher Snyder

A Thesis Presented in Partial Fulfillment
of the Requirements for the Degree
Master of Science

Approved April 2011 by the
Graduate Supervisory Committee:

T. Agami Reddy, Chair
Marlin Scott Addison
Harvey John Bryan

ARIZONA STATE UNIVERSITY

May 2011

ABSTRACT

The modeling and simulation of airflow dynamics in buildings has many applications including indoor air quality and ventilation analysis, contaminant dispersion prediction, and the calculation of personal occupant exposure. Multi-zone airflow model software programs provide such capabilities in a manner that is practical for whole building analysis. This research addresses the need for calibration methodologies to improve the prediction accuracy of multi-zone software programs. Of particular interest is accurate modeling of airflow dynamics in response to extraordinary events, i.e. chemical and biological attacks.

This research developed and explored a candidate calibration methodology which utilizes tracer gas (e.g., $CO_2$) data. A key concept behind this research was that calibration of airflow models is a highly over-parameterized problem and that some form of model reduction is imperative. Model reduction was achieved by proposing the concept of macro-zones, i.e. groups of rooms that can be combined into one zone for the purposes of predicting or studying dynamic airflow behavior under different types of stimuli.

The proposed calibration methodology consists of five steps: (i) develop a "somewhat" realistic or partially calibrated multi-zone model of a building so that the subsequent steps yield meaningful results, (ii) perform an airflow-based sensitivity analysis to determine influential system drivers, (iii) perform a tracer gas-based sensitivity analysis to identify macro-zones for model reduction, (iv) release $CO_2$ in the building and measure tracer gas concentrations in at least one room within each macro-zone (some replication in other rooms is highly

desirable) and use these measurements to further calibrate aggregate flow parameters of macro-zone flow elements so as to improve the model fit, and (v) evaluate model adequacy of the updated model based on some metric.

The proposed methodology was first evaluated with a synthetic building and subsequently refined using actual measured airflows and $CO_2$ concentrations for a real building. The airflow dynamics of the buildings analyzed were found to be dominated by the HVAC system. In such buildings, rectifying differences between measured and predicted tracer gas behavior should focus on factors impacting room air change rates first and flow parameter assumptions between zones second.

# DEDICATION

This work is dedicated to my parents, Blaine and Peggy, whose love and support have made me the person I am today and whose guidance has instilled in me a desire to continue learning. I also dedicate this work to my wife Stefanie and daughter Olivia who give meaning to all that I do.

ACKNOWLEDGMENTS

I gratefully acknowledge the following individuals who contributed to this research by way of advice, help and sharing of information:

Dr. T. Agami Reddy, my committee chair, whose guidance and support has made this work possible and has allowed me to pursue higher education. His leadership, encouragement, and advice made invaluable contributions to this work.

Joseph Firrantello and Pongpeera Sae Kow whose previous work on multi-zone calibration methodologies, tracer gas releases, PCW development and field testing provided the foundation of this research.

Dr. Amy Musser, Vandemusser Design LLC, whose experience with the PCW program provided crucial guidance in understanding and implementing PCW throughout this research.

Dr. William Bahnfleth, Pennsylvania State University, whose advice and assistance helped in finalizing this research.

This research was funded by the Technical Support Working Group – Combating Terrorism Technical Support Office.

TABLE OF CONTENTS

Page

CHAPTER Page

CHAPTER Page

CHAPTER Page

CHAPTER Page

CHAPTER Page

LIST OF TABLES

Table Page

LIST OF FIGURES

Figure Page

Figure Page

Figure Page

Figure Page

# CHAPTER 1: INTRODUCTION AND BACKGROUND

## 1.1 Research Problem

Multi-zone airflow model software programs provide the capability to evaluate an existing building's vulnerability and dynamic response to various extraordinary event scenarios (i.e., either accidental or intentional airborne contaminant releases). There is a need for calibration methodologies to be developed to provide confidence in the predictions of these models so that event response plans can be formulated and the effectiveness of possible mitigation measures can be analyzed.

## 1.2 Research Background

The September 11, 2001 (9/11) terrorist attacks on New York City, New York, Arlington County, Virginia, and Shanksville, Pennsylvania and the subsequent anthrax mailing attacks have had significant impacts on American society in the years since. Relevant to this research, one such impact is the way in which we address building vulnerability to possible terrorist threats. For example, in response to the 2001 attacks, "government, construction industry, and facilities management organizations initiated efforts to identify and disseminate guidance for making buildings less vulnerable to terrorist threats" (Bahnfleth, 2004).

Terrorist attacks can take many forms and typically have the objectives of "disruption of a routine, creation of an economic loss, disruption of critical resources and vital services, loss of lives and emotional devastation" (Bahnfleth et al., 2008). This discussion will focus on the use of airborne chemical and

biological (CB) agents as weapons in terrorist attacks on buildings. Bahnfleth et al. (2008) identified that the key vulnerabilities of buildings to airborne CB attacks include:

1. Ability of small quantities of agents to result in hazardous indoor concentrations;
2. Rapid spread of airborne agents by HVAC systems;
3. Multiplicity of pathways for agent entry into a building, including easily accessible outdoor air (OA) intakes, infiltration, mail, water, surface contact or resuspension of deposited material, and others;
4. Long term loss of building use due to contamination.

Heating, ventilation, and air-conditioning (HVAC) systems in buildings are designed to disperse fresh and conditioned air throughout the occupied spaces to maintain certain indoor environmental conditions. For airborne CB attacks, such building systems under normal operation can become the prime movers of a released contaminant and can quickly expose a large number of building occupants. Therefore, reducing building vulnerability to airborne CB attacks requires studying building airflow dynamics and analyzing the impact of HVAC systems on contaminant behavior. The use of calibrated multi-zone airflow models is one option for performing this analysis.

### *1.2.1 Reducing Building Vulnerability*

Reducing building vulnerability in "critical" infrastructure (i.e. government buildings), which often have the budgets for maximizing security, can involve gaseous filtration technologies, high minimum efficiency reporting

value (MERV) particulate filters, ultraviolet germicidal irradiation technologies, the latest in sensing and alarm equipment, etc. Other buildings which may not be considered "critical", in terms of their likelihood of being terrorist targets, could be high impact (e.g., large loss of life). Such "non-critical" but high impact buildings could include schools, hospitals, churches, college dormitories, office buildings, courthouses, stadiums, etc. These building types typically do not have the budget for investing in security technologies specific to reducing building vulnerability to terrorist threats. Also, since the probability of being a target of terrorist activity is so small and since it has been over nine years since 9/11, most building owners have little or no interest in investing in building security for extraordinary events. Therefore, having the ability to quantify risk and being able to perform some cost-benefit analysis is essential if building owners are to make decisions on implementing security measures (Bahnfleth et al., 2008). The use of a multi-zone modeling software program, such as CONTAM developed by the National Institute of Standards and Technology (Walton and Dols, 2005 and NIST, 2008) or COMIS developed by the Lawrence Berkeley National Laboratory (LBNL, 1989), provides one option for building owners to assess their building's vulnerability, analyze the building's response to various contaminants and attack scenarios, and investigate possible low cost mitigation methods if there is an interest.

As mentioned earlier, building HVAC systems provide opportunities for terrorists to quickly disperse a contaminant throughout a building. In particular, since physical security limiting building access to mechanical spaces is typically

robust in many buildings, the most vulnerable point then becomes the OA intake louvers. The OA intake is the location where the building's air handling units draw in outside air to provide the building's ventilation needs. A contaminant released at the outside air louvers will quickly find its way throughout the building via the supply air fans and ductwork. Thus, one of the most common mitigation strategies is to protect the OA intakes or make them inaccessible by locating them high on the side of the building or on the roof.

If advanced filtration or agent inactivating technologies are not within the budget, then response plans and mitigation options will typically involve control strategies. In particular, how to control the HVAC system fans, dampers, etc. Janus et al. (2005) discusses that system design or control strategies typically involve the four following approaches: (i) exclusion (e.g., positive space pressurization, damper control), (ii) containment (e.g., HVAC zone separation or isolation), (iii) removal (e.g., dedicated exhausts, filtration technologies, manipulation of outside air percentage), and (iv) evasion (e.g., evacuation, protective masks or suits). Depending on the release scenario, there could be different building responses. If there is an outdoor release, other than entering the OA intake, the contaminant can enter through windows or leakage paths in the building envelope. In some cases, an outdoor release may require closing certain dampers or shutting off certain fans. Indoor releases in critical areas such as lobby spaces or mail rooms may require purging the building by running certain exhaust fans at full power. Generic guidance such as this should be used with caution and actual response plans should be building specific. The most appropriate response

strategy will be dependent on the release location, the type of release, and even the contaminant that was released. For example, separate response plans may be developed for chemical agents versus biological agents due to differences in their properties (e.g., density) and due to differences in the way they interact with building surfaces and materials (e.g., absorption, chemical reactions). If pursuing filtration options, most chemical agents will require gaseous filtration technologies, such as carbon filters, whereas many biological agents can be controlled with certain particulate filters.

Other common response or mitigation strategies include the following:

1. Have critical areas such as lobby spaces and mail rooms on their own dedicated HVAC systems with ducted returns to limit the transfer of a contaminant to adjacent spaces. Utilize intelligent HVAC zoning to minimize contaminant spread.
2. Provide physical security to limit access to mechanical spaces containing air handling units or water supplies.
3. Use ducted returns rather than plenum returns throughout the building to minimize air mixing between zones.
4. Use the highest efficiency particulate air filters that are compatible with the current HVAC system (i.e., do not require increasing the size of fans to overcome additional pressure drop). Chemical agents will typically require some type of gaseous filtration and sensing equipment.

5. Locate outdoor air intakes at high elevations or other inaccessible areas. If at ground level, provide some physical security measures and surveillance equipment.
6. Provide central control locations for the HVAC system so that operations personnel or "first responders" can shut down any system, close or open any dampers, or switch any system to 100% outside air.
7. Reduce building envelope leakiness to reduce infiltration of a contaminant from an outdoor release. Make windows resistant to thrown objects.
8. Positively pressurize egress routes such as stairwells to keep them contaminant free.
9. Make sure building occupants are well informed and trained for various attack scenarios. Practice pre-developed response plans and make building plans and HVAC controls readily accessible to "first responders".

Janus et al. (2005) and Nakano et al. (2007) provide two examples of applications of multi-zone modeling in assisting the analysis of building vulnerability to CB threats and the effectiveness of certain mitigation strategies. Janus et al. (2005) uses the multi-zone model program CONTAM to examine the following strategies on an office building in response to both external and internal CB attacks: sheltering-in-place, building exhaust, low level filtration without pressurization, and high level filtration with pressurization. The authors conclude that expensive technologies and mitigation strategies are not always required and due to the high levels of uncertainty associated with CB threats (i.e., large number of possible attack scenarios and contaminants, weather conditions, occupancy

patterns, etc.) it is difficult to assign "one-size-fits-all" design solutions. This stresses the importance of using modeling to provide building specific guidance. Nakano et al. (2007) also uses CONTAM as part of a building assessment procedure that includes the following steps: design and problem definition, baseline design modeling, model alterations for specific design strategies, and a multi-criteria decision making process. The authors use CONTAM to develop a multi-zone model of the building, evaluate different strategies based on an exposure metric for different attack scenarios and contaminant types, and suggest using some sort of multi-criteria optimization procedure to choose the best strategy based on financial issues (equipment costs, operation and maintenance costs, etc.) as well as other considerations. This work illustrates how multi-zone modeling can be used to assist in the decision making process for reducing building vulnerability to CB threats.

Bem (2008) proposed a security design procedure which identifies possible design features to reduce building vulnerability and then uses CONTAM modeling to analyze the effectiveness of the various features in mitigating CB threats. A book by Kowalski (2003) discusses immune building system design and technologies, a threat assessment procedure, and the use of multi-zone modeling such as CONTAM to quantitatively evaluate possible response strategies. Kowalski et al. (2003) discusses the use of both steady-state and transient single zone multi-zone airflow models to analyze the effectiveness of different air-cleaning and air-disinfecting technologies (e.g. high efficiency particulate filtration, ultraviolet germicidal irradiation, ventilation strategies) on

reducing the occupant dose to a contaminant and the subsequent number of fatalities.

### *1.2.2 Existing Knowledge, Guidance Documents, and Tools*

The post 9/11 atmosphere led to the development of guidance documents and software programs which were designed to analyze building vulnerability to various attack scenarios, perform risk analysis, propose some metric for vulnerability, suggest mitigation strategies for reducing risk, etc. There are similarities and differences in the guidance provided in these documents and programs. However, in general, most of the guidance provided is heuristic. The format of these tools varies from checklists to spreadsheets to detailed documents to interactive software programs.

Bahnfleth (2004) discusses a variety of the guidance documents developed post 9/11 that are specific to reducing building vulnerability to airborne chemical and biological attacks. The documents have the goal of "adopting security as a design parameter" which is not a straight forward task. Therefore, not all documents agree on how this should be accomplished and no consensus on design criteria has been reached. Before 9/11, guidance documents were almost exclusively developed by government departments (e.g., Department of Defense) for use on government facilities. Post 9/11, guidance documents were developed by a wide spectrum of organizations for public use. The American Institute of Architects (AIA) and the American Society of Heating, Refrigerating, and Air-Conditioning Engineers (ASHRAE) both developed their own guidance documents (AIA, 2001 and ASHRAE, 2003). The ASHRAE Presidential Ad Hoc

Committee report (ASHRAE, 2003) entitled "Risk Management Guidance for Health, Safety, and Environmental Security Under Extraordinary Incidents" discusses a risk management process including four steps: risk analysis, risk treatment planning, risk treatment plan implementation, and re-evaluating the plan after implementation and modifying it as needed. The main body of the document discusses typical building vulnerabilities and typical mitigation measures (i.e., HVAC system control strategies) to reduce vulnerability. Appendix C of ASHRAE (2003) contains an empirical risk analysis example. This approach is largely heuristic with the user specifying the categories and weighting factors for an exposure level matrix which calculates the exposure level of the building using some numerical scale. The assessor then completes two more tables, the probability of successful occurrence table, and the impact classification table. Based on these two tables, the assessor can create a risk-rating chart that compares the probability of a successful threat and the resulting impact to give a risk rating. The document also provides a life cycle cost analysis and discusses how to create a risk mitigation plan. Bahnfleth (2004) also discusses documents developed by Lawrence Berkeley National Laboratory, the U.S. Army Corps of Engineers, and the National Institute for Occupational Safety and Health, among others.

A report by Bahnfleth et al. (2008) provides a literature review that summarizes "existing knowledge in terms of available documents, guidance, and tools as applicable to non-critical buildings targeted towards, (i) risk assessment procedures, (ii) airborne CB agents and building attack scenarios, (iii) metrics

used to quantify building security, (iv) design methods, available technology and existing guidance to enhance resiliency of new buildings as well as existing buildings, (v) an overall classification of the various analysis methods, (vi) published guidance, procedures and protocols and on risk reduction, (vii) identifying the multiple related impacts of security design, and (viii) the economics of building resiliency for "non-critical" facilities." The focus of the report is on airborne contaminant distribution through buildings and how HVAC systems and other building features can be used to control or mitigate that distribution. Some of the technological knowledge reviewed includes air filtration technologies and chemical and biological sensing technologies. The report also discusses airflow management, HVAC system zoning, interior space pressurization, and HVAC system selection in terms of how they can affect the dispersion of a contaminant throughout the building. The authors identify and discuss the following methods of analysis: compartmental models, detailed deterministic simulation programs, and probabilistic modeling and simulation programs. Multi-zone modeling programs fall under the compartmental model category. For risk reduction procedures and guidance, the report reviews literature based on how threat/vulnerability assessment is treated (i.e., heuristic, empirical, or formal) and what type of remedial action or guidance is provided (i.e., heuristic, semi-quantitative, or quantitative). Finally, the report discusses the economics of resiliency and possible additional benefits of resiliency. Additional benefits of considering building security and resiliency in designs could include improved indoor air quality (IAQ) and reduced energy use. If reducing a

building's vulnerability to terrorist threats via the implementation of certain design features can simultaneously reduce energy consumption and improve IAQ, building owners will be more inclined to desire building security as a design consideration.

A subsequent report by Bahnfleth et al. (2009) evaluated five tools and protocols available in the open literature that allow building owners to assess their building's vulnerability to possible airborne CB attacks. The subset of tools analyzed and compared were those identified to be developed to the extent that they could be pragmatically used by building owners, practicing engineers, or building security professionals. Two of the tools evaluated were simple checklist documents to evaluate vulnerability with corresponding appendices providing general guidance. The other three tools evaluated were interactive software programs of varying formats. These tools were evaluated in terms of how they perform risk assessment or quantify vulnerability and based on what guidance they provide. The tools were also compared in terms of their ease of use, the quantity and content of the guidance provided, the gaps in coverage, etc. Each tool identified was applied to specific buildings so that the vulnerability assessment and guidance could be compared.

From these two reports by Bahnfleth et al. (2008 and 2009) it was concluded that for technologies and design practices for reducing building vulnerability to airborne CB attacks, "there are a fair number of documents (largely repetitive) that provide guidance, but their recommendations are mainly heuristic and rarely supported by quantitative data" (Bahnfleth et al., 2009). Only

a few studies utilized simulations or field testing to analyze vulnerability or assess the benefit of certain resiliency measures. Whole building analysis through multi-zone modeling provides a pragmatic way to produce building specific guidance. By accurately modeling a building and simulating various attack scenarios, building owners, facilities management personnel, or building security professionals can develop response plans, identify egress routes, propose shelter-in-place locations, estimate personal exposure, develop HVAC system control strategies, and understand the behavior of various contaminants for various attack scenarios.

### *1.2.3 Context in this Research*

The main focus of previous research efforts on multi-zone model calibration, discussed in Chapter 2, as well as this research is to provide multi-zone model calibration methodologies for improving model prediction accuracy in response to extraordinary events. Other applications for multi-zone model calibration methodologies are left for future research. One such application could include quantifying IAQ for the purposes of "green" building design and achieving points or credits from some rating system such as the LEED (Leadership in Energy and Environmental Design) rating system (USGBC, 2010). This is similar to how detailed building energy simulation programs are used to quantify energy savings for a particular design above some baseline design. Another application could be in assisting the design of healthcare facilities (e.g., hospitals) where zonal pressurization design and interior airflow dynamics may be critical. For example, hospital clean rooms or certain patients rooms (i.e., burn

victims) need to remain positively pressurized with respect to the surrounding spaces to prevent infections. Conversely, rooms containing patients with possible infectious diseases need to remain negatively pressurized with respect to the surrounding spaces. Similarly, certain industrial facilities or laboratories which house potentially harmful chemicals may require the careful consideration indoor airflow dynamics. Finally, the design of naturally ventilated buildings could significantly benefit from calibrated multi-zone airflow models.

For developing multi-zone airflow model calibration methodologies, this research uses carbon dioxide as a tracer gas. Since carbon dioxide is not harmful to humans, in certain concentrations, it can easily be used for testing in real buildings so that real data can be collected and used in the calibration process. "It is important to realize that [a multi-zone model] implements mathematical relationships to model airflow and contaminant related phenomenon and therefore incorporates assumptions that simplify the model from that of the modeled phenomenon" (Walton and Dols, 2005). As implied by this statement, accurate modeling requires some attempt at model calibration.

## 1.3 Multi-Zone Airflow Modeling

### *1.3.1 Introduction to Multi-Zone Modeling*

Multi-zone airflow models, which are also commonly referred to as "Network", "Macro", or "Compartmental" models, consist of a set of nodes connected by links to other nodes. For airflow modeling specifically, the actual building must be idealized into nodes where each node represents the volume of air in a building zone and the links between nodes are mathematical relationships,

typically nonlinear, between the volumetric flow rate through and the pressure difference across various airflow paths. These airflow paths can be windows, doorways, small cracks in building construction, transfer ducts, etc. Figure 1.1 (NIST, 2008) shows the building idealization in multi-zone modeling. "The network model predicts zone-to-zone airflows based on the pressure-flow characteristics of the path models, and pressure differences across the paths. Three types of forces drive flow through the paths: wind, temperature differences (stack effect), and mechanical devices such as fans" (ASHRAE, 2009). Although this discussion focuses on multi-zone modeling of airflow transport and contaminant dispersion through a building, multi-zone or network models are also commonly adapted to heat transfer analysis (ASHRAE, 2009).

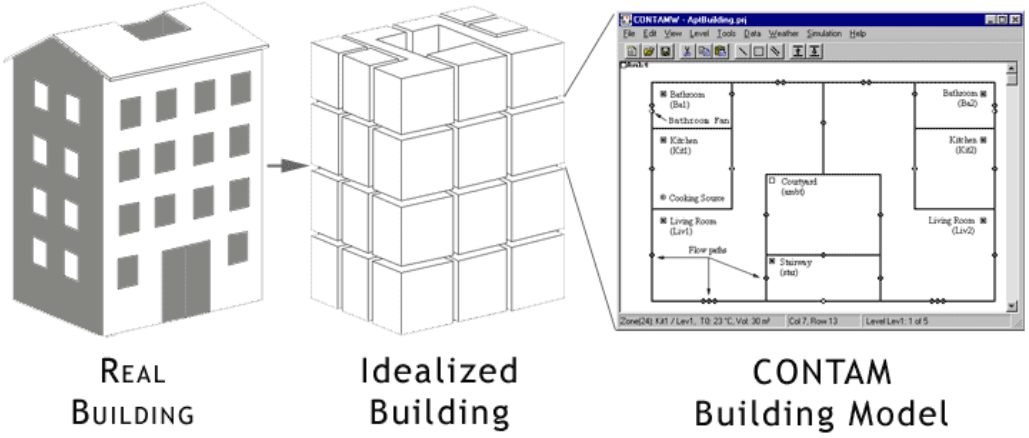


*Figure 1.1*: Multi-Zone Model Building Idealization

The fundamental basis of multi-zone modeling is the "well-mixed" assumption. The well-mixed assumption means that any zone, which is a volume of air, is "characterized by a discrete set of state variables, i.e., temperature, pressure and contaminant concentrations" (Walton and Dols, 2005). This also

means that for a contaminant release, by the first time step, the contaminant is diluted with the entire zone volume. Although this assumption sacrifices some accuracy and prevents the analysis of airflow/contaminant distribution within a zone, it is the reason that multi-zone models have short simulation times and are currently the only pragmatic option for whole building airflow and contaminant dispersion analysis. In terms of the mathematics, when setting up the differential equations which account for the change in contaminant concentration over time, the derivatives are with respect to time only rather than with respect to time and the three spatial dimensions. Therefore, the mass balance equations are ordinary differential equations rather than partial differential equations thus simplifying the calculation.

To illustrate how multi-zone models handle contaminant dispersion, the following example shows a single zone model for contaminant concentration change over time.

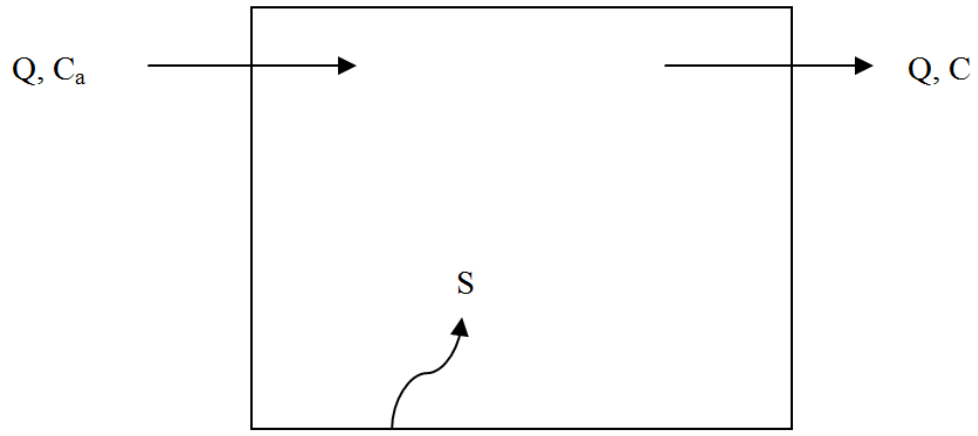


*Figure 1.2*: Single Zone with Contaminant Source

Figure 1.2 shows a single zone with a contaminant source and mechanical ventilation at a volumetric flow rate "Q". It is assumed that the contaminant

concentration in the supply air is equal to the contaminant concentration in the ambient air "$C_a$". The contaminant concentration in the room "C" is the concentration of the air leaving via the exhaust or return airflow. Based on this diagram, the change in contaminant concentration over time can be modeled by the concentration mass balance in Equation 1.1.

$$V\frac{dC}{dt} = QC_a - QC + S \tag{1.1}$$

In Equation 1.1, "V" is the zone volume and "S" is the rate of contaminant generation within the zone (e.g., kg/hr). The solution to this differential equation is given by Equation 1.2.

$$C(t) = C_{ss} - [C_{ss} - C(0)]e^{-At} \tag{1.2}$$

In Equation 1.2, "$C_{ss}$" is the steady-state contaminant concentration (as time approaches infinity) and is given by Equation 1.3, "C(0)" is the initial concentration, and "A" is the air change rate as given by Equation 1.4.

$$C_{ss} = \frac{QC_a + S}{Q} \tag{1.3}$$

$$A = \frac{Q}{V} \tag{1.4}$$

By taking the natural log of both sides of Equation 1.2 and rearranging, one can find an expression (Equation 1.5) for the time it will take the zone to reach any specified concentration.

$$t = -\frac{1}{A} ln\left[\frac{C_{ss} - C(t)}{C_{ss} - C(0)}\right] \tag{1.5}$$

The single zone analysis becomes more complicated once more factors are considered. For example, Figure 1.3 accounts for air infiltration and exhfiltration through the envelope, contaminant adsorption to zone surfaces, and the use of a contaminant filtration device within the zone.

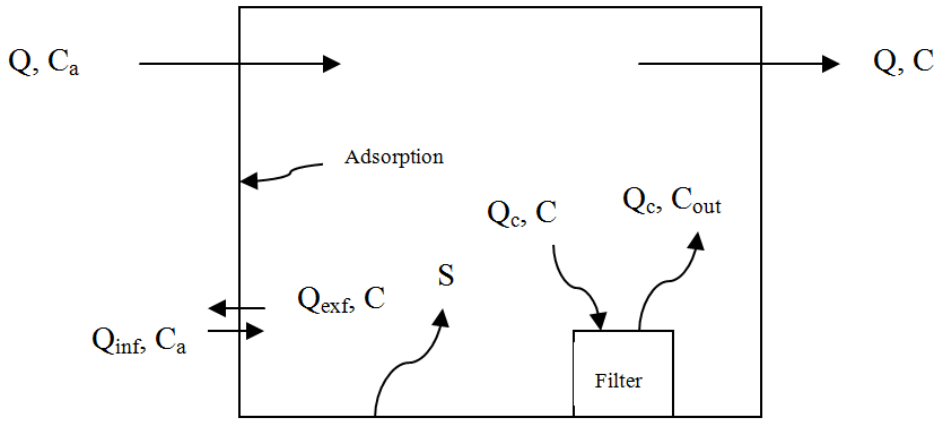


*Figure 1.3*: Single Zone with Contaminant Source, Filtration, Adsorption, Infiltration, and Exfiltration

With these factors taken into consideration, Equation 1.1 becomes Equation 1.6 below where "$Q_{inf}$" is the infiltration rate, "$Q_{exf}$" is the exfiltration rate, "$Q_c$" is the volumetric flow rate of air flowing through the filtration device, and "$C_{out}$" is the concentration of contaminant leaving the filtration device. This differential equation can be analytically solved in the same manner as before.

$$V\frac{dC}{dt} = QC_a - QC + Q_{inf}C_a - Q_{exf}C + Q_cC_{out} - Q_cC + S - Adsorption \tag{1.6}$$

This analysis can be further complicated by accounting for air recirculation in the mechanical system, series and parallel filtration arrangements, and chemical reactions between multiple contaminants.

Multi-zone modeling includes these contaminant mass balance equations for each zone and will have terms accounting for flow between zones. Matrix notation is typically employed to describe these systems of equations. In order to perform these contaminant mass balances, one must first identify all of the airflow rates. Mechanical airflow rates can be measured or determined from design documents. Infiltration, exhfiltration, and inter-zonal airflow rates are more difficult to measure and are impacted by pressure differences due to wind, temperature difference (stack effect), and mechanically induced pressure differences. Multi-zone models can calculate these airflows by making an initial guess of the building pressures and using an iterative solution method of air mass balance equations while accounting for the various factors impacting pressure differences.

Multi-zone modeling concepts and assumptions directly related to this research are discussed in Section 4.1.2 and a more detailed discussion of the mathematics behind multi-zone modeling is provided in Appendix C.

### *1.3.2 Multi-Zone Models vs. Computational Fluid Dynamics*

The most accurate airflow modeling is accomplished by computational fluid dynamics (CFD). However, as will be discussed here, the computational effort and time needed for CFD modeling makes it impractical for whole building analysis. However, one could first model the whole building with a multi-zone

program and then switch to CFD modeling for a specific zone of importance where more detail is warranted.

CFD models, also referred to as "micro" models, determine the flow fields within a zone thus providing the detail that multi-zone models lack. "CFD modeling can be used for a microscopic view of a building or its components by solving Navier-Stokes equations to obtain detailed flow field information and pollutant concentration distributions within a space" (ASHRAE, 2009). The Navier-Stokes equations are the microscopic momentum balances for Newtonian fluids derived by the application of Newton's motion laws or the impulse-momentum principle to a control volume of fluid (Street et al., 1996). The CFD model "interprets a specific problem of the indoor environment through a mathematical form of the conservation law and situation-specific information (boundary conditions)" (ASHRAE, 2009). CFD involves the simultaneous solution of the coupled partial differential equations describing mass, momentum in all flow directions, energy (Navier-Stokes), and contaminant dispersion. Therefore, CFD can accurately predict the flow field within a zone whereas multi-zone models, which do not model momentum, are based on the well-mixed assumption. However, few useful analytical solutions are known to the set of CFD equations and therefore one must resort to computer-based numerical procedures within CFD software programs (Street et al., 1996). ASHRAE (2009) presents a common form, shown in Equation 1.7, of the CFD equations which can be used for airflow analysis, convective heat transfer analysis, or contaminant dispersion analysis. This equation shows the change in time of a variable at a certain location

due to the "amount of variable flux (e.g., momentum, mass, thermal energy)" (ASRHAE, 2009). Essentially, transient changes plus convection equals diffusion plus sources.

$$\frac{\partial}{\partial t}(\rho\phi) + \frac{\partial}{\partial x_j}(\rho U_j \phi) = \frac{\partial}{\partial x_j}\left(\Gamma_\phi \frac{\partial \phi}{\partial x_j}\right) + S_\phi \qquad (1.7)$$

In Equation 1.7, "t" is time, "ρ" is density, "ϕ" is the transport property (e.g., air velocity, temperature, species concentration) at any point, "$x_j$" is the distance in the "j" direction, "$U_j$" is the velocity in the "j" direction, "$\Gamma_\phi$" is the generalized diffusion coefficient or transport property of the fluid flow, and "$S_\phi$" is the source or sink.

According to ASHRAE (2009), the total description of flow consists of eight coupled and non-linear differential equations containing both first and second derivatives expressing the convection, diffusion, and source of the variables being analyzed. CFD computer programs divide the air volume being analyzed into a grid of cells where the CFD equations are solved for each cell. ASHRAE (2009) provides an example illustrating the computational effort and power required for using CFD analysis even on a single zone:

> "Assuming a room is typically divided into 90 x 90 x 90 cells, the eight differential equations are replaced by eight difference equations in each point, giving a total of $5.8 \times 10^6$ equations with the same number of unknown variables. The numerical method typically involves 3,000 iterations, which means that a total of $17 \times 10^9$ grid point calculations are made for the prediction of a flow field" (ASHRAE, 2009).

Significant simulation time is needed to perform the large number of calculations required by CFD analysis. This makes CFD analysis of entire buildings impractical for most applications and for most users. The ability of CFD models to accurately predict flow fields within zones makes them more appropriate for modeling specific small scale phenomenon. This could include designing displacement ventilation systems, modeling clean room airflow, predicting thermal comfort, etc. (ASHRAE, 2009).

Another issue with CFD programs is the specification of boundary conditions. Boundary conditions describe the physical (and chemical) characteristics at the boundaries of the air volume being analyzed. "Boundary conditions are integral to CFD modeling's ability to solve the general Navier-Stokes equations for a particular problem in an indoor environment" (ASHRAE, 2009). For airflow analysis, boundary conditions typically involve HVAC supply diffuser and return registers, wall surfaces, contaminant sources and sinks, etc. Properly identifying and modeling the boundary conditions for a specific problem is critical to the success of the CFD analysis. This requires a certain level of user expertise.

Table 1.1 below (reproduced from Spengler, 2001) provides a quick comparison of multi-zone modeling and CFD modeling. The main difference is that CFD involves the numerical solutions of nonlinear partial differential Navier-Stokes equations, continuity equations, and energy conservation equations, whereas multi-zone models involve the solution of ordinary differential equations (only one independent variable) which can be solved analytically. As discussed

above, multi-zone models fail to model spatial variation of variables within a zone whereas CFD analysis provides this detail. However, the increased accuracy comes at the price of computational power and time. CFD programs are expensive, require significant simulation run times, and are limited by their complexity. The successful use of CFD programs and the correct interpretations of the results is dependent on the knowledge and expertise of the user. Namely, the program user must be familiar with thermal/fluid sciences and must successfully identify and model boundary conditions. Multi-zone models, on the other hand, are efficient for whole building analysis, but limited by oversimplification.

*Table 1.1*

Multi-Zone Models Versus CFD Models

| **Characteristic** | **Multi-Zone** | **CFD** |
|---|---|---|
| Ordinary Differential Equations | YES | NO |
| Partial Differential Equations (Navier Stokes) | NO | YES |
| Prediction of Spatial Distribution of Indoor Parameters | NO | YES |
| Computation Time and Computer Power | LOW | HIGH |
| Accuracy | GOOD | EXCELLENT |
| Prediction of Airflow Conditions (e.g., velocity) | NO | YES |

### *1.3.3 CONTAM*

CONTAM is a multi-zone model software program for indoor air quality and ventilation analysis (Walton and Dols, 2005 and NIST, 2008). Several versions of the program exist, all of which were developed by the National

Institute of Standards and Technology (NIST). CONTAM has several functions and can be used for a variety of applications. The program is designed to help determine building airflows (through the envelope and between interior zones), contaminant concentrations, and personal exposure. For airflow analysis, the program considers driving forces such as mechanical ventilation system airflows, wind pressures, stack effects, terrain characteristics, and temperature differences. By defining contaminants and specifying the nature of the contaminant source, the program can predict the dispersion of these contaminants through the various airflow paths throughout the building. In calculating concentration levels, the program takes into account how the contaminant may interact with building surfaces (adsorption, desorption, and deposition) and any filtration devices that are present. The main applications of CONTAM include assessing adequacy of ventilation rates, design and analysis of smoke systems, assessing indoor air quality performance, predicting contaminant dispersion, and estimating personal exposure (Walton and Dols, 2005). CONTAM is comprised of a graphical user interface called "CONTAMW" and a numerical solver called "CONTAMX".

### *1.3.4 Project Creation Wizard (PCW) – "Rapid Semi-Empirical Tool for Estimating Airflow in Facilities"*

"PCW 1.0 is a Project Creation Wizard that is based on and uses the simulation engine of NIST's CONTAMW series" (Vandemusser, 2007). PCW, which was developed by Vandemusser Design, LLC and runs on the CONTAMX engine, differs from CONTAM in that it has a more "user friendly" graphical user interface that helps to reduce the time and effort needed to develop an airflow

model. PCW has more built-in default values, as compared to CONTAM, to help reduce the amount of information that needs to be manually entered into the program (i.e., default leakage values which were derived from Persily, 1998). PCW was also designed to facilitate and simplify the model calibration process. The program contains a built-in "tuning" process which accepts actual measured data and updates the model based on those measurements to improve model accuracy. PCW also performs a factorial analysis to identify significant input parameters on the percentage of correctly predicted airflow directions and a regression analysis to optimize certain parameters which are too difficult to measure. At the end of the simulation, PCW has a fully integrated results viewer which includes color coded contaminant distribution diagrams. PCW also contains a scenario manager to allow the user to compare various contaminant release scenarios.

The model calibration process in PCW occurs between the "input phase" and the "analysis or simulation phase" in the "measurements" phase. After the "input phase" and an initial simulation, the program calculates the magnitude and direction of airflow through every single airflow path for a certain set of operating and climatic conditions. PCW then compares actual, i.e. measured, airflow directions entered by the user to model predictions. This is presuming that the user has measured all airflow directions in the building (using chemical smoke bottles, for example) at the same operating and climatic conditions specified in the simulation. PCW graphically displays which flow directions were predicted incorrectly based on the actual measurements. Next, the user is encouraged to

perform measurements of HVAC system airflows in rooms where incorrect flow directions are being predicted and update the model with these measurements.

As part of the tuning process, PCW then performs a $2^7$ factorial analysis to determine the effects (main and interaction) of seven variables on the percentage of incorrectly predicted flow directions. Refer to Appendix B for a discussion on "design of experiments" or experimental design methods such as factorial designs. The seven variables include: terrain factors, interior wall leakage, exterior wall leakage, shaft wall leakage, wind direction, wind velocity, and outside air temperature. The user is then encouraged to get more accurate measurements on those variables which are found to have a large effect or influence. However, some of these variables are too difficult to measure or too ambiguous to define (e.g., terrain factors and leakage), therefore, PCW performs a regression analysis to try to optimize the values of these variables as well as any other variables that the user is unable to measure. Finally, after the calibration phase, PCW's "analysis phase" is similar to CONTAM except that PCW has slightly better results graphics. Refer to Section C.4 of Appendix C for a summary outline of the PCW simulation process.

This research specifically focuses on using the PCW version of CONTAM to develop a calibration process that builds upon the current calibration procedure by explicitly using $CO_2$ tracer gas data. Refer to Appendix C for a more detailed discussion on PCW and CONTAM.

## 1.4 Research Objectives and Scope

This research builds upon previous research efforts (Firrantello, 2007 and Sae Kow, 2010) whose purpose was to develop methods that allow for quick calibration of a CONTAM multi-zone airflow model. Through these research efforts, the calibration oriented and user-friendly wizard version of CONTAM, PCW, was developed and validated. Although $CO_2$ tracer gas measurements from releases in air handling units (AHUs) were available in these previous studies, these measurements were not used in the calibration process. Rather, they were used for evaluating/validating the calibration process. Experience with these tracer gas tests indicates that they are relatively simple and inexpensive to perform as long as research grade $CO_2$ monitoring equipment is not needed.

The purpose of this research is to develop a methodology for explicitly using $CO_2$ tracer gas tests in the airflow model calibration process and in refining the overall calibration process currently utilized in PCW. Application to real buildings within this research was limited to evaluation of data collected from prior field tests performed by Firrantello (2007) and Sae Kow (2010). This research included the following objectives:

1. Review relevant literature including general calibration literature, tracer gas testing literature, multi-zone model performance characterization literature and other relevant areas.
2. Review past work done on PCW and the existing PCW calibration procedure.

3. Develop a candidate calibration methodology that explicitly incorporates $CO_2$ tracer gas data into the procedure. Start with methods that complement and do not fundamentally alter the basic approach currently implemented in PCW and continue to methods that are integrated with or require modifications of the current approach.
4. Evaluate the candidate methodology using a synthetic or virtual building approach. Refine and re-evaluate the methodology with synthetic building testing.
5. Evaluate the suitability of existing data sets (Firrantello, 2007 and Sae Kow, 2010) from a real building for testing the proposed methodology and apply to that building if feasible.
6. Provide a summary and identify important conclusions.
7. Outline extensions of this methodology which could potentially be investigated in future research efforts.

# CHAPTER 2: LITERATURE REVIEW

This chapter presents a review of relevant literature on general calibration methodologies, multi-zone airflow models, and tracer gas techniques.

## 2.1 General Literature Review

### *2.1.1 Reddy and Bahnfleth (2006)*

This paper proposes a decision methodology for reducing vulnerability of building occupants to chemical, biological, and radiological attack scenarios. In the step to predict system dynamic response, a case was made that representing the building in simplified multi-zone or compartmental models could be beneficial in many ways. Compartmental models represent the building as a series of well-mixed compartments connected by airflow paths. Generally the building is "aggregated" into simple one or two zone models. Mass balances of contaminant concentrations can be applied to each compartment in the form of first-order ordinary differential equations (ODEs). Closed form solutions to these ODEs can then be easily found. This simplified mathematical representation of the airflow system allows for model parameterization, model calibration, and uncertainty analysis. Compartmental models can also be used to infer information regarding certain physical parameters (e.g., leakage values, inter-zonal flow rates, etc.) for different scenarios.

It was hypothesized that the use of these simplified compartmental models may help in the current investigation on the use of $CO_2$ tracer gas data for better model calibration. For example, solving the mass balance equations for $CO_2$ in

each compartment could yield useful information on aggregated building leakage values (internal and external). Developing macro-zones simplifies the analytical solution for the network model. Using aggregated leakage parameters could be a robust step towards model calibration.

### *2.1.2 Reddy (2006)*

This paper presents a literature review on the various uses and benefits of calibrated simulation in the context of building energy simulation. Current calibration simulation processes are discussed and broken into the following categories: general references; calibration based on manual, iterative, and pragmatic intervention; calibration based on a suite of informative, graphical comparative displays; calibration based on special tests and analytical procedures; and analytical or mathematical methods of calibration. Then, issues with error and uncertainty are discussed including: improper input parameters, improper model assumptions, lack of robust and accurate numerical algorithms, error in writing simulation code, and external vs. internal error types. Finally, calibration tools and capabilities including daytyping and data visualization tools are discussed. Although energy and airflow simulations are very different, there are numerous similarities in the way that one might approach model calibration. It is possible that some of these calibration procedures for energy discussed in this paper could be applied to airflow models. Of particular interest are some of the iterative, graphical, and analytical methods of calibration.

### *2.1.3 Reddy, Maor, and Panjapornpon (2007)*

This paper develops a calibration methodology for energy simulation programs that is a combination of heuristic and analytical procedures. The steps of this methodology include: heuristically define a set of influential parameters, perform a coarse grid search using Latin Hypercube Monte Carlo simulations to identify strong parameters and a small set of solutions, use the small solution set to predict changes to the building and building systems, and compute uncertainty in the calibrated model solutions. The objective is to tune the various inputs into the simulation program so that the predicted energy use matches the actual energy use. Once the calibration provides a good fit with the observed utility data, the program can also be able to accurately predict building performance after operational and equipment changes. Finally, the methodology allows for predicting uncertainty in the results. A literature review is presented on different types of models, sensitivity analysis methods, and experimental design methods. As mentioned previously, although there are similarities between energy and airflow simulations, there are also significant differences. It is unclear whether this type of methodology could be applied to airflow models.

### *2.1.4 Heinsohn and Cimbala (2003)*

The fifth chapter of this book discusses well-mixed models and how they can be used to calculate contaminant concentrations through the transient solution of first order ODEs in certain zones for different scenarios. The well-mixed concept is an assumption of spatial uniformity (i.e., constant temperature and contaminant concentration throughout the zone). This chapter adopts a lumped

parameter or macro-model analytical representation of zones for determining contaminant concentrations. These macro-models are then compared to micro-models that employ computational fluid dynamics (CFD). A few examples, similar to those presented in Section 1.3.1, of one and two zone macro-models are presented where concentration mass balances on each zone are performed and the resulting first order ODEs are solved to determine contaminant concentrations or airflow rates. Included in these mass balance equations are the effects of air filters, adsorption of building materials, exfiltration, infiltration, ventilation strategies, and contaminant sources.

Such macro-model, or compartmental model, representations of buildings are useful for easy determination of physical parameters (e.g., flow rates, contaminant concentrations, etc.) in zones under different conditions. It was hypothesized that for the current investigation of $CO_2$ tracer gas-based calibration, such simplified models could be very useful. Again, the concept of macro-zone analysis to identify aggregated model parameters (e.g. leakage coefficients) could help in calibrating a model beyond the current capabilities of PCW.

### *2.1.5 Musser and Persily (2002)*

This paper discusses a contaminant-based approach to assist certain design practices such as ventilation control strategies, purge strategies, depressurization fan sizing, etc. Contaminant-based designs involve determining ventilation rates from target contaminant concentrations. CONTAM was used to create a multi-zone model for a case study to implement contaminant-based designs. It was proposed that such contaminant-based designs could provide better indoor air

quality, energy conservation, and reduced environmental impact as compared to prescriptive ventilation rates from building codes. The leakage components for the building were specified based on published data and pressurization test studies. It was mentioned that easy to determine leakage paths should be added to the model if possible to "fine tune" the model. The case study model was used to implement demand controlled ventilation, analyze post construction VOC levels, and size a depressurization fan.

### *2.1.6 Price, Chang, and Sohn (2004)*

This paper discusses a methodology to determine where to take measurements to create an accurate building model. The methodology is summarized as follows: "Create a preliminary model that relies only on the connectivity of the zones (what is connected to what) and on easily observable parameters such as zone volumes. Describe other parameters with uncertainty distributions. Sample from the parameter distributions using Monte Carlo methods and exercise the preliminary model, and analyze the results to determine what measurements will most reduce the uncertainties in the parameters that affect a specific question of interest" (Price et al., 2004). Due to the large number of parameters in any given building, it is not practical to conduct exhaustive measurements. Also, due to the complexity of many parameters, it may not be possible to perform experiments that can directly measure them. This paper focuses on determining which measurements should be made to reduce the uncertainty in the input parameters that have the greatest influence on the response.

Tracer gas measurements can be used along with zone pressure measurements to estimate model parameters that describe airflow links between zones. It is mentioned that a good approach is to "directly investigate the relationship between the pressure measurements and the time-average concentration" (Price et. al, 2004).

### *2.1.7 Etheridge and Sandberg (1996)*

The tenth chapter of this book focuses on measurement techniques for determining flow characteristics in buildings and how uncertainty issues in measurements are a concern for each technique. The chapter discusses measurement devices, accuracy, measurement techniques, and calibration techniques for volumetric flow rates and pressure differences. For volumetric flow rate measurements, the various techniques are characterized by the level of flow (i.e., low, high, and very high flow rates). Pressure measurements are discussed for single-cell buildings and multi-cell buildings. The effects of wind and buoyancy on pressure measurements are also mentioned. Finally, this chapter goes into the analysis of leakage data. Results from leakage tests are usually in the form of pairs of values of flow and pressure difference. This data is then fit to a curve which most likely follows either a power law or quadratic equation. How regression equations can be used to estimate flow rates or pressure differences is also covered.

The eleventh chapter of this book discusses one approach of multi-zone representation of buildings that may be adopted for the investigation of $CO_2$ tracer gas-based calibration, namely the inverse problem approach. The inverse problem

is where outside air and inter-zonal flow rates are determined from concentration measurements of a tracer gas. Multi-zone representation of buildings consists of mass conservation (or continuity) equations of air and tracer gas for each zone in the form of first order ODEs. Rules of thumb for simplifying a building into a multi-zone model are presented. The continuity equations are combined and represented in matrix format. Once in matrix form, physical interpretations of the matrices can be made. For example, the sum of any row in the flow matrix is the flow into that zone and the sum of the columns is the flow out of the zone. In the inverse flow matrix, the diagonals are the purging flow rates of each zone and the non-diagonals are the transfer index values between the injection zone and another zone. Manipulation of the continuity equation in matrix format provides an expression for the steady state concentration of the contaminant. The results show that the steady state concentration depends only on the flow terms and not the volume of the zones. The tau ($\tau$) matrix, which is the product of the volume matrix and the inverse flow matrix, is also amenable to physical interpretation. The sum of any row is equal to the mean age of air in that zone. It is also shown that the equilibrium concentration in a zone is directly proportional to the mean age of air in that zone. The chapter also discusses the meanings of matrix eigenvalues and matrix determinants. Transforming the network of equations for a multi-zone model in matrix form not only simplifies the representation but also allows for easy physical interpretations of the mathematical model.

The twelfth chapter of this book discusses how tracer gas techniques can be used to measure certain flow rates such as the total outside air flow rate and

infiltration. These measurements are accomplished by injecting a tracer gas into a space and measuring the concentration history of that gas. For a particular space, the inflow of air that is tracer gas free can be determined from this concentration history. Four tracer gas techniques are discussed in this chapter including: decay method, constant injection method, pulse technique, and constant concentration method. The decay method involves a short burst of tracer gas injected into a space to establish a uniform concentration within the space. The concentration of tracer gas is then recorded over time. The constant injection method involves injecting tracer gas at a constant rate and measuring the concentration response of the space over time. The pulse technique involves a short duration gas pulse into the space and the concentration response of the space is recorded over time. Finally, the constant concentration method involves injecting tracer gas at a rate that maintains constant concentration in the space.

The basis for all of these methods is the mass balance of tracer gas and air in each zone. Two general approaches are discussed. The direct approach is to solve the mass balance equation for flow rate. The alternative approach is to view the mass balance equation as a state equation where the unknown flow rate is regarded as a coefficient in the equation and statistical estimation theory is used to obtain the flow rate. The tracer gas techniques are divided into two broad categories, active and passive techniques. Active techniques involve the use of pressurized systems. Passive techniques involve the transportation of gas and air samples by molecular diffusion.

The theoretical basis for the above mentioned tracer gas techniques are also discussed in this chapter. The decay method includes mathematical expressions for after the release, i.e. no gas injection during measurement. The concentration as a function of time is defined mathematically. The plot of the natural log of concentration versus time yields a straight line of negative slope equal to the flow rate divided by the volume i.e., the air change rate. Thus, the flow rate is equal to the room volume times the slope of the decay curve. The constant injection method involves integrating the mass balance equation over the measurement period. The equilibrium concentration is equal to the mass divided by the flow rate. For the constant concentration method, the injection of the tracer gas into the room is controlled so that the concentration is maintained at some target level. Thus, the equilibrium concentration is equal to the target concentration. Therefore, for an individual room, the flow rate of outside air to the room is equal to the release rate of tracer gas into the room divided by the target concentration. Feedback control with proportional, integral, and derivative (PID) compensation is used to maintain the target concentration. All three methods require complete mixing and any departure from that will introduce errors.

Identification methods can be applied to any injection strategy. This is where one "disturbs" the physical system to observe the system response in terms of changing concentrations. The mass balance equation is called the "state equation" where the actual concentrations are the state of the system and the flow rate and ventilated volume are the coefficients of the equation. Statistical estimation theory (such as the least squares method) can be used to infer these

coefficients. For example, the mass balance in Equation 2.1 below is the state equation where the release rate of tracer gas "m" is the input or control and Q/V and 1/V are the coefficients or model parameters.

$$\frac{dC}{dt} = -\frac{Q}{V}C + \frac{1}{V}m \tag{2.1}$$

The "inverse problem" is to determine these model parameters. Integrating the solutions of the mass balance equation over one sample period will result in a difference equation. This equation will predict the concentration at certain times and certain release rates. The least squares method minimizes the sum of squares of the differences between the recorded concentrations and the predicted concentrations.

Next, the chapter discusses methods for measuring inter-zonal airflow rates. For a building with "N" rooms or zones, there will be "N*(N+1)" inter-zonal flow rates. Thus, there will be "N*(N+1)" equations, expressed in matrix form for simplicity, that need to be solved to determine all of these flow rates. These equations can be obtained by using one tracer gas and making concentration measurements in each room or zone or by simultaneously using different tracer gases. It is noted that as the number of zones increase, the number of unknown airflows also increase. There will be a point when it is not practical to determine all the flow rates. Inter-zonal flow rates are difficult to determine because they are affected by buoyancy forces and thus are vulnerable to indoor temperature variations. Such forces could result in the reversal of flow through a particular flow path.

This chapter also discusses the various physical components of a tracer gas system. Typical components include: gas, injection system, artificial mixing system, sampling system, gas analyzer, and control system. Selecting the right tracer gas to use is also an important decision. An ideal tracer gas should not be a normal constituent of the environment being investigated, should be easily measured at low concentrations, should be non-toxic, non-allergenic, non-reactive, non-flammable, environmentally friendly, and economical to use. There are various injection systems and sampling techniques available. There are also various methods of gas analysis including infrared spectroscopy, gas chromatography, and mass spectrometry.

Another important consideration is where to inject the tracer gas and where to sample the tracer gas. Most methods assume "well-mixed" zones which are almost never achieved in reality. The authors suggest injecting the gas in rooms where outside air enters, and to sample in rooms where air leaves the building. "This strategy gives the maximum possibility for the gas to be diluted with all incoming air" (Etheridge and Sandberg, 1996). If one cannot determine where outside air is entering and leaving the building, the best strategy is to inject a sample in each room. Practical applications of the three tracer gas methods are presented by testing each method on an actual house. The results and differences in equipment needed are presented and discussed.

### *2.1.8 Evans (1996)*

It is common to represent indoor air quality models as systems of linear, ordinary differential equations. This paper reviews the state-variable formulation,

which utilizes vector/matrix notation, of these systems and discusses what useful information can be extracted without explicitly solving the differential equations that comprise the system. This mathematical modeling of building airflows, sometimes referred to as compartmental modeling, can have problems of "observability", structural or deterministic "identifiability", and "redundancy". The term "observability" refers to the problem of determining whether or not the state variables can be determined from observations before any measurements are made. Identifiability occurs when trying to "extract information about a linear system's parameters from observations of that system's response to a forcing function" (Evans, 1996). The identifiability problem involves not being able to uniquely estimate system parameters from an experiment. This can happen no matter how good the measurements are. This condition, however, can be detected before experimentation begins and before any data is collected by using compartmental models. "Identifiability is tested most commonly through the use of the Laplace transform method" (Evans, 1996). Finally, "redundancy" occurs when there is an "inability to obtain unique parameter estimates from the data, even if the experiment is identifiable" (Evans, 1996). In other words, "redundancy" refers to the problem where multiple models may fit the data equally well and one cannot determine which model is the right one. Thus, a selected model may provide parameter estimates that are not the best for the systems being modeled. Such a "redundancy" problem is "intimately related to that of "ill-conditioning" of the matrices in the estimation process" (Evans, 1996).

The author combines the "identifiability" and "redundancy" issues using instead the term "estimability."

The author first provides an introduction to compartmental models, linear systems, and the well-mixed assumption. For indoor air quality (IAQ) models, the rooms of the building are the compartments in the model. These models predict the time varying movement of a contaminant through the building. Since partial differential equations are not used (i.e., derivatives are taken only with respect to time), these models do not simulate spatial variance.

The state-variable formulation is presented in Equation 2.2 below where "x(t)" is the "state vector" (mass of material in each compartment), "A" is the rate-parameter matrix, "u(t)" is the input vector, and "B" is the matrix which distributes the number of inputs to the number of compartments.

$$x'(t) = Ax(t) + Bu(t) \tag{2.2}$$

The "A" matrix is of particular importance. "The column sums are the negative of the rate constant for transfer to the environment ("excretion rate") from the compartment corresponding to each column. If all these sums are zero, one has a "closed" system; if at least one is nonzero, one has an "open" system" (Evans, 1996). Also, the negative diagonal elements are the sum of losses to the environment and all other compartments. The off-diagonal elements are the transfer rates between compartments. A simple example of a three-compartment (source, room, and sink) IAQ model is presented to illustrate the concept of the "A" matrix. It is noted that the benefit of this linear systems formulation is that

the “A” matrix contains a lot of information that can be extracted without having to solve the system’s differential equations.

The eigenvalues of the “A” matrix are important because they “control the dynamic response of the system, since the eigenvalues appear in the exponentials which comprise the time-domain solutions of the [multi-compartment system] ODEs” (Evans, 1996). If the eigenvalues are real and distinct, the response is exponential. If the eigenvalues are real and repeated, the response is a time-exponential product. If the eigenvalues are complex (conjugate pairs), the response is an exponentially-damped sinusoid. The eigenvalues cannot be obtained in closed form for small systems. However, software packages are available to numerically find these eigenvalues. The inverse of the “A” matrix can be useful for determining the long-term or equilibrium concentrations in each compartment without having to solve the system’s differential equations.

Next, the author discusses solution methods for compartmental systems including single-compartment analytical solutions, multiple-compartment analytical solutions, and numerical methods of solutions. The single-compartment analytical solution involves evaluating the scalar convolution integral for a source term. The multiple-compartment analytical solution is more complex and involves using a Laplace transform approach. The concept of a “transfer function” is introduced here. The transfer function “is a way of expressing how an input function is transformed into the output of the system” (Evans, 1996). In this case, the transfer function is the ratio of the Laplace transform of the output to the Laplace transform of the input. To get the Laplace

transform of the output, one multiplies the Laplace transform of the input by the transfer function. Taking the inverse Laplace transform of the output then gives the solution to the multi-compartment system. This is typically in the form of a sum of exponentials. Numerical methods are not discussed at any length in this paper. It is noted, however, that numerical solutions may be more advantageous for larger systems since analytical solutions quickly become algebraically cumbersome.

The remainder of the paper deals with parameter estimation. First, a brief background of linear and nonlinear estimation is presented. Linear estimation models in the least squares estimate of the parameters and are typically in the form of a polynomial in the independent variable. However, these models usually have no physical or mechanistic basis and thus the parameters have no physical interpretation. "In nonlinear estimation, where the [estimation model] is nonlinear in the parameters, the normal equations turn out to be nonlinear, and have no closed-form solution, so we must use search methods in order to find the least-squares estimates of the parameters" (Evans, 1996). This search begins with a best guess of the parameter values and continues until some convergence criterion is met. The surface plot of the residual sum of squares for linear models would reveal that there is one unique minimum. Similar surface plots for nonlinear models can take any shape and can thus have local minima. Multiple search methods should be utilized to find the global minimum. Parameter estimation in multi-compartment systems can result in parameter estimates that are unstable and unreliable. Here author presents several examples of "estimability" problems.

### *2.1.9 Lawrence and Braun (2005)*

This paper evaluates different modeling approaches for predicting carbon dioxide levels in small single zone commercial buildings served by packaged air-conditioning units. It is important to note that the authors found that a transient $CO_2$ model did not yield significant improvements in model prediction accuracy as compared to a quasi-static model. The paper discusses CFD models as well as simplified $CO_2$ models.

Three simplified models were used to compare with the results of the CFD models. These simplified models include: a quasi-static (equilibrium) model, a two-zone transient model with inter-zonal airflow, and a three-zone transient model with inter-zonal airflow. All three models involve a mass balance of $CO_2$ concentration within the zone(s) being analyzed. The two and three zone model mass balance equations are first order ordinary differential equations since there is a change in zone concentration over time. For the single zone quasi-static model, the authors use a ventilation effectiveness term defined as "a measure of how well the supply airflow mixes with the occupied zone for removal of $CO_2$ or other pollutants" (Lawrence and Braun, 2005). The ventilation effectiveness "$\eta_v$" is presented in Equation 2.3 below.

$$\eta_v = \frac{(C_r - C_s)}{(C_z - C_s)} \tag{2.3}$$

In Equation 2.3, "$C_r$", "$C_s$", and "$C_z$" are the $CO_2$ concentrations in the return air, supply air, and zone air, respectively. This ventilation effectiveness term attempts to account for some of the realistic deviations from the "well-mixed"

assumption. In the two and three zone models, this ventilation effectiveness term is replaced by inter-zonal flow terms. A parameter estimation process was used to learn unknown values in the two and three zone models. This process was conducted using a commercially available optimization routine to obtain estimates of these parameters. The paper compares the prediction accuracy of CFD models with the simplified models by calculating the cost savings associated with using demand controlled ventilation (DCV) for some typical small commercial buildings.

### *2.1.10 Awbi (1991)*

The third chapter of this book discusses three areas of air infiltration and natural ventilation including the following: airflow characteristics of building envelope and components and how airflow through them is calculated, measurement and calculation of air infiltration through the whole building envelope, and how to combine this knowledge and apply it to the design of passive and natural ventilators.

Flow rates or leakage rates through openings in the building envelop are affected by the size and distribution of the leakage path, the flow characteristics of the leakage path, and the pressure difference across the leakage path. These three factors must be known in order to evaluate leakage through the envelope. There are several methods available for estimating these factors. The mass balance equation across the building envelope is used to estimate the air leakage through the envelope.

The author mentions two basic equations for calculating the airflow through building components. The equation used depends on the type of opening. One equation deals with fully turbulent flow and the other deals with laminar or transitional flow. For large openings with turbulent flow, the orifice equation is used where effective leakage area values are obtained from tables published by the American Society of Heating, Refrigerating, and Air-Conditioning Engineers (ASHRAE). For smaller openings with laminar flow, the "Couette" flow equation is used. When there are wide cracks where flow is in the transition region (i.e., neither laminar nor turbulent), the orifice equation and the "Couette" equation are lumped into a single power law equation called the "crack flow equation" which says that the flow rate is proportional to the pressure difference raised to some exponent. The proportionality constant is a function of the geometry of the crack and the exponent is dependent on the flow regime. This power law equation is not dimensionally homogeneous so some suggest using the dimensionally homogenous quadratic form which is a second order polynomial relating the pressure difference to the flow rate and the square of the flow rate. The first order term represents laminar flow and the second order term represents turbulent flow. These equations are typically written in a form that fits compartmental models. These compartmental models form the multi-zone models that are used in computer simulation programs. The solution of the compartmental model "is achieved by an iteration process in which an arbitrarily guessed internal pressure value is successively improved until a flow balance is achieved across the building fabric" (Awbi, 1991).

The driving force for air leakage across an opening is the pressure difference on either side of the opening. The magnitude and direction of the pressure difference can be affected by wind, temperature difference (stack effect), and operation of mechanical ventilation systems. “Total pressure acting on an opening or the building envelope as a whole is the sum of the pressure due to wind, stack and mechanical ventilation taking into consideration the sign of each pressure component” (Awbi, 1991). The author presents an equation for pressure due to wind flow. The wind pressure coefficient can be estimated using wind tunnel testing. Wind pressure on a building façade depends on wind velocity, direction, and the terrain surrounding the building. An equation for the time-averaged wind speed profile is also presented. This wind speed depends on the weather conditions, the height where it is being calculated, and the terrain surrounding the building. Stack pressure effects are driven by buoyancy forces, i.e. the variation in air density with air temperature. The author presents equations for the stack pressure difference between two vertical openings separated by a vertical difference. Finally, the effect of mechanical air infiltration is “determined by matching the building’s air leakage curve with the fan’s characteristic curve in a similar way as in fan and duct system matching” (Awbi, 1991).

To calculate air infiltration using the expressions mentioned above, the following quantities need to be known or evaluated: wind speed and direction, internal and external air temperature, position and flow characteristics of all openings, and pressure distribution over the building for the wind direction under consideration. It is often difficult or impossible to determine all of these

measurements so some simplifications are typically necessary. The author discusses the following three simplified solution methods to calculate infiltration rate: empirical methods, simplified theoretical methods, and network models.

Two empirical methods are discussed, the ASHRAE method and the British Standards Method. For the ASHRAE method, flow is a function of the total effective leakage area, a stack coefficient times the temperature difference, and a wind coefficient times the wind velocity. ASHRAE provides values for the coefficients based on different situations. The British Standards Method gives tables of formulations for calculating air infiltration rate due to wind, buoyancy and combined wind and buoyancy for openings at different situations. Two simplified theoretical models are discussed, the Building Research Establishment (BRE) Model and the Lawrence Berkeley Laboratory (LBL) Model. The BRE model uses a power law expression that relates the infiltration rate for any given internal and external conditions to the leakage characteristics of the building determined by a pressurization test. The LBL model is a simple model for a single zone building. Infiltration due to wind and stack effect are calculated separately and then added in quadrature to obtain the total infiltration.

Next, the author discusses these methods in the context of multi-zone modeling. “In a multi-zone building, the flow through the external envelope is also affected by the flow resistance of the internal zones and the prediction of infiltration rates requires a multi-zone network analysis” (Awbi, 1991). The external pressure nodes in a multi-zone model are usually known and the internal pressure nodes usually need to be determined. “Because of the non-linear

dependency of the volume flow rate on the pressure difference the internal pressures can only be determined by an iterative solution of the flow equations" (Awbi, 1991). These multi-zone models allow one to calculate the mass flow interaction between different zones. This flow between zones is usually given by a power law equation. When the flow coefficients and exponents are known, the flow can be calculated by an iterative solution process after an initial guess on the pressure differences. The system of equations in the multi-zone model is obtained by performing a mass balance on each node.

This chapter also discusses the measurement of air infiltration through the building envelope and through building components. For the building envelope, one can adopt steady-state pressurization/depressurization tests or dynamic pressurization tests. The results of these pressurization, or depressurization, tests are values of flow rate for corresponding pressure differences. Constructing a logarithmic plot of $\log_{10}Q$ vs. $\log_{10}\Delta P$ produces a straight line with slope = n and y-intercept equal to $\log_{10}k$ where "n" and "k" are the flow exponent and flow coefficient, respectively. Thus the pressurization tests can be used to obtain the coefficients and exponents of the power law equations that describe the flow through the envelope.

The measurement of air leakage rates can be obtained from tracer gas techniques where a tracer gas mass balance is performed in the rooms or zones of the building. Three methods are discussed; namely, the concentration decay method, the constant tracer injection method, and the constant concentration method. The concentration decay method is the most common and requires the

least sophisticated equipment. This method involves solving the differential mass balance equation as a function of time. A plot of the natural log of the tracer gas concentration versus time results in a straight line with negative slope equal to the air change rate during the measurement period. The constant injection method has a similar mass balance expression as the decay method only with a constant source term. For the constant concentration method, flow is directly proportional to the tracer gas injection rate required to maintain a target concentration.

Tracer gas techniques can also be used for the measurement of inter-zonal air leakage. Again, for "N" zones there are "N*(N+1)" equations that need to be solved for all the inter-zonal flow rates. The author describes various ways of assembling these "N*(N+1)" equations. Also discussed, are various release and measurement locations and situations.

Finally, the chapter discusses passive ventilation designs and the tradeoff between reducing infiltration for energy reasons and keeping infiltration for indoor air quality reasons. Passive or natural ventilation design requires careful and detailed selection of ventilation opening and their optimum positioning on the building envelope. Equations for sizing passive ventilation openings are presented.

### *2.1.11 Spengler, Samet, and McCarthy (2001)*

Chapter 51 of this book discusses technologies for measuring and monitoring indoor air quality and provides a procedure for properly selecting instrumentation for a particular situation. The selection process includes the following steps: select the concentration threshold level for the pollutant, define

data quality objectives (DQOs), evaluate operational requirements, evaluate available technologies, and document selections and rationale. Current measurement technologies are discussed for bio-aerosols, carbon dioxide and carbon monoxide, ozone, particulate matter, organics, and air exchange.

When selecting measurement systems one needs to consider operating characteristics and performance characteristics. Operating characteristics include logistics, mobility, sampling mode and approach, power requirements, size, weight, and costs. Performance characteristics include range, method detection limit, precision, calibration, and output.

Air exchange measurement is important for tracking contaminant migration in a building due to a source. Included in air exchange measurements are infiltration, natural and mechanical ventilation, inter-zonal flows, and local circulation. The authors discuss two basic tests for determining air exchange: pressurization tests and tracer gas techniques. The constant concentration, pulse injection, and constant injection tracer gas techniques are briefly discussed.

Chapter 52 of this book discusses various measurement techniques related to building ventilation. First, a brief background is provided on ventilation, the various flows involved, and the various driving forces for those flows. Next, current instrumentation is briefly described for the following: air temperature, relative humidity, differential pressure, Pitot-static tubes, hot-wire anemometers, rotating-vane anemometers, flow hoods, tracer gas monitors, and smoke tubes. The author then describes various measurement techniques for pressure differences (across exterior and interior walls), tracer gas concentrations, percent

outside air (using flows, temperatures, or tracer gas concentrations), and airflow rates (using Pitot traverses, hot-wire traverses, tracer gas concentrations, vane anemometers, flow hoods, etc.).

For whole building air change rates, the author discusses the tracer gas decay method which is a single zone approach. The assumption is that the building can be represented by a single well-mixed zone. If there is a constant air change rate, the tracer gas concentration will decay according to Equation 2.4 below.

$$C(t) = C_0 e^{-It} \tag{2.4}$$

In Equation (2.4), "t" is time, "$C_0$" is the initial tracer gas concentration (at time t=0) and "I" is the air change rate. Therefore, "I" is the ratio of the outside air flow rate into the building (mechanical and infiltration) to the building volume. Another expression is given for a non-constant air change rate. The author also mentions the constant concentration approach and the constant injection approach. In the constant concentration approach, the volume of tracer gas injected over a period of time is used to determine the air change rate. This requires more sophisticated instrumentation as compared to the decay method and is generally only used in research studies. The constant injection approach uses the build-up of tracer concentration to determine air change rate.

Finally, measurement of outside air distribution is discussed. It is pointed out that even though a building as a whole receives the proper amount of ventilation, some spaces may be under-ventilated while other spaces may be over-ventilated. Two ways to evaluate this phenomenon (providing there is proper

outside air distribution), is to directly measure airflow rates or conduct tracer gas measurements in various zones to determine the local age of air. The age of air is a measure of how long the air has been in the space since it entered from the outdoors.

Chapter 57 of this book discusses the complex, dynamic characteristics of the indoor environment. The indoor air environment is influenced by outdoor climate parameters, occupants and their activities, the HVAC system, building materials (off-gasing), etc. In order to model such a complex environment, mathematical representations are used. For indoor air environment modeling, the author distinguishes these mathematical models into microscopic and macroscopic models. Macro-models use mass balance equations and the well-mixed assumption to form lumped parameter formulations, which are ordinary differential equations. Macro-models or CFD models are simple to solve but do not model spatial distribution or surface phenomena. Micro-models are based on the Navier-Stokes equations of fluid motion. Advanced numerical methods are used to solve these equations. Thus, micro-models require greater computational time and power as compared to macro-models; however, they can predict spatial distribution of indoor parameters.

Chapter 58 of this book discusses IAQ modeling and its role in risk analysis. IAQ models can be used for estimating population exposure to various indoor pollutants, estimating the impact of individual sources on pollutant concentration, and estimating the impact of individual sources on IAQ control options. Models that estimate population exposure use statistical models such as

Monte Carlo techniques. Models that estimate individual sources use mass balance equations.

Mass balance models allow for the estimation of how sources, sinks, and IAQ control impact the concentration of contaminants. They can be represented by single zone or multi-zone models. The author presents a typical mass balance equation for a room. One important term in this equation is the penetration factor for outdoor pollutants. The penetration factor accounts for pollutant penetration into the space through small cracks and openings in the building shell assuming there is an ambient concentration of the contaminant. A table of penetration factors for some typical pollutants is provided. The source and sink terms in the mass balance equation are typically not constant, and thus yield additional coupled equations to the set of equations based on mass balance considerations. IAQ models must solve all of these equations using numerical methods. The multi-zone program CONTAM uses finite element techniques to solve this set of equations.

The well-mixed assumption made in mass balance IAQ models is valid under the following situations: time scales of interest are several minutes or longer, concentrations very close to the large sources are not of interest, and there are no local flow disturbances close to the location of interest. There are some modifications that can be made to these models to improve the predictions near large sources. These mass balance models can be verified by using quantitative criteria established by the American Society for Testing and Materials (ASTM). These criteria include the following: absolute value of the fractional residual

between the measured or observed concentration and the predicted concentration, correlation coefficient between the observed and predicted concentrations, normalized mean square error, least squares best fit regression line between observed and predicted concentration, and the normalized or fractional bias. ASTM has recommendation values for each of these criteria that correspond to a "satisfactory" model.

The author also discusses source and sink models. Source models are split between empirical decay models and mass transfer based models. For empirical decay models, the time step of the model should be compared with the decay constant. A large decay constant relative to the time step used will not effectively show the source behavior. The section on sink models is limited to volatile organic compounds (VOCs).

## 2.2 Review of Previous Work and the Existing PCW Calibration Procedure

### *2.2.1 "Development of a Rapid, Data Driven Method for Tuning Multizone Airflow Models" (Firrantello, 2007)*

#### *2.2.1.1 Introduction*

The work by Firrantello (2007) entitled "Development of a Rapid, Data Driven Method for Tuning Multizone Airflow Models" utilized NIST's multi-zone airflow modeling program, CONTAM. "The objective of this work was to develop an algorithm that can be used to tune multi-zone airflow models of buildings with the aid of measurements taken at the building site" (Firrantello, 2007). The main purpose of this type of airflow model calibration is for accurate predictions of contaminant dispersion and occupant exposure during extraordinary

events, i.e. chemical or biological attacks. The original intent of this research was to develop a tuning algorithm based on analytical methods. However, as the algorithm development progressed, heuristic methods were determined to be more practical and relevant. Although CONTAM was used in this work, the resulting turning algorithm led to the development of the PCW version of CONTAM described earlier.

*2.2.1.2 Research Methods*

The extreme case of model calibration would involve physically performing all possible release scenarios within the building and measuring contaminant concentrations in each space for various weather conditions and operational settings. With this data, an airflow model would not even be necessary. However, the time, effort, and cost associated with such procedures make this type of calibration prohibitive. This implies to the need for developing simpler, cheaper, and less time-consuming methods of calibration.

The calibration algorithm developed by Firrantello (2007) was based on a combination of analytical and heuristic methods. Tests on two virtual buildings and two real buildings were conducted to determine which methods were most suitable for the algorithm. Tests on virtual buildings were used to develop the algorithm, while tests on the real buildings were used to validate the algorithm. The analytical methods included sensitivity analysis and regression optimization; both conducted using a full factorial experimental design. For both of these analytical approaches, the response variable was the percentage of correctly predicted airflow directions. Another measure of model adequacy utilized was the

percentage of satisfactory metrics specified in ASTM Standard D5157 – "Standard Guide for Statistical Evaluation of Indoor Air Quality Models" (ASTM, 2003). The full factorial design was chosen over fractional factorial and Plackett-Burman (PB) designs due to the resulting robust data set which accounts for all interaction effects. Fractional factorial and PB designs result in the aliasing of effects of certain factors or factor interactions (Montgomery, 2009). The sensitivity analysis was used to determine input factors that significantly contribute to the number of correctly predicted airflow directions and the number of satisfactory ASTM D5157 metrics. The regression equation was used to determine optimal values of factors that are too difficult or impossible to measure (e.g., interior leakage, exterior leakage, shaft wall leakage, and terrain constant and exponent).

The tuning methodology was intended to be based on measured data, i.e. HVAC airflows and inter-zonal airflow directions, rather than some sort of numerical optimization to achieve an optimal value of a model quality metric (Firrantello, 2007). Further, the tuning methodology was designed to be rapid, low-cost, and easy to use. The scope of the methodology included commercial buildings with mechanical ventilation systems. Residential scale buildings were not included. The intended users of this methodology include building owners or operations personnel who are concerned with occupant vulnerability under possible extraordinary events.

*2.2.1.3 Model Evaluation*

Two metrics were chosen to evaluate model accuracy during calibration: the percentage of correctly predicted inter-zonal airflow directions and the percentage of satisfactory ASTM D5157 metrics. It was noted that the ASTM Standard D5157 is the only published standard for indoor air quality model evaluation. The percentage of correctly predicted inter-zonal airflow directions is a semi-quantitative, heuristic measure of model accuracy that considers only the flow direction and not the magnitude of the flows between zones. Knowing the correct flow directions requires actual measurement using smoke bottles, for example. Thus, this metric is limited by the operating conditions under which the flow directions were observed as well as by the number of places where inter-zonal flow directions can be practically measured, e.g. under doors. Using ASTM D5157 metrics provides a more formal and quantitative measure of model accuracy. The standard specifies six statistical measures that need to be calculated for each zone including: correlation coefficient, line of regression slope and intercept, normalized mean square error, normalized or fractional bias, and fractional variance. These metrics are calculated by comparing $CO_2$ tracer gas concentrations measured in the real building to those predicted by the airflow model. Section 3.1.2 “Model Evaluation” from Firrantello (2007) discusses criteria for evaluating “satisfactory” levels of these metrics. Firrantello (2007) also discusses advantages and disadvantages of both of these metrics and notes the difficulty encountered in selecting a robust metric. In particular, the heuristic metric of percent correctly predicted airflow directions was selected because of its

simplicity and its potential for pragmatic applications. In order for either of these metrics to be used, actual building measurements need to be taken, i.e. air flow directions and $CO_2$ concentrations.

*2.2.1.4 Virtual Building Testing*

The first part of the tuning algorithm development involved testing two virtual buildings modeled using CONTAM. The advantage of using virtual buildings is that any parameter can be measured and measurement uncertainty is eliminated. The first building was a one story, 4,290 $ft^2$ building with three constant air volume (CAV) air handling units (AHUs). The second building was a ten story, 64,700 $ft^2$ building with four CAV AHUs. After the two virtual buildings were created, various parameters (e.g., leakage values and airflows) were arbitrarily changed on the order of 10-20% so as to randomize the process and determine whether the tuning algorithm was able to detect these changes. In this manner, the two virtual building models were used to mimic "real" buildings, while the two models with the altered inputs became the airflow models that needed to be tuned.

*2.2.1.5 Field Testing*

Next, the tuning algorithm was tested and validated on two real buildings since virtual buildings, despite their advantages, will not completely capture the response of actual buildings. The CONTAM models for these real buildings were developed using as-built drawings and available literature on leakage values (e.g., Persily, 1998). Once developed, the CONTAM models were tuned using the algorithm developed from the virtual buildings. Finally, $CO_2$ tracer gas data was

used to evaluate model predictive accuracy. In order to compare the real buildings to the models, the following measurements were made: zone temperatures, diffuser airflow rates, zone pressures, bulk HVAC airflows at the AHU (supply, return, and outside air), weather conditions, airflow directions, and $CO_2$ concentrations. Airflow directions between zones were measured using chemical smoke bottles. The $CO_2$ concentrations for each release were measured only in the AHU return ducts. The $CO_2$ concentrations predicted by the model after each calibration step were compared to the measured concentrations. The first real building was a three story, 41,000 $ft^2$ building with three variable air volume (VAV) AHUs. The second real building was a five story, 74,500 $ft^2$ building with five VAV AHUs. For both real buildings, the AHUs were held to constant flow operation during all testing to simplify the situation and mimic constant air volume conditions.

*2.2.1.6 Algorithm Development*

In order for the percentage of correctly predicted airflow directions to be used as a response metric, it is required that inter-zonal airflow directions are measured. The response variable for the factorial and regression analyses is the inter-zonal airflow directions for a quasi-static state of the system. The basis of the original tuning algorithm was a formal sensitivity analysis where factors most impacting the response variable are identified, measured, and updated within the model with the hopes of improving model accuracy. The originally proposed algorithm included the following steps (Firrantello, 2007):

1. Choose factors or independent variables for simulation (e.g., bulk HVAC airflows, leakage parameters, etc).
2. Perform a $2^k$ full factorial analysis on the selected factors. (Examples of factor levels include: airflows varied to +/- 30%, leakage values set to high and low, etc).
3. Identify significant effects (main and interaction). User experience is needed to identify the line between significant and insignificant factors.
4. Physically measure factors associated with the most significant effects. Measurement feasibility and cost must be considered for this step.
5. Revise the CONTAM model based on these measurements. This now becomes the new "best guess" model.
6. Determine the incorrect flow directions by comparing actual measurements to flow directions predicted by the CONTAM model.
7. Evaluate model quality based on the percentage of correctly predicted airflow directions and the percentage of satisfactory ASTM D5157 metrics. If the model is not satisfactory, repeat the process. User experience is needed to determine the stopping criteria for the algorithm.

This algorithm was then tested on the first virtual building (VB-1). For the first iteration, factors such as bulk HVAC airflows and leakage values were selected for the factorial analysis. Factors for each subsequent iteration were selected based on areas of the building where there were incorrectly predicted airflow directions. This process showed that the most significant model

improvements resulted from the first iteration via bulk HVAC airflow measurements.

After testing the algorithm on VB-1, some improvements were made to the algorithm (Firrantello, 2007):

1. It was heuristically identified that bulk HVAC airflows (supply, return, and outside air) should always be measured.
2. Easy to measure factors (e.g., outside air temperature) should always be measured.
3. Eliminate Step 2 and Step 3 of the algorithm for branch and diffuser flows since they are almost always significant. Instead, replace these steps by identifying incorrectly predicted airflow directions and measuring diffuser and branch flows in areas associated with these incorrect airflow directions.

Based on these improvements, the updated algorithm included the following steps (Firrantello, 2007):

1. Measure all bulk AHU airflows.
2. Identify the airflow paths with incorrectly predicted airflow directions.
3. Identify the lowest unmeasured branch levels associated with incorrectly predicted airflow directions.
4. Measure the associated airflows in these areas.
5. Revise the model based on these measurements. This becomes the new "best guess" model.
6. Evaluate model quality. If unsatisfactory, then repeat starting at Step 2.

7. Perform regression analysis and maximize the difficult or impossible to measure factors (e.g., average interior and exterior leakage, shaft leakage, and terrain constant/coefficient).

From these steps it is clear that the formal sensitivity analysis led to a shift towards a more heuristic approach. The factorial sensitivity analysis was dropped and replaced with heuristically recommended measurements. A regression optimization step was added; however, whether this step improves the calibration is questionable based on the results. This new algorithm was tested on the second virtual building (VB-2). The percentage of correctly predicted airflow directions improved with each iteration. However, the optimization step did not adjust all the variables correctly. The values of the tuned parameters were not close to the actual "design" values. The results of the ASTM D5157 metrics showed that the regression step was actually detrimental to the model. Also, while the percentage of correctly predicted airflow directions influenced the ASTM D5157 metrics, the nature of the influence was found to be inconsistent among the various metrics (i.e., not all ASTM D5157 metrics yielded the same conclusion). Thus, one cannot look at any single metric in isolation if conclusions are to be made. From testing on VB-2 it was recognized that duct branch airflow measurements can be too time consuming. It is quicker and easier to measure diffuser airflows using a flow hood.

*2.2.1.7 Real Building Testing*

The algorithm developed from the virtual building was then tested on the two real buildings. The algorithm steps, specific to the real buildings, are as follows (Firrantello, 2007):

1. Model Development (0 iterations)
    a. Construct the multi-zone model in CONTAM.
    b. Measure all possible interior airflow directions.
    c. Enter interior airflow directions into the model.
2. Initial Measurements (1 iteration)
    a. Measure all bulk HVAC airflows.
    b. Measure weather conditions.
    c. Measure exterior and shaft leakage (optional).
    d. Enter these values into the model.
3. Iterative Measurements (2 to "n" iterations)
    a. Note location of incorrectly predicted airflow directions.
    b. Measure diffuser or branch airflows in areas/rooms associated with incorrectly predicted airflow directions.
    c. Enter measured airflow rates into model. Distribute "remaining" flow to unmeasured diffusers.
4. Automatic Tuning ("n+1" iterations)
    a. Use regression to automatically tune remaining leakage parameters and terrain coefficient. A maximum to the regression equation is

found and the parameters are adjusted to the values recommended by the equation.

In order to evaluate model quality by calculating the ASTM D5157 metrics, $CO_2$ measurements were made in the real buildings. The measured $CO_2$ concentrations are then compared with predicted $CO_2$ concentrations from the model. These comparisons were made after each iteration so as to evaluate the model quality at each step. $CO_2$ releases were conducted in each AHU of the real buildings and concentrations were measured only in the main return duct of each AHU. It was noted that having $CO_2$ concentration measurements in individual rooms rather than just the AHU returns would result in improvements in the calculated ASTM D5157 metrics.

Note that this real building tuning was done only for one set of operating and climatic conditions. These conditions at which the airflow and $CO_2$ measurements were taken are input into the model and are fixed throughout the tuning process. Therefore, this tuning does not consider how the building will behave, in terms of airflows, for other operating conditions.

*2.2.1.8 Tracer Gas ($CO_2$) Measurements*

From this point on, this summary will only focus on the first real building (RB-1) since it will be used in the subsequent analyses of this thesis. For details on the results of the second real building (RB-2), see Firrantello (2007).

Six burst $CO_2$ tracer gas releases (two in each of the three AHUs on two different days) were performed in RB-1. Using fire extinguishers, $CO_2$ was released in an amount necessary to bring the spaces served by the AHU to a

concentration of 1600 PPM (parts per million) above ambient. This is a procedure recommended by NIST. Firrantello (2007) records the actual amounts (lbs) of $CO_2$ released by weighing the fire extinguishers before and after each release. The $CO_2$ was injected on the suction side of the supply air fans in each AHU. Transient $CO_2$ concentrations were measured in the return ducts of each AHU. It was noted that AHU2 has two return mains and thus two measurements (Unit 2 and Unit 3) were taken for AHU2. The ambient $CO_2$ concentrations were also measured for both days of testing and the mean and standard deviation of ambient $CO_2$ concentrations for each day and each AHU release were calculated. Ambient concentrations were typically between 350 and 450 PPM. The first set of releases occurred on 3/09/06 and the second set of releases occurred on 3/10/06. Section 5.1.1 "RB-1 Building $CO_2$ Releases" from Firrantello (2007) provides a detailed explanation of these measured $CO_2$ concentrations for each release including a discussion on possible short circuiting, instrument failure, and outliers that could have caused some of the unusual characteristics in plotted data. Figures 2.1 through 2.6 below are the $CO_2$ decay curves for RB-1 developed by Firrantello (2007).

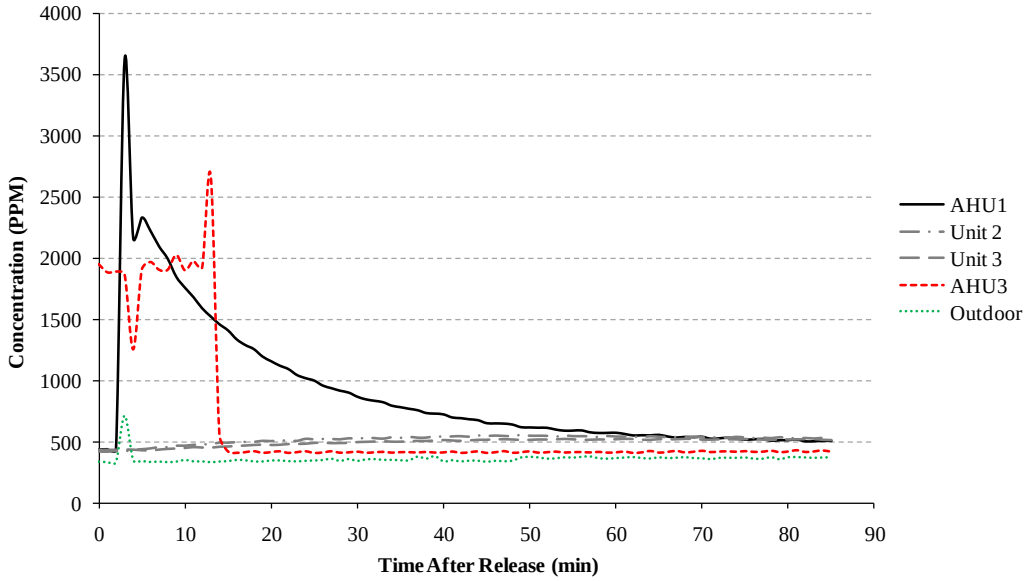


*Figure 2.1*: Time Plots of $CO_2$ Concentration with Release in AHU1 (3/09/06)

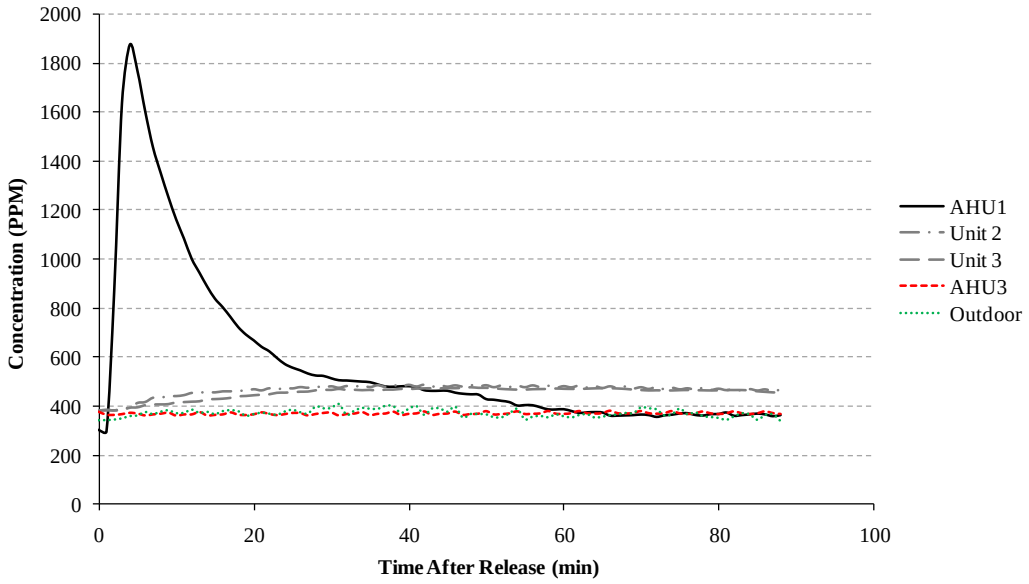


*Figure 2.2*: Time Plots of $CO_2$ Concentration with Release in AHU1 (3/10/06)

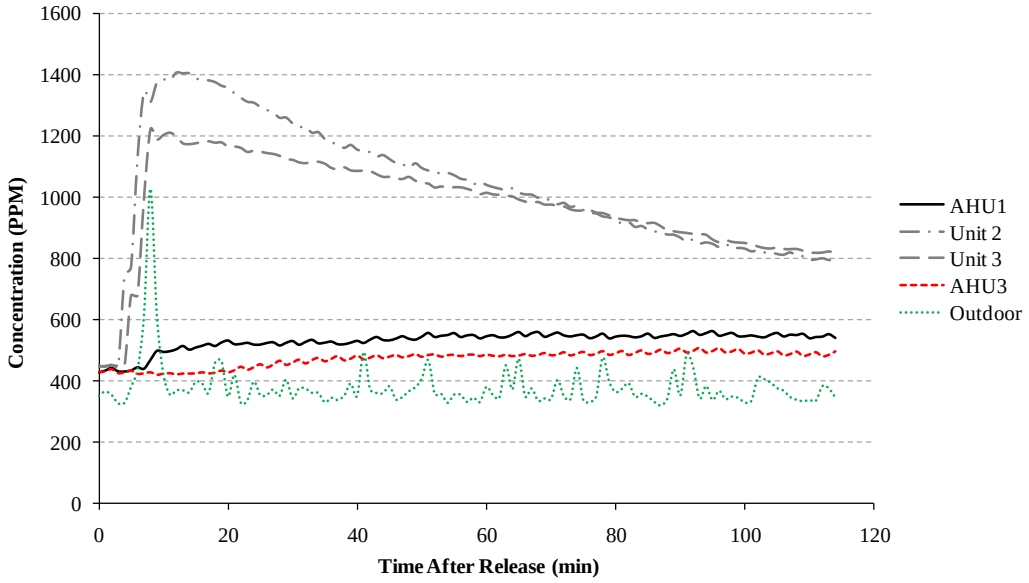


*Figure 2.3*: Time Plots of $CO_2$ Concentration with Release in AHU2 (3/09/06)

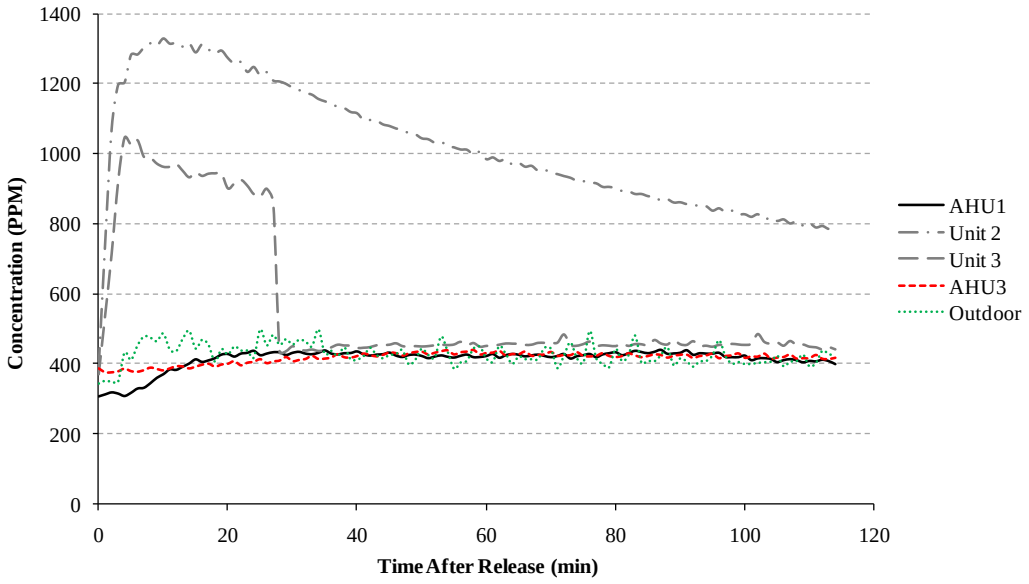


*Figure 2.4*: Time Plots of $CO_2$ Concentration with Release in AHU2 (3/10/06)

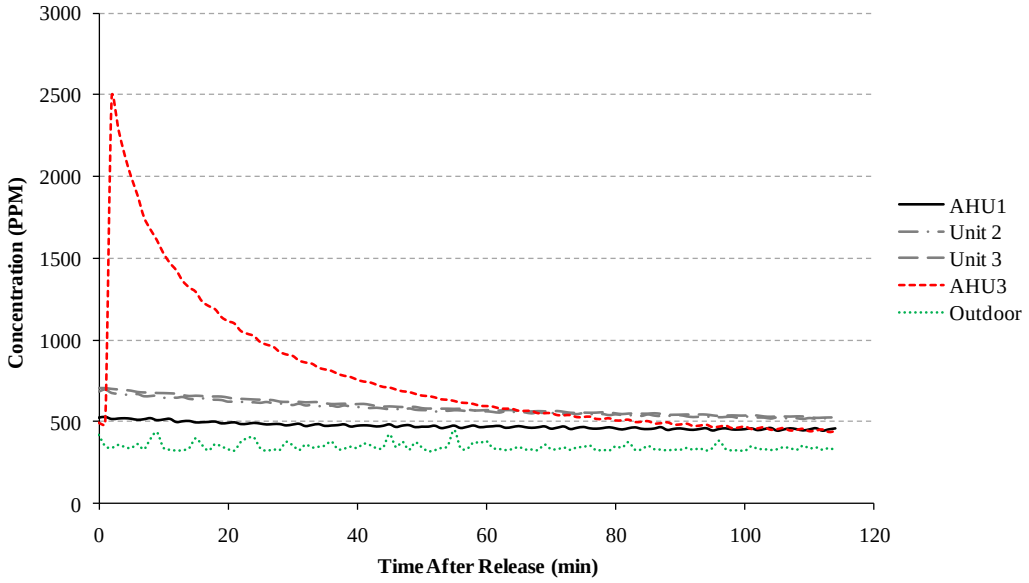


*Figure 2.5*: Time Plots of $CO_2$ Concentration with Release in AHU3 (3/09/06)

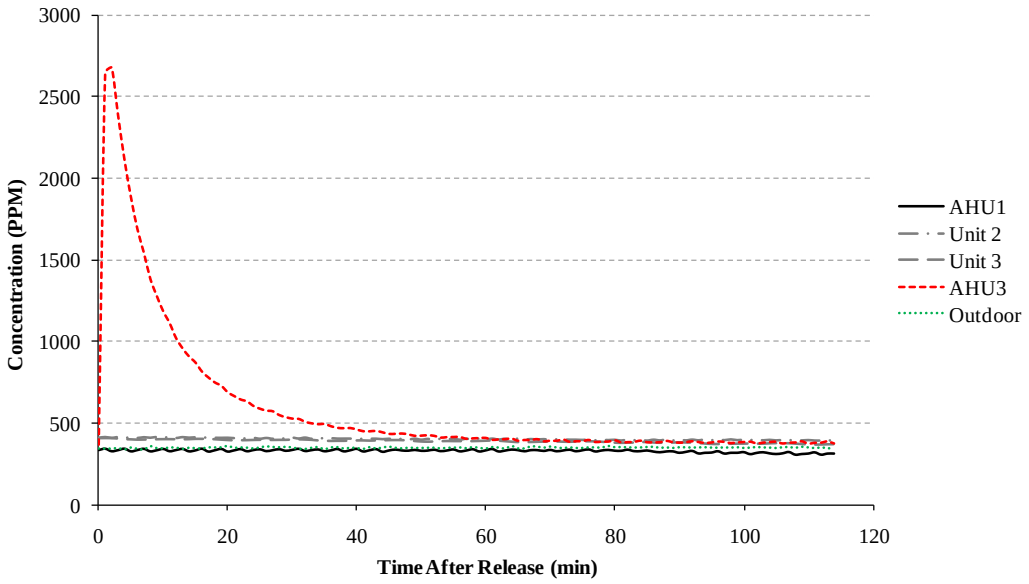


*Figure 2.6*: Time Plots of $CO_2$ Concentration with Release in AHU3 (3/10/06)

For the releases in AHU1, Figures 2.1 and 2.2 clearly reveal uptake and decay curves for the concentration in the zones served by AHU1. Notice also that there are slight increases in concentrations measured in both AHU2 return ducts.

This indicates the presence of some cross contamination between zones served by AHU1 and zones served by AHU2.

For releases in AHU2, Figures 2.3 and 2.4 clearly reveal uptake and decay curves for the concentration in the zones served by AHU2. The dramatic drop in $CO_2$ in Unit 3 on the 3/10/06 release was found to be due to a failure of the $CO_2$ sensor. Both curves also show some slight increase in AHU1 and AHU3 concentrations, indicating some cross contamination between these zones.

For releases in AHU3, Figures 2.5 and 2.6 clearly reveal uptake and decay curves for the concentration in the zones served by AHU3. There is almost no noticeable change in the concentrations for AHU1 and AHU2. The zones served by AHU3 are isolated on the third floor of the building and thus there is little cross contamination between these zones and the zones served by AHU1 and AHU2.

For each of the seven iteration steps in the tuning algorithm, the model predicted $CO_2$ concentrations in each AHU return were compared to actual measured $CO_2$ concentrations shown in the previous graphs. These comparison graphs are shown in Section 5.2.2 "RB-1 Results" from Firrantello (2007). It was noted that the measurement of the bulk HVAC airflows (or Step 1 of the tuning algorithm) resulted in the improvements towards matching the uptake and decay curves predicted by the model to the measured data.

Firrantello (2007) also made some observations with regard to the relationship between model prediction accuracy and the locations of $CO_2$ release and measurement. In general, the models were able to better predict concentrations in

the return duct that is associated with the AHU where the release occurred. For example, following an AHU2 release, the predicted concentration at the AHU2 return would be modeled well, while the predicted concentrations at AHU1 and AHU3 were not as accurate. This is not surprising, as the dominant mode of transport is mechanical system flow, as opposed to the interior leakage equations that dominate the transfer between zones. It is clear that the effect of transport through the air distribution system is fairly well modeled. When the pathway from release point to measurement location is through inter-zonal path, model accuracy is diminished.

*2.2.1.9 Results and Conclusions*

Some of the main conclusions drawn from the development of the algorithm and the subsequent testing on the virtual and real buildings included the following:

1. Analytical sensitivity analysis can be abandoned for heuristic methods. Regression optimization can then be used to handle the influence of factors difficult to measure.
2. The heuristic algorithm, along with some analytical features, was found to be more efficient and practical than a primarily analytical algorithm.
3. Measurement of bulk HVAC airflows in the first iteration produced the most improvement in the percentage of correctly predicted airflow directions and the percentage of satisfactory ASTM D5157 metrics.
4. Conducting more $CO_2$ measurements in the real building will improve model quality in terms of satisfactory ASTM D5157 metrics.

5. ASTM D5157 metrics are not an absolute measure of model quality. In any one situation, it is not guaranteed that all ASTM D5157 metrics yield the same conclusion on whether or not a certain tuning iteration has improved the model accuracy.
6. Regression refinements had little, and sometimes detrimental, effects on the model.
7. For a certain release scenario the model more accurately predicts $CO_2$ concentrations in zones served by the AHU where the release occurred.

*2.2.1.10 Future Work*

Recommendations of future work include establishing applicable boundaries for the algorithm, exploring more complex mechanical systems (e.g. variable air volume systems), and exploring other metrics that can evaluate model accuracy.

### *2.2.2 "Field Verification of a Semi-Empirical Multizone Airflow Modeling Calibration Method" (Sae Kow, 2010)*

*2.2.2.1 Introduction*

The work by Sae Kow (2010) entitled "Field Verification of a Semi-Empirical Multizone Airflow Modeling Calibration Method" is a continuation of the work by Firrantello (2007). The work by Firrantello (2007) led to the creation of a specialized version of CONTAMW called Project Creation Wizard (PCW). The use of the PCW program, which runs on the CONTAMX simulation engine, was used throughout this work by Sae Kow (2010). "The objective of this research is to perform field tests to further investigate PCW modeling and

calibration performance" (Sae Kow, 2010). The research involved the field testing of two buildings on The Pennsylvania State University (PSU) campus.

*2.2.2.2 Testing Plan*

The objectives of the research are described as follows (Sae Kow, 2010):

1. To study the performance of the PCW model tuning method for particular buildings under different operating conditions (e.g., interior doors closed and interior doors opened) against field tests.
2. To investigate the prediction accuracy of a model calibrated for one set of conditions for different conditions (specifically, a calibrated closed door model simulating a condition with some doors opened).
3. To examine the repeatability of PCW calibration by developing and tuning a real building model for the same building calibrated in the previous research by Firrantello (2007).
4. To collect data on the time and effort reduction in model development achieved by PCW as compared to CONTAM.

The "MBNA" building on PSU's campus is the same building as the first real building (RB-1) selected by Firrantello (2007). The subsequent tasks in this thesis use the MBNA model and the field measurement data collected by both Sae Kow (2010) and Firrantello (2007). Therefore, this summary will only discuss the sections of the work by Sae Kow (2010) that involve the MBNA building and not the second building ("Rackley" building). The MBNA building is a 44,000 $ft^2$ building with three floors and three variable air volume air handling units. The MBNA building is described further in Section 5.1.

The MBNA building was tested under two conditions, "all interior doors closed" and "some interior doors opened." Similar to the procedure used by Firrantello (2007), the variable air volume AHUs in the building were held at steady state conditions (i.e., fixed damper positions and constant air volume operation). Sections 3.4 and 3.5 from Sae Kow (2010) discuss the measured variables and the measurement equipment used, respectively. A weather station recorded outside air temperature, wind velocity, and wind direction during testing. Flow sensors were used to measure bulk AHU airflows as well as branch duct airflows. Smoke bottles were used to measure the airflow direction through each doorway. Flow hoods were used to measure diffuser airflows. Tracer gas ($CO_2$) releases were conducted following the same NIST recommended procedure used by Firrantello (2007). Infrared absorption gas analyzing equipment was used to measure $CO_2$ concentrations over time in specific locations.

*2.2.2.3 Data Analysis*

Two PCW models of the MBNA building were developed (one for each test condition) and tuned using the bulk AHU and diffuser airflow measurements according to the final version of the tuning algorithm proposed by Firrantello (2007). After each tuning step, the models were evaluated using the following two metrics: percentage of correctly predicted airflow directions and percentage of satisfactory ASTM D5157 metrics. Also, predicted versus measured $CO_2$ concentrations over time were plotted for each tuning step. Visual comparison of these tracer gas concentration curves allows for a simple method of evaluating

model adequacy. Sae Kow (2010) describes how the two test conditions were used in the project:

> "One objective of this research was to investigate the suitability of the model calibrated based on one test condition for predicting another test condition. Therefore, the simulated $CO_2$ concentration for the refined closed door model with added doors opened was compared to the $CO_2$ concentration calculated from the opened door model which was calibrated directly with the data obtained from the door opened test condition. Also, the closed door model with added doors opened was compared against the actual building behavior during the door opened conditions. Compared to the measured data from the test buildings, the percentage of correct airflow directions and satisfactory ASTM D5157 metrics were calculated" (Sae Kow, 2010).

Sae Kow also tested the PCW calibration repeatability by comparing his calibration results to those of Firrantello (2007). It was noted that Sae Kow's work was conducted under conditions different than those of Firrantello, e.g. different HVAC operating conditions. "To examine the repeatability, the final percentages of correct airflow directions and the improvement trend of the percentages of correct airflow directions from both models were compared to each other" (Sae Kow, 2010). The modeling efficiency of PCW was also evaluated by comparing the modeling time required as compared to the original CONTAM interface.

*2.2.2.4 Results*

AHU operating conditions and measured climatic conditions for the MBNA building field testing are documented in Section 4.2.1 and Section 4.2.2 from Sae Kow (2010) for the "all doors closed" test and for the "some doors opened" test, respectively. The measurement of AHU bulk airflows were also provided along with the uncertainty in their values. The supply and return AHU flows were measured using fan inlet sensors. The outside air flow rates were measured differently in each AHU. For AHU1 a duct traverse was used to measure the outside airflow rate. For AHU2 a duct mounted sensor was used. For AHU3 the outside air fraction method using temperatures to calculate the air flow rate was used. This calculation was necessary because it was not feasible to install sensors in AHU3. Due to a small difference between the return air temperature and the outside air temperature, the air temperature fraction method resulted in high uncertainty for the AHU3 outside airflow rate (approximately 70%). Results of the smoke bottle airflow direction measurements and the flow hood diffuser measurements are provided in the appendices of Sae Kow (2010).

2.2.2.4.1 "All Doors Closed" Tracer Gas Release Results

For the "all doors closed" test condition, a total of six $CO_2$ releases were conducted in the MBNA building. Two releases were performed in each AHU on two separate days. The releases are labeled MBNA-C1 through MBNA-C6. Section 4.2.1.2 "$CO_2$ Tracer Gas Release Test Results" from Sae Kow (2010) provides details on the actual amount (in lbs) of $CO_2$ used in each release. For these releases, the transient $CO_2$ concentrations were measured at five

measurement locations: the main return duct of each AHU, a room on the second floor, and a room on the third floor. Floor plans were provided showing the exact location of these rooms. Three AHUs, two releases per AHU, and five measurement locations resulted in a total of 30 sets of $CO_2$ data collected for this test condition. Sae Kow (2010) also discusses a few plots of these $CO_2$ concentration decay curves. One example plot of a release in AHU2 shows increases in $CO_2$ concentrations in both the AHU2 return as well as the AHU1 return. This indicates some cross contamination between the AHU2 and AHU1 zones. A sharp peak and sharp decay in the second floor room measurement location were attributed to the lack of "well-mixed" conditions and the higher air change rate, respectively. Another example plot is that of a release in AHU3 which shows that only $CO_2$ concentration increases in the AHU3 return and the third floor room measurement location. This result indicates that there is no cross contamination between the AHU3 zones and the rest of the building. A plot of an AHU1 release showed similar results of no cross contamination. The overall conclusions for the "all doors closed" condition were that an AHU1 release only affects zone 1, an AHU2 release affects all zones, and an AHU3 release affects only zone 3 (i.e., the third floor).

Figures 2.7 through 2.12 show the transient $CO_2$ concentration curves for the MBNA-C1 through MBNA-C6 releases produced by Sae Kow (2010). These graphs only show three of the five measurement locations, i.e. the main return ducts at each AHU. They are similar to the $CO_2$ concentrations decay curves measured by Firrantello (2007) shown previously.

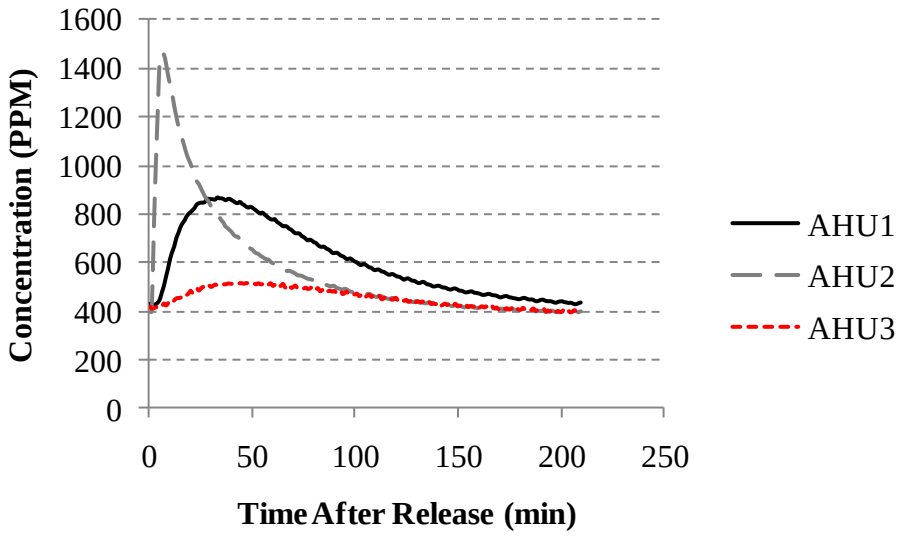


*Figure 2.7*: Time Plots of $CO_2$ Concentration with Release in AHU2 (MBNA-C1)

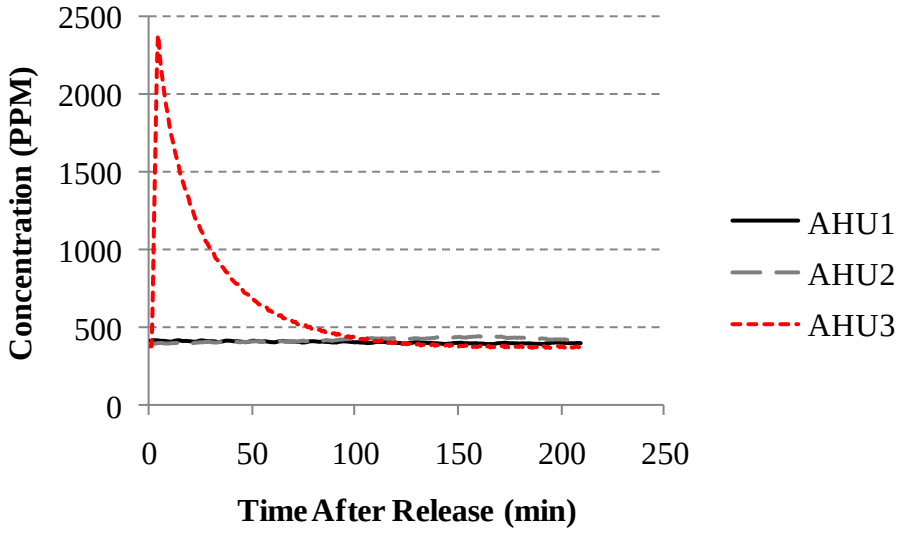


*Figure 2.8*: Time Plots of $CO_2$ Concentration with Release in AHU3 (MBNA-C2)

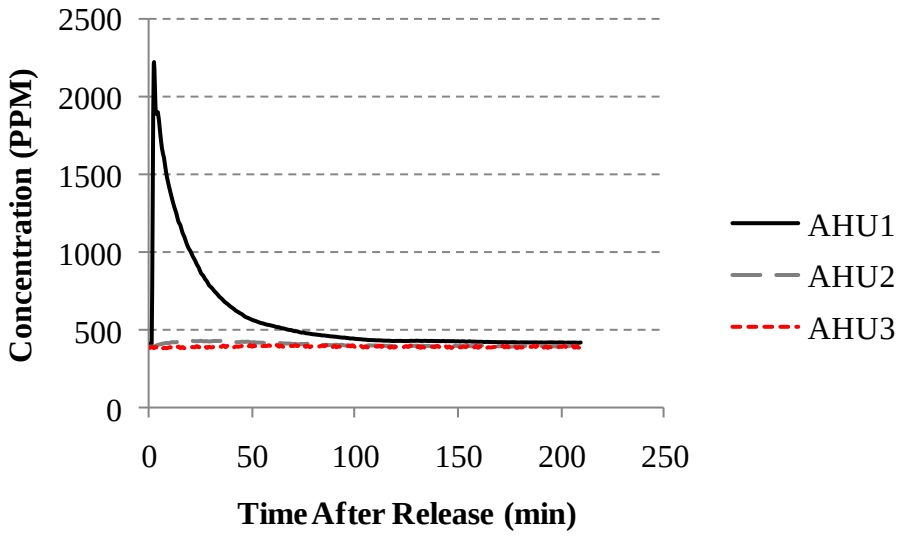


*Figure 2.9*: Time Plots of $CO_2$ Concentration with Release in AHU1 (MBNA-C3)

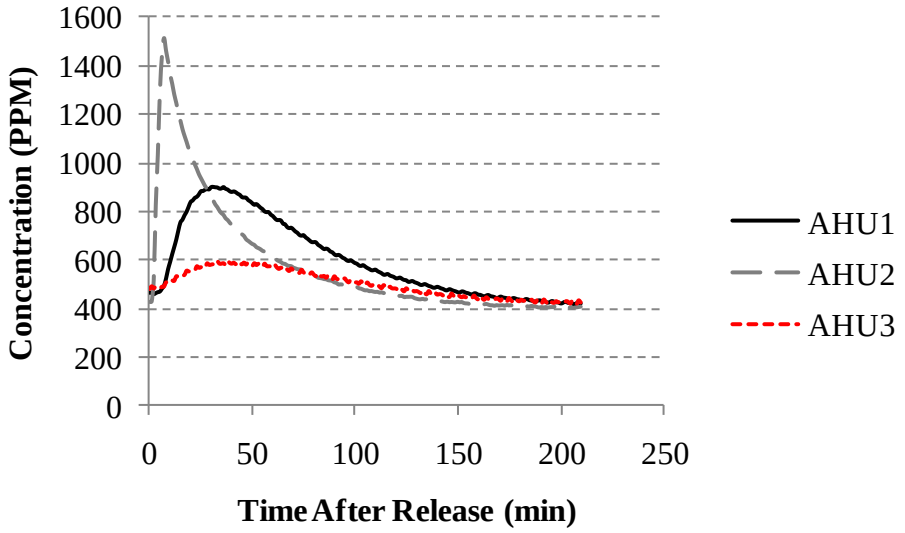


*Figure 2.10*: Time Plots of $CO_2$ Concentration with Release in AHU2 (MBNA-C4)

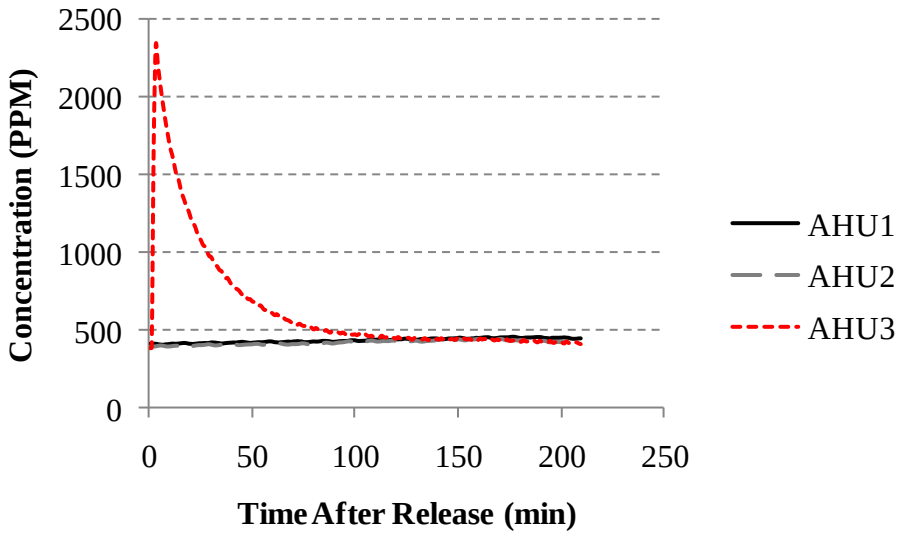


*Figure 2.11*: Time Plots of $CO_2$ Concentration with Release in AHU3 (MBNA-C5)

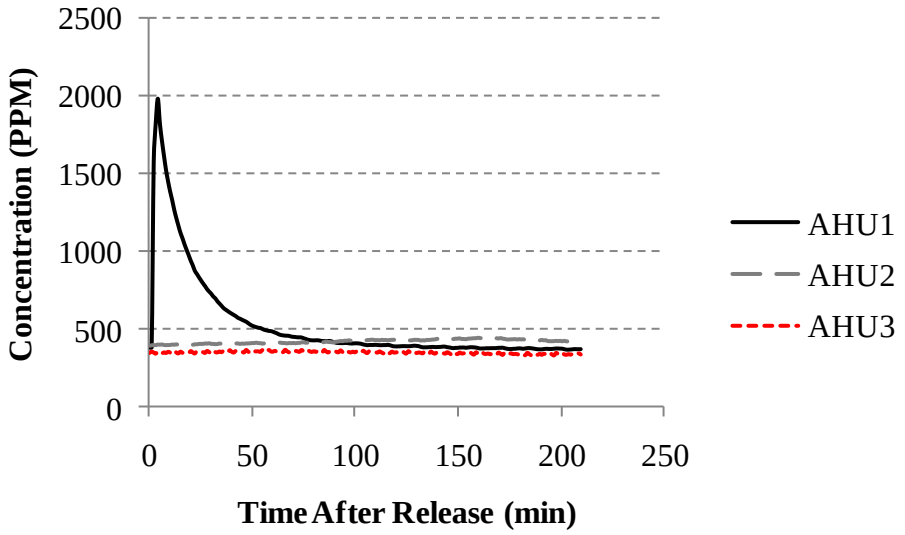


*Figure 2.12*: Time Plots of $CO_2$ Concentration with Release in AHU1 (MBNA-C6)

2.2.2.4.2 “All Doors Closed” Tuning Results

Next, the PCW model for the MBNA building was subjected to the tuning algorithm developed by Firrantello (2007). Specifically, the algorithm for this test condition included the following steps (Sae Kow, 2010):

0. Develop the multi-zone model based on design documents.
1. Adjust total supply, return, and outside air flow rates of each air handling unit based on measurements.
2. Input 181 measured diffuser airflows associated with incorrectly predicted airflow directions.
3. Input 14 measured diffuser airflows associated with incorrectly predicted airflow directions.
4. Adjust exterior leakage, interior leakage, shaft leakage, terrain factors based on PCW automatic tuning (regression analysis).

At each tuning step, predicted $CO_2$ concentration decay curves were plotted and compared to actual measured concentrations at each measurement location. Of the 30 total sets of $CO_2$ data, 14 of the graphs are flat i.e., no time-dependent behavior. These correspond to the measurement locations that were not affected by the particular release. For the remaining 16 graphs, the tuning steps that actually resulted in a visible difference in the predicted $CO_2$ concentration decay curves were documented. For the majority of the data sets, only iteration 1 (measurement of bulk AHU flows) showed a noticeable difference in the predicted $CO_2$ concentration curve. The number of satisfactory ASTM D5157 metrics was also documented for each tuning step at each measurement location.

These metrics help to indicate improvements even if there is no visible difference. Sae Kow (2010) also provided some sample graphs showing the measured $CO_2$ concentration curves for a certain release and measurement location as compared to the model predicted $CO_2$ concentration curves for each tuning iteration. These graphs show that some tuning steps helped improve tracer gas prediction accuracy while other tuning steps were actually detrimental to the model. System level tracer gas concentration curves for the AHU main return measurement locations did not show any visible improvement as measured diffuser flows were added to the model in the middle tuning steps. However, at zone level concentration curves, diffuser measurements did affect the model prediction of $CO_2$ concentrations in particular rooms.

Some modeling errors were found which contributed to model disagreement with measured values. Two examples of such errors include underestimating HVAC system volume which affected the peak concentrations predicted at room measurement locations and the incorrect measurement of outside airflow rate at AHU3 which affected the decay rate. Underestimating system volume resulted in higher peak concentrations. Overestimating the outside air percentage resulted in faster concentration decay rates.

After completing the tuning algorithm, the model was evaluated using the percentage of correctly predicted airflow directions and the percentage of satisfactory ASTM D5157 metrics. “The model improved from 46% to 67% as indicated by correct airflow direction. The largest improvement was from tuning the model with total AHU airflows (iteration 1). There was no model

improvement from PCW automatic tuning" (Sae Kow, 2010). The PCW automatic tuning is the regression optimization step described in Section 1.3.4 and mentioned above as part of the calibration procedure developed by Firrantello (2007). In terms of the ASTM D5157 metrics, the model improved from 51% to 53% satisfactory metrics from iteration 0 to iteration 1. However, the next two iterations where diffuser flows were entered, the model worsened by 2%. The PCW automatic tuning also resulted in no improvement. Closer examination of the ASTM D5157 metrics showed that the overall model improves for the zones served by the AHU where the release occurred while the model does not improve for zones not served by the AHU where the release occurred.

2.2.2.4.3 "Some Doors Opened" Tracer Gas Release Results

Similar to the "all doors closed" test conditions, the "some doors opened" condition involved six tracer gas releases labeled MBNA-O1 through MBNA-O6. Two releases were performed in each AHU and the same five measurement locations were used. Identical to the "all doors closed" test condition the results show that an AHU1 release only affects zone 1, an AHU2 release affects all zones, and an AHU3 release affects only zone 3 (i.e., the third floor).

2.2.2.4.4 "Some Doors Opened" Tuning Results

The specific tuning steps performed for this test condition include (Sae Kow, 2010):

0. Add opened doors to the original MBNA PCW model.
1. Adjust total supply, return and outside air flow rates of each air handling unit based on measurements.

2. Input 129 measured diffuser airflows associated with incorrectly predicted airflow directions.
3. Input 32 measured diffuser airflows associated with incorrectly predicted airflow directions.
4. Input 6 measured diffuser airflows associated with incorrectly predicted airflow directions.
5. Adjust exterior leakage, interior leakage, shaft leakage, terrain factors based on PCW automatic tuning.

Again, the tuning iterations which yielded noticeable differences in the predicted $CO_2$ concentrations for each release were documented. For the majority of the releases only iteration 1 and 2 showed noticeable differences. More example plots of predicted versus measured $CO_2$ concentrations for various releases were provided. Some of the same modeling errors from the "all doors closed" condition (incorrect system volume and poor outside air flow rate measurement) were documented again for this test condition. It was noted that model tuning affected the zone level $CO_2$ concentration decay curves more so than the AHU or system level $CO_2$ concentration decay curves.

Once the tuning was complete, the model was evaluated using the percentage of correctly predicted airflow directions and the percentage of satisfactory ASTM D5157 metrics. In terms of airflow directions, the model improved from 52% to 72%. Iteration 1 again showed the largest improvement. The PCW automatic tuning step actually lowered model accuracy by 1%. In terms of satisfactory ASTM D5157 metrics, the first iteration showed a 1% decrease,

the second iteration showed a 1% increase, and the remaining iterations showed no change. Again, the ASTM D5157 metrics were broken down by iteration and by measurement location.

*2.2.2.5 Discussion*

2.2.2.5.1 Model Development Time

Sae Kow (2010) found that model development time was significantly shortened when PCW was used as compared to the original CONTAM interface. Some simplifying assumptions and default settings in PCW, combined with PCW's series of menus, were identified as reasons for this decrease in modeling time. However, PCW sacrifices some accuracy with these assumptions and does not allow for some of the detailed modeling features of CONTAM (e.g., ductwork and controls modeling).

2.2.2.5.2 Calibration Repeatability

It was noted earlier that PCW calibration repeatability was to be tested by comparing the tuned MBNA model to the tuned MBNA model developed by Firrantello (2007). "Since the models were not calibrated based on exactly the same test conditions (different ambient conditions and HVAC operating conditions), the tracer gas results simulated from both models cannot be compared to indicate the calibration repeatability" (Sae Kow, 2010). Section 5.2 "Calibration Repeatability" from Sae Kow (2010) provides a comparison of these two MBNA models based on the percentage of correctly predicted airflow directions. Both models show the same trend in the increase in this percentage as the iterations proceed with the largest improvement coming from the first

iteration. Also the last step in both tuning procedures (i.e., regression optimization and PCW automatic tuning) did not improve the model as indicated by the percentage of correctly predicted airflow directions.

2.2.2.5.3 Applicability of Calibrated Models to Other Conditions

Another objective was to investigate how a model calibrated under one condition would predict indoor contaminant dynamics under another condition. The conditions used by Sae Kow (2010) were open and closed doors. Specifically, the "all doors closed" model was used to simulate the "some doors open" condition. "For comparison purposes, both closed door model with added opened doors and opened door model were set to the same conditions. For example the ambient conditions (outdoor temperature, wind speed and wind direction), HVAC operating conditions (total airflow and the percentage of outside air) and door opened locations of the opened door test condition were followed" (Sae Kow, 2010). The calibrated model from the "all doors closed" test condition was altered so that some of the doors were open in a consistent manner to that of the "some doors open" model and so that both models had the same conditions. Then, the "all doors closed with some added doors open" model's prediction results were compared to the "some doors open" results. ASTM D5157 metrics were used to evaluate the prediction agreement by assuming that the "some doors open" prediction values were "measured" values. Also, the percentage of correctly predicted airflow directions for both models was compared.

Plots of $CO_2$ concentration curves predicted by the two models for different measurement locations showed fairly close agreement between the two

models. Agreement was closer at the AHU or system level than at the zone level. Calculated ASTM D5157 metrics also showed fairly close agreement while the percentage of correctly predicted airflow directions did not. The “all doors closed with some added doors open” had 47% satisfactory ASTM D5157 metrics whereas the “some doors opened” model had 52% satisfactory ASTM D5157 metrics. The “all doors closed with some added doors open” had 57% correct airflow directions whereas the “some doors opened” model had 80% correct airflow directions.

*2.2.2.6 Conclusions*

The final sections discuss the significance of how measurement uncertainty can affect model calibration and the significance of one specific error found during model tuning (i.e., underestimating system volume). Both were found to be fairly significant. The main conclusions drawn from this research included the following (Sae Kow, 2010):

1. PCW has the built-in capability to improve model accuracy as measured by the percentage of correctly predicted airflow directions.
2. Measurement of bulk HVAC flows (main supply, return, and outside air flow rates) yield the best improvement in correctly predicted airflow directions.
3. “In terms of ASTM D5157 metrics, the model calibration results, which were evaluated at the AHU level, indicated that the improvement of model quality indicated by the percentage of satisfactory ASTM D5157 metrics was not consistent to the improvement of model quality indicated by the

percentage of correct airflow directions. However, model tuning did change the simulated transient concentration profile at the zone level. It is possible that the improvement of correct airflow direction would be paralleled to the improvement of satisfactory ASTM metrics if more measurement points were at the zone level" (Sae Kow, 2010).

4. The automatic tuning (regression analysis) feature of PCW did not always improve model quality. It was found that it either resulted in no change or it was a detriment to the model.
5. PCW can save approximately 30-35% in model development time as compared to CONTAM.
6. Measurement accuracy and uncertainty can have a significant impact on model calibration.
7. Calculation of outside air flow rate based on temperatures was not suitable since the small difference between outside air and return air temperature yielded large errors and uncertainties.
8. It is important to accurately gather building information. In this case, an underestimation of HVAC distribution system volume resulted in significant errors in the peak concentrations predicted by the model.
9. Calibration repeatability showed similar improvement trends in percentage of correctly predicted airflow directions throughout the tuning process between two separate models of the same building.

10. The calibrated model for one condition predicted fairly well when subjected to a different condition. AHU level predictions were more accurate than zone level predictions.

*2.2.2.7 Subsequent Field Testing on MBNA Building*

In addition to the testing procedures described above, Sae Kow (2010) performed two subsequent tracer gas releases in the MBNA building. The intent was to obtain tracer gas measurements in more room level locations. It was hypothesized that these room level measurements would help to increase model adequacy as measured by the ASTM D5157 metrics. Both releases were conducted on the third floor, i.e. in AHU3, using the same procedures as the previous releases. In response to previous conclusions, the number of zone level measurement locations was increased during these releases. $CO_2$ concentrations were measured at seven locations on the third floor including: AHU3 main return duct, office room 322, office room 327, the computer room, the resource room, the conference room, and the intern room. Refer to Sae Kow (2010) for a floor plan showing the location of these $CO_2$ sensors. Since the results of previous releases showed that AHU3 releases impacted the third floor only, no sensors were placed on the first or second floors. Figure 2.13 and Figure 2.14 show the measured $CO_2$ data from these two releases.

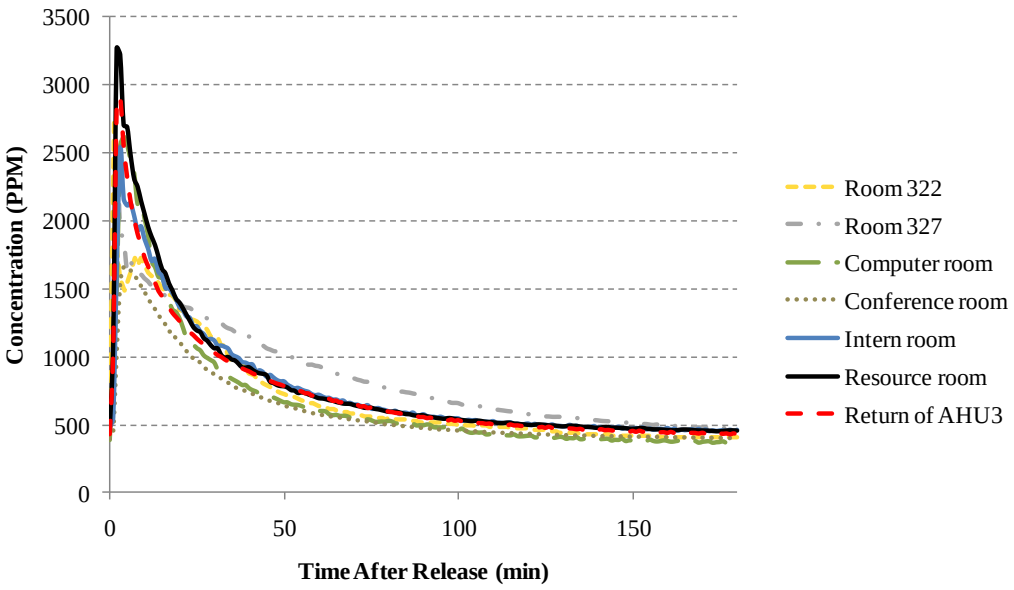


*Figure 2.13*: Results of Subsequent Testing - AHU3 Release 1

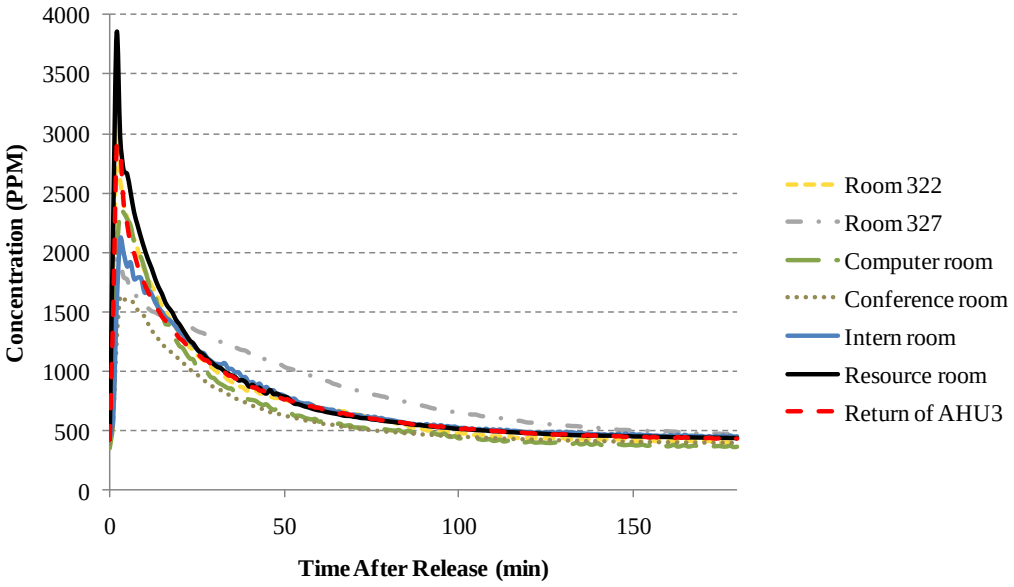


*Figure 2.14*: Results of Subsequent Testing - AHU3 Release 2

Sae Kow (2010) was able to reach some additional conclusions from these subsequent tests by comparing measured and predicted $CO_2$ concentration curves in the various rooms. First, some of the discrepancies between measured and

predicted curves were due to the assumption of "well-mixed" zones. Specifically, some of the measured $CO_2$ concentrations may have high peaks due to the fact that the room was not well-mixed and the sensor was placed in a location that had high concentrations. Deviations from the well-mixed assumption are very likely to occur in many real buildings. It was also identified that system volume has a significant impact on peak concentrations predicted by the model. Thus, it is important to get an accurate estimate of the volume of ductwork from HVAC design drawings or site surveys. Finally, it was noted that the outside air measurement in for AHU3 was conducted using the air temperature fraction method. Due to the fact that the temperature difference between the outside air and the return air was quite small, the calculated outside air percentage had a large uncertainty associate with it. Uncertainty in the outside air fraction can also have significant impacts on the prediction accuracy of the multi-zone model.

## CHAPTER 3: PROPOSED GENERAL CALIBRATION METHODOLOGY

Calibrating a multi-zone airflow model such as CONTAM or PCW with numerous parameters specified by the user is a highly over-parameterized or underdetermined problem. When faced with such problems, the traditional approach is to reduce the order of the model and then identify relevant model parameters of the reduced model. For this research, the general calibration approach is to take an approximately tuned multi-zone model, use it to identify macro-zones, i.e. groups of rooms which have similar airflow dynamics and tracer gas behavior, and then estimate aggregate flow parameters of the macro-zone flow elements. The basis of this methodology is to explicitly use $CO_2$ tracer gas data during the calibration process. The proposed calibration methodology involves the following steps:

1. Preliminary Model Tuning: To develop a "somewhat" realistic multi-zone model. This step is necessary for steps 2 and 3 to provide meaningful insights about the building.
    a. One approach is to use PCW to initially tune the model following the approach developed by Firrantello (2007) discussed in Section 2.2.1 hereby referred to as the "PSU tuning algorithm". The PSU tuning algorithm relies on measuring airflows in certain key locations (ducts and diffusers) and then uses inter-zonal airflow directions and ASTM D5157 metrics calculated with single point measurements to evaluate the model. The use of airflow directions as a metric may not be the best approach for to evaluating a

calibrated model whose subsequent purpose is to predict occupant exposure under extraordinary events. However, they appear to be an adequate preliminary measure of model adequacy. Following the PSU tuning algorithm implies that all room volumes, HVAC airflow rates, outside air percentages, etc. have been accurately measured.

b. Alternatively, one could tune the model in any fashion that somewhat correctly captures the overall dynamic behavior of the building (i.e., $CO_2$ concentration behavior predicted in the main AHU return matches measured values assuming such a test has been conducted).

2. Airflow-Based Sensitivity Analysis: To evaluate whether the airflow dynamics are climate or HVAC system dominated and also to identify the significant or important drivers of the airflow dynamics. (Refer to Appendix B for a discussion on "design of experiments" or experimental design methodologies including the sensitivity analyses or factorial analyses mentioned throughout this research.)

   a. Select possible influential drivers of the airflow system. These will most likely include ambient air temperature, wind direction, wind velocity, building leakage severity, and HVAC system airflow rates.

   b. Use a full factorial experimental design to set up simulations to run (i.e., a $2^k$ design if the effects have a linear relationship with the

factor levels, or a $3^k$ design if the effects have a non-linear relationship with the factor levels).

c. Perform a semi-quantitative airflow-based sensitivity analysis based on the magnitude and direction of airflow in each airflow path in each room of the building. Due to the lack of a robust response variable and the deterministic nature of multi-zone models, which limits the ability to perform statistical significance tests, a formal sensitivity analysis where main and interaction effects are calculated is not proposed here. Rather it is proposed that graphical methods be utilized to analyze the results.

    i. Scatter plots help to illuminate changes in airflow behavior under different stimuli and to distinguish whether the building is HVAC dominated or climate dominated.

    ii. If climate dominated (which most low-rise commercial buildings typically are not), future research is needed since this was determined to be outside the scope of this research.

3. Identify Macro-Zones for Model Reduction: It is improbable that an airflow-based sensitivity analysis alone will reveal enough information about building airflow dynamics to allow for sufficient macro-zone formation. Therefore, group rooms into macro-zones based on the following considerations:

    a. HVAC Zoning (e.g., rooms supplied by the same terminal unit or AHU, ducted vs. plenum returns, etc.)

b. Building Geometry: It would be ideal if rooms with similar airflow dynamics were adjacent to one another.

c. Tracer Gas-Based Sensitivity Analysis ($CO_2$ Concentration Curves and Decay Coefficients): To determine how significant the influential system drivers are in determining macro-zones and to identify rooms with similar dynamic responses to the tracer gas releases. The overall goal is to group rooms into macro-zones in a manner such that the macro-zones do not change under varying climate and operating conditions. Instead of using individual room airflows for this purpose, $CO_2$ concentration curves are used for identifying such macro-zones.

    i. Plot $CO_2$ concentration curves in each room for all rooms served by a given AHU. Try to visually identify macro-zones based on these plots. (If available, one could utilize software packages which feature statistical classification methods to identify macro-zones from the $CO_2$ data generated). Simulations can be performed for different release scenarios, different air handling units, different weather conditions, etc. A factorial analysis can again be used during this process.

    ii. The above approach could be daunting if a large number of rooms are to be considered simultaneously. An alternative approach is to use natural log data transformation, linearize

the exponential decay curves for each room and use linear regression to identify the decay coefficient for each room. Then, macro-zones could be identified based on groups of rooms with similar decay coefficients under various conditions.

iii. Along with decay coefficients, peak concentrations must also be considered. Due to varying supply air flow rates, rooms will reach different peak contaminant concentrations. Isolate rooms which have similar decay coefficients and peak concentrations under varying climatic and operating conditions. Form macro-zones based on these observations.

4. Model Calibration:

   a. Measure transient $CO_2$ tracer gas concentrations in at least one room for each of the macro-zones identified under a central AHU release scenario. This procedure is limited to releases in the AHU.

   b. Estimate new aggregate flow parameters (e.g., the coefficient and exponent of the power law relation), one set for exterior airflow paths and one set for interior airflow paths, for each of the identified macro-zones by adopting one of the following approaches:

      i. Set up a factorial sensitivity analysis to determine the effects of varying airflow parameters (coefficients and

exponents) for all airflow paths. The response for this analysis will be the match between predicted and measured $CO_2$ concentration curves for each macro-zone. The quality of the match between the two curves can be evaluated visually or by some statistical measure, i.e. root mean square error. The factorial analysis will tune flow parameters in each macro-zone in an attempt to yield predicted $CO_2$ concentrations that match the measured values. This is the approach adopted in this research.

ii. Set up a compartmental model for the macro-zones identified and solve the tracer gas mass balance equations, using actual $CO_2$ data, for aggregate flow parameters. Due to the definition of macro-zones, i.e. rooms with similar dynamic behavior, assume that all rooms in that particular macro-zone will have the same numerical values for the flow parameters.

iii. Rather than change flow parameters, one could use tracer gas mass balance equations and measured $CO_2$ data to calculate HVAC flows, i.e. air changes, supply flows, return flows, etc. Appropriately distribute these calculated flows into the PCW model. Since PCW does not explicitly model ductwork, these mass balance calculations will

account for contaminant loss through duct leakage and other practical issues related to a ductwork system.

c. Update model with new flow parameters.

d. If significant differences between predicted and measured concentrations still remain, investigate possible measurement errors and uncertainties for factors impacting room air changes, such as HVAC airflows, room volumes, and outside air percentages.

5. Evaluate Model Adequacy: Evaluate the adequacy of the updated model based on some metric. Since a robust metric for airflow model "goodness-of-fit" has yet to be determined, and since previous research has questioned the validity and relevance of any one metric, the evaluation of the model can be based on several metrics such as:

   a. Percentage of correctly predicted airflow directions. This metric is arguable since the magnitude of the flow also influences indoor air contaminant concentrations. Also, the number of flow directions that can be practically measured is limited.

   b. ASTM Standard D5157 statistical metrics or some modified form thereof.

   c. Predicted vs. measured $CO_2$ concentration curves during portions of the decay when the contamination is high (i.e., the first hour after a release).

# CHAPTER 4: APPLICATION AND REFINEMENT OF PROPOSED CALIBRATION METHODOLOGY USING A SYNTHETIC BUILDING

## 4.1 Introduction

### *4.1.1 Introduction to Synthetic Building*

The proposed calibration methodology consists of five steps. The first step is to begin with a "somewhat" realistic or partially calibrated multi-zone model of a building so that the subsequent steps yield meaningful results. This preliminary model tuning is taken to be akin to the PSU tuning algorithm described in several papers (Firrantello, 2007; Firrantello et al., 2005; Firrantello et al., 2007). The second and third steps involve model sensitivity analysis and identifying macro-zones for model reduction, respectively. A macro-zone is a group of rooms which can be combined into one zone for the purposes of predicting or studying dynamic airflow and contaminant behavior under different types of stimuli. The proposed approach to identifying such aggregation is done as per three primary pragmatic criteria: (i) the similarity of room airflow dynamics and tracer gas behavior, (ii) geometric relationships between rooms, and (iii) HVAC zoning. Once this is done, the next step calls for estimating aggregate flow parameters of the macro-zone flow elements so as to update the model. Finally, the updated model is to be evaluated based on some metric for model adequacy.

The first three steps of the methodology were developed and refined using a synthetic, or virtual, building (i.e., one whose dynamic behavior can be entirely simulated on a computer and does not need any real building data). This is similar

to the procedure used by Firrantello (2007) for the development of the PSU tuning algorithm. To assist with developing the proposed methodology, the first virtual building (VB-1) developed by Firrantello (2007) was utilized. Figure 4.1 is a diagram of the synthetic building from the PCW interface and Table 4.1 assembles pertinent building details. This single story building has 29 modeled zones (25 rooms, and 4 corridors) and three air handling units (north perimeter, south perimeter, and core). The data in Table 4.1 was obtained from the PCW file for VB-1 provided by Firrantello (2007). Thus, the proposed methodology begins with a partially tuned PCW model with a network node or zone for each and every room of the building. Note however, that tuning a model of a synthetic building is quite arbitrary. This is because the creation of a model that corresponds to a synthetic building is done by arbitrarily perturbing model parameters. Therefore, the calibration step is really meaningful only when developing a model for a real building. If the model had been tuned with respect to a real building, it would include measured flow directions using smoke bottles, measured diffuser airflow rates, and measured main duct and sub-branch duct HVAC airflow rates. The advantage of using a synthetic building for early development of a calibration methodology, however, is its flexibility and lack of measurement uncertainty. Also, a synthetic building would not suffer from model deficiencies in representing real building details.

For evaluating model adequacy, Firrantello (2007) and Sae Kow (2010) used the percentage of correctly predicted airflow directions as a metric. The results of both of those research papers found that even after implementing the

PSU tuning algorithm, the model was still incorrectly predicting some airflow directions. Therefore, further model calibration is necessary and advisable. The objective of this research was to develop a methodology that utilizes tracer gas ($CO_2$) data in an explicit manner to further calibrate the model and thereby improve prediction accuracy. As discussed by Firrantello (2007) and Sae Kow (2010), the percentage of correctly predicted airflow directions and the ASTM D5157 metrics both have inherent limitations. A subsequent objective, which is reserved for future work, is to propose and develop a more robust metric for evaluating model adequacy.

The development of the proposed calibration methodology began by pointing out that the PSU tuning algorithm (Firrantello, 2007) considered only one set of operating conditions. In other words, it did not account for varying ambient temperatures, wind speeds, assumed leakage parameters, wind direction, or HVAC airflow rates. Thus, a detailed calibrated model for only one set of typical conditions may provide a false sense of accuracy and may not be accurate when extrapolated to different conditions. Therefore, the first intent of this methodology was to look at how sensitive the simple synthetic building PCW model was to varying operating conditions. It must be pointed out that the methodology used by Firrantello (2007) and Sae Kow (2010) involved using constant airflow path leakage parameter assumptions obtained from literature (Persily, 1998).

Next, it was hypothesized that model reduction or reducing the complexity of the model by grouping rooms into macro-zones is likely to yield a more

aggregated model that may provide greater accuracy under different climatic conditions, operating conditions, and leakage parameter assumptions. With macro-zones identified, tracer gas ($CO_2$) concentration decay data can be used to find aggregate leakage parameters for the airflow paths of each macro-zone which are more representative of varying conditions.

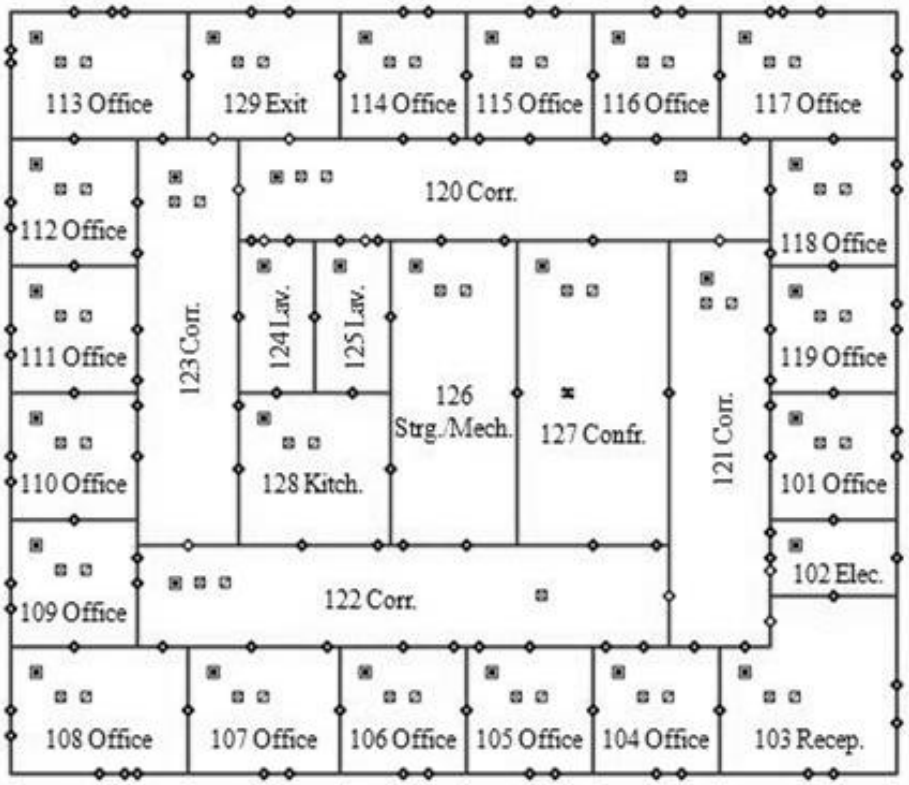


*Figure 4.1*: Virtual Building (VB-1) Developed by Firrantello (2007)

Table 4.1

*Synthetic Building Room Information*

| Room Name | Area | Supply Air | Return Air | Exhaust Air | HVAC |
|---|---|---|---|---|---|
| | $ft^2$ | CFM | CFM | CFM | Zone |
| 101 Office | 100 | 160 | 144 | N/A | South |
| 102 Elec. | 50 | N/A | N/A | 30 | South |
| 103 Recep. | 200 | 300 | 270 | N/A | South |
| 104 Office | 100 | 160 | 144 | N/A | South |
| 105 Office | 100 | 160 | 144 | N/A | South |
| 106 Office | 100 | 160 | 144 | N/A | South |
| 107 Office | 100 | 160 | 144 | N/A | South |
| 108 Office | 150 | 320 | 288 | N/A | South |
| 109 Office | 100 | 150 | 135 | N/A | South |
| 110 Office | 100 | 150 | 135 | N/A | South |
| 111 Office | 100 | 150 | 135 | N/A | North |
| 112 Office | 100 | 150 | 135 | N/A | North |
| 113 Office | 150 | 230 | 207 | N/A | North |
| 114 Office | 100 | 150 | 135 | N/A | North |
| 115 Office | 100 | 150 | 135 | N/A | North |
| 116 Office | 100 | 150 | 135 | N/A | North |
| 117 Office | 150 | 230 | 198 | N/A | North |
| 118 Office | 100 | 160 | 144 | N/A | North |
| 119 Office | 100 | 160 | 144 | N/A | North |
| 120 Corr. | 336 | 380 | 180 | N/A | Core |
| 121 Corr. | 256 | 180 | 135 | N/A | Core |
| 122 Corr. | 336 | 200 | 180 | N/A | Core |
| 123 Corr. | 256 | 150 | 135 | N/A | Core |
| 124 Lav. | 84 | N/A | N/A | 90 | Core |
| 125 Lav. | 84 | N/A | N/A | 90 | Core |
| 126 Strg./Mech. | 200 | 140 | 126 | N/A | Core |
| 127 Confr. | 200 | 300 | 270 | N/A | Core |
| 128 Kitch. | 168 | 100 | 90 | N/A | Core |
| 129 Exit | 100 | 80 | 72 | N/A | North |
| **Total** | **4120** | **4780** | **4104** | **210** | |

### *4.1.2 Review of CONTAM/PCW Basic Concepts*

There are some basic concepts, definitions, and assumptions used by the CONTAM and PCW software programs that are very relevant to this research. The first major assumption of these multi-zone programs is the "well-mixed" assumption. A "well-mixed" zone is a zone that is "characterized by a discrete set of state variables, i.e., temperature, pressure, and contaminant concentrations" (Walton and Dols, 2005). The only difference is zone pressure which does vary hydrostatically within a zone. Each zone is identified as a specific volume of air that is connected to other zones by various airflow paths.

Airflow paths and leakage parameters are mentioned often in this research and need to be properly defined. "An airflow path indicates some building feature by which air can move from one zone to another. Such features include cracks in the building envelope, open doorways, and fans" (Vandemusser, 2007). Airflow through any airflow path is governed by the air pressures on either side of the path and the characteristics of the flow path itself. An "airflow element" is the mathematical relationship, used in the multi-zone model, between the flow through an airflow path and the pressure difference across that airflow path. PCW and CONTAM provide several different options of mathematical models or airflow elements for airflow paths. The most common airflow elements are the one-way flow using power law models or one-way flow using quadratic models. Two-way flow models, forced flow or fan models, and damper models are also available. Refer to Walton and Dols (2005) and Vandemusser (2007) for a complete discussion on the various types airflow elements.

One-way flow using power law models take the form of Equation 4.1 below.

$$Q = k(\Delta P)^n \tag{4.1}$$

In Equation 4.1, "k" is the airflow coefficient and "n" is the airflow exponent. Along with the form of the airflow element, these coefficients and exponents for each airflow path are sources of uncertainty in multi-zone models. Throughout this research, the terms "leakage parameters, values, or coefficients" refer to the "k" and "n" in Equation 4.1. The one-way flow using quadratic models usually take the form of Equation 4.2 below.

$$\Delta P = aQ + bQ^2 \tag{4.2}$$

In Equation 4.2 "a" and "b" are the flow coefficients. Awbi (1991) provides a more detailed discussion on the formation and use of Equations 4.1 and 4.2 as models for airflow paths as mentioned in Section 2.1.10. Besides picking from these predetermined airflow elements, the user has the option to create custom airflow elements of any form. When using CONTAM, the user must manually identify each airflow element either from the library of elements or a custom element. One simplification that is built into PCW is that building leakage severity can be automatically assigned. This capability of PCW to automatically assign airflow paths and airflow elements contributes to the reduction in modeling time and effort as compared to CONTAM. When using this automatic feature in PCW, the leakage severity is selected by the user from a menu. The user specifies either "normal" (or "average"), "tight", or "leaky" for leakage severity. "A suggestion is to select 'normal' unless you have reason to believe that the

building's leakage is significantly different from other buildings" (Vandemusser, 2007). The details of these leakage severity assumptions are explained by Vandemusser (2007):

> "Your selection of leakage severity sets the airflow elements that PCW uses to represent the exterior walls, roof, interior walls, and floors of the building. This includes unintentional leakage in these walls such as cracks, as well as the effect of closed doors and windows. Thus, you do not need to account for closed doors and windows separately. The 'normal' condition for exterior walls and roofs is the mean of all buildings summarized by Persily (1998). The 'tight' and 'leaky' conditions are defined as ±1 standard deviation from the mean in the same survey. Interior walls and floors are then defined as having twice the airflow as the exterior walls/roofs at the same pressure condition."

This default feature uses the one-way flow power law airflow element from Equation 4.1. The flow exponent is 0.65 for all leakage paths and the flow rate ($m^3$/hr) is specified for a reference pressure difference (75 Pa). The flow coefficinents can then be deduced from Equation 4.1.

PCW also contains default leakage parameters for elevator walls, stairs, and shafts. Refer to Vandemusser (2007) for a complete discussion on these leakage assumptions. After using all default leakage values from the program, PCW's built-in tuning process attempts to calibrate the building's overall leakage using a full factorial parametric analysis feature. However, the accuracy and

utility of this step has come into question based on the results discussed by Firrantello (2007) and Sae Kow (2010).

Some additional features of airflow paths include contaminant filtration, schedules, and wind pressure. A filter can be assigned to any airflow path to remove contaminants. Various filtration models are available. Schedules can be assigned to vary flow through an airflow path to mimic opening and closing of a window, opening and closing of a damper, turning on and off a fan, etc. For exterior airflow paths, the direct effects of wind pressure can be accounted for by specifying a wind pressure profile which is a function of the incidence angle of the wind. The elevation of an airflow path also needs to be specified. This accounts for how the airflow path responds to or influences building stack effect.

Another important concept is the simplified air handling unit or "Simple AHU" feature of PCW which is used throughout this research. Although CONTAM allows for more detailed HVAC system modeling (i.e. drafting ductwork systems, controls, etc.), PCW is limited to only the Simple AHU type of model where ductwork is not explicitly modeled. In this simplified model, the entire HVAC duct system is modeled as two implicit airflow nodes or zones, the supply duct volume and the return duct volume. As any other zone in a multi-zone model, the "well-mixed" assumption applies. Therefore, for example, if a contaminant is released in the supply duct system, the contaminant concentration is uniform throughout the entire supply duct volume at the first time step. This is obviously a simplification from reality. Another limitation with this Simple AHU assumption is that duct leakage is not accounted for in the simulation. For the

Simple AHU model, there are three implicit airflow paths: recirculation air, outside air, and exhaust air. Additionally, there are an infinite possible number of supply diffusers and zone returns in any given model. Refer to Walton and Dols (2005) and Vandemusser (2007) for a complete discussion on how the various airflows are calculated for the Simple AHU model.

Another important concept to discuss is the different types of simulations that can be performed. Airflow simulations are used to determine inter-zonal airflows and pressure differences. Contaminant simulations are used to determine contaminant concentrations throughout the building. Airflow simulations and contaminant simulations can be performed under the following methods: no simulation, steady state, transient, or cyclical. Steady state simulations calculate airflows and concentrations under constant building and weather conditions. Transient simulations calculate airflows under changing conditions and calculate contaminant concentration histories within each zone. For transient simulations, separate weather files must be uploaded to the program to simulate varying outdoor weather conditions. Similarly, separate contaminant files can be uploaded to simulate varying outdoor contaminant concentrations. Refer to Walton and Dols (2005) and Vandemusser (2007) for instructions on how to create such files.

For this research, all simulations were performed with steady state airflow analysis and transient contaminant analysis. This means that the airflows and pressure differentials are calculated for one set of conditions (i.e. constant weather condition and constant air volume HVAC flows) while contaminant concentrations were allowed to vary over time under these steady state airflow

conditions. No contaminant file was used and therefore the outdoor concentration (approximately 400 PPM for $CO_2$) was assumed to remain constant. These simulation assumptions are identical to those used by Firrantello (2007) and Sae Kow (2010).

## 4.2 Airflow-Based Sensitivity Analysis

The objectives of the sensitivity analysis were to evaluate whether the airflow dynamics of the building are climate or HVAC dominated, to identify the significant or important drivers of the airflow dynamics, and to assist with reducing the model complexity by identifying macro-zones.

### *4.2.1 Airflow-Based Sensitivity Analysis Methodology*

1. Identify influential drivers of the building airflow dynamics (e.g., climatic and operating parameters). These will most likely include ambient air temperature, wind direction with respect to the orientation of the building, wind velocity, building leakage severity, and HVAC system airflow rates.
2. Identify characteristic values representative of low, medium, and high values for each parameter.
3. Perform a $2^k$ full factorial analysis assuming that the relationships between the effects and the factor levels are linear. For this synthetic building example, a $3^k$ analysis was performed so as to evaluate the non-linearity effects of the drivers; however, it was found that a $2^k$ factorial was adequate.

4. Graphically evaluate the results of the sensitivity analysis. Scatter plots are a convenient way of distinguishing whether the building airflow dynamics are HVAC dominated or climate dominated.
5. If the building is found to be climate dominated (which most mechanically heated, cooled, and ventilated low-rise commercial buildings are not), further research is needed. This was deemed outside the scope of this research and left to a future study.

### *4.2.2 Data Generation*

Initially, the sensitivity analysis included a $3^3$ full-factorial experimental design using multiple PCW simulations to determine the effects of varying ambient temperature, wind speed, and building leakage severity on the direction and magnitude of airflow through all model airflow paths. Value ranges for ambient temperature and wind speed that would be commonly encountered by the building were used. The default building leakage severity is specified in PCW as either "leaky", "average", or "tight." The user-specified building leakage severity level then corresponds to a set of default leakage values that PCW uses when assigning leakage as discussed in Section 4.1.2.

PCW has its own built in factorial analysis in the "measurements phase" of the program. It performs a $2^7$ factorial to determine the main and interaction effects of the following variables: terrain factors, interior wall leakage, exterior wall leakage, shaft wall leakage, wind direction, wind velocity, and outside air temperature. Based on these results, the user can enter measured values to update the factors with the most significant effects. The response variable for this

sensitivity analysis is the percentage of correctly predicted airflow directions predicted by the model for one set of conditions. The factorial analysis being proposed here aims to determine the influence of certain variables on building behavior between different sets of conditions rather than one set of conditions. It is important to make a distinction between these two types of factorial analyses.

A $3^3$ factorial analysis involves a total of 27 simulations which were performed on the single story synthetic building for the combinations of three wind speeds (0 mph, 5 mph, and 10 mph), three ambient temperatures (40°F, 70°F, and 100°F), and the three default leakage settings in PCW ("leaky", "average", and "tight"). Refer to Table 4.2 for the summary of these simulations. This part of the sensitivity analysis did not include the effect of wind direction or mechanical ventilation conditions. For each simulation, the wind direction is kept unaltered, i.e. from the north. Also, for each simulation, the supply and return volumetric airflow rates from each air handling unit are the same (i.e., a constant air volume HVAC system is assumed). This constant air volume assumption is significant since most buildings today will operate under some type of variable air volume system. The methods used by Firrantello (2007) and Sae Kow (2010) also use the constant air volume assumption since it simplifies the airflow calibration problem. Researching methods to calibrate variable air volume systems was left for future work. The interior temperature remains the same for each simulation (72°F) and the terrain condition remains the same ("Large obstruction within 40-100 feet"). Each simulation was performed as a steady state airflow simulation

and thus airflow magnitudes and directions do not change with time. No tracer gas release was simulated for this part of the analysis methodology.

Table 4.2

*Synthetic Building Airflow-Based Sensitivity Analysis Summary*

| **Wind Speed (mph)** | **Ambient Temperature (°F)** | | |
|---|---|---|---|
| | 0 | 70 | 100 |
| 0 | Leaky | Leaky | Leaky |
| | Average | Average | Average |
| | Tight | Tight | Tight |
| 5 | Leaky | Leaky | Leaky |
| | Average | Average | Average |
| | Tight | Tight | Tight |
| 10 | Leaky | Leaky | Leaky |
| | Average | Average | Average |
| | Tight | Tight | Tight |
| Wind Direction is from the North | | | |
| Indoor Air Temperature = 72°F | | | |

### *4.2.3 Data Analysis*

#### *4.2.3.1 Bar Graphs*

The results of the sensitivity analysis were evaluated by first plotting bar graphs that showed the absolute magnitude and direction of each flow path in each zone (e.g. flow from outdoors to indoors through building envelope, flow to adjacent zones, etc.). Each bar corresponds to a single airflow path, and thus each room has several bars corresponding to the various airflow paths in that room. The sign convention that PCW uses is that airflows are positive (+) if the air travels into the room and are negative (-) if air travels out of the room. Refer to Appendix A and Figures A1.1 and A1.2 for examples of these bar graphs. Due to the large number of airflow paths, it became obvious that identifying macro-zones

based on such plots would be too difficult and tedious. The utility of such graphs is unclear.

*4.2.3.2 Normalized Bar Graphs*

A subsequent manner of re-plotting the data was to normalize all of the flows from each simulation with respect to a base case situation (i.e., 70°F, 0mph, and "Average") and generate similar bar graph diagrams for these normalized flows. Although these graphs did reveal some global trends in airflow behavior between different conditions, it was still too difficult to reach any conclusions towards trying to group rooms in to macro-zones. Therefore these graphs were no more useful than the other bar graphs.

*4.2.3.3 Scatter Plots*

It was discovered that a very useful representation of the effects of various operating conditions on airflow dynamics was obtained by using scatter plots. The results of the $3^3$ factorial seemed to display linear relationships between the effects and the factor levels. Therefore, eight simulations were selected, which were somewhat representative of a $2^3$ factorial, to generate scatter plots. Due to the linear relationships, the same conclusions could be drawn from eight simulations as from the total 27. Each scatter plot generated compares the airflow magnitudes and directions of two different scenarios (one scenario per axis) which differ in only one condition. The unit on each axis is the volumetric flow rate of air in cubic feet per minute (CFM). The direction of airflow is accounted for in the sign convention. Each point in the scatter plot represents a single flow path. The scatter plots generated are summarized in Table 4.3.

Table 4.3

*Synthetic Building Airflow-Based Sensitivity Analysis Scatter Plot Summary*

| Figure | Description | X-Axis Scenario | Y-Axis Scenario |
|---|---|---|---|
| **4.2** | Effect of airflow path leakiness at high wind | 70°F, 10mph, Tight | 70°F, 10mph, Leaky |
| **4.3** | Effect of airflow path leakiness at low wind | 70°F, 0mph, Tight | 70°F, 0mph, Leaky |
| **4.4** | Effect of temperature at high wind | 100°F, 10mph, Average | 40°F, 10mph, Average |
| **4.5** | Effect of temperature at low wind | 100°F, 0mph, Average | 40°F, 0mph, Average |

The scatter plots allow one to visualize how varying operating conditions affect the magnitude and direction of airflows through all airflow paths. It was at this stage that it was determined that a $2^k$ factorial analysis would suffice since using the "high" and "low" values yielded the same conclusions as using "high" and "medium" or "medium" and "low" values. Important conclusions about model sensitivity to these factors and on the building's airflow dynamics can be revealed by the structure of these scatter plots:

1. Points which fall within the positive/positive and negative/negative quadrants of the scatter plot indicate that the altered condition did not result in a change in the airflow direction in those airflow paths.
2. Points that fall within the positive/negative and negative/positive quadrants indicate that the altered condition did change the airflow direction in those airflow paths.
3. Points that fall on the "y = x" line indicate that the altered condition did not change the magnitude of airflow through those airflow paths.

4. Points that fall off of the "y = x" line indicate that the altered condition did change the airflow magnitude through those airflow paths.

Despite illustrating the impact of various conditions on airflow dynamics, this type of graph by itself is inadequate in allowing the collection of rooms into macro-zones for the purpose of model reduction. The large number of airflow paths and the fact that there are multiple paths per room, makes it too difficult and tedious to isolate individual rooms on these scatter plots.

*4.2.3.4 Effect of Wind Direction*

The sensitivity analysis described above did not account for varying wind directions due to the number of simulations that would be required to add another factor to the factorial analysis. Realizing that this may be a significant omission, four more PCW simulations were performed so that the effect of varying wind direction could be analyzed. Besides wind from the north, two other wind directions were chosen; a 90° change (wind from the west) and a 45° change (wind from the northwest). Table 4.4 summarizes these additional simulations. The different wind directions were compared to the simulations of north wind for both the "leaky" and "tight" airflow path leakage severities. See Figures 4.6 through 4.9 for scatter plots of these comparisons. Specifically, note that changing wind direction can alter the direction of flow through a certain airflow path as seen by the points in the negative/positive and positive/negative quadrants of Figure 4.6 and Figure 4.7. The significant influence of wind suggests that wind speed and wind direction should both be included in the original factorial analysis.

Table 4.4

*Summary of Simulations Performed to Investigate the Effect of Wind Direction*

| **Wind Direction** | **Leakage Severity** | |
|---|---|---|
| Northwest | Leaky | Tight |
| West | Leaky | Tight |
| Ambient Temperature = 70°F | | |
| Wind Speed = 10mph | | |
| Indoor Temperature = 72°F | | |

*4.2.3.5 Preliminary Macro-Zoning Based on Building Geometry and HVAC Zoning*

A final attempt towards model reduction using airflow-based sensitivity analysis was made by plotting the magnitude and direction of airflows through each airflow path for all rooms and then separating out airflow paths for assumed macro-zones. These graphs were only generated for two scenarios (70°F, 5mph, Average and 70°F, 0mph, Average). The assumed macro-zones were formed based on the geometry of the floor plan layout and HVAC zoning. Refer to Table 4.5 for details of the assumed macro-zones. The intent was to visually segregate rooms which may have similar airflow dynamics so that they could be lumped into macro-zones. The results show significant scatter for each assumed macro-zone, and this type of analysis was inconclusive. Further thought lead to the conclusion that since each room will have multiple flow paths with varying magnitudes and directions of airflow such variation is to be expected. Refer to Appendix A and Figures A1.3 and A1.4 for examples of these graphs.

Table 4.5

*Assumed Macro-Zones Identified from Floor Plan Geometry and HVAC Zoning*

| **Assumed Macro-Zone** | | | | | | | |
|---|---|---|---|---|---|---|---|
| 1 | 2 | 3 | 4 | 5 | 6 | 7 | 8 |
| 111 Office | 129 Exit | 117 Office | 101 Office | 104 Office | 108 Office | 120 Corr. | 124 Lav. |
| 112 Office | 114 Office | 118 Office | 102 Elec. | 105 Office | 109 Office | 121 Corr. | 125 Lav. |
| 113 Office | 115 Office | 119 Office | 103 Recep. | 106 Office | 110 Office | 122 Corr. | 126 Strg./Mech. |
| | 116 Office | | | 107 Office | | 123 Corr. | 127 Confr. |
| | | | | | | | 128 Kitch. |

### *4.2.4 Airflow-Based Sensitivity Analysis Conclusions*

None of graphical methods of visualizing the sensitivity analysis results allowed for the proper grouping of rooms in macro-zones based on airflow simulations alone. Each room has several airflow pathways which can have varying airflow magnitudes and directions. This natural scatter does not allow for any such macro-zone grouping. An alternative and more appropriate method which utilized tracer gas simulations is described in the next section.

This airflow-based sensitivity analysis did, however, provide useful information on the significant drivers of the airflow dynamics. Flow magnitudes and directions did not change significantly for varying ambient temperature or when there is no wind. With wind from one direction, it appears that wind only changes flow magnitudes when the building has the most severe leakage condition, i.e. “leaky.” Airflow directions through airflow paths only changed when wind direction changed. The 90° wind direction change resulted in more airflow direction changes than the 45° wind direction change. Again, wind direction change was only significant when the building was “leaky.”

These results indicate that wind velocity and wind direction are the most significant drivers. However, their significance is a function of the building severity, with “leaky” yielding the most significance. Buildings with average or tight leakage severity will be less sensitive to climatic conditions. Also, since most magnitude changes were small and since only wind direction seemed to affect airflow directions, it would appear that the building is mostly HVAC dominated. In other words, the HVAC induced airflows define the interior airflow behavior almost independent of climatic conditions. Also note that it is difficult to determine what magnitude of airflow through the various building airflow paths should be considered significant. If the purpose of the model calibration is to improve contaminant prediction accuracy, then the magnitude and directions of airflow through airflow paths are only important in how they impact the movement and concentration decay of contaminants, and thereby the dose of contaminant that an occupant is exposed to. Therefore, moving to a tracer gas based sensitivity analysis, as suggested in the next section, would provide a better indication of whether these climatic conditions affect the tracer gas histories in each room.

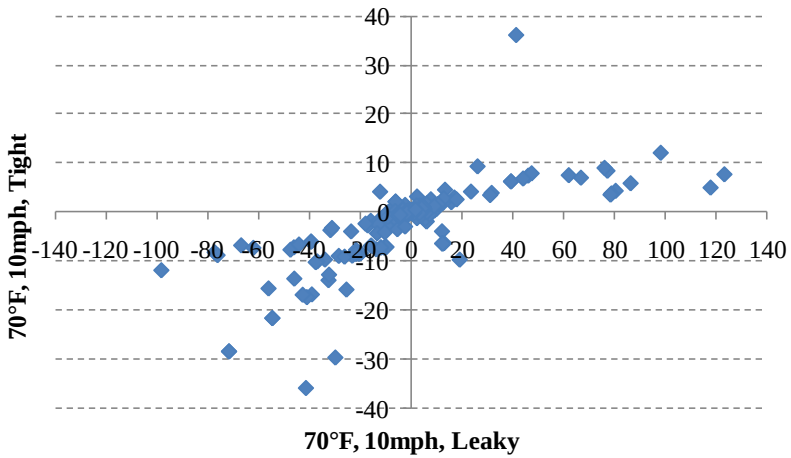


*Figure 4.2*: Effect of Leakage Severity at High Wind

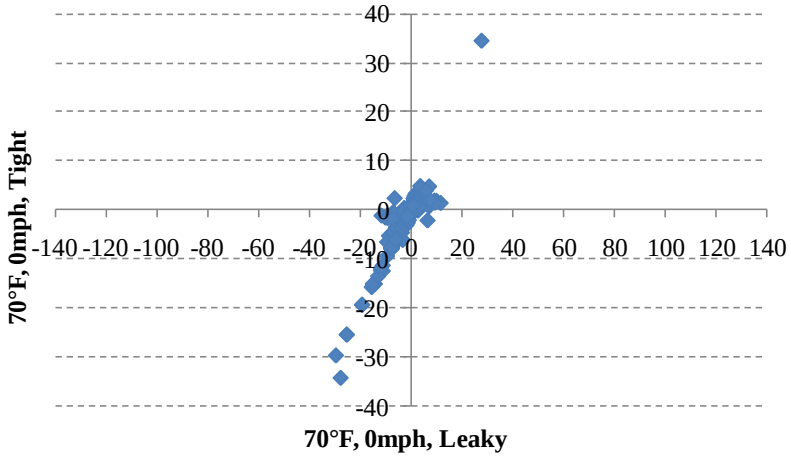


*Figure 4.3*: Effect of Leakage Severity at No Wind

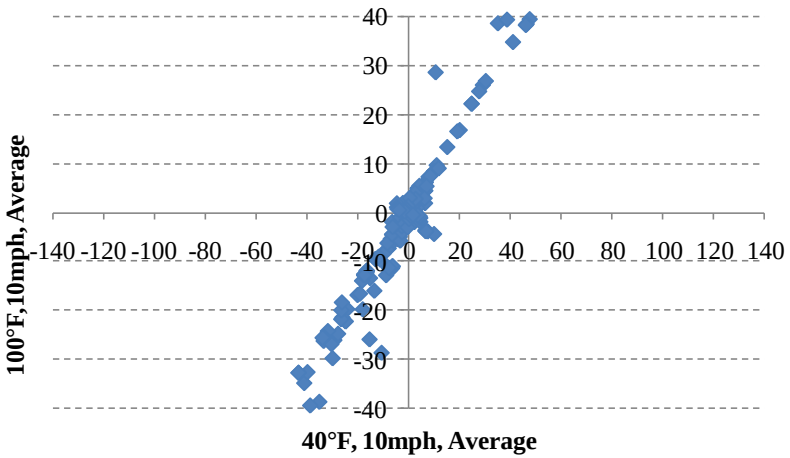


*Figure 4.4*: Effect of Temperature at High Wind

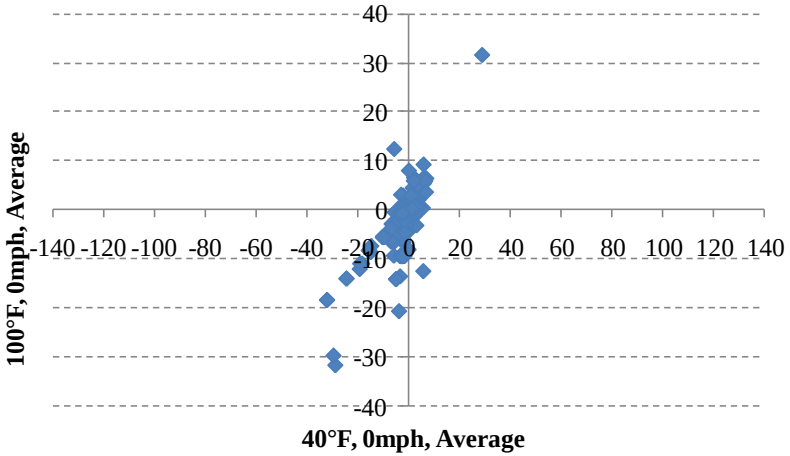


*Figure 4.5*: Effect of Temperature at No Wind

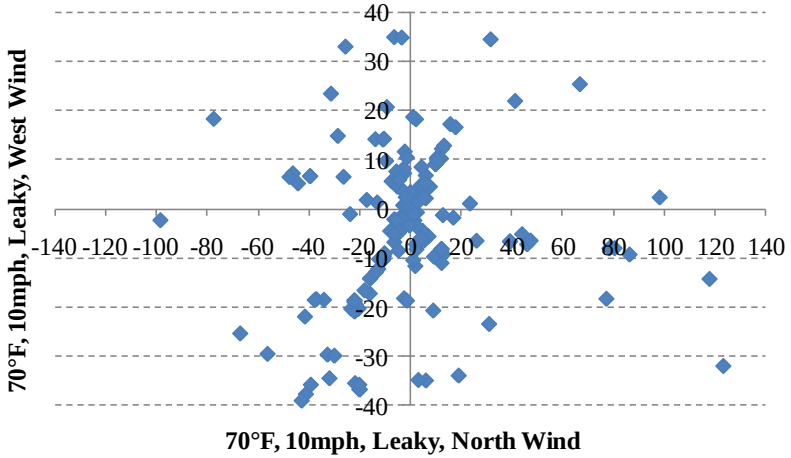


*Figure 4.6*: Effect of Wind Direction (90° Change) at “Leaky”

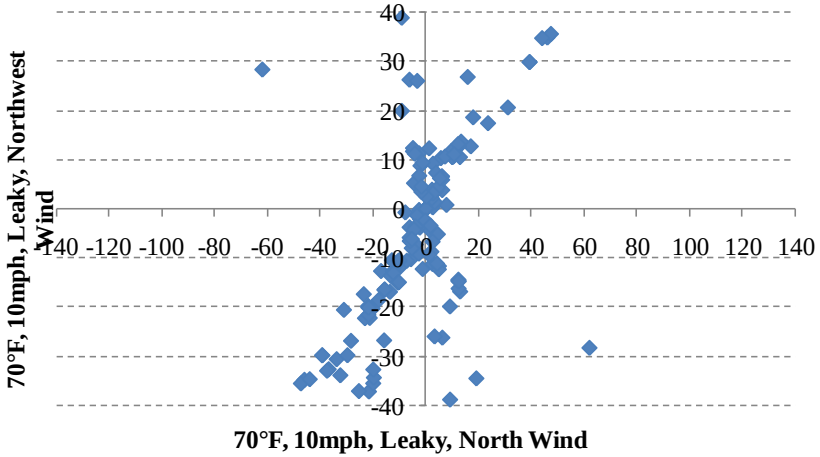


*Figure 4.7*: Effect of Wind Direction (45° Change) at "Leaky"

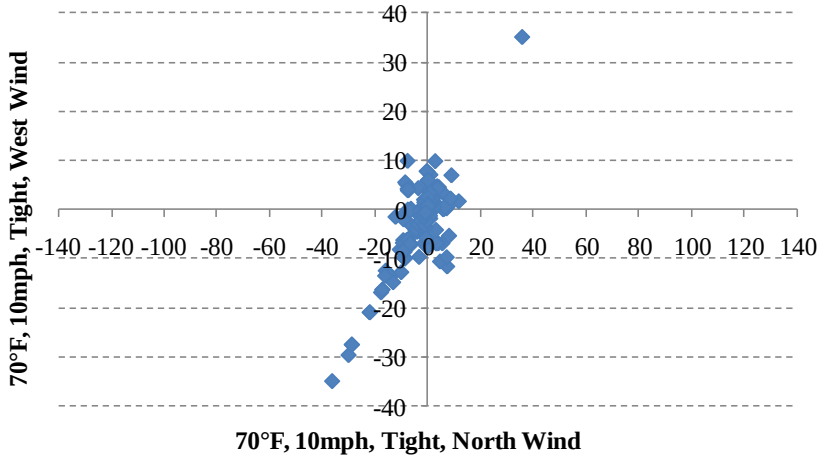


*Figure 4.8*: Effect of Wind Direction (90° Change) at "Tight"

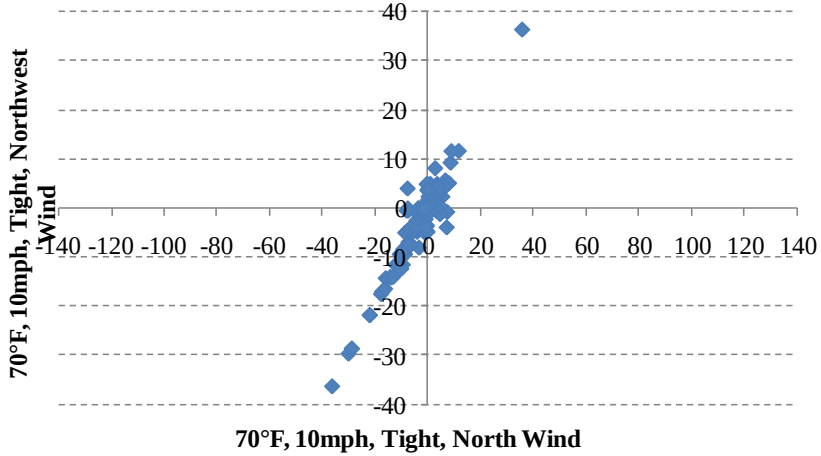


*Figure 4.9*: Effect of Wind Direction (45° Change) at "Tight”

### 4.3 Identification of Macro-Zones for Model Reduction Using Tracer Gas ($CO_2$) Simulations

Since model reduction based on airflows alone proved to be too problematic, the next step was to perform tracer gas simulations and try to group rooms into macro-zones based on similar tracer gas dynamic behavior. Moving to a tracer gas-based sensitivity analysis provides an indication of how changing conditions impact the contaminant histories in each room which may also help in identifying macro-zones for model reduction. The ideal situation for macro-zone grouping would be to find rooms that are geometrically adjacent and have similar tracer gas behavior for all conditions.

The overall goal is to select macro-zones that do not change under varying climatic and operating conditions. Instead of using individual room airflows for this purpose, tracer gas, namely $CO_2$, data is used for identifying such macro-zones. The results of the airflow-based sensitivity analysis described in the previous section clearly showed that wind velocity and direction have the greatest potential to change the results of macro-zone grouping. Therefore, the impact of wind on tracer gas behavior was specifically analyzed. To start, one set of operating conditions (70°F, 5mph, and "Average") out of the 27 simulations from the airflow-based sensitivity analysis was selected to use with tracer gas simulations. Subsequent simulations involved changes in these conditions.

Using PCW, simulations were performed where $CO_2$ was released in each AHU. The synthetic building has three AHUs, one serving the north perimeter zones, one serving the south perimeter zones, and one serving the core zones. For

these simulations, $CO_2$ concentration decay data was obtained for each room. Next, a release was simulated in one room, 129 Exit, rather than in an AHU. Then tracer gas simulations were performed for a 90° and 180° change in wind direction with a leakage severity of "leaky" for both north AHU and south AHU releases. Refer to Table 4.6 for a summary of all of the tracer gas release simulations. The release simulated in each case was an amount of $CO_2$ that would bring each room served by that AHU to a concentration of 1600 PPM above ambient concentration (assumed to be 400 PPM). This is the procedure recommended by NIST, which was used by Firrantello (2007) and Sae Kow (2010) for their $CO_2$ releases. This was specifically modeled in PCW by specifying an initial concentration of 2000 PPM in each room served by the AHU where the release occurred. Thus, the HVAC system volume is initially ignored, and the $CO_2$ concentration curves show only the decay and not the uptake of $CO_2$ concentration. The unit of concentration of $CO_2$ in all of the graphs in this section is kg/kg since this is the default units given in PCW. Finally, the use of plotting $CO_2$ decay coefficients for each room under varying conditions for the identification of macro-zones was also evaluated. For these last few simulations only wind speed and wind direction for a model with 70°F ambient temperature, "Leaky" leakage severity, and a north AHU release were varied.

Table 4.6

*Synthetic Building Tracer Gas Release Simulation Summary*

| Release | Tracer Gas Simulation Summary | |
|---|---|---|
| | Leakage Severity | Wind Direction |
| North AHU - Figure 4.10 | Average | North |
| South AHU - Figure 4.11 | Average | North |
| Core AHU - Figure 4.12 | Average | North |
| 129 Exit - Figure 4.13 | Average | North |
| North AHU - Figure 4.14 | Leaky | West |
| South AHU - Figure 4.15 | Leaky | West |
| North AHU - Figure 4.16 | Leaky | South |
| South AHU - Figure 4.17 | Leaky | South |
| Ambient Temperature = 70°F | | |
| Wind Speed = 5mph | | |

### *4.3.1 Model Reduction Methodology*

The primary considerations for grouping rooms into macro-zones include the following:

1. HVAC Zoning
2. Building Geometry
3. Tracer Gas-Based Sensitivity Analysis ($CO_2$ concentration curves, decay coefficients, and peak concentrations)

In buildings where the airflow dynamics are HVAC dominated, rooms that are served by the same HVAC system are likely to have similar dynamic airflow and contaminant concentration behaviors. This is especially true for constant air volume systems and for contaminant releases in air handling units.

### *4.3.2 Preliminary Macro-Zoning – Release in All AHUs*

An initial simulation was performed where $CO_2$ was released in all AHUs simultaneously. Similar to when analyzing airflows, rooms were first grouped into

macro-zones based on floor plan geometry and HVAC zoning alone. For these assumed macro-zones:

- The north AHU serves Zone 1, Zone 2, and Zone 3.
- The south AHU serves Zone 4, Zone 5, and Zone 6.
- The core AHU serves Zone 7 and Zone 8.

Refer to Table 4.5 which specifies which rooms fall into which assumed macro-zones. If the tracer gas dynamics in these rooms are similar, this would provide the necessary justification of clustering them into these macro-zones. For this simulation the results for 0 min, 5 min, 10 min, and 15 min after the release were exported. Refer to Appendix A and Figures A1.5 through A1.8 for these plots. From these graphs, one can quickly ascertain visually whether the assumed macro-zoning is appropriate or not. Large variations in concentrations within one of the assumed zones would suggest that those rooms should not be grouped into the same-macro zone. This simulation served only as a test since a simultaneous release in all AHUs is unlikely.

### *4.3.3 Preliminary Macro-Zoning – Release in Individual AHU*

A more realistic situation is to consider a release in only one AHU. Therefore, a release was simulated in each AHU individually. In an effort to compress all these graphs, the concentration values for five minutes after the release were arbitrarily selected to be plotted for the rooms in each assumed macro-zone. Refer to Appendix A and Figures A1.9 through A.11 for these plots. Again, these graphs can help to determine whether the assumed macro-zones are justified, or whether they need to be adjusted. Each point on these graphs

represents a single room. For any time step after the release, all rooms within the same macro-zone should have similar $CO_2$ concentrations. Any significant scatter would indicate that the rooms are behaving differently in response to the release and should not be combined within the same macro-zone. Comparing these graphs between different release scenarios shows how the macro-zones react to different release locations. A disadvantage of these plots is that it is difficult to indicate which point corresponds to which room.

Another way of visualizing this same information is by plotting the $CO_2$ concentration curves for all of the rooms within each macro-zone. Refer to Appendix A and Figures A1.12 through A1.14 for plots of the first 30 minutes of concentration decay. These decay curves for the assumed macro-zones are slightly misleading because they are the average of the concentrations of the rooms within them. Thus, one cannot visualize if certain rooms within a macro-zone should actually be part of another macro-zone.

#### *4.3.4 Individual Room $CO_2$ Concentration Curves – Release in Individual AHU*

Since the grouping of rooms into assumed macro-zones yielded some misleading results, the $CO_2$ concentration decay curves for each room, rather than for assumed macro-zones, were plotted.

Figure 4.10 shows the tracer gas concentration curves for each room after a release in the north AHU. For this north AHU release, the spaces served by the north AHU (rooms 111, 112, 113, 114, 115, 116, 117, 118, and 119) all have similar decay curves. Only room 129 Exit has a noticeably different decay curve.

This may be attributed to the fact that it is an entrance/exit space and has significantly lower HVAC flows than the adjacent offices. Figure 4.10 also shows some slight cross contamination to some of the adjacent spaces (corridors, lavatories, and Office 110).

Figure 4.11 assembles the tracer gas concentration curves for each room after a release in the south AHU. Rooms 101, 103, 104, 105, 106, 107, 109, and 110 all have similar concentration curves. Room 108 decays faster than the other room likely due to a larger air change rate. Electrical room 102 has no HVAC supply and thus only showed a slight increase in $CO_2$ concentration due to the exhaust fan pulling air in from the corridor via a transfer grille and adjacent spaces. There was little cross contamination to other spaces.

Figure 4.12 shows the tracer gas concentration curves for each room after a release in the core AHU. For this core release there was greater variation in behavior among the core rooms. From Figure 4.12 it appears that the core spaces can be grouped into four separate zones (124 and 125; 122 and 128; 121, 123, and 126; 120 and 127). There was significant cross contamination into room 102 Electric due to its exhaust fan.

### *4.3.5 Individual Room $CO_2$ Concentration Decay Curves – Release in Room 129-Exit*

An additional tracer gas simulation was performed to see how the building reacts to a release in a single room rather than in an AHU. Room 129 Exit was chosen for this simulation. Figure 4.13 shows the tracer gas decay curves for each room. For this release, there was only a small amount of cross contamination to

the adjacent corridor, 123. All of the other spaces were unaffected by the release. This shows that the results are specific to the release scenario. From this point on, this research will focus only on releases within the air handling units.

### *4.3.6 Individual Room $CO_2$ Concentration Curves – Changing Wind Direction 90° and 180°*

Four additional tracer gas simulations were performed to see how changing the wind direction by 90° and by 180° would impact the macro-zone groupings. Each new wind direction was simulated with a north AHU release and a south AHU release. See Figures 4.14 through 4.17 for the $CO_2$ concentration curves for all rooms for these simulations. The building leakage severity was set to "leaky" for these simulations. It was noted from Figure 4.6 that a change in wind direction had the most impact when the building leakage was set to "leaky." Thus, this represents a worst case scenario. The north AHU release with west wind in Figure 4.14 shows the same room groupings as the north wind scenario in Figure 4.10. The only difference is a slightly larger variation in decay rates among the north perimeter offices. Whether this variation in decay curves among these rooms is large enough to justify assigning them into separate macro-zones would depend on the subsequent dose to which the occupants are likely to be exposed to. Such factors are to be specified by the analyst at the onset of the calibration process depending on the circumstance and the criticality of the consequence. Similarly, the south AHU release with west wind in Figure 4.15 shows the same room groupings as the north wind scenario in Figure 4.11. However, now room 109 and room 110, which have west facing exterior walls, have slightly faster

decay rates. The simulations with south wind in Figure 4.16 and Figure 4.17 show the same trends and the rooms with south facing exterior walls have faster decay rates. For all of these wind direction changes, whether the slight variations in decay are significant or not would depend on the circumstances under which the model calibration is being performed. Also, the changes in the wind direction seem to impact which adjacent zones receive cross contamination. Adjacent zones are those that are not served by the AHU where the release occurred. In most cases, the small amount of cross contamination is probably insignificant; however, it would depend on the situation.

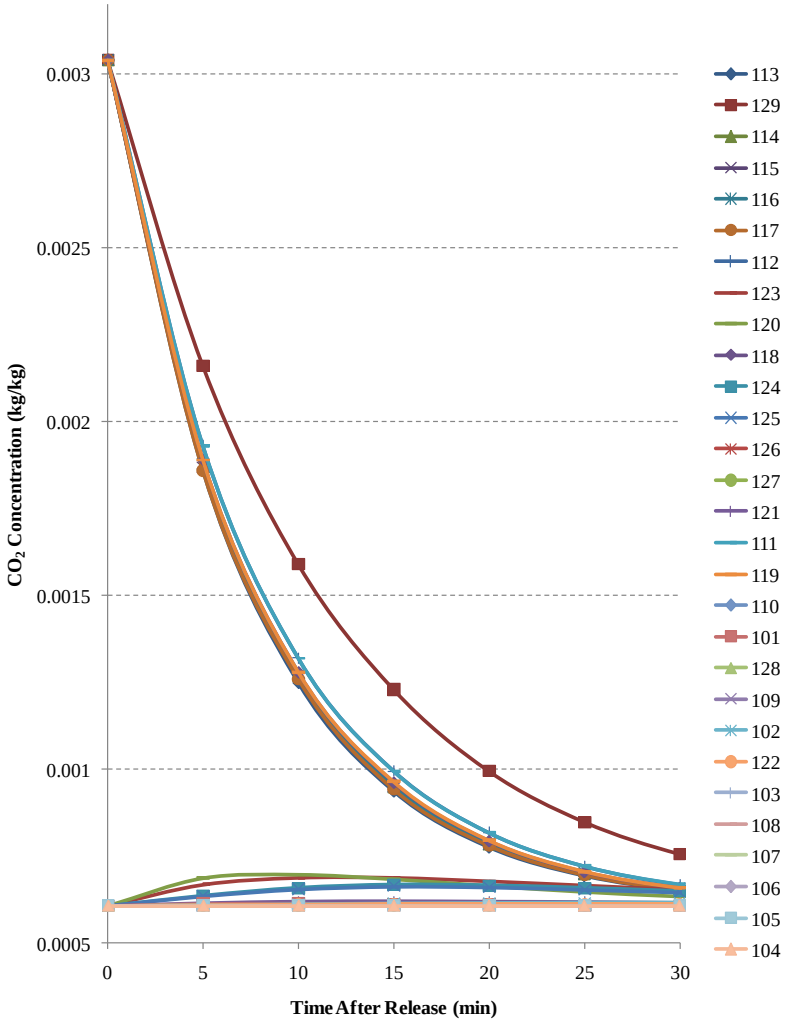


*Figure 4.10*: $CO_2$ Concentration Curves in Individual Rooms (North AHU Release)

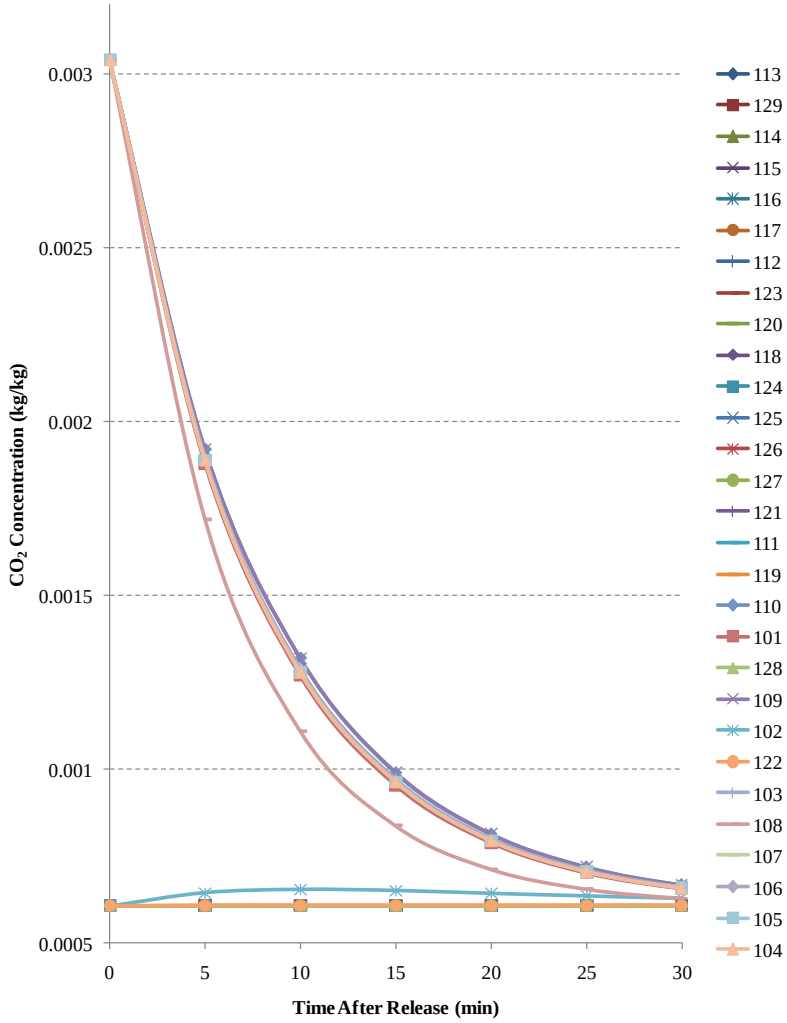


*Figure 4.11*: $CO_2$ Concentration Curves in Individual Rooms (South AHU Release)

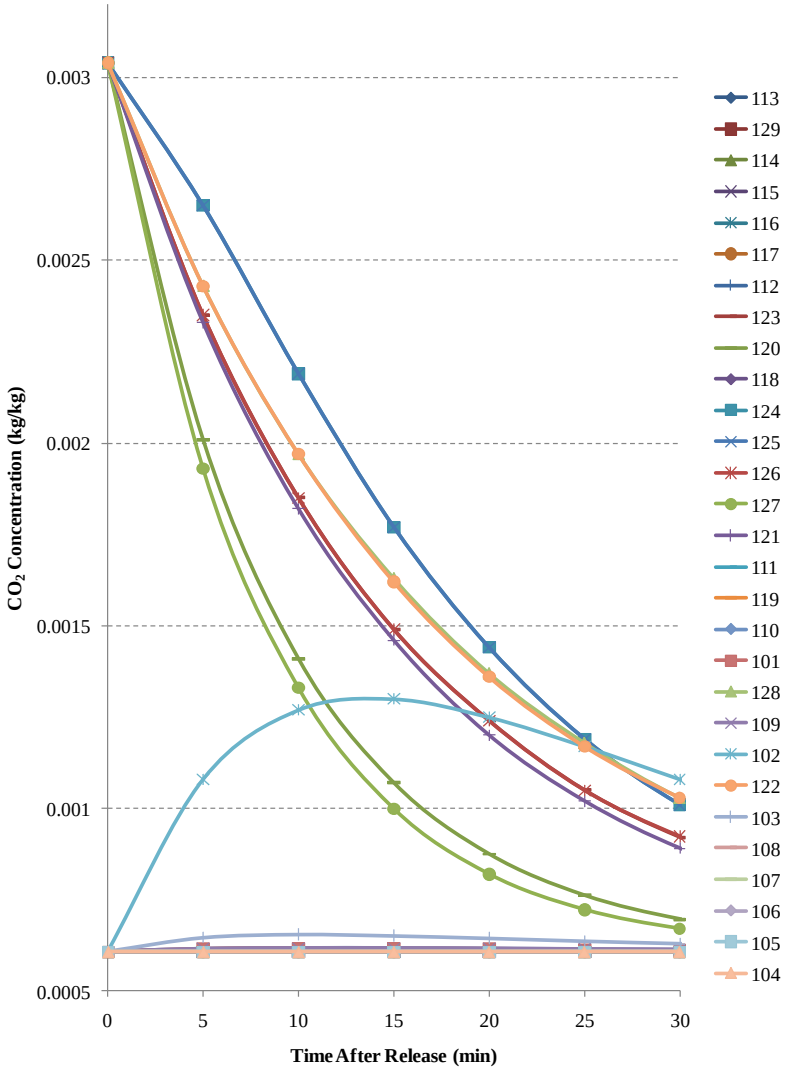


*Figure 4.12*: $CO_2$ Concentration Curves in Individual Rooms (Core AHU Release)

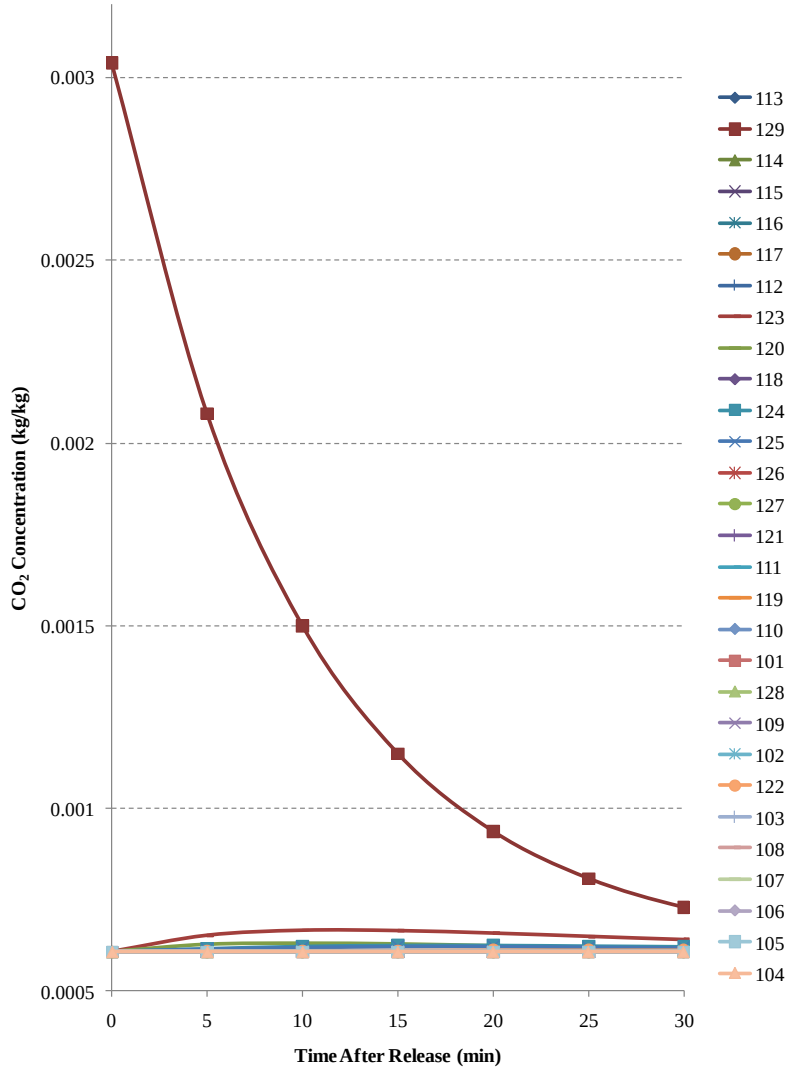


*Figure 4.13*: $CO_2$ Concentration Curves in Individual Rooms (129 Release)

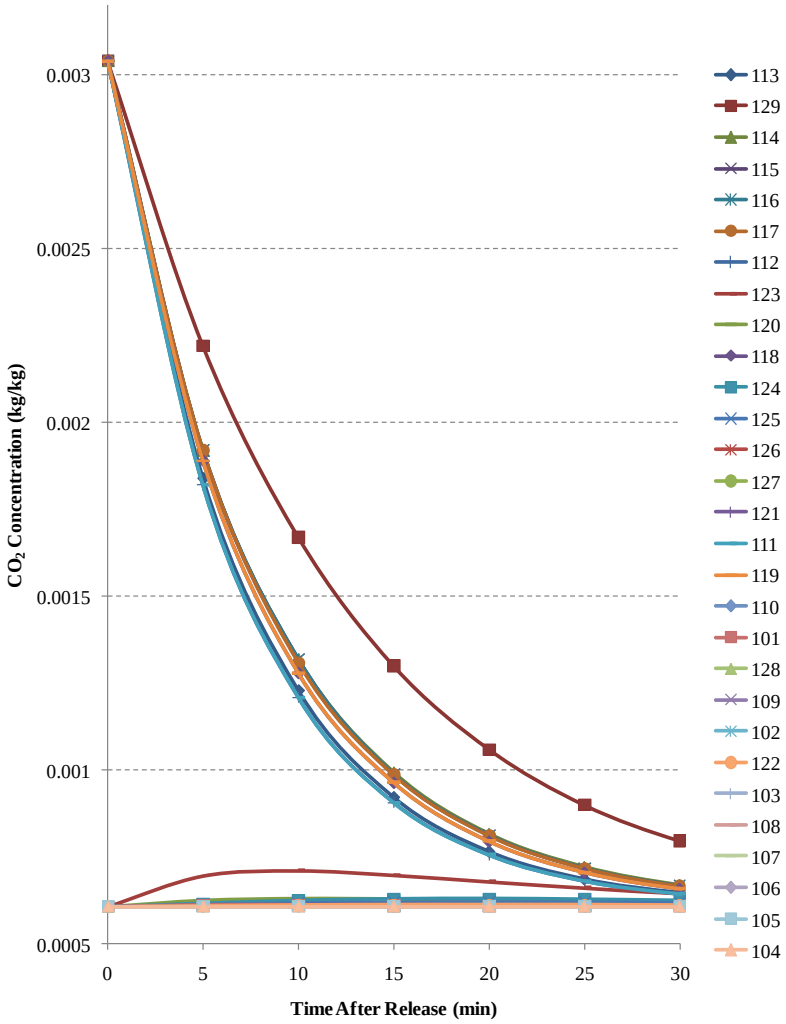


*Figure 4.14*: $CO_2$ Concentration Curves in Individual Rooms (North AHU Release with West Wind at "Leaky")

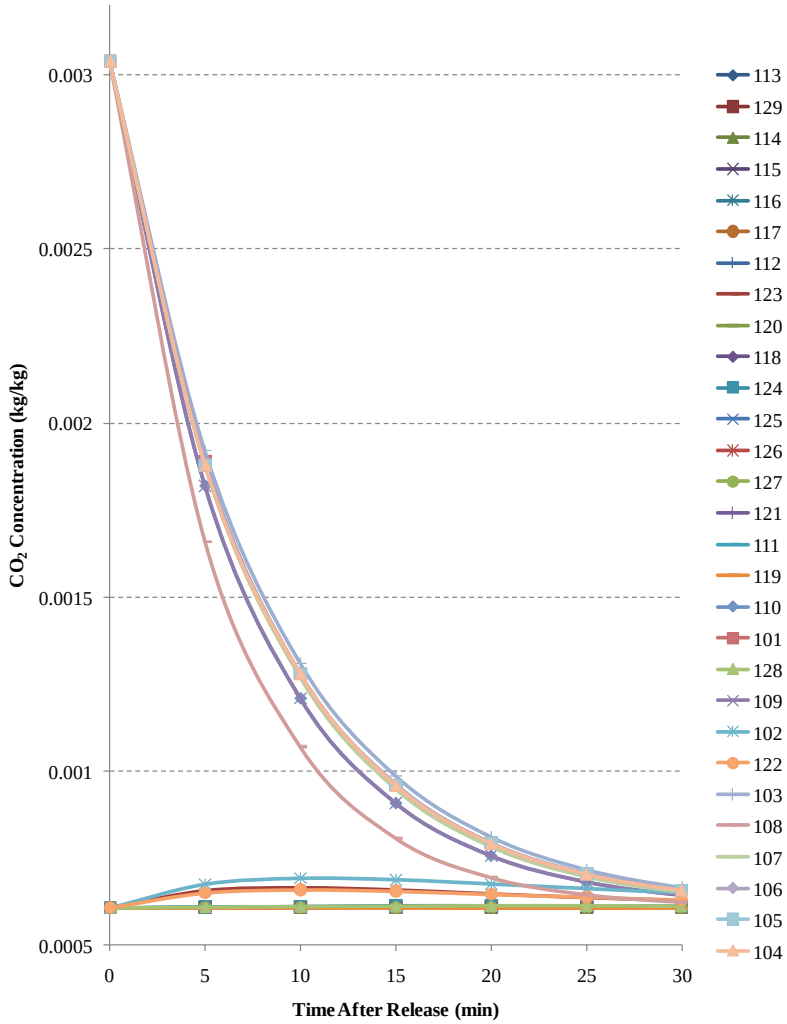


*Figure 4.15*: $CO_2$ Concentration Curves in Individual Rooms (South AHU Release with West Wind at "Leaky")

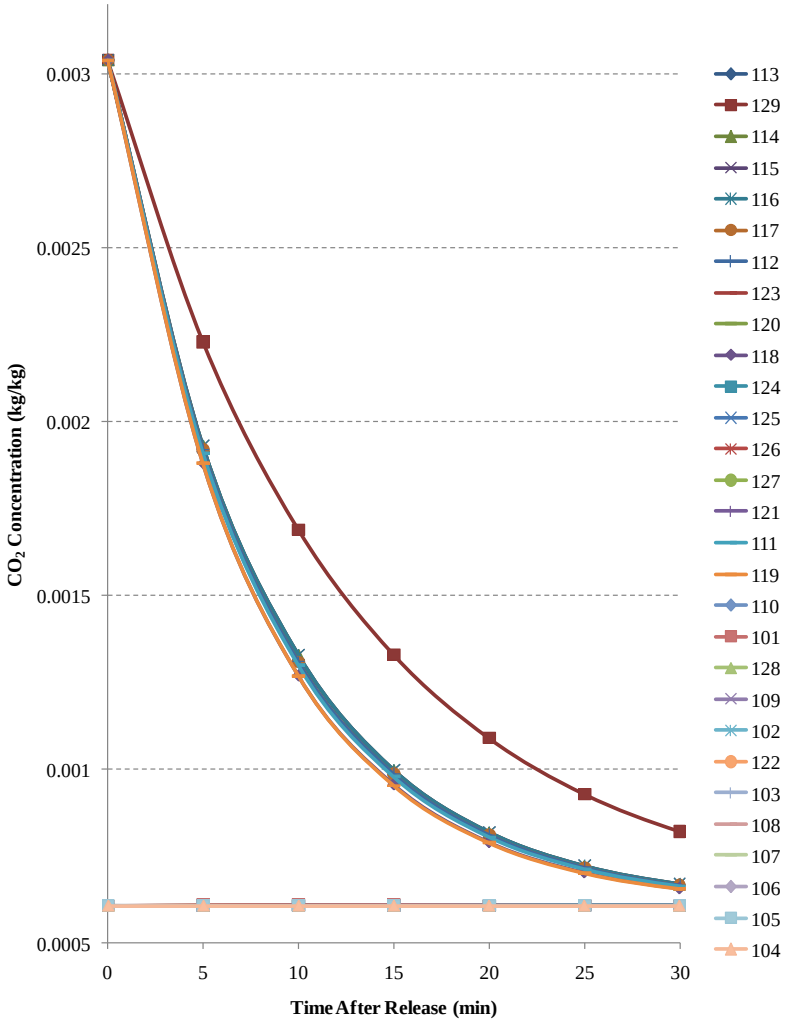


*Figure 4.16*: $CO_2$ Concentration Curves in Individual Rooms (North AHU Release with South Wind at "Leaky")

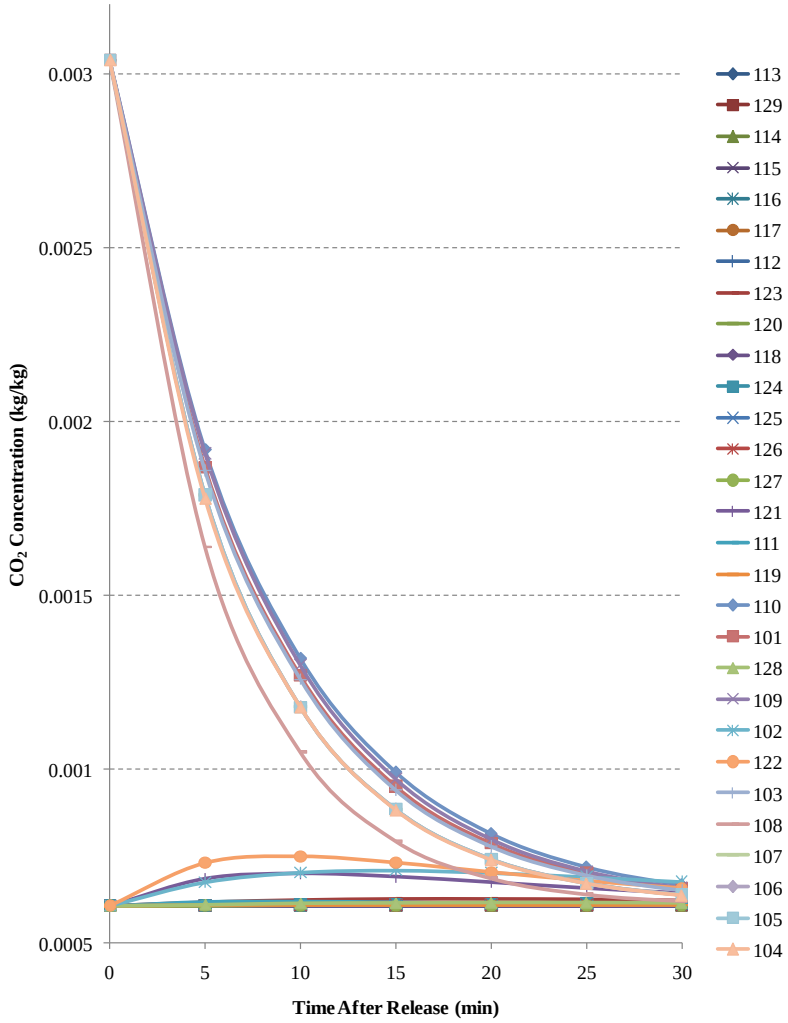


*Figure 4.17*: $CO_2$ Concentration Curves in Individual Rooms (South AHU Release with South Wind at "Leaky")

### *4.3.7 Tracer Gas Decay Coefficients*

The previous section revealed that under different conditions, there were variations in the decay of $CO_2$ in each room. Visually observing these numerous concentration decay curves in cases when there are a large number of rooms, with the intent of ascertaining those which have similar dynamics, is a daunting task. A procedure which could be automated and which makes use of statistical concepts such as clustering methods would be valuable. The decay curve of a first-order system can be represented by Equation 4.3 below.

$$y(t) = Ce^{(-kt)} \tag{4.3}$$

In Equation 4.3, "t" is time, "k" is the decay coefficient, "y" is the $CO_2$ concentration, and "C" is a constant.

Therefore, another tracer gas-based approach is to estimate the exponential decay coefficients for each room under various conditions and use scatter plots of these coefficients for macro-zone identification. The $CO_2$ concentration decay coefficients can also help to determine how significant the influential system drivers are in determining macro-zones. The above equation can be linearized by a natural log data transformation, and so the decay coefficient for each room can be identified by simple linear regression as shown in Equation 4.4. This procedure is similar to the "decay method" that is mentioned in the literature as discussed in Section 2.1.7 and 2.1.10. Those authors found that for first order exponential decay, the decay coefficient is equal to the room air change rate.

$$\ln(y) = C - kt \tag{4.4}$$

Figure 4.18 shows the natural log transformation of one set of concentration decay curves for the synthetic building from one of the conditions in Table 4.6. Similar plots were generated for the other scenarios but were not included here. Contrary to what was expected, the resulting curves are not linear and this suggests that a model of higher order than the first-order model in Equation 4.3 would be more appropriate. A possible reason for this higher order behavior is the fact that $CO_2$ is being re-circulated via the return ducts, mixed with outside air, and being re-supplied to each zone. A 100% outside air system would be more likely to show a first order decay. Rather than to follow this approach with a higher order model, a simpler option is to stick to the first-order model but to only consider a shorter portion of the dynamic decay curve. A preliminary analysis of the log-transformed curves revealed that only considering the first twenty minutes of decay as shown in Figure 4.19 would result in a log-transformed plot which is approximately linear. Note that this is rather case specific and different circumstances may require different segments of time to be taken. Hence, the decay coefficient for each room in this study was determined using only the first 20 minutes after the release and was interpreted as the slope of the line for the first twenty minutes only.

The next step was to plot these decay coefficients for each room under varying climatic and operating conditions. The final intent was to identify macro-zones based on these observations. Figure 4.20 (a) through (e) shows conceptual representations illustrating HVAC influence on the exponential decay coefficient of individual rooms. The different scatter plots illustrate five conceptually

different instances of HVAC interaction for a building with four rooms. Each scatter plot represents two sensitivity runs, one per axis, similar to the airflow-based sensitivity scatter plots from Section 4.2. The resulting plot shows how the exponential decay coefficients for each room are likely to change under different types of climatic and operating conditions. There are several possibilities for the resulting structure of these plots:

1. The first possibility is to have multiple macro-zones that are HVAC dominated as shown in Figure 4.20 (a). In this situation, the altered condition has no effect on the decay coefficient for each room. This would indicate that the rooms are dominated by HVAC flows and not by climatic conditions. However, each room has a significantly different decay coefficient, and therefore, should not be grouped into the same macro-zone.
2. The second possibility is to have only one macro-zone that is HVAC dominated as shown in Figure 4.20 (b). In this situation, all rooms have similar decay coefficients that do not change with the altered condition.
3. The third possibility is to have multiple macro-zones that are not HVAC dominated as shown in Figure 4.20 (c). In this situation, all rooms have significantly different decay coefficients that change with the altered condition.
4. The fourth possibility relates to the instance when one macro-zone is not HVAC dominated as shown in Figure 4.20 (d). In this situation, all rooms have similar decay coefficients that do change with the altered condition.

5. The fifth possibility is have multiple macro-zones of which some are HVAC dominated and some are not as shown in Figure 4.20 (e).

This decay coefficient approach was analyzed with only five simulations which are summarized in Table 4.7. The condition of 70°F ambient temperature, "Leaky" leakage severity, and a north AHU release was used. Only wind speed and wind direction were varied.

Table 4.7

*Summary of Release Simulations Performed for Decay Coefficient Analysis*

| Release | Wind Speed | Wind Direction |
|---|---|---|
| 1 | 0 mph | N/A |
| 2 | 5 mph | North |
| 3 | 10 mph | North |
| 4 | 5 mph | West |
| 5 | 10 mph | West |
| North AHU Release | | |
| Ambient Temperature = 70°F | | |
| Leakage Severity = "Leaky" | | |
| Indoor Air Temperature = 72°F | | |

Figure 4.21 shows the scatter plot of decay coefficients for each room for the 10 mph north wind versus no wind cases. Each point represents the decay coefficient for one room. Notice that many of the points are near the origin of the plot. These points represent the rooms that were not affected by the tracer gas release. In this case, they represent the core and south zones that were not affected by the north AHU release. At this scale, the rooms that were impacted by the release appear to have decay coefficients that are fairly well clustered. Figure 4.22 zooms in on these decay coefficients to get a better view of the clustering. Figure 4.23 plots the decay coefficients for changing wind speed from 5 mph to 10 mph

for north wind. Figure 4.24 plots the decay coefficients for changing wind speed for west wind. Finally, Figure 4.25 plots the decay coefficients for changing wind direction from north to west at 10 mph. For all of these plots, there is one room that clearly acts differently than the others. This is room 129 Exit and its different behavior agrees with the previous results.

Figure 4.22 shows the results of adding wind at 10mph as against the no wind case. Compared to the conceptual situations mentioned above, this graph appears to be not HVAC dominated with multiple macro-zones. However, the scale of the plot is an important consideration. The changes in decay coefficient are fairly small. Thus, the situation is actually more HVAC dominated than not. Similar to the differences in the decay curves from Section 4.3.4 – 4.3.6, the resolution of decay coefficients that is significant depends on the circumstance of the problem. Other than room 129, there appears to be two or three clusters. The cluster with higher decay coefficients (more negative) includes rooms 113, 114, 115, 116, and 117 and the cluster with the lower decay coefficients includes rooms 111, 112, 118, and 119. Thus, the rooms that are directly impacted by the north wind decay faster. Within the upper cluster, the rooms in the same side of the building have decay coefficients that are closer together (i.e., rooms 111 and 112 are similar and rooms 118, and 119 are similar).

Figure 4.23 and Figure 4.24 both show the results of changing wind speed. In both cases, the rooms seem to be mostly HVAC dominated since the decay coefficients do not significantly change with wind speed. For Figure 4.23, other than the point for room 129 Exit, there appears to be two other clusters. These

results are almost identical to the results mentioned above for Figure 4.22. For Figure 4.24, other than the decay coefficient point for room 129 Exit, there appear to be three clusters. The cluster with higher decay coefficients are rooms 111, 112, and 113. The middle cluster includes rooms 118 and 119. The cluster with lower decay coefficients are rooms 114, 115, 116, and 117. Here again, the rooms that are directly impacted by the wind (i.e., rooms 111, 112, and 113) decay faster.

Figure 4.25 shows the effect of changing wind direction. As seen from the previous airflow analysis and tracer gas analysis, wind direction appears to be the most significant climatic condition. Figure 4.25 shows the highest scatter among the decay coefficient plots. Compared to the conceptual situations mentioned above, this graph points to a situation this not HVAC dominated with multiple macro-zones. Again, scale is an important consideration here. The lower left point (highest decay coefficient) is room 113. The lower right cluster includes rooms 111 and 112. The upper right cluster includes rooms 118 and 119. The upper left cluster includes rooms 114, 115, 116, and 117. The exterior rooms have a higher decay coefficient, and thus decay faster, when the wind is coming from the direction normal to their exterior wall. On Figure 4.25, room 113 is positioned as the highest decay coefficient in both cases because it has two exterior walls with different orientations and it is thus directly impacted by wind in both situations.

Figure 4.26 is a plot of decay curves for varying decay coefficients in the range of those that were found in the above analysis. The curves with a higher decay coefficient (more negative) result in faster concentration decay. Figure 4.27

and Figure 4.28 are plots of the $CO_2$ concentration decay for the two simulations whose decay coefficients comprise the scatter plot in Figure 4.25. It was not apparent whether or not these plots provide a physical justification for keeping rooms grouped together in the same macro-zone even though Figure 4.25 shows scatter.

### *4.3.8 Analysis of Results and Conclusions for Model Reduction of the Synthetic Building*

From this analysis, it can be concluded that this building is HVAC dominated rather than climate dominated. The $CO_2$ concentration curves in Figures 4.10 through 4.17 show similar room groupings even under different climatic conditions. It is noted however, that wind speed and wind velocity changes do result in slight variations in the concentration decay rate. The analysis of the decay coefficients in Figures 4.21 through 4.25 shows these variations very clearly. Rooms that are directly impacted by wind have faster concentration decay, which can be explained by the higher air change rates and lower time constants. Although there are slight variations, it again appears that the overall groupings remain the same. Also, although scatter plots of decay coefficients resemble a non-HVAC dominated situation, the scale of these graphs must be taken into consideration. The decay coefficients are close enough between the different situations that they are actually more HVAC dominated than not. Between the analysis of $CO_2$ concentration curves in Sections 4.3.2 through 4.3.6 and the decay coefficient analysis in Section 4.3.7, it seems that one could

confidently reduce the complexity of the model by grouping rooms into macro-zones.

Based on the $CO_2$ concentration curve analysis of Sections 4.3.2 through 4.3.6, it appears that the macro-zoning is dependent on the location of the contaminant release. If the goal of the analysis is to determine possible dosage impacts of a contaminant, then the forming of macro-zones is only important in the rooms that are affected by the release. For a release in an AHU, which was the main consideration of this analysis, the rooms affected were those served by the AHU and some adjacent rooms which received cross contamination. The amount of cross contamination that should be considered significant will depend on the situation. For the releases in the north AHU, Figure 4.10, Figure 4.14, and Figure 4.16 show two groupings of rooms with similar concentration decay curves. Based on these groupings there could be at least two macro-zones for the north AHU rooms. For the releases in the south AHU, Figure 4.11, Figure 4.15, and Figure 4.17 also show two groupings of rooms with similar concentration decay curves. Based on these groupings there could be at least three macro-zones for the south AHU rooms. For the core release shown in Figure 4.12, there appears to be several groupings. This can be attributed to the large variation in room sizes and HVAC airflows within the core zone. Based on these groupings of rooms there could be at least four macro-zones for the core AHU rooms. Table 4.8 provides a summary of these groupings of rooms with similar dynamics. Since the results of the airflow-based sensitivity analysis, the tracer gas simulations, and the decay coefficient calculations all revealed HVAC dominance of airflow dynamics, the

identified macro-zones were compared to room air changes. Table 4.9 shows this comparison by aligning the macro-zones with the air changes per hour in each room. It is clear that macro-zones are fairly well correlated to air changes per hour, after HVAC zoning is taken into account. Some slight deviations from a strictly air change rate determination of macro-zones may be attributed to the impact of exhaust fans and transfer grills in the bathrooms and the electrical room as well as varying leakage areas.

Table 4.8

*Macro-Zone Identification for the Synthetic Building*

| **Macro-Zone** | **Rooms** | **AHU** |
|---|---|---|
| 1 | 111, 112, 113, 114, 115, 116, 117, 118, 119 | North |
| 2 | 129 | |
| 3 | 101, 103, 104, 105, 106, 107, 109, 110 | South |
| 4 | 108 | |
| 5 | 102 | |
| 6 | 120, 127 | Core |
| 7 | 121, 123, 126 | |
| 8 | 122, 128 | |
| 9 | 124, 125 | |

Table 4.9

*Observed Macro-Zones and Room Air Change Rates*

| Macro-Zone | PCW Room Name | Volume | Supply Air Flow | Return Air Flow | Exhaust Air | Air Changes | HVAC |
|---|---|---|---|---|---|---|---|
| | | $ft^3$ | CFM | CFM | CFM | 1/hr | Zone |
| 1 | 111 Office | 900 | 150 | 135 | N/A | 10.00 | North |
| 1 | 112 Office | 900 | 150 | 135 | N/A | 10.00 | North |
| 1 | 113 Office | 1350 | 230 | 207 | N/A | 10.22 | North |
| 1 | 114 Office | 900 | 150 | 135 | N/A | 10.00 | North |
| 1 | 115 Office | 900 | 150 | 135 | N/A | 10.00 | North |
| 1 | 116 Office | 900 | 150 | 135 | N/A | 10.00 | North |
| 1 | 117 Office | 1350 | 230 | 198 | N/A | 10.22 | North |
| 1 | 118 Office | 900 | 160 | 144 | N/A | 10.67 | North |
| 1 | 119 Office | 900 | 160 | 144 | N/A | 10.67 | North |
| 2 | 129 Exit | 900 | 80 | 72 | N/A | 5.33 | North |
| 3 | 101 Office | 900 | 160 | 144 | N/A | 10.67 | South |
| 3 | 103 Recep. | 1800 | 300 | 270 | N/A | 10.00 | South |
| 3 | 109 Office | 900 | 150 | 135 | N/A | 10.00 | South |
| 3 | 110 Office | 900 | 150 | 135 | N/A | 10.00 | South |
| 3 | 104 Office | 900 | 160 | 144 | N/A | 10.67 | South |
| 3 | 105 Office | 900 | 160 | 144 | N/A | 10.67 | South |
| 3 | 106 Office | 900 | 160 | 144 | N/A | 10.67 | South |
| 3 | 107 Office | 900 | 160 | 144 | N/A | 10.67 | South |
| 4 | 108 Office | 1350 | 320 | 288 | N/A | 14.22 | South |
| 5 | 102 Elec. | 450 | N/A | N/A | 30 | 4.00 | South |
| 6 | 120 Corr. | 3024 | 380 | 180 | N/A | 7.54 | Core |
| 6 | 127 Confr. | 1800 | 300 | 270 | N/A | 10.00 | Core |
| 7 | 121 Corr. | 2304 | 180 | 135 | N/A | 4.69 | Core |
| 7 | 123 Corr. | 2304 | 150 | 135 | N/A | 3.91 | Core |
| 7 | 126 Strg./Mech. | 1800 | 140 | 126 | N/A | 4.67 | Core |
| 8 | 122 Corr. | 3024 | 200 | 180 | N/A | 3.97 | Core |
| 8 | 128 Kitch. | 1512 | 100 | 90 | N/A | 3.97 | Core |
| 9 | 124 Lav. | 756 | N/A | N/A | 90 | 7.14 | Core |
| 9 | 125 Lav. | 756 | N/A | N/A | 90 | 7.14 | Core |

If geometry is an important factor, these groupings need to be further separated by analyzing the proximity of rooms with similar dynamics, before the final macro-zones are identified. Table 4.10 shows the further separation of macro-zones once geometry was taken into account.

Table 4.10

*Macro-Zone Identification for Synthetic Building Considering Floor Plan Geometry*

| Macro-Zone | Rooms | AHU |
|---|---|---|
| 1 | 111, 112, 113 | North |
| 2 | 129 | North |
| 3 | 114, 115, 116, 117, 118, 119 | North |
| 4 | 101, 103 | South |
| 5 | 102 | N/A |
| 6 | 104, 105, 106, 107 | South |
| 7 | 108 | South |
| 8 | 109, 110 | South |
| 9 | 120, 127 | Core |
| 10 | 121 | Core |
| 11 | 123 | Core |
| 12 | 126 | Core |
| 13 | 122, 128 | Core |
| 14 | 124, 125 | N/A |

This analysis has reduced the building of 29 rooms to at least 9 macro-zones. It is also noted that the effect of wind direction does have an impact on the individual decay coefficients of each room as well as the magnitude of cross contamination with adjacent spaces during a specific release. However, the overall macro-zone groupings do not change. The question of whether or not these variations in decay coefficients and cross contamination levels are significant is dependent upon the situation (i.e., the toxicity of the contaminant and the uncertainty in the $CO_2$ measurements).

The decay coefficient analysis of Section 4.3.7 showed how wind velocity and wind speed impact the $CO_2$ concentration decay of individual rooms. Depending on the scale at which the difference in decay coefficients becomes

significant, this analysis could result in increasing the model complexity by separating the previously identified 9 macro-zones into a larger number of macro-zones. Table 4.9 shows that the identified macro-zones are directly correlated to room air change rates. The apparent HVAC dominance of the airflow dynamics and tracer gas behavior indicates that room air changes may be the most important factor to tune in the multi-zone model to improve prediction accuracy.

It should be noted that the types of plots that were generated in this analysis (airflow scatter plots, $CO_2$ decay curves for individual rooms, and decay coefficient scatter plots) all have the same problem of point identification. For the scatter plots, it is a tedious task to determine which point corresponds to which flow path or room. For the $CO_2$ decay curves, it is difficult to determine which rooms have overlapping curves. This problem is exacerbated as the number of rooms increase and could pose potential problems for the analysis of larger buildings.

The next step in our general methodology is model tuning and calibration. This step was not performed on the synthetic building because the process of perturbing flow coefficient values, HVAC flow magnitudes, and other model parameters of a synthetic building to mimic a "real" building is very arbitrary, and would not lead to a meaningful evaluation. The calibration step is only meaningful when trying to tune and calibrate a model of a real building with real building data.

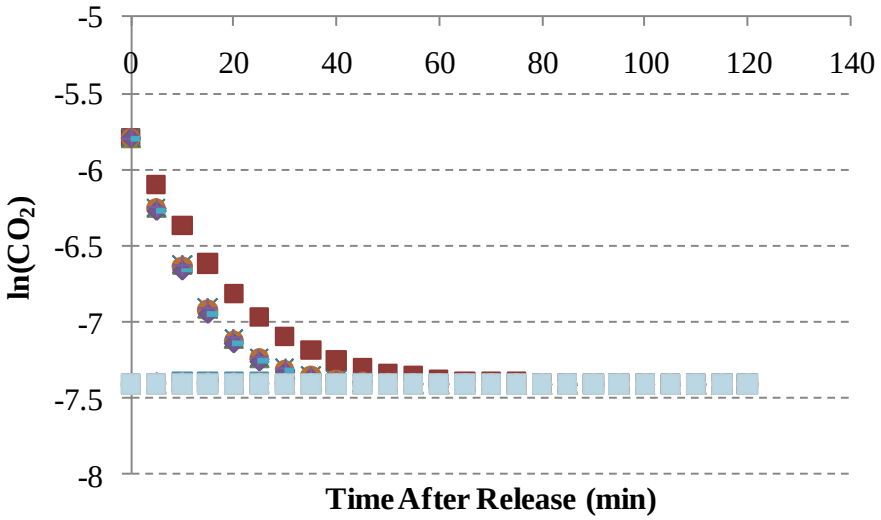


*Figure 4.18*: Tracer Gas Decay After Natural Log Transformation

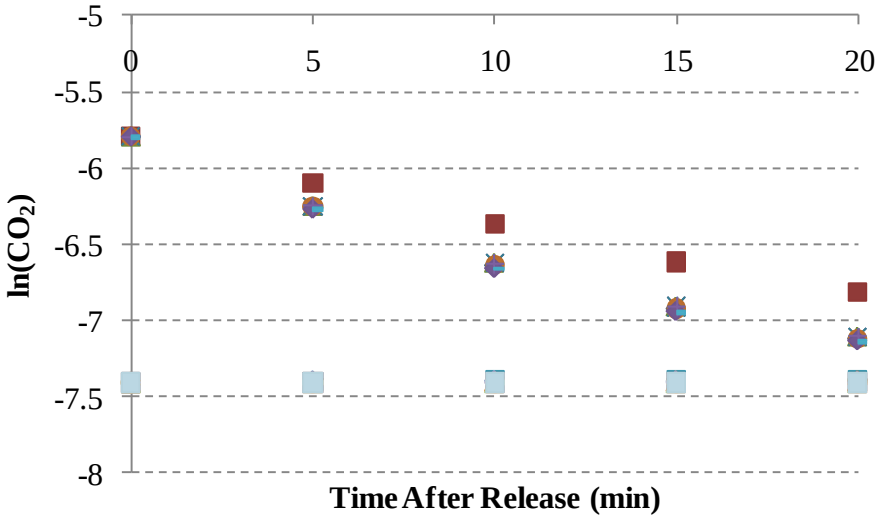


*Figure 4.19*: Tracer Gas Decay After Natural Log Transformation for the First 20 Minutes

*Figure 4.20*: Conceptual Plots of Decay Coefficients

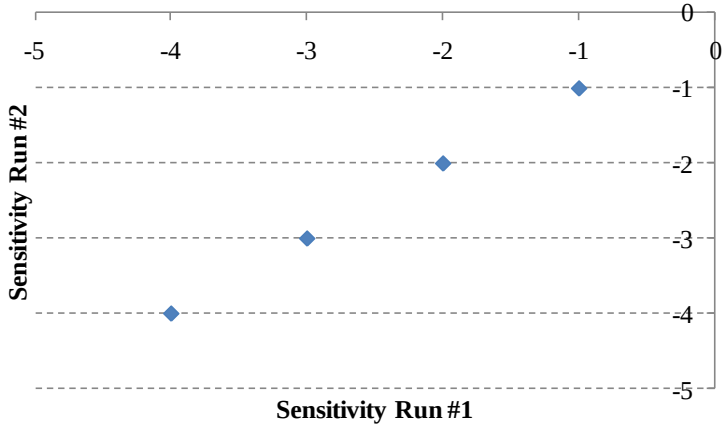


(a) Multiple Macro-Zones – HVAC Dominated

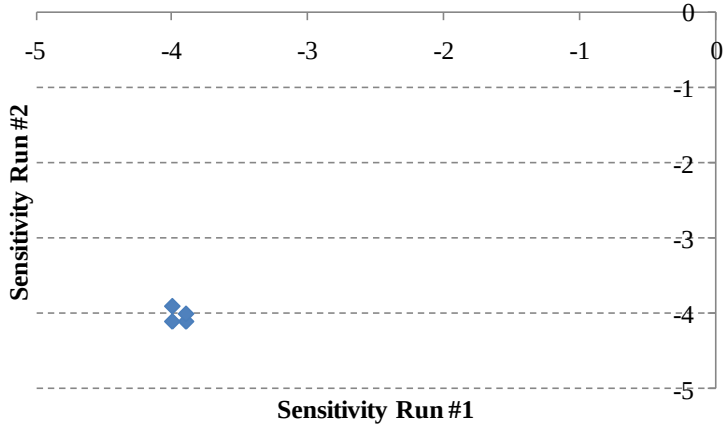


(b) One Macro-Zone – HVAC Dominated

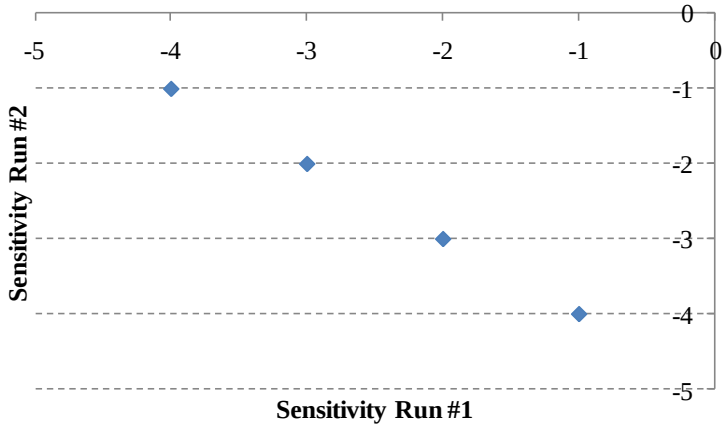


(c) Multiple Macro-Zones – Not HVAC Dominated

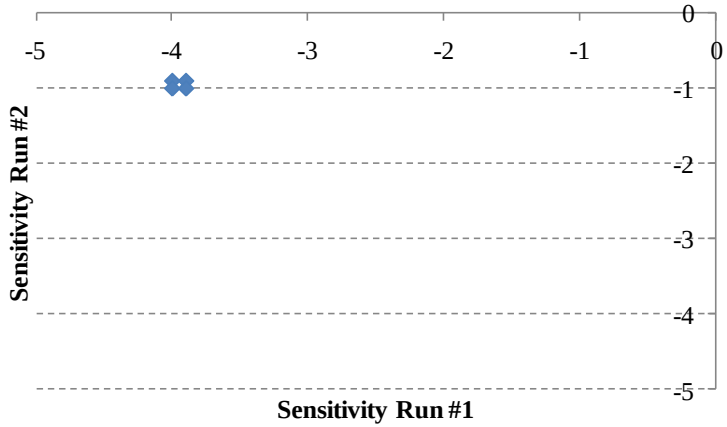


(d) One Macro-Zone – Not HVAC Dominated

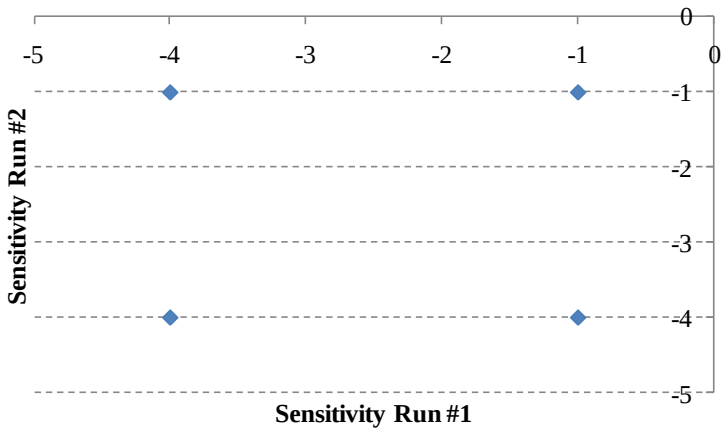


(e) Some Zones HVAC Dominated and Some Zones Not HVAC Dominated

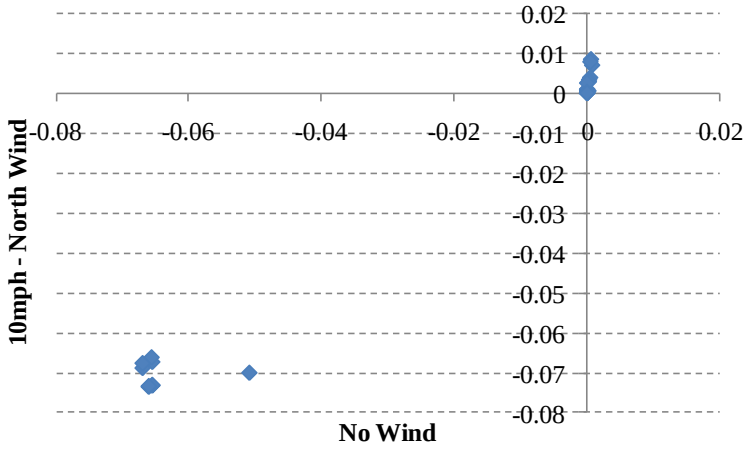


*Figure 4.21*: The Effect of Wind on Decay Coefficients

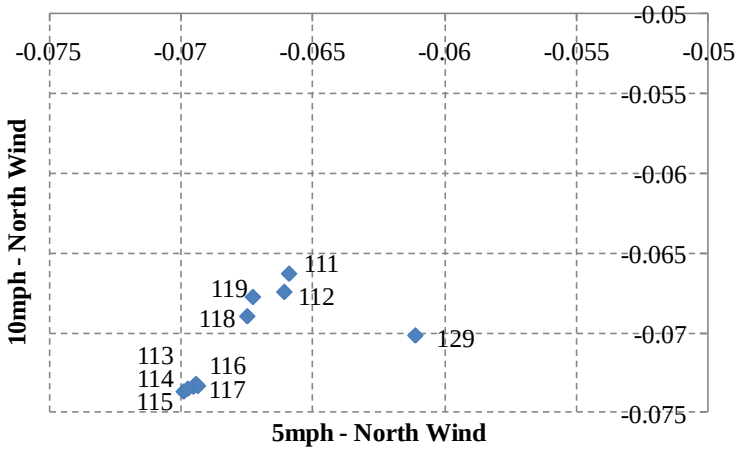


*Figure 4.23*: The Effect of Wind Velocity (North Wind) on Decay Coefficients

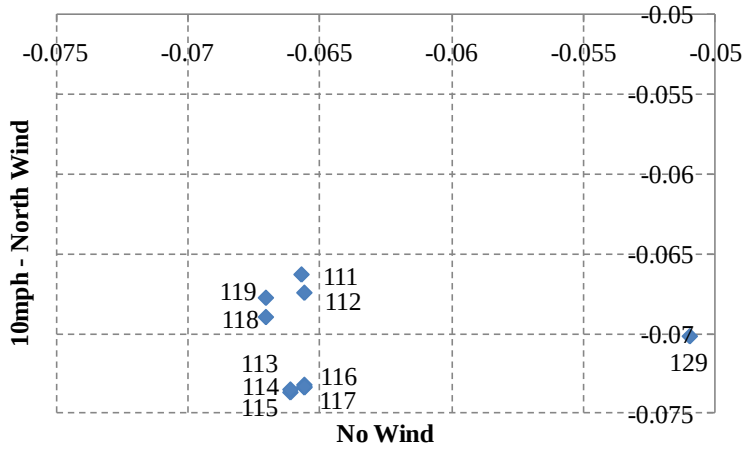


*Figure 4.22*: The Effect of Wind on Decay Coefficients (Enlarged Plot)

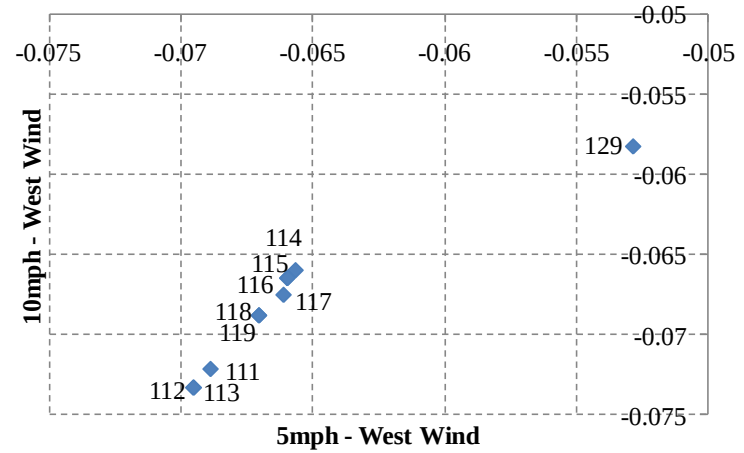


*Figure 4.24*: The Effect of Wind Velocity (West Wind) on Decay Coefficients

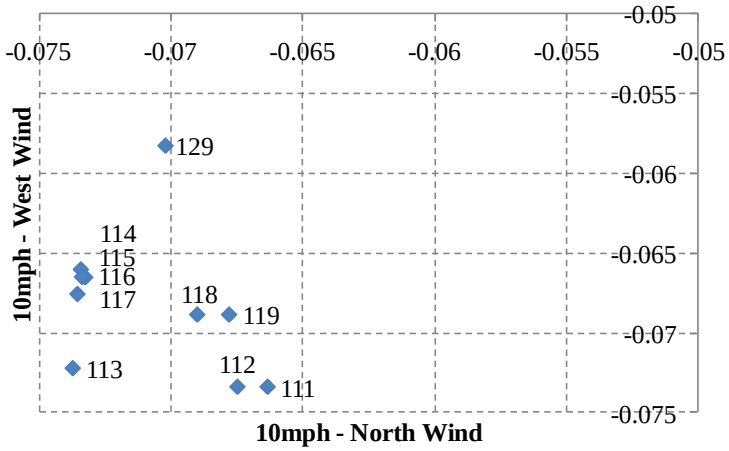


*Figure 4.25*: The Effect of Wind Direction on Decay Coefficients

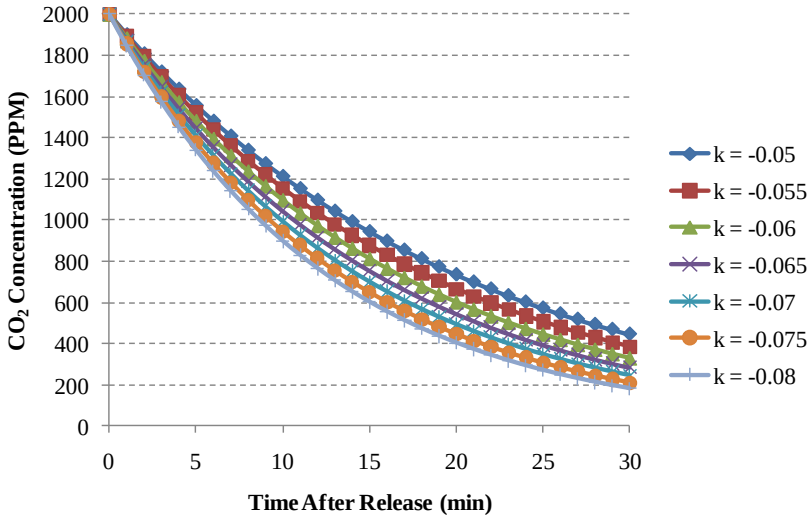


*Figure 4.26*: $CO_2$ Concentration Curves for Various Decay Coefficients

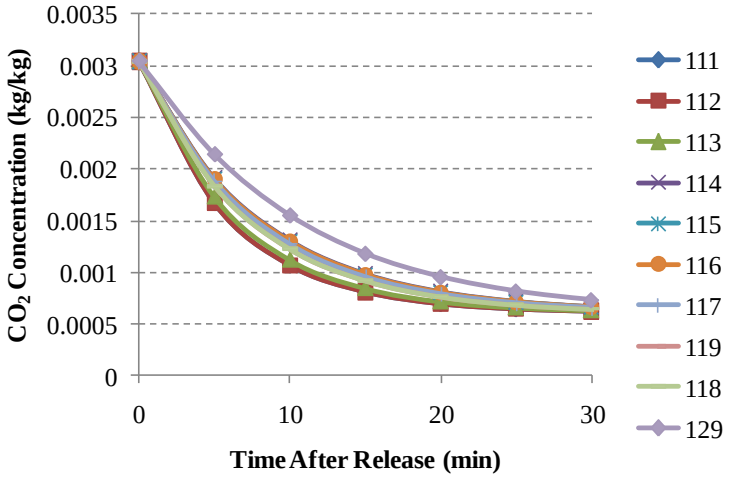


*Figure 4.27*: $CO_2$ Concentration Curves for 10 mph West Wind - North AHU Release

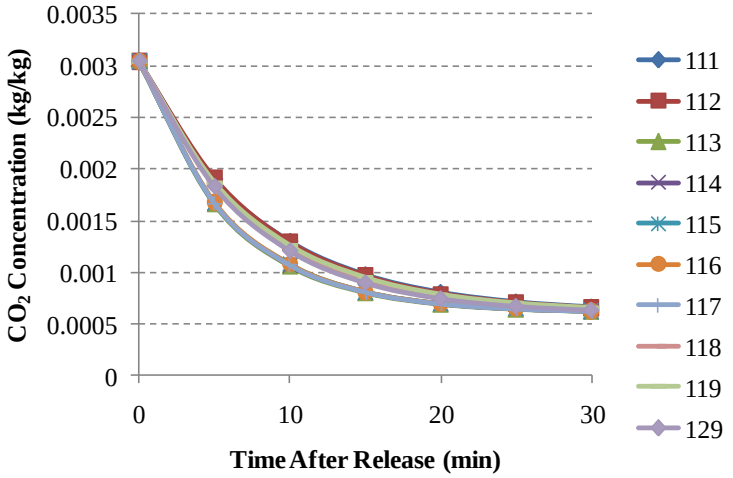


*Figure 4.28*: $CO_2$ Concentration Curves for 10 mph North Wind – North AHU Release

# CHAPTER 5: APPLICATION OF PROPOSED CALIBRATION METHODOLOGY TO A REAL BUILDING

## 5.1 Introduction

After evaluating the first few steps of the proposed methodology with a synthetic building model, it was apparent that the model calibration step needed to be conducted on a real building model with measured $CO_2$ data. Since calibration requires real building data, the MBNA building on PSU's campus was selected for which measured $CO_2$ data and measured airflow directions were available from the field testing performed by Sae Kow (2010). Also obtained for use in this research was a PCW model of the MBNA building that was developed and tuned by Sae Kow (2010). The tuning was done following the PSU methodology proposed by Firrantello (2007) involving measured HVAC flows (i.e., main and branch flows, supply diffuser flows, return grille flows) as well as inter-zonal airflow directions. The procedure being developed in this research starts where the previous PSU tuning approach left off but intends to improve the calibration by explicitly using measured $CO_2$ data.

The MBNA building is a three story, 44,000 $ft^2$ office and administration building on the PSU campus. The building is served by three variable air volume (VAV) air handling units. Two of the AHUs (AHU1 and AHU2) are located in an unconditioned basement. The third AHU (AHU3) is located in a mechanical room on the third floor of the building. AHU1 serves conference rooms on the first floor. AHU2 serves the rest of the first floor and the entire second floor. AHU3

serves the entire 3rd floor. The terminal units are VAV boxes with reheat coils and the building has a mixture of plenum and ducted returns. Refer to Table 5.1 for room names, areas, and HVAC airflows. Figure 5.1 provides a floor plan of the MBNA building.

In order to properly and completely analyze the proposed methodology, it would be ideal to have real $CO_2$ data for all rooms in a building or for at least one room in each identified macro-zone. For this research, however, the available $CO_2$ data was limited to the data that had been collected earlier by Firrantello (2007) and Sae Kow (2010). Firrantello (2007) only measured $CO_2$ concentrations in the main return duct of each AHU in the MBNA building. No zone level measurements were collected. Sae Kow (2010) initially added only two zone level measurements (a room on the second floor and a room on the third floor) to the same return duct measurements. In subsequent testing, however, Sae Kow (2010) focused on just the third floor of the MBNA building and collected $CO_2$ data for seven locations (AHU return duct and six rooms). The details of this field testing were discussed in Section 2.2.2.7.

The results presented by both Firrantello (2007) and Sae Kow (2010) revealed that the tracer gas releases on the third floor of the MBNA building in AHU3 resulted in no cross-contamination to the floors below. In other words, the third floor zones could be considered as isolated from all other building zones, and hence can be treated as a separate building by itself in the event of a release in AHU3. Therefore, airflow from the third floor to the second floor below via cracks, stairwells, the elevator shaft, etc. can be assumed to be negligible. It was

for this reason that Sae Kow (2010) chose to focus solely on the third floor for subsequent testing. For evaluating the proposed methodology in this research, the third floor of the MBNA building was also selected. All releases were performed in AHU3 and the $CO_2$ data collected by Sae Kow (2010) was used as the basis for calibration. Refer to Table 5.1 for room names, areas, and volumes and refer to Table 5.2 for HVAC airflows. Figure 5.1 shows a floor plan of the third floor of the MBNA building. In Table 5.2, the design HVAC airflows are those which appear on the mechanical design drawings for the MBNA building. The initially tuned HVAC flows are the values measured during field testing by Sae Kow (2010) using a flow hood. The measured HVAC airflows show that the third floor is served with approximately 1 CFM/$ft^2$ of supply air under constant air volume operation.

Table 5.1

*MBNA Building Third Floor Room Information*

| Room Name | PCW File Name | Area ($ft^2$) | Volume ($ft^3$) |
|---|---|---|---|
| Meeting 301/312 | Conference | 158 | 1392 |
| Server 303/311 | Zone_1 | 132 | 1159 |
| Programmer 304/309 | Zone_2 | 124 | 1091 |
| Staff. Asst. 305/307 | Zone_3 (Intern) | 171 | 1500 |
| Staff Lounge 307/305 | Zone_4 | 186 | 1637 |
| Mechanical 308/M305 | M305 | 220 | 1936 |
| Men M3/R301 | Zone_5 | 95 | 832 |
| Meeting 318/301 | 301 | 618 | 5436 |
| Women W3/R315 | Zone_6 | 144 | 1271 |
| Counselor 320/318 | 318 | 144 | 1241 |
| Counselor 321/319 | Zone_7 | 138 | 1213 |
| Counselor 322/322 | 322 | 138 | 1213 |
| Counselor 323/323 | Zone_9 | 138 | 1213 |
| Counselor 324/326 | Zone_10 | 138 | 1213 |
| Counselor 325/327 | 327 | 138 | 1213 |
| Stair S2/2301 | Zone_12 | 144 | 1267 |
| Elevator E1/V301 | Zone_13 | 58 | 508 |
| Lobby 333/F301, Reception 316/302, Lounge 331/328, Corridor 309/0301 | F301 | 2743 | 24134 |
| Programmer 302/313 | 313 | 77 | 678 |
| Stair S1/Z302 | Z302 | 216 | 1901 |
| Director 310/310 | Zone_14 | 236 | 2077 |
| Work Room 311/308 | Zone_15 | 1440 | 1267 |
| Admin. Asst. 312/306 | Zone_16 | 184 | 1619 |
| Resource 313/304 | Computer | 212 | 1866 |
| L.S. Coord. 319/316 | Resource | 132 | 1159 |
| Counselor 326/317 | Zone_19 | 132 | 1159 |
| Counselor 327/320 | Zone_20 | 132 | 1159 |
| Counselor 328/321 | Zone_21 | 132 | 1159 |
| Counselor 329/324 | Zone_22 | 132 | 1159 |
| Counselor 330/325 | Zone_23 | 132 | 1159 |
| Stair S3/Z304 | Zone_24 | 156 | 1374 |
| P.T. Staff 317/314 | Zone_25 | 110 | 970 |
| Copy Room 315/303 | Zone_26 | 168 | 1478 |
| **Total** | | **9215** | **69650** |

Table 5.2

*Design and Measured HVAC Airflows for the MBNA Building Third Floor*

| PCW File Name | Design | | PSU Tuned Model | | Supply |
|---|---|---|---|---|---|
| | Supply Air Flow (CFM) | Return Air Flow (CFM) | Supply Air Flow (CFM) | Return Air Flow (CFM) | CFM/sf |
| Conference | 330 | 330 | 180 | 137 | 1.14 |
| Zone_1 | 100 | 100 | 70 | 63 | 0.53 |
| Zone_2 | 180 | 180 | 139 | 110 | 1.12 |
| Zone_3 (Intern) | 230 | 230 | 148 | 121 | 0.87 |
| Zone_4 | 580 | 580 | 420 | 246 | 2.26 |
| M305 | N/A | N/A | N/A | N/A | N/A |
| Zone_5 | 120 | N/A | 85 | N/A | 0.90 |
| 301 | 690 | 690 | 570 | 393 | 0.92 |
| Zone_6 | 160 | N/A | 118 | N/A | 0.82 |
| 318 | 180 | 180 | 130 | 96 | 0.90 |
| Zone_7 | 180 | 180 | 116 | 96 | 0.84 |
| 322 | 180 | 180 | 107 | 93 | 0.78 |
| Zone_9 | 180 | 180 | 118 | 76 | 0.86 |
| Zone_10 | 180 | 180 | 115 | 52 | 0.83 |
| 327 | 300 | 300 | 95 | 41 | 0.69 |
| Zone_12 | N/A | N/A | N/A | N/A | N/A |
| Zone_13 | N/A | N/A | N/A | N/A | N/A |
| F301 | 2450 | 2450 | 1095 | 920 | 0.40 |
| 313 | 190 | 190 | 121 | 80 | 1.57 |
| Z302 | 50 | N/A | 44 | N/A | 0.20 |
| Zone_14 | 260 | 260 | 167 | 141 | 0.71 |
| Zone_15 | 180 | 180 | 110 | 106 | 0.08 |
| Zone_16 | 210 | 210 | 124 | 126 | 0.67 |
| Computer | 400 | 400 | 256 | 192 | 1.21 |
| Resource | 190 | 190 | 132 | 96 | 1.00 |
| Zone_19 | 190 | 190 | 171 | 100 | 1.30 |
| Zone_20 | 190 | 190 | 173 | 101 | 1.31 |
| Zone_21 | 190 | 190 | 166 | 101 | 1.26 |
| Zone_22 | 190 | 190 | 166 | 85 | 1.26 |
| Zone_23 | 190 | 190 | 158 | 74 | 1.20 |
| Zone_24 | 50 | N/A | 44 | N/A | 0.28 |
| Zone_25 | 190 | 190 | 109 | 101 | 0.99 |
| Zone_26 | 380 | 380 | 225 | 191 | 1.34 |
| **Total** | **9090** | **8710** | **5672** | **3938** | **0.94** |

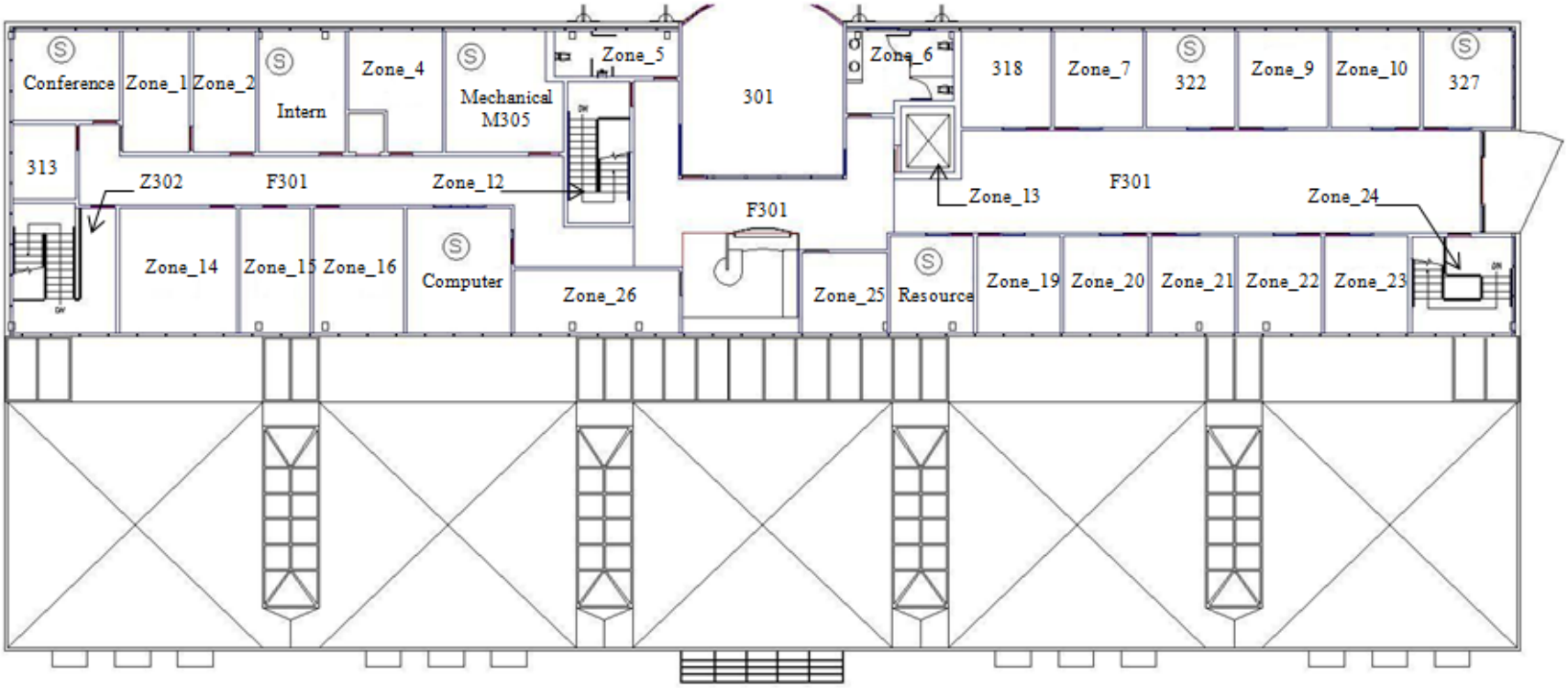


*Figure 5.1*: MBNA Third Floor Plan with PCW Zone Designations

## 5.2 Airflow-Based Sensitivity Analysis for Real Building

To reiterate the work done previously on the synthetic building, the objectives of the airflow-based sensitivity analysis were to: (i) evaluate whether the airflow dynamics of the building are climate or HVAC dominated, (ii) identify the significant or influential drivers of the airflow dynamics, and (iii) assist with reducing the model complexity by identifying macro-zones. From the synthetic building testing, it was discovered that the use of scatter plots provided the best way to visualize the results of the sensitivity analysis. Therefore, in this analysis only scatter plots were generated and studied. A full factorial analysis was used to set up the simulation runs. Since the effects of various factors are only visualized by scatter plots, this is not a formal quantitative sensitivity analysis where all the effects (main and interaction) are calculated with respect to some response variable. This is in part due to the lack of a robust response variable and the inability to have an estimate of error from deterministic simulations (as discussed in Appendix B).

### *5.2.1 Airflow-Based Sensitivity Analysis Methodology*

1. Identify influential drivers of the building airflow dynamics (e.g., climatic and operating parameters). These will most likely include ambient air temperature, wind direction with respect to the orientation of the building, wind velocity, building leakage severity, and HVAC system airflow rates.
2. Identify characteristic values representative of low and high values for each parameter.

3. Perform a $2^k$ full factorial analysis assuming that the relationships between effects and factor levels are linear.
4. Graphically evaluate the results of the sensitivity analysis using scatter plots.
5. If the building is found to be climate dominated (which most mechanically heated, cooled, and ventilated buildings are not), further research is needed. This was deemed outside the scope of this research and left to a future study.

### *5.2.2 Data Generation*

Another conclusion drawn from analyzing the synthetic building was that wind speed, wind direction, and leakage severity seem to be influential drivers of the airflow dynamics under constant air volume operating conditions. Ambient temperature, on the other hand, appeared to have only small effects. For the analysis of the real building, all four of these variables were analyzed. As discovered from the synthetic building, since the relationships between the effects and the factor levels seem to be linear, the $3^4$ full factorial was reduced to a $2^4$ full factorial which only requires 16 simulations.

The 16 simulations were performed on the PCW model of the third floor of the MBNA building for which preliminary tuning was already performed by Sae Kow (2010). Therefore, the model was already tuned with measured HVAC airflow rates and airflow directions and the first step of the calibration methodology has thus already been completed. The 16 sensitivity analysis simulations included the combinations of two wind speeds (0 mph and 10 mph),

two wind directions (north and northwest), two ambient temperatures (19°F and 67°F), and two of the default leakage settings in PCW ("leaky" and "tight"). Refer to Table 5.3 for the summary of these simulations. This sensitivity analysis did not include the effect of mechanical ventilation airflow rate which was assumed to be held constant at approximately 1 CFM/ft$^2$ of supply air. Refer to Table 5.2 for the HVAC airflow rates. The interior temperature remained the same for each simulation (at 72°F) and the terrain condition was also unaltered ("Large obstruction within 40-100 feet"). Each simulation was performed as a steady state airflow simulation, and thus airflow magnitudes and directions do not change with time. No tracer gas release was simulated for this part of the analysis.

Table 5.3

*Real Building Airflow-Based Sensitivity Analysis Summary*

| **Wind Direction** | **Wind Speed (mph)** | **Ambient Temperature (°F)** | |
|---|---|---|---|
| | | 19°F | 67°F |
| North | 0 | Leaky | Leaky |
| | | Tight | Tight |
| | 10 | Leaky | Leaky |
| | | Tight | Tight |
| Northwest | 0 | Leaky | Leaky |
| | | Tight | Tight |
| | 10 | Leaky | Leaky |
| | | Tight | Tight |
| Indoor Air Temperature = 72°F | | | |

The values of the weather variables used in this sensitivity analysis were not arbitrarily selected. Rather, they were determined by using the climate analysis software program Climate Consultant (version 4.0) developed by the University of California, Los Angeles (http://www.energy-design-

tools.aud.ucla.edu). The Climate Consultant program uses the weather files from the EnergyPlus detailed building energy simulation software (http://apps1.eere.energy.gov/buildings/energyplus/cfm/weather_data.cfm) and uses powerful its graphical techniques to display the data. The weather file for "State College – Penn State Campus" was downloaded and analyzed. Rather than selecting the extremes in the range of the dry-bulb temperature, the inter-quartile range values were deemed more realistic. Thus for ambient temperatures, the 25$^{th}$ and 75$^{th}$ percentiles of the annual range were 19°F and 67°F respectively. See Figure 5.2 for the ambient temperature ranges by month. For wind speed, the low value of 0 mph was selected to represent the extreme condition of no wind. The high value of 10 mph was selected as approximately the 75$^{th}$ percentile of the annual average wind speeds. See Figure 5.3 for the wind velocity range. The "wind wheel" in Figure 5.4 was used to select the two wind directions. Clearly, the predominant wind direction is from the northwest. This also happens to be the direction that wind was measured during the $CO_2$ testing performed by Sae Kow (2010). The next most frequent direction is from the west. However, wind from the north was chosen to be analyzed instead. This decision was because of the orientation of the building with respect to its rectangular shape. Plan north is parallel to the cardinal direction north in Figure 5.1. It can be seen that the north façade is longer than the west façade. It is logical to assume that wind striking a larger façade will have a more significant effect on building airflow dynamics than wind striking a smaller façade. Therefore, the second wind direction was

chosen to be north rather than west. The leakage severities of "leaky" and "tight" were selected to represent the extreme cases.

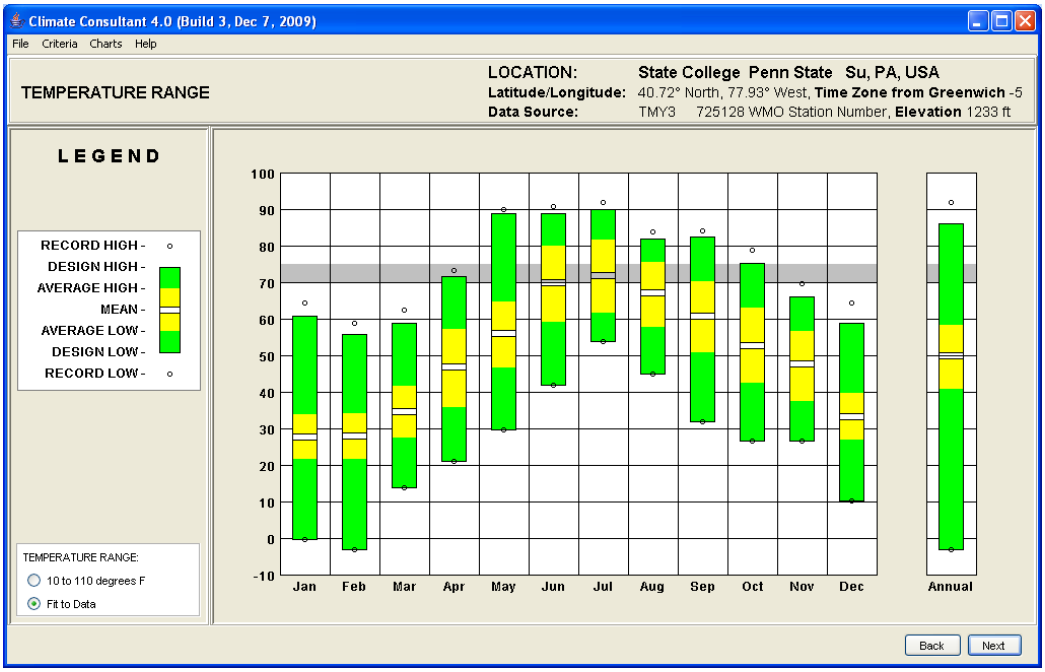


*Figure 5.2*: Temperature Range of State College, PA as Displayed by Climate Consultant Software Using Typical Meteorological Year Data

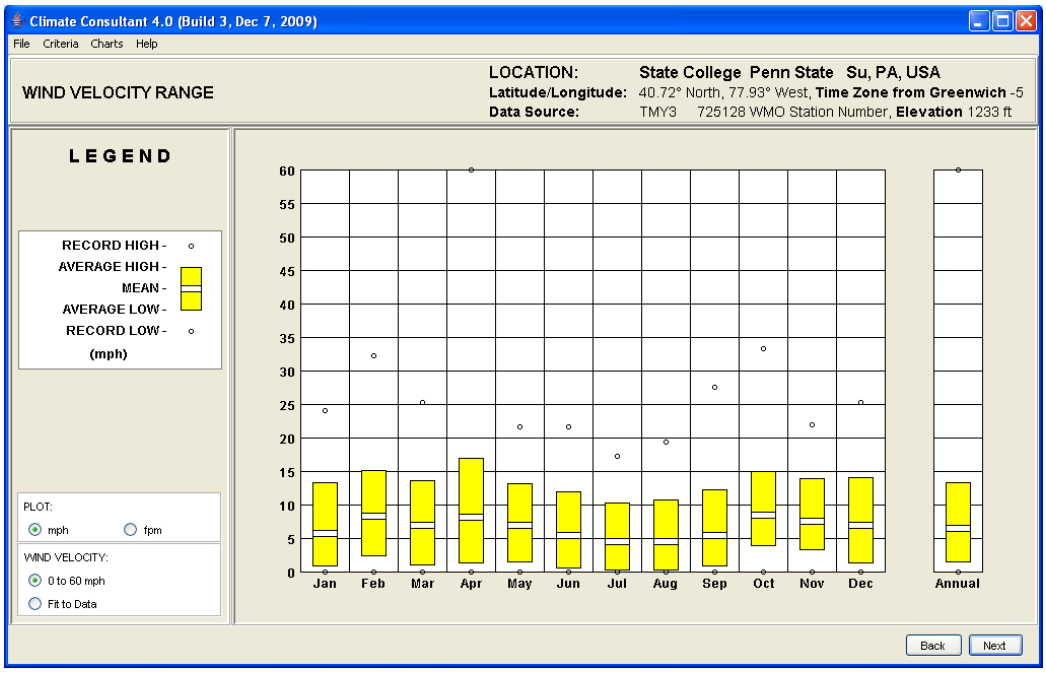


*Figure 5.3*: Wind Velocity Range of State College, PA as Displayed by Climate Consultant Software Using Typical Meteorological Year Data

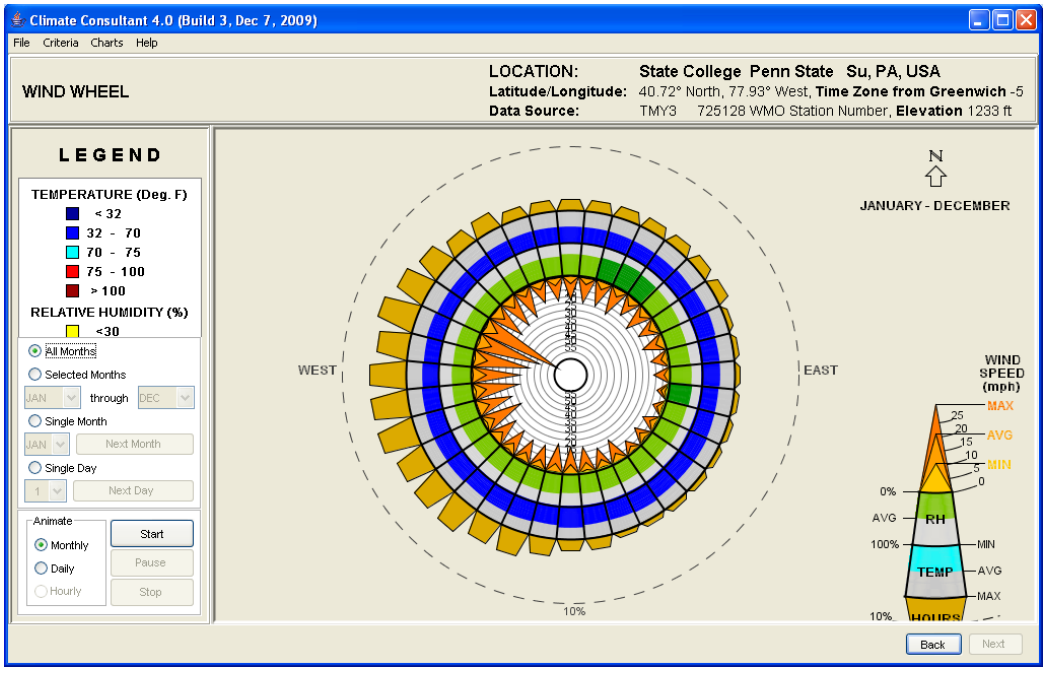


*Figure 5.4*: Wind Wheel for State College, PA as Displayed by Climate Consultant Software Using Typical Meteorological Year Data

### *5.2.3 Data Analysis*

Once the PCW simulations were performed, the next step was to display the information gathered in scatter plots for convenient interpretation of the results. Using the same format as with the synthetic building, each scatter plot contains the information for two scenarios, one on each axis. With 16 simulations, this yields 8 scatter plots. However, since the low value for wind speed is 0 mph, there were some repetitive simulations. For example, simulations with 0 mph and north wind will be the same as 0 mph and northwest wind. Thus, the 8 scatter plots generated do not include all 16 sets of data but do contain all the necessary sensitivity information. The data sets were selected so that the effects of each variable could be clearly seen in the data scatter. Each scatter plot compares the airflow magnitudes and directions of two different scenarios with only one different condition. The unit on each axis is the volumetric flow rate in cubic feet per minute (CFM). The direction of airflow is accounted for in the sign convention. Each point in the scatter plot represents a single airflow path. The various scatter plots generated are summarized in Table 5.4.

Table 5.4

*Real Building Airflow-Based Sensitivity Analysis Scatter Plot Summary*

| Figure | Description | X-Axis Scenario | Y-Axis Scenario |
|---|---|---|---|
| **5.5** | Effect of temperature at high wind and "leaky" | 19°F, 10mph, NW, Leaky | 67°F, 10mph, NW, Leaky |
| **5.6** | Effect of temperature at high wind and "tight" | 19°F, 10mph, NW, Tight | 67°F, 10mph, NW, Tight |
| **5.7** | Effect of wind speed at "leaky" | 67°F, 0mph, NW, Leaky | 67°F, 10mph, NW, Leaky |
| **5.8** | Effect of wind speed at "tight" | 67°F, 0mph, NW, Tight | 67°F, 10mph, NW, Tight |
| **5.9** | Effect of wind direction at high wind and "leaky" | 67°F, 10mph, N, Leaky | 67°F, 10mph, NW, Leaky |
| **5.10** | Effect of wind direction at high wind and "tight" | 67°F, 10mph, N, Tight | 67°F, 10mph, NW, Tight |
| **5.11** | Effect of leakage severity at high north wind | 19°F, 10mph, N, Tight | 19°F, 10mph, N, Leaky |
| **5.12** | Effect of leakage severity at high northwest wind | 19°F, 10mph, NW, Tight | 19°F, 10mph, NW, Leaky |

The sensitivity analysis scatter plots, summarized in Table 5.4, illuminate the numerical results of the sensitivity analysis; namely, how varying the operating conditions impact the magnitude and direction of building airflows. As discussed for the synthetic building, recall that points which fall within the positive/positive and negative/negative quadrants of the scatter plot imply that altering the operating condition will not result in a change in the airflow direction of those particular airflow paths. On the other hand, points that fall within the positive/negative and negative/positive quadrants indicate that the altered condition did change the airflow direction in those airflow paths. Points that fall on the “y = x” line indicate that the altering the operating condition did not change the magnitude of airflow through those airflow paths. Points that fall off of this line indicate that the altered condition did change the airflow magnitude.

As was concluded from the synthetic building evaluation, these scatter plots are inadequate for determining macro-zones for the purpose of model reduction.

### *5.2.4 Airflow-Based Sensitivity Analysis Conclusions*

Compared to the synthetic building, the MBNA building airflows appear to be much more influenced by HVAC operation. Most of the sensitivity scatter plots show an approximately "y=x" relationship indicating that neither airflow magnitudes nor directions were impacted with the changing conditions. This is especially true when the leakage severity is "tight". Under this condition, the HVAC flows seem to completely dictate the airflow dynamics within the building. As expected, the effect of ambient air temperature was very small on the airflow dynamics even under the "leaky" condition. Wind speed and wind direction again appear to be significant influences since they result in changes in airflow magnitudes and even directions in some cases. The last two scatter plots, Figure 5.11 and Figure 5.12 show that changing the leakage severity from "tight" to "leaky" increased the magnitude of many of the airflows. These graphs are somewhat repetitive since the previous graphs also show the effects of leakage severity. This can be seen, for example, by comparing Figure 5.5 and Figure 5.6. However, Figure 5.11 and Figure 5.12 allow for easier interpretation.

These results, which are consistent with those of the synthetic building, indicate that after HVAC airflows, wind velocity and wind direction are the most significant drivers of the building's airflow dynamics. However, their significance is a function of the leakage severity of the building. The tighter the building, the less influential these external drivers become. These conclusions reiterate the fact

that buildings of this size which are mechanically ventilated are likely to have airflow dynamics dominated by the HVAC system. Again it is important to note that the magnitudes of airflows through the envelope and between interior zones that are significant depend on the situation, i.e. the type of contaminant analyzed and the resulting occupant exposure. Thus, the practical significance of the scatter in Figures 5.5 through 5.12 will be case specific.

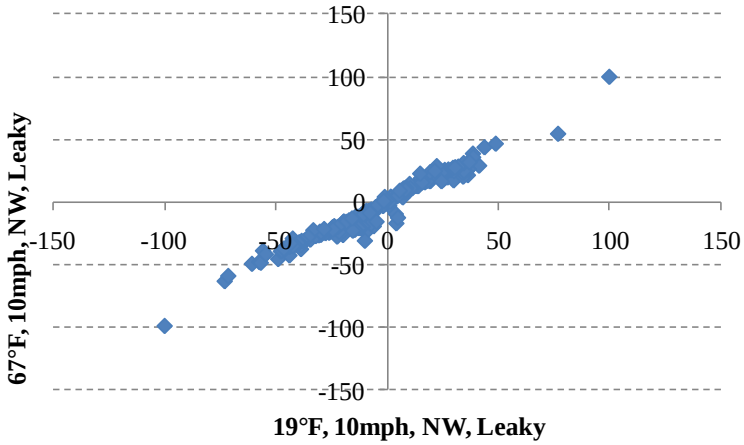


*Figure 5.5*: Effect of Temperature at High Wind and "Leaky"

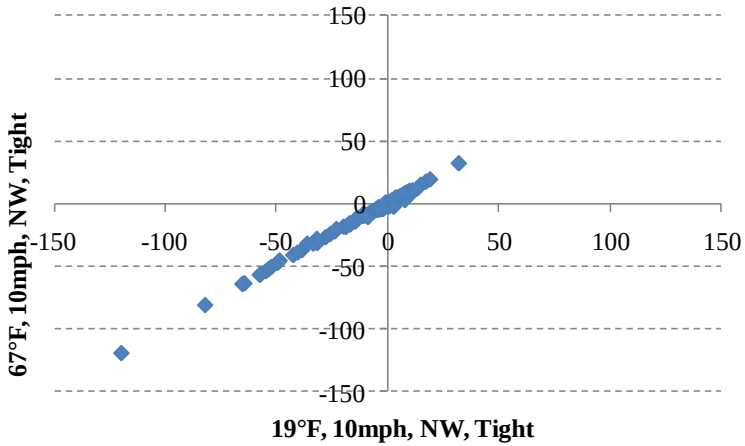


*Figure 5.6*: Effect of Temperature at High Wind and "Tight"

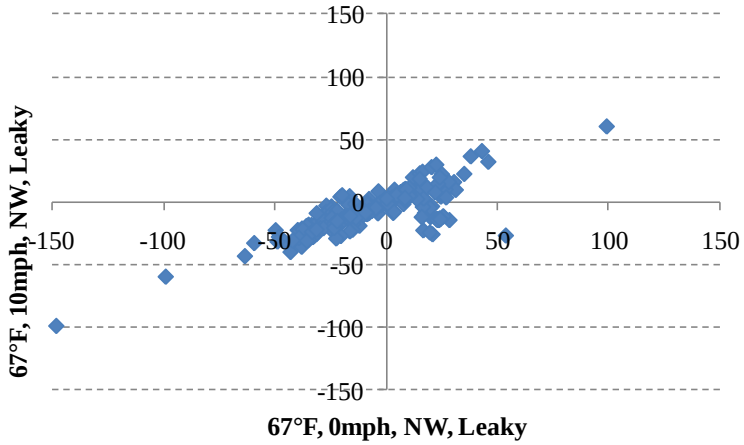


*Figure 5.7*: Effect of Wind Speed at "Leaky"

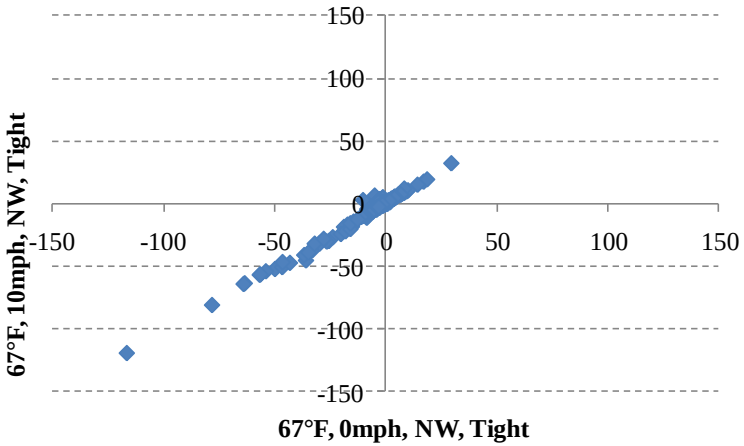


*Figure 5.8*: Effect of Wind Speed at "Tight"

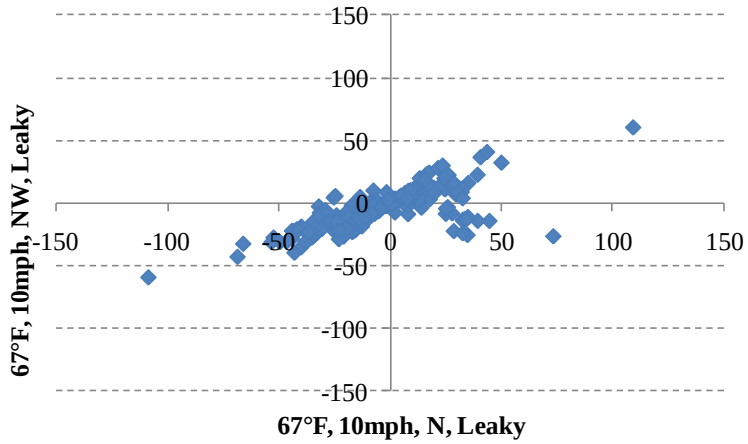


*Figure 5.9*: Effect of Wind Direction (45° Change) at "Leaky"

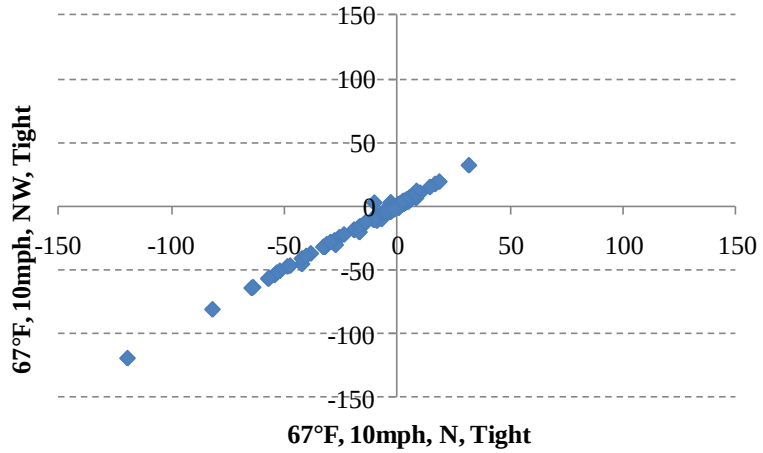


*Figure 5.10*: Effect of Wind Direction (45° Change) at "Tight"

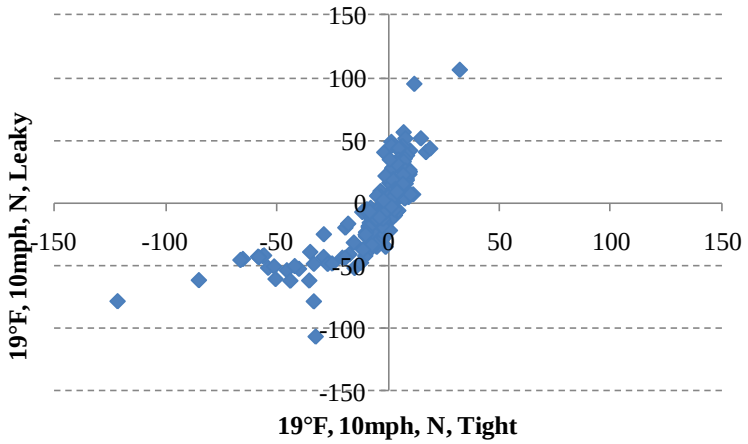


*Figure 5.11*: Effect of Leakage Severity at North Wind

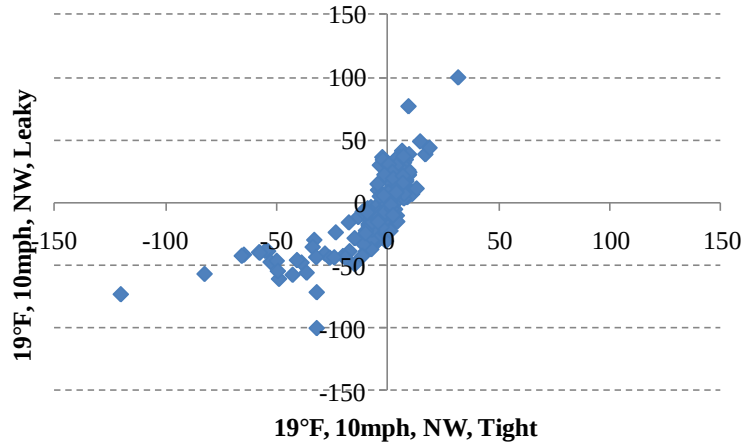


*Figure 5.12*: Effect of Leakage Severity at Northwest Wind

## 5.3 Identification of Macro-Zones for Model Reduction Using Tracer Gas ($CO_2$) Simulations

The next step in the tuning methodology was to perform a tracer gas-based sensitivity analysis. As seen with the synthetic building, the airflow-based sensitivity analysis did not provide opportunities for the identification of macro-zones for model reduction. Moving towards a tracer gas-based method is more appropriate. Macro-zones can be more readily identified by observing tracer gas behavior in the various rooms of the building under changing conditions.

### *5.3.1 Individual Room $CO_2$ Concentration Curves*

The identification of macro-zones via tracer gas simulations was first attempted by simulating a release in the air handling unit (AHU3) and plotting $CO_2$ concentration curves for each room on the third floor of the MBNA building. The airflow-based sensitivity analysis showed that wind speed, wind direction, and leakage severity are potentially important factors. Thus, a tracer gas-based sensitivity analysis was performed to analyze changes in tracer gas behavior by altering these variables. Several releases in AHU3 were simulated for varying wind conditions and leakage severity. In each simulation, the ambient air temperature remained constant since its effects were assumed to be insignificant. For these tracer gas simulations, the synthetic building was more complex in that it had three air handling units serving different zones. For the third floor of the MBNA building, there is only one air handling unit that serves all rooms on the floor. Subsequently, since this research is focused only on releases in air handling units, other release scenarios did not have to be considered for this analysis of the

MBNA building third floor. With three factors at two levels each, a $2^3$ factorial analysis was used resulting in eight $CO_2$ release simulations. Again, instead of performing a formal quantitative sensitivity analysis and calculating effects, graphs of the data were used to visually determine how the changing conditions impact apparent macro-zones. Table 5.5 summarizes the tracer gas simulations performed.

Table 5.5

*Real Building Tracer Gas Release Simulation Summary*

| **Tracer Gas Simulation Summary** | | | |
|---|---|---|---|
| **Figure** | **Wind Speed (mph)** | **Wind Direction** | **Leakage Severity** |
| 5.13 | 10 | N | Leaky |
| A2.1 | 10 | NW | Tight |
| A2.2 | 10 | N | Leaky |
| A2.3 | 10 | NW | Tight |
| A2.4 | 0 | N | Leaky |
| A2.5 | 0 | NW | Tight |
| A2.6 | 0 | N | Leaky |
| A2.7 | 0 | NW | Tight |
| Indoor Air Temperature = 72°F | | | |
| Ambient Air Temperature = 67°F | | | |

Figure 5.13 shows the individual decay curves for each room on the third floor of the MBNA building for the first set of conditions (i.e. 10 mph north wind and "Leaky"). Clearly, there is a wide range of responses to the release in the AHU. Each release simulated in Table 5.5 adopted the same procedure. For the actual testing in the MBNA building performed by Sae Kow (2010), a fire extinguisher was used to release $CO_2$ into the AHU supply duct. The exact amount of $CO_2$ released was measured by weighing the fire extinguisher before and after the release. As for the synthetic building, the amount of $CO_2$ released

was enough to bring each room served by the AHU to 1,600 PPM above ambient concentrations (assumed to be approximately 400 PPM). This is the experimental release procedure adopted by both Firrantello (2007) and Sae Kow (2010). Mimicking such a release in PCW is not exactly straight forward. Remember that PCW uses the Simple AHU model where the entire duct system is defined by two volumes or zones, one for the supply ductwork and one for the return ductwork. Since a contaminant source cannot be specified in the supply zone, the release must be performed by specifying an initial concentration within the supply volume. The supply duct volume for the third floor of the MBNA building was approximated from mechanical design drawings by Sae Kow (2010) to be 876 $ft^3$. The following is a calculation of the initial concentration that needs to be specified in PCW to mimic one of the releases performed by Sae Kow (2010):

- Volume of $CO_2$ Released = 116.292 $ft^3$ (Sae Kow, 2010)
- Approximate Total Volume of MBNA Third Floor = 69,650 $ft^3$
- Initial Concentration for All Rooms = $\frac{116.292 ft^3}{69{,}650 ft^3} * 10^6 = 1{,}670\ PPM$
- Initial Concentration in PCW Supply Volume = $\frac{116.292 ft^3}{876 ft^3} * 10^6 = 132{,}753\ PPM$

Note that there is a major difference in the assumptions used for the $CO_2$ simulations for the synthetic building as compared to those in this real building analysis. For the synthetic building, an initial $CO_2$ concentration was specified in each room ignoring the supply duct volume. Therefore, all rooms were initially at the same concentration and all that was observed was the concentration decay

with time. Here, however, with a release more realistically simulated accounting for the supply duct volume; the entire concentration curve is shown including the uptake, peak, and decay of $CO_2$. The rooms have varying peaks due to different supply air flow rates. Even in this situation, however, the PCW assumptions reflect important simplifications to real conditions. In reality, the complexity of the supply duct system would not result in a uniform concentration at the first time step immediately after a release. Also, in reality, not all zones would receive the contaminant at the first time step.

The overall goal of these tracer gas simulations was to be able to identify macro-zones that do not change when climatic and operating conditions change. Since observing individual room airflows was inadequate for this purpose, the hope was that tracer gas data could be used for identifying such macro-zones. The difficulty encountered at this point can be seen in Figure 5.13. With so many decay curves on one plot, it is too difficult to identify individual rooms or overlapping decay curves. Also, with the variations in peak concentrations and decay rates, there do not appear to be clearly defined macro-zones (as were apparent for the synthetic building). Properly identifying macro-zones requires closer inspection of these graphs. Besides the conditions in Figure 5.13, the other conditions simulated appear to yield very similar results. Refer to Appendix A and Figures A2.1 through A2.7 for these other plots. It is clear that simply observing these $CO_2$ plots with a concentration curve for each room is too difficult. This process was easier for the synthetic building which did not have as

many zones. The synthetic building also had multiple air handling units which simplified these $CO_2$ plots by creating some macro-zones from HVAC zoning.

Despite not being able to identify macro-zones, there were a few conclusions that were drawn from this sensitivity analysis. In order to better visualize the impacts of the changing conditions, the $CO_2$ concentration curves were plotted for each condition for each room. See Figures 5.14 through 5.17 for examples. Each plot includes a $CO_2$ concentration curve in that room for each of the eight conditions described in Table 5.5. Note that only six curves are plotted since the wind direction changes during no wind are redundant data sets. Figure 5.14 shows how the tracer gas behavior changed in Zone_1 which is in the northwest corner of the MBNA building (refer to Figure 5.1). The main conclusion that was drawn from this graph was that wind direction and wind speed have little impacts on the decay curves since the resulting variations in decay are very small. However, leakage severity does have a large impact when there is wind. This is indicated by the faster decay in the rooms that are "leaky" under the high wind condition. The decay curves for "tight" leakage severity and high wind are almost identical to when there is no wind and leakage paths set at "leaky" or "tight". Even closer inspection of this graph revealed that wind in any condition increases the rate of decay of the tracer gas. This can be attributed to higher air change rates with wind induced infiltration. Also, wind from the north results in faster decay in Zone_1 than wind from the northwest. This is due to the fact that Zone_1 has only a north facing exterior wall. Almost all of the rooms on the north side of the MBNA building show the same behavior as Figure 5.14. The

rest of these individual room plots are provided in Appendix A (Figures A2.8 through A2.37).

Figure 5.15 shows how the tracer gas behavior changed in the mechanical room or M305. The mechanical room has no HVAC supply or return terminals. Therefore, it can only receive a contaminant via inter-zonal airflows. This graph shows that the "leaky" condition with no wind resulted in the largest contaminant concentration. With wind added, the peak concentration is less and the decay is much faster. Under "tight" conditions, with and without wind, the peak concentration is smallest but the decay rate is much slower. Again, wind from the north results in faster decay than wind from the northwest. Comparing this graph to Figure 5.14 shows how there can be conflicting conclusions about leakage severity depending on whether or not HVAC airflows are involved. In terms of reducing contaminant concentrations due to a release in an AHU, mechanically ventilated rooms benefit from "leaky" conditions. On the other hand, unventilated rooms benefit from "leaky" conditions only if there is wind or some other force that drives contaminant out of the space. Otherwise, a "tight" condition is preferred because it limits the transfer of the contaminant from other zones.

Figure 5.16 shows how the tracer gas behavior changed in Zone_20 which is one of the spaces on the south side of the MBNA building. This graph shows almost no change in the $CO_2$ behavior under the various conditions. Since this space does not have exterior walls normal to the two wind directions analyzed, it was not directly impacted by the wind. This graph also agrees with the previous conclusion that the only significant impact is the "leaky" condition with wind

present. The other spaces on the south side of the building show similar behavior (See Figure A2.8 through Figure A2.37 in Appendix A). Closer inspection does reveal slight variations among the curves. The importance of these slight variations in peak concentrations and decay rates in all of these plots is dependent on the type of contaminant and the corresponding occupant exposure differences.

### *5.3.2 Tracer Gas Decay Coefficients*

The previous section revealed that under different conditions, there were slight variations in the decay of $CO_2$ in each room. From Figure 5.13, it is clearly noted that visually observing these numerous concentration decay curves with the intent of ascertaining those which have similar dynamics is a daunting task. As stated during the analysis of the synthetic building, a procedure which could be automated and which makes use of statistical concepts such as clustering methods would be valuable. One possible method is to represent the decay curve as a first-order system, evaluate the decay coefficient for each room following Equation 4.3, and then cluster the rooms into macro-zones on the basis of the decay coefficients. To identify the decay coefficients, Equation 4.3 can be linearized by a natural log data transformation and the decay coefficient can be extracted from simple linear regression to the model given by Equation 4.4.

Figure 5.17 shows the natural log transformation of the set of concentration decay curves from Figure 5.13. Similar to what was discovered for the synthetic building, the transformed curves are not linear and suggest that the system should be described by a higher order exponential model. Performing a natural log transformation on the actual measured $CO_2$ data from Sae Kow (2010)

for the third floor of the MBNA building showed similar higher order behavior. As hypothesized for the synthetic building, one possible reason for this is the fact that $CO_2$ is being recirculated via the return ducts, mixed with outside air, and being re-supplied to each zone. A 100% outside air system would be more likely to show first-order decay.

For the synthetic building, the calculation of the decay coefficients was performed by simply taking the first twenty minutes after the release on the natural log transformation plots, which were approximately linear. From Figure 5.17, it was clear that this approach will not work in this case. The nature of the release causes various peak concentrations which makes it difficult to identify a time where all transformed decay curves are approximately linear. One way to determine decay coefficients in this case was to simulate a release in the same way as in the synthetic building where each room starts with the same initial concentration. Although this is somewhat unrealistic and ignores the effect of supply duct volume, it does allow one evaluate just the decay rates of each room. Figure 5.18 shows a plot of this type of release for the third floor of the MBNA building and Figure 5.19 shows the natural log transformation. From Figure 5.19, the first twenty minutes could be considered linear and the decay coefficients for each room could be calculated.

Although this alternative type of release will allow determination of decay coefficients, the peak concentration is also important. In the first order model, the peak would be represented by the y-intercept or "C" in Equation 4.4. The peak concentration will have a significant impact on occupant exposure. Therefore,

both the peak concentration and the decay coefficient need to be taken into account. This requires analyzing the results of both types of releases.

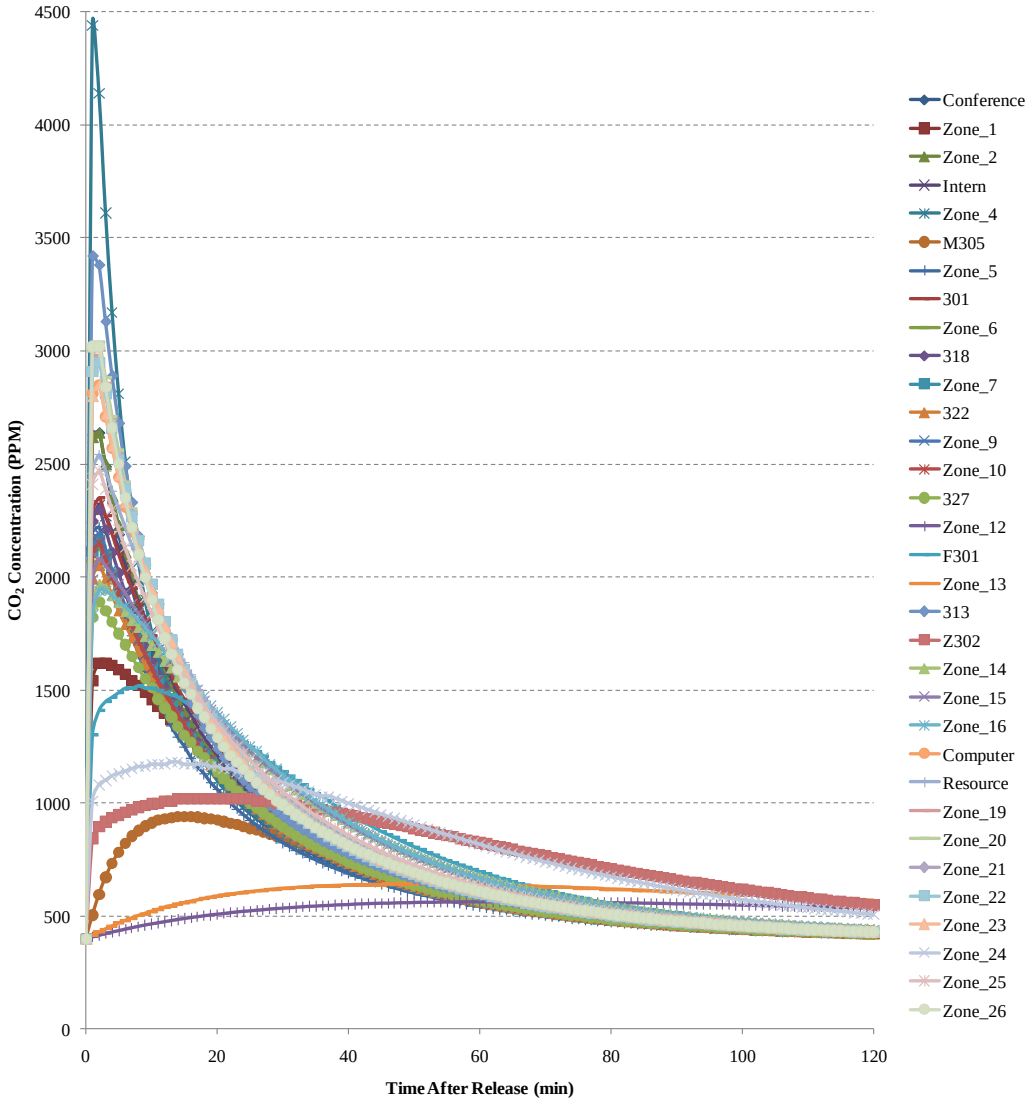


*Figure 5.13*: $CO_2$ Concentration Curves in Individual Rooms (67°F, North Wind at 10 mph, "Leaky")

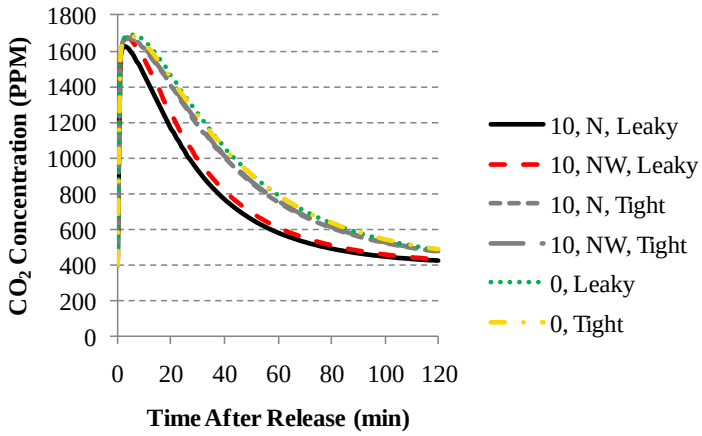


*Figure 5.14*: Zone_1 Tracer Gas-Based Sensitivity Analysis

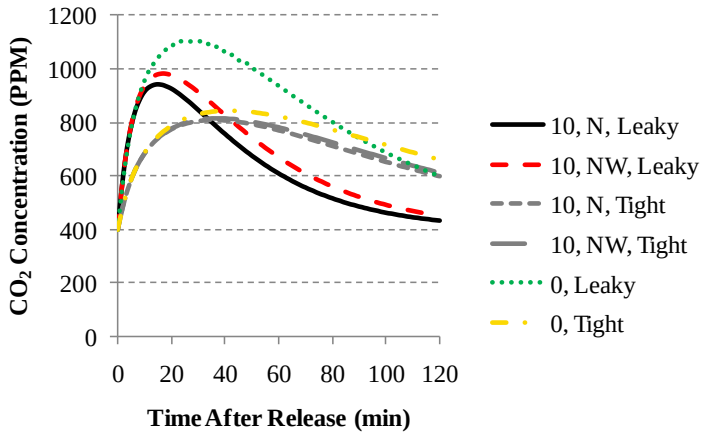


*Figure 5.15*: M305 Tracer Gas-Based Sensitivity Analysis

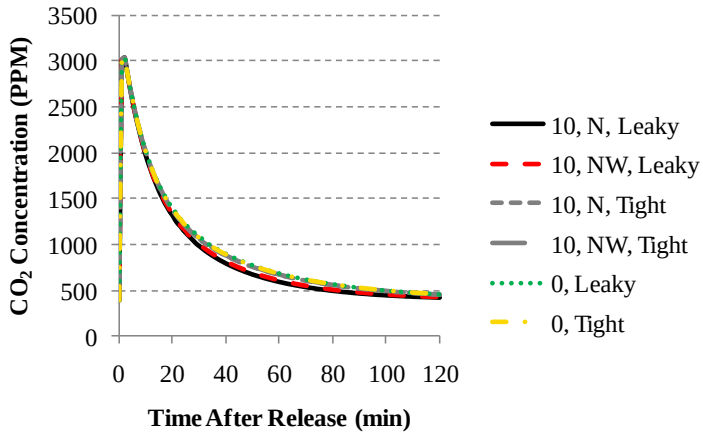


*Figure 5.16*: Zone_20 Tracer Gas-Based Sensitivity Analysis

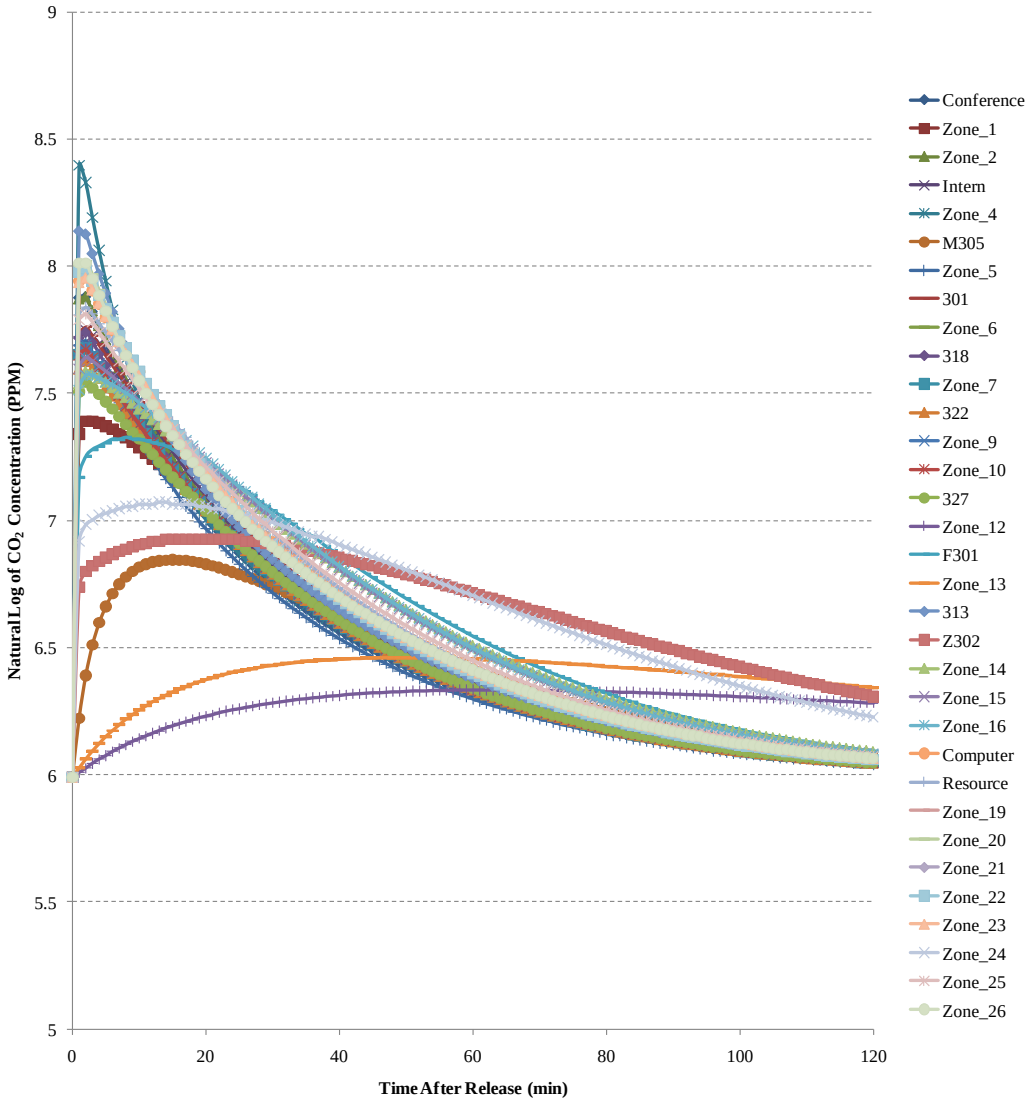


*Figure 5.17*: Natural Log Transformation of $CO_2$ Concentration Curves in Figure 5.13

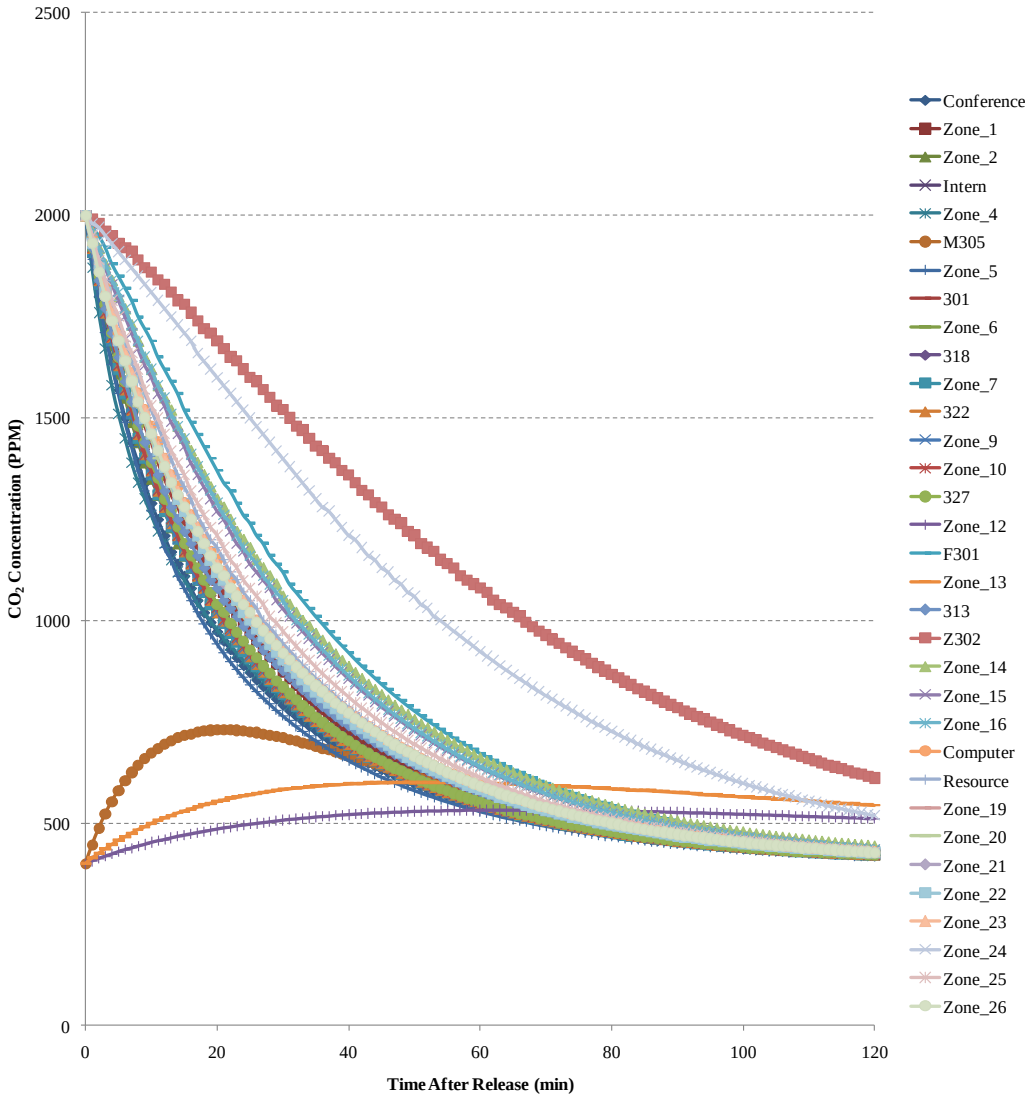


*Figure 5.18*: Alternative Release - $CO_2$ Concentration Curves in Individual Rooms (67°F, North Wind at 10 mph, "Leaky")

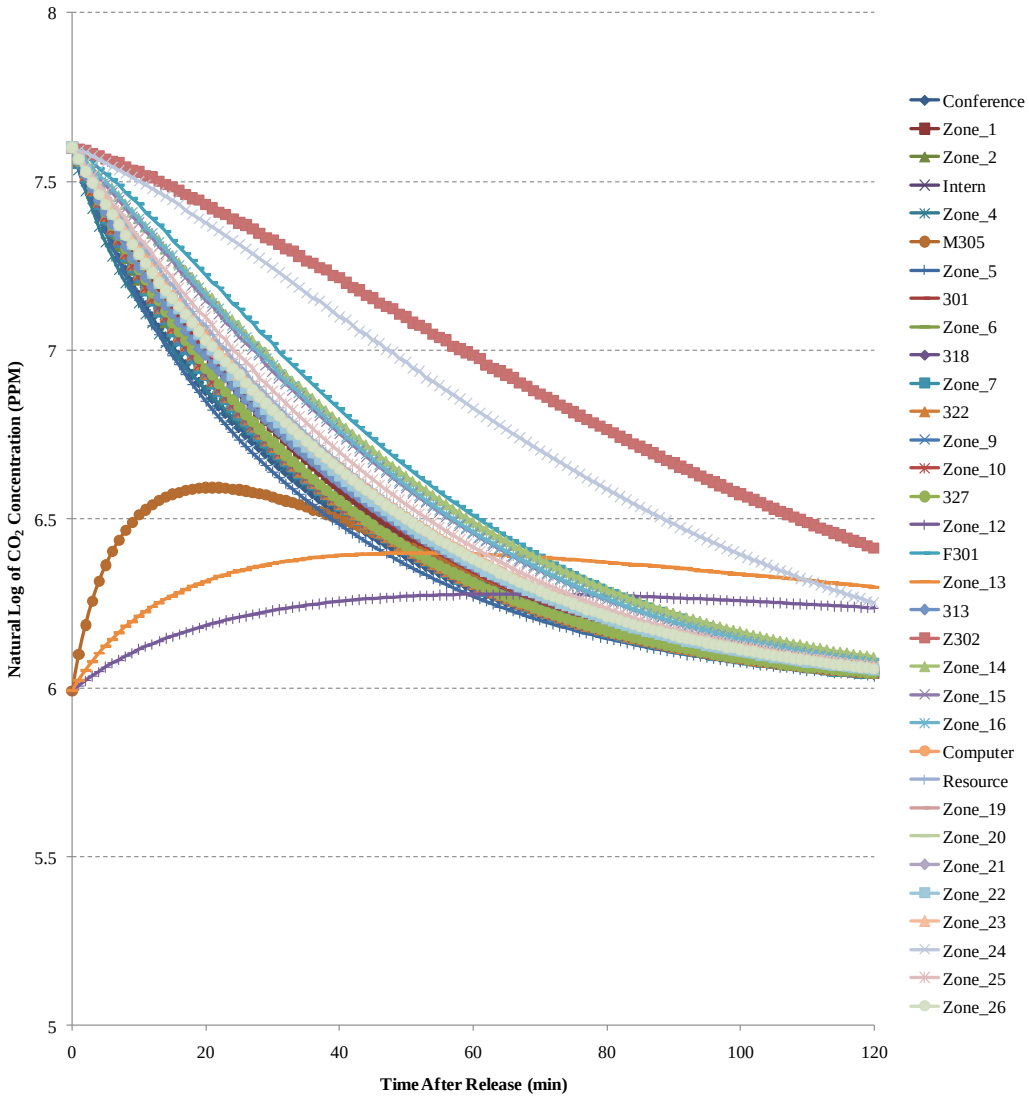


*Figure 5.19*: Natural Log Transformation of $CO_2$ Concentration Curves in Figure 5.18

### *5.3.3 Individual Room $CO_2$ Concentration Curves for Assumed Macro-Zones*

Before simulating new releases similar to those of the synthetic building, i.e. constant initial concentration in each room, further analysis was performed on the figures listed in Table 5.5. In order to solve the issue of macro-zone identification from the tracer gas curves (e.g. Figure 5.13), an attempt was made

to analyze the $CO_2$ data based on assumed macro-zones. Using the floor plan of the third floor of the MBNA building, preliminary macro-zones were identified based on geometry. Then separate sets of $CO_2$ concentration curves were plotted for each assumed macro-zone. Significant differences in the peak concentrations and decay rates would indicate the need for further adjustments to the macro-zones identified.

Analyzing Figure 5.1, five macro-zones were assumed based on floor plan geometry. Since the entire floor is served by the same air handling unit, and since PCW does not explicitly model ductwork, there was no HVAC zoning basis for these assumed macro-zones. The five macro-zones included the northwest perimeter spaces, the northeast perimeter spaces, the southeast perimeter spaces, the southwest perimeter spaces, and the core/bathroom/stairwell spaces. These assumed macro-zones are listed below in Table 5.6.

Table 5.6

*Assumed Macro-Zone Groupings*

| **Assumed Macro-Zones** | | | | |
|---|---|---|---|---|
| **1** | **2** | **3** | **4** | **5** |
| 313 | 318 | Zone_19 | Zone_14 | M305 |
| Conference | Zone_7 | Zone_20 | Zone_15 | Zone_5 |
| Zone_1 | 322 | Zone_21 | Zone_16 | 301 |
| Zone_2 | Zone_9 | Zone_22 | Computer | Zone_6 |
| Intern | Zone_10 | Zone_23 | Zone_26 | Zone_12 |
| Zone_4 | 327 | Resource | | Zone_13 |
| | | Zone_25 | | F301 |
| | | | | Zone_23 |
| | | | | Z302 |

Figure 5.20 (a) through (e) shows the $CO_2$ concentration curves of these assumed macro-zones for the first set of conditions from Table 5.5 (i.e. 10 mph north wind and "leaky"). Clearly, these assumed macro-zones do not meet the criteria for forming macro-zones. As one might expect, similar floor plan geometry does not guarantee similar tracer gas behavior. These same plots were generated for the remaining seven conditions listed in Table 5.5 in the sensitivity analysis. It was found that the same groupings occurred in each case. Therefore, these plots were not included. Although the macro-zones selected initially were not correct, they did eliminate some of the confusion of Figure 5.13. Therefore, a second iteration of macro-zones, listed in Table 5.7, was formed based on the peak concentrations and decay rates observed in Figure 5.20 (a) through (e). Figure 5.21 (a) through (h) shows the decay curve plots for these new macro-zones under the first set of conditions from Table 5.5 (i.e. 10 mph north wind and "leaky").

Table 5.7

*Second Iteration of Macro-Zone Groupings*

| **Revised Macro-Zones** | | | | | | | |
|---|---|---|---|---|---|---|---|
| **1** | **2** | **3** | **4** | **5** | **6** | **7** | **8** |
| Intern | 322 | Computer | Conference | Zone_4 | 313 | Zone_1 | M305 |
| Zone_5 | 327 | Zone_19 | Zone_2 | | | | Zone_12 |
| 301 | Zone_14 | Zone_20 | Zone_25 | | | | F301 |
| Zone_6 | Zone_15 | Zone_21 | Resource | | | | Zone_13 |
| 318 | Zone_16 | Zone_22 | | | | | Z302 |
| Zone_7 | | Zone_23 | | | | | Zone_24 |
| Zone_9 | | Zone_26 | | | | | |
| Zone_10 | | | | | | | |

From these plots, it is clear that this second iteration of macro-zones more appropriately matches rooms with similar tracer gas behavior. Zone_1, Zone_4, and Room 313 appear to have unique tracer gas behavior and were binned into separate own macro-zones. Macro-zone 8 is not so much a macro-zone as it is a grouping of those rooms who have either no HVAC terminals or who have very small HVAC airflow rates. The exception is room F301 which is the main corridor and lobby space on the third floor of the MBNA building. This space is unique due to its large volume. It is unclear how the remainder of the calibration methodology would be applied to the types of spaces in macro-zone 8.

Since previous results for the MBNA building and for the synthetic building suggested that the building's airflow dynamics are largely HVAC dominated, these newly formed macro-zones were compared to the HVAC airflows that were measured by Sae Kow (2010). Table 5.8 shows that the macro-zones are directly related to the air changes per hour in each space. Although it appears that the HVAC airflows dictate the macro-zones, the airflows through the building envelope and between interior zones do have an impact. Note that in Figure 5.21 (b) and (d), there appear to be two separate decay rates even though the peak concentrations are similar for all rooms in those macro-zones. This is caused by the 10 mph north wind. In both of these macro-zones, there are rooms on both the north and south side of the MBNA building. The rooms on the north side decay faster due to infiltration caused by the wind. Figure 5.22 and Figure 5.23 show the same macro-zones under the same conditions except with no wind (i.e. 0 mph north wind and "leaky"). With no wind, all rooms in these two macro-

zones have almost identical behavior. The plots in Figure 5.21 were also generated for the remaining seven conditions listed in Table 5.5 in the sensitivity analysis. Refer to Figure A2.38 through Figure A2.42 in Appendix A for these graphs. Again, there are only six sets of these plots since there are redundant data sets for different wind directions with no wind velocity. For each condition, the slight variations in peak concentrations and decay rates, as discussed previously, due to wind changes and leakage severity changes, are not large enough to alter the macro-zones identified by the air changes per hour criterion. However, the significance of such variations may depend on the release scenario and the type of contaminant.

Table 5.8

*Identified Macro-Zones and Room Air Change Rates*

| Macro-Zone | PCW File Name | Volume ($ft^3$) | Measured Airflows (PSU Tuned Model) | | Air Changes (1/hr) |
|---|---|---|---|---|---|
| | | | Supply Airflow Rate (CFM) | Return Airflow Rate (CFM) | |
| 1 | Zone_3 (Intern) | 1500.4 | 148 | 121 | 5.92 |
| 1 | Zone_5 | 831.6 | 85 | N/A | 6.13 |
| 1 | 301 | 5435.99 | 570 | 393 | 6.29 |
| 1 | Zone_6 | 1270.5 | 118 | N/A | 5.57 |
| 1 | 318 | 1240.8 | 130 | 96 | 6.29 |
| 1 | Zone_7 | 1212.75 | 116 | 96 | 5.74 |
| 1 | Zone_9 | 1212.75 | 118 | 76 | 5.84 |
| 1 | Zone_10 | 1212.75 | 115 | 52 | 5.69 |
| 2 | 322 | 1212.75 | 107 | 93 | 5.29 |
| 2 | 327 | 1212.75 | 95 | 41 | 4.70 |
| 2 | Zone_14 | 2076.8 | 167 | 141 | 4.82 |
| 2 | Zone_15 | 1267.2 | 110 | 106 | 5.21 |
| 2 | Zone_16 | 1619.2 | 124 | 126 | 4.67 |
| 3 | Computer | 1865.6 | 256 | 192 | 8.23 |
| 3 | Zone_19 | 1158.85 | 171 | 100 | 8.85 |
| 3 | Zone_20 | 1158.85 | 173 | 101 | 8.96 |
| 3 | Zone_21 | 1158.85 | 166 | 101 | 8.59 |
| 3 | Zone_22 | 1158.85 | 166 | 85 | 8.59 |
| 3 | Zone_23 | 1158.85 | 158 | 74 | 8.18 |
| 3 | Zone_26 | 1478.4 | 225 | 191 | 9.13 |
| 4 | Conference | 1391.5 | 180 | 137 | 7.76 |
| 4 | Zone_2 | 1091.2 | 139 | 110 | 7.64 |
| 4 | Resource | 1158.85 | 132 | 96 | 6.83 |
| 4 | Zone_25 | 969.652 | 109 | 101 | 6.74 |
| 5 | Zone_4 | 1636.8 | 420 | 246 | 15.40 |
| 6 | 313 | 677.6 | 121 | 80 | 10.71 |
| 7 | Zone_1 | 1159.4 | 70 | 63 | 3.62 |
| 8 | M305 | 1936 | N/A | N/A | 0.00 |
| 8 | Zone_12 | 1267.2 | N/A | N/A | 0.00 |
| 8 | Zone_13 | 508.203 | N/A | N/A | 0.00 |
| 8 | F301 | 24134 | 1095 | 920 | 2.72 |
| 8 | Z302 | 1900.8 | 44 | N/A | 1.39 |
| 8 | Zone_24 | 1374.45 | 44 | N/A | 1.92 |

*Figure 5.20*: $CO_2$ Concentration Curves for Assumed Macro-Zones

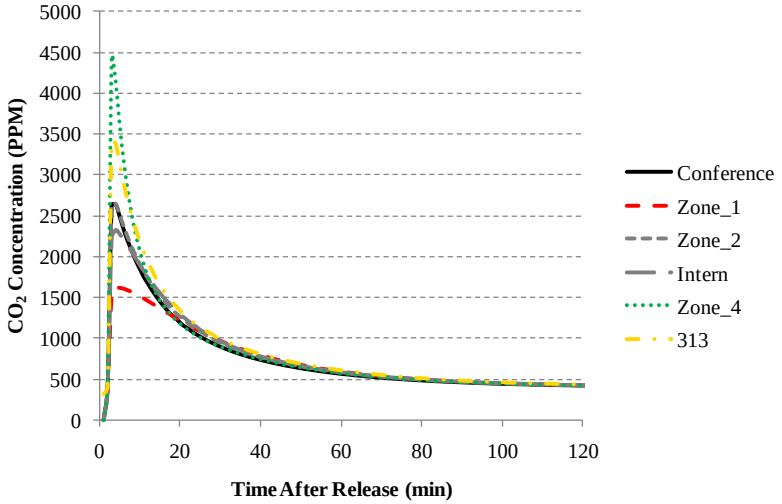


(a) Assumed Macro-Zone 1

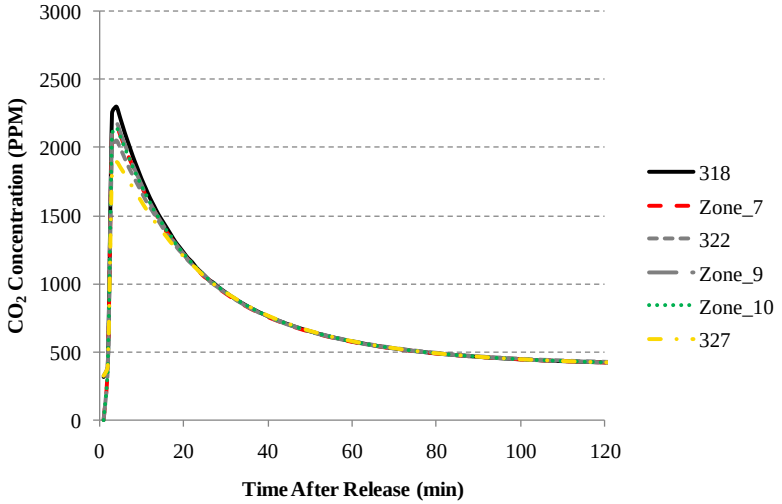


(b) Assumed Macro-Zone 2

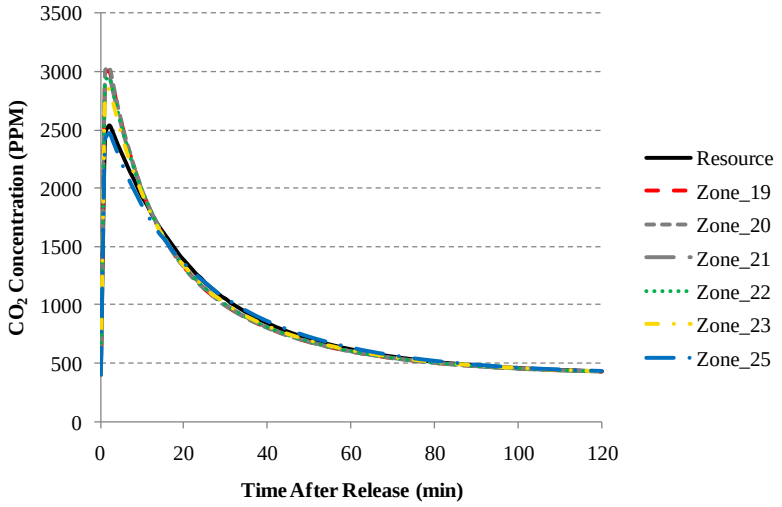


(c) Assumed Macro-Zone 3

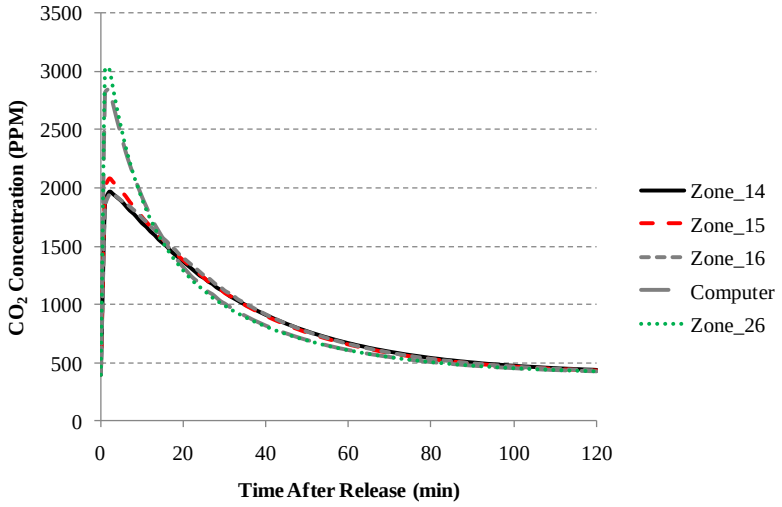


(d) Assumed Macro-Zone 4

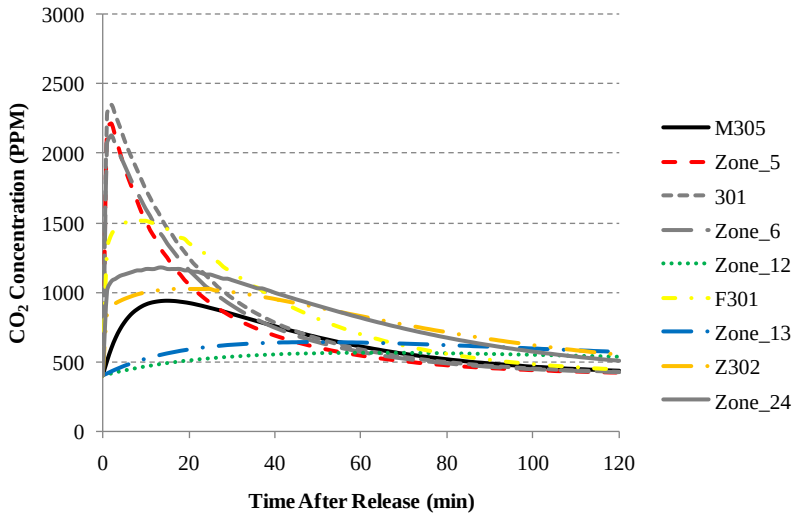


(e) Assumed Macro-Zone 5

*Figure 5.21*: $CO_2$ Concentration Curves for Second Iteration of Macro-Zones

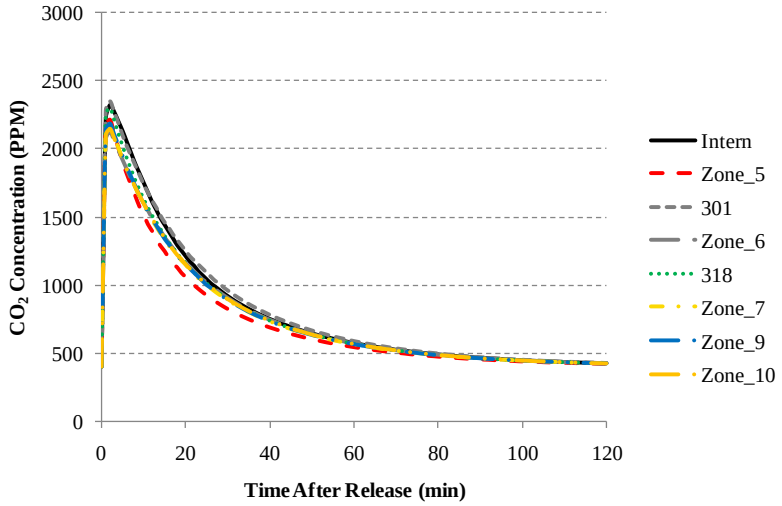


(a) Macro-Zone 1

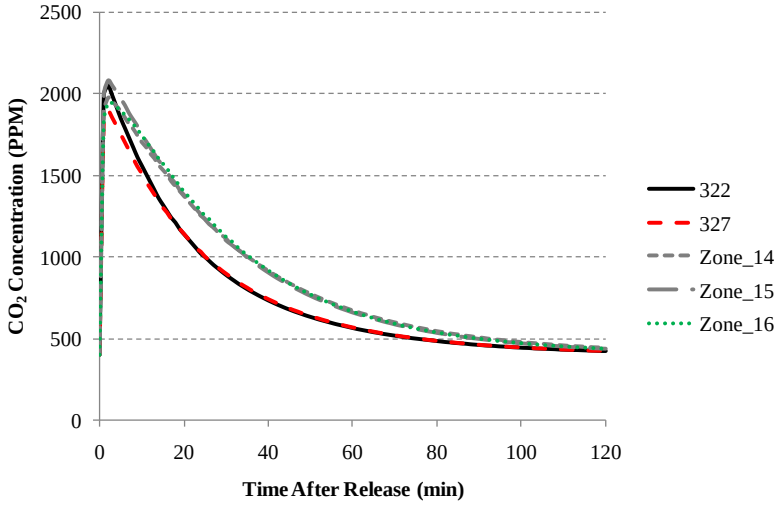


(b) Macro-Zone 2

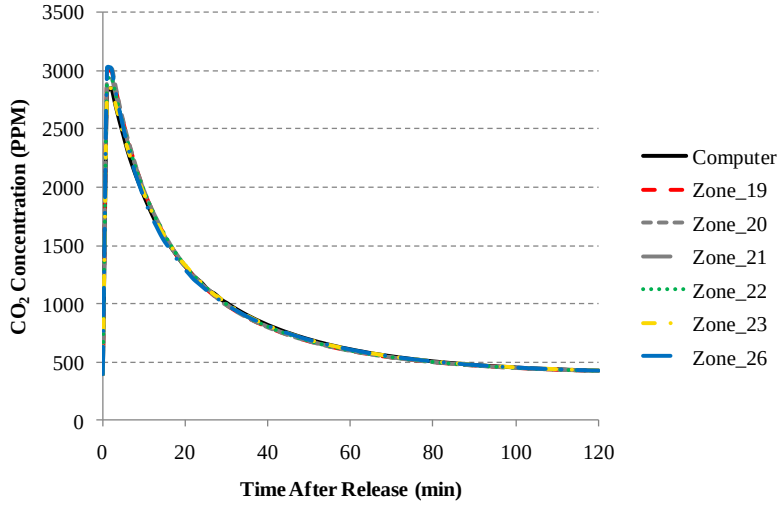


(c) Macro-Zone 3

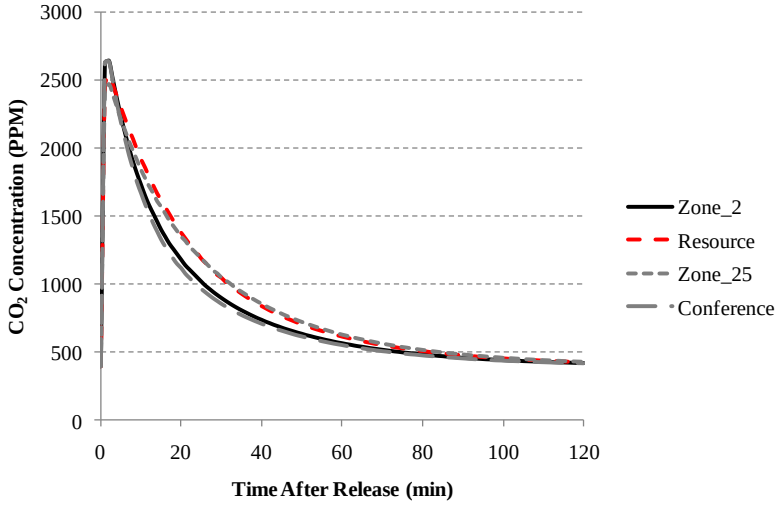


(d) Macro-Zone 4

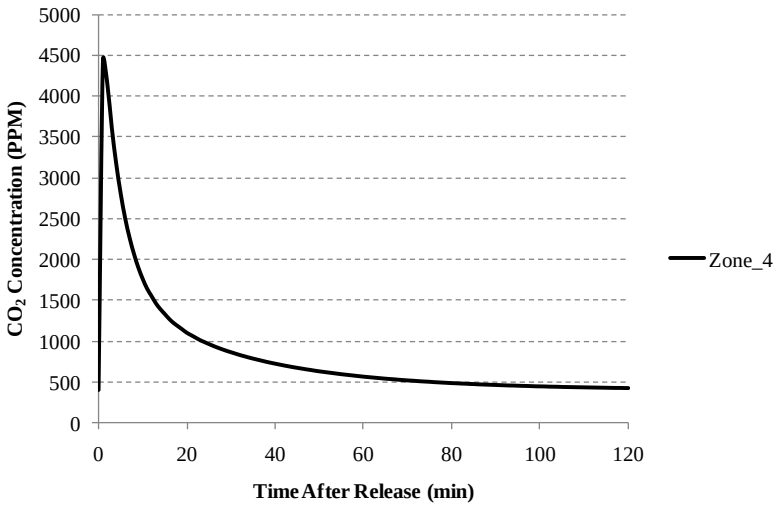


(e) Macro-Zone 5

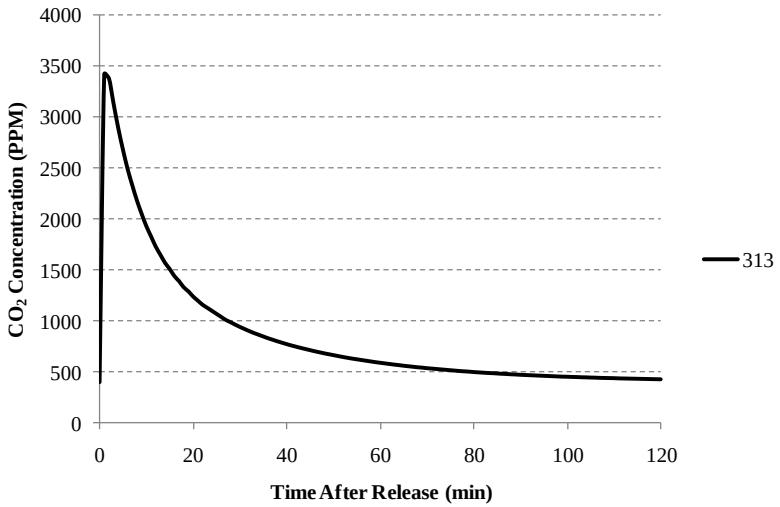


(f) Macro-Zone 6

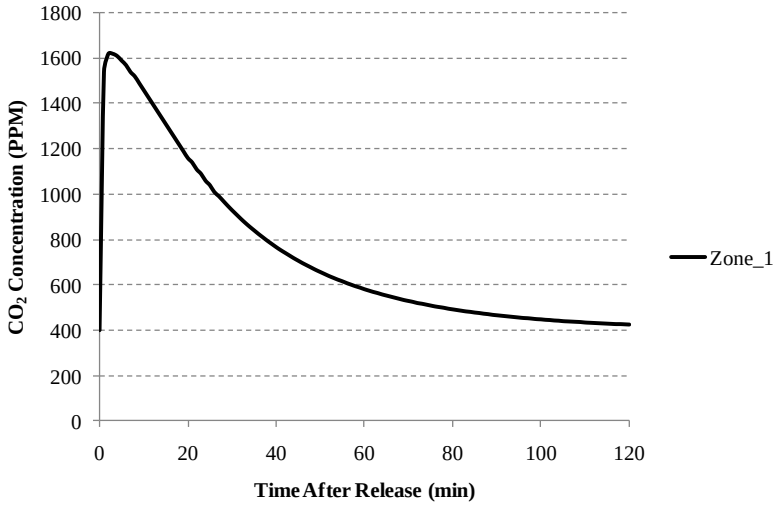


(g) Macro-Zone 7

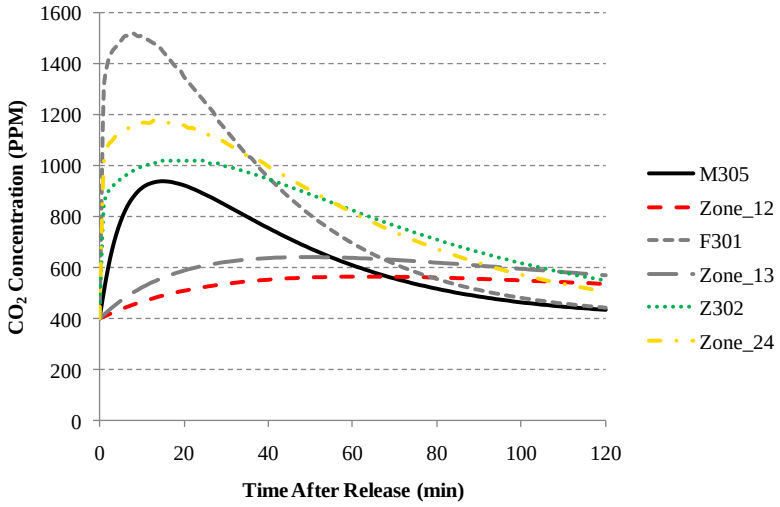


(h) Macro-Zone 8

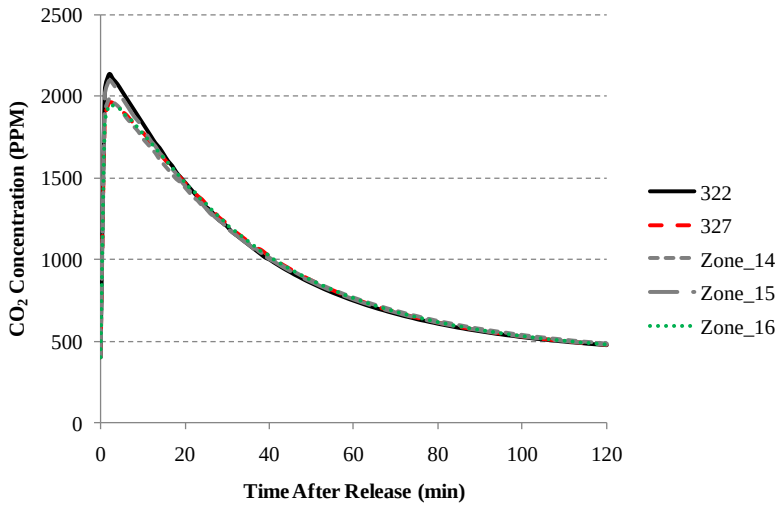


*Figure 5.22*: Macro-Zone 2 with No Wind

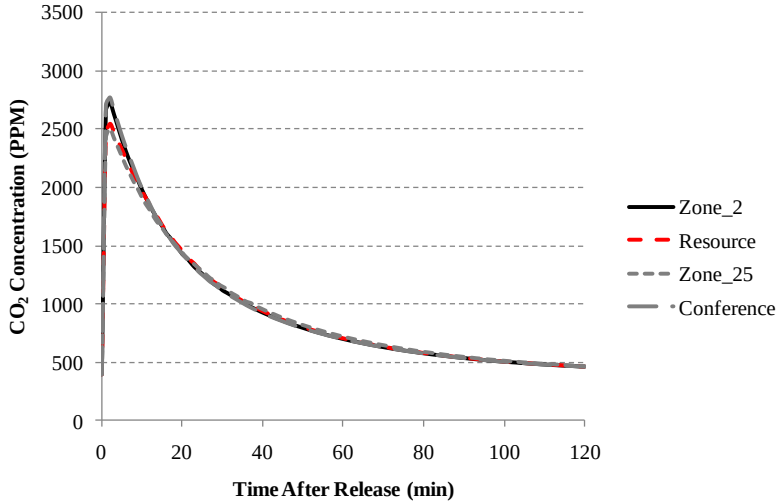


*Figure 5.23*: Macro-Zone 4 with No Wind

### *5.3.4 Macro-Zone Formation with Tracer Gas Decay Coefficients*

The identification of decay coefficients for each room is another method of macro-zone identification. The $CO_2$ decay plots above appear to identify macro-zones quite well. Therefore, the decay coefficients determined here serve as a verification of the macro-zones identified. As discussed in Section 5.3.2, some difficulty was encountered when trying to identify the macro-zones due the nature of the $CO_2$ release in the AHU and due to the apparent high order exponential behavior of the decay. Therefore, some simplifications and assumptions had to be made. First, the release type was changed to that described in the synthetic building procedure. Each room is given an initial concentration of $CO_2$ thus ignoring the effect of supply duct volume and providing an identical peak concentration for each room. Figure 5.18 shows an example of the $CO_2$ decay curves resulting from this type of release and Figure 5.19 shows the natural log transformation. The second observation was that approximately the first twenty minutes of the natural log transformation plots are linear and that the decay coefficients can be determined from linear regression of those twenty data points.

Figure 5.24 below shows the decay coefficients determined for each room from the first twenty minutes of the natural log transformation plot for the first simulation condition (10 mph north wind and "Leaky"). They are grouped by the macro-zones identified above. The large scatter for macro-zone 8 is expected since it is a more of a mixture of rooms with unique behaviors than a macro-zone, as mentioned earlier. Within the rest of the macro-zones, the rooms appear to

have fairly similar decay coefficients. The separation in decay coefficients seen in macro-zone 2 and macro-zone 4 are due to wind and have been discussed above. Despite the fact that many of the rooms have very similar decay coefficients they have significant variations in peak concentrations. Therefore, Figure 5.24 shows that macro-zones probably should not be separated by decay coefficients alone. Peak concentrations must also be accounted for.

Figure 5.25 below shows how changing wind direction impacts the decay coefficients. The decay coefficients for the second simulation condition (10mph northwest wind and "Leaky") are plotted along with the coefficients from the first condition. The "y = x" nature indicates that there is HVAC dominance (i.e. wind has little effect) and the scatter indicates that there are multiple macro-zones. This is consistent with the findings from the previous section. However, it is unclear from such a plot where one would draw the line between one macro-zone and the next. Overall, it appears that the use of this decay coefficient approach was not very helpful in the analysis of the MBNA building.

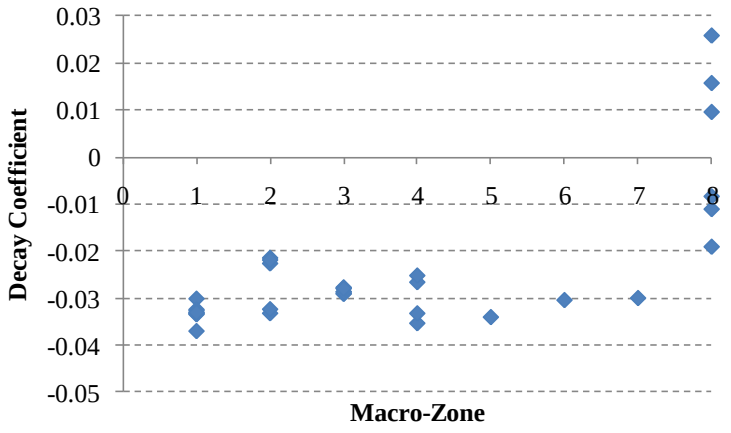


*Figure 5.24*: Decay Coefficients Grouped by Macro-Zone

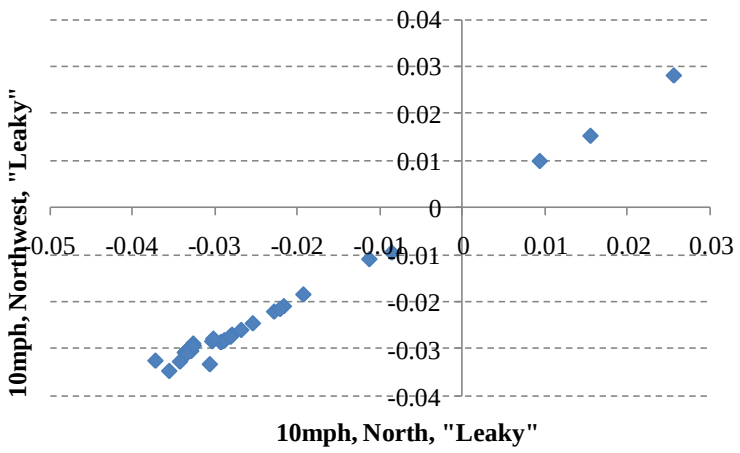


*Figure 5.25*: Effect of Wind Direction on Decay Coefficients

### 5.4 Model Calibration

The first step in model calibration was to gather the real building tracer gas data. As mentioned previously, the data used for this research was collected by Sae Kow (2010) and includes two releases in AHU3 on the third floor of the MBNA building. $CO_2$ concentrations were measured every minute for three hours in the main return duct of AHU3 as well as in the following six rooms: Conference, Intern, Room 322, Room 327, Computer, and Resource. For this methodology, the ideal situation would be to have tracer gas data in at least one room of each macro-zone. Since this methodology was developed after the releases were performed by Sae Kow (2010) there was no guarantee that the identified macro-zones would match up with the measurement locations. However, should this methodology be applied to other buildings, the identification of macro-zones would assist in determining in which rooms it would be advantageous to place $CO_2$ sensors during real building testing.

Comparing the measurement locations used by Sae Kow (2010) and the macro-zones identified above, it became apparent that four of the identified macro-zones could be calibrated with real data. Table 5.9 below shows how the measurement locations match up with the identified macro-zones. For macro-zone 2 and macro-zone 4 there were two measurement locations and thus two sets of measured data to compare with predicted $CO_2$ concentrations.

Table 5.9

*Identified Macro-Zones and $CO_2$ Measurement Locations*

| **Macro-Zones and $CO_2$ Measurement Locations** | | | | | | | |
|---|---|---|---|---|---|---|---|
| **1** | **2** | **3** | **4** | **5** | **6** | **7** | **8** |
| Intern | 322 | Computer | Conference | Zone_4 | 313 | Zone_1 | M305 |
| Zone_5 | 327 | Zone_19 | Zone_2 | | | | Zone_12 |
| 301 | Zone_14 | Zone_20 | Zone_25 | | | | F301 |
| Zone_6 | Zone_15 | Zone_21 | Resource | | | | Zone_13 |
| 318 | Zone_16 | Zone_22 | | | | | Z302 |
| Zone_7 | | Zone_23 | | | | | Zone_24 |
| Zone_9 | | Zone_26 | | | | | |
| Zone_10 | | | | | | | |

In order to calibrate the model, a factorial sensitivity analysis can be set up where the response variable is the match between predicted $CO_2$ decay curves and measured $CO_2$ decay curves for each macro-zone. Initially, the quality of the match between the two curves can be evaluated graphically. An alternative measure of improvement could be some statistical metric such as the root mean square error. The factorial analysis evaluates the effect of increasing and decreasing flow parameters in each macro-zone on how well the predicted $CO_2$ decay curves match the measured curves. More specifically, the flow coefficient "k" and the flow exponent "n" in the power-law equation for each airflow path

can be adjusted. It is recommended that the exterior airflow path flow parameters be changed separately from the interior airflow path flow parameters. However, in each macro-zone, all of the exterior parameters should be changed in the same manner and all interior parameters should be changed in the same manner. Thus the identification of macro-zones has significantly reduced the number of individual parameters that need to be tuned in a detailed multi-zone model. Therefore, this methodology does not provide a means of isolating individual airflow paths that may be causing the differences between measured and predicted decay curves. Also, this calibration is performed one macro-zone at a time. This methodology does not provide a means for simultaneous calibration across all macro-zones. Therefore, there is still some ambiguity as to how to tune the flow parameters for airflow paths that connect two different macro-zones. The individual calibration of each macro-zone will most likely suggest changing the flow parameters for these airflow paths differently. The factorial analysis for flow parameters could include many levels of increasing and decreasing the exterior coefficient, the exterior exponent, the interior coefficient, and the interior exponent (i.e. an $X^4$ analysis).

Figure 5.26 and Figure 5.27 below show the measured $CO_2$ decay curves for the seven measurement locations from the testing conducted by Sae Kow (2010) (Same as Figures 2.13 and 2.14 from Section 2.2.2.7). The two graphs represent the two separate releases that were performed. The conditions under which these releases were performed were also measured and include: 1 mph northwest wind, 24°F ambient air temperature, 73.4°F interior air temperature,

and 20% outside air. The PCW model was set to match these conditions and the leakage severity of "Average" was used for all interior airflow paths and the leakage severity of "Leaky" was used for all exterior paths. Therefore, the assumption made by Sae Kow (2010) is that the exterior envelope of the MBNA building is "leakier" than average. Based on design documents, the supply duct system volume was estimated to be 876 $ft^3$ and the return duct system volume was estimated to be 920 $ft^3$. Using the procedure discussed in Section 5.3.1, the initial concentration of $CO_2$ specified in the PCW supply volume was calculated based on the 876 $ft^3$ and the amount of $CO_2$ used in the second release by Sae Kow (2010). Therefore, the rest of this calibration was only with respect to the second set of release data (Figure 5.27). To calibrate with respect to the other release, the initial concentration in PCW needs to be recalculated to match the amount of $CO_2$ released for the first release, which was 114.5 $ft^3$ (Sae Kow, 2010).

The PCW model that was obtained from Sae Kow (2010) was already tuned with measured HVAC airflows in all rooms. The $CO_2$ release in AHU3 under the conditions mentioned above was first simulated in PCW and compared to the measured data. Figure 5.28 through Figure 5.33 show the measured versus predicted $CO_2$ concentration curves for the six room measurement locations. The predicted concentrations were obtained by a simulation from the tuned PCW model. The graphs show that even after using the PSU tuning algorithm, there were still some discrepancies between the measured and predicted tracer gas behavior. Assuming the HVAC flows were measured accurately, it was initially hypothesized that these differences must be attributed to airflow into and out of

the room via the exterior envelope or inter-zonal airflow paths. Consequently, this methodology attempts to adjust the flow parameters for these airflow paths. By first identifying macro-zones, the complexity of the model has been reduced and locations where $CO_2$ needs to be measured have been identified. Reducing the complexity of the model also reduces the complexity of these flow parameter adjustments. The macro-zones identify groups of flow paths whose parameters can be changed by the same amount. Other sources of discrepancies between measured and predicted behavior could include uncertainties or errors in HVAC airflows and $CO_2$ measurements, errors in the development of the PCW model, and possible contaminant loss through duct leakage which is not modeled in PCW. If the peak concentration does not match correctly, this could be a result of poor estimation of the supply or return duct volume or even room volume. Sae Kow (2010) discusses the impact of system volume in more detail.

As discussed in Section 4.1.2, the default mathematical relationship, or airflow element, used by PCW to relate the volumetric flow rate of air through an airflow path to the pressure difference across that path is of the form given by Equation 4.1. For model calibration, this methodology suggests that a sensitivity analysis be utilized to alter the values of the flow coefficient "k" and the exponent "n" for the interior and exterior airflow paths of each macro-zone in an attempt to yield a closer match between the measured and predicted tracer gas decay curves. In PCW, the assumption is that all exterior airflow paths are the same and all interior airflow paths are the same. The only exception is that stairwell and shaft walls have slightly different leakage conditions.

Figure 5.28 through Figure 5.33 reveal a problem that impacts the ability to try to tune this model in the manner proposed. For macro-zone 2 and macro-zone 4, there are two $CO_2$ measurement locations. In macro-zone 2 for example, the measurement locations are Room 322 and Room 327. From the above analysis, it was concluded that these two rooms have similar airflow dynamics and similar tracer gas histories and should therefore be grouped into the same macro-zone. However, Figure 5.29 and Figure 5.30 show that the predicted $CO_2$ curves, which are similar for both rooms as one would expect based on the macro-zone definition, vary from the measured $CO_2$ curves differently in each room. This could be attributed to errors in the development of the PCW model or errors in $CO_2$ and HVAC airflow measurements. With the proposed methodology, the flow parameters for the airflow paths in all rooms of a macro-zone should be changed consistently. However, it is clearly impossible to reconcile the discrepancies between the measured and predicted curves in Room 322 and Room 327 by changing flow parameters in the same manner. A similar phenomenon is seen for Conference and Resource which are both in macro-zone 4.

Noting this problem, the simpler case of macro-zone 3 was selected to demonstrate the calibration step. The leakage settings specified by Sae Kow (2010) in the tuned model of the third floor of the MBNA building were collected and are specified in Table 5.10. Macro-zone 3 includes the Computer room, Zone_19, Zone_20, Zone_21, Zone_22, Zone_23, and Zone_26. These rooms have a total of 7 airflow paths through the exterior envelope and 16 interior airflow paths. One possible manner of proceeding is described as follows:

1. A formal sensitivity analysis can be set up where the internal flow coefficients, external flow coefficients, and flow exponents are varied at several factor levels (i.e. an $X^4$ factorial analysis). Or one could perturb the flow parameters and see which direction they need to be altered to provide a better match. For example, vary the exterior and interior flow coefficients by ±15% and ±30% to see how sensitive the $CO_2$ decay curves are to the values of these flow coefficients.
2. Vary the flow exponent between 0.5 and 0.7 (this represents the range of typical flow exponents discussed by Walton and Dols, 2005) to see how sensitive the $CO_2$ decay curves are to the values of these flow exponents.
3. After some initial simulations, it may become apparent which way the flow coefficients or exponents need to be altered to obtain a better match between predicted and measured curves. In the case of macro-zone 3, since the model was over predicting concentrations, increasing the "leakiness" of the airflow paths helped to reduce the predicted concentrations. Once this was discovered, the number of simulations needed was reduced since decreased leakage severity need not be considered. Therefore, the flow coefficient was also increased by 50% and 75%. The 75% increase was almost equivalent to changing from exterior "Leaky" to interior "Leaky" leakage severity. Beyond that would represent unrealistic leakage according to the data gathered from real buildings by Persily (1998).

Table 5.10

*Tuned Model Leakage Settings*

| PSU Tuned Model Leakage Settings | | | | |
|---|---|---|---|---|
| **Path Type** | **Volumetric Flow Rate** | **Pressure Difference** | **Flow Exponent** | **Flow Coefficient** |
| | Q ($ft^3$/min) | $\Delta P$ ($inH_20$) | n | ($ft^3$/min)/($inH_20^n$) |
| Exterior | 28.61 | 0.30 | 0.65 | 62.41 |
| Interior | 31.90 | 0.30 | 0.65 | 69.61 |

Figure 5.34 below shows that despite all of these increases of the leakage coefficient, there were no noticeable differences in the predicted $CO_2$ concentration curves. The data shows that the increase to extreme leakiness resulted in approximately 10 PPM to 30 PPM decrease for most time steps whereas the average difference between the measured and predicted concentrations was approximately 100 PPM. The leakage exponent did have a more noticeable impact by shifting the entire curve. Changing the flow exponent to 0.5 provides a better match for the decay part of the curve. However, the peak concentration is still poorly captured. It appears that these changes fail to provide significant progress in matching the predicted curve to the measured curve.

Other possible causes for discrepancies between the measured and predicted $CO_2$ decay curves include incorrect supply duct system volume, return duct system volume, room volume, HVAC airflow rates, and outside air percentage. It was assumed that the HVAC airflow rates were measured accurately by Sae Kow (2010). To investigate if supply duct or return duct volume is an issue, Figure 5.35 below was generated to show the measured vs. predicted $CO_2$ concentrations in the AHU3 Return. From the graph it is quite clear that the two curves match fairly well. The main difference is in the peak

concentration. The measured concentration is approximately 525 PPM higher than the predicted concentration. This could be due to an incorrect estimate in system duct volume in the model. Decreasing the duct volume in the model would help to bring up the predicted peak concentration. However, as seen from Figure 5.28 through Figure 5.33, not all measurement locations result in higher than predicted peak concentrations. Thus, rather than adjusting the system volume, there may be errors in individual room volume estimates.

Figure 5.36 below shows the impact of varying room volume on the Computer room which is the measurement location in macro-zone 3. This was done in PCW by changing the ceiling height. Increasing the room volume, similar to the effects of system volume, results in a significant drop in the peak concentration in that room and negligible change in the concentration decay rate. Decreasing the room volume resulted in an increase in the peak concentration in that room and a negligible change in the concentration decay rate. Clearly, changing the ceiling height to 10 ft provides a much better match between curves. This stresses the importance of room volume measurements. Estimating room volumes from design documents may not be accurate enough. For example if the room has an accessible ceiling, the typical acoustic ceiling tile system may result in considerable air leakage from the room to the plenum space above. This could have a significant impact on the tracer gas behavior of that particular room. To account for this one could alter the room volume in the multi-zone model or model a separate plenum zone and account for air leakage between the two.

Figure 5.37 below shows the impact of changing the outside air percentage in AHU3. In the field testing performed on the MBNA building, Sae Kow (2010) noted difficulty in accurately measuring the outside air percentage for AHU3. Due to physical constraints, the only practical option for measuring the outside air percentage was to use the air temperature fraction method as shown in Equation 5.1 below.

$$\%OA = \frac{T_{MA} - T_{RA}}{T_{OA} - T_{RA}} * 100 \quad (5.1)$$

In Equation 5.1, "$T_{MA}$" is the mixed air temperature, "$T_{RA}$" is the return air temperature, and "$T_{OA}$" is the outside air temperature. The outside air, return air, and mixed air temperatures were measured using hot wire anemometers. However, the calculated outside air percentage based on these measurements had a very large uncertainty (approximately 60-70%). This was due to the small temperature difference between the outside air and the return air. Therefore, it is fair to assume that the outside air percentage of 20% initially used in the model is not accurate. Figure 5.37 shows that the small change from 20% to 40% outside air provides a much better match. Therefore, accurate outside air measurement is significant.

The fact that the identified macro-zones align with room air changes, as found in Table 5.8 and based on the results in Figure 5.36 and 5.37, it appears that the most important parameters to measure correctly and subsequently tune are those which impact room air change rates.

## 5.5 Analysis of Results and Conclusions

Due to limitations with the available real building $CO_2$ data, only a few of the identified macro-zones could be calibrated in this analysis. By demonstrating the proposed methodology on one such macro-zone, it was found that altering the flow parameters in the airflow paths of macro-zones did not seem to significantly improve the match between measured and predicted tracer gas curves. It was hypothesized that after all of the HVAC airflows had been measured and entered into the model, the remaining discrepancies between predicted and measured curves would be the result of incorrect flow parameters in the mathematical models describing the airflow through the building envelope and between internal zones. For the building tested here, all of the HVAC airflows were measured by Sae Kow (2010). The fact that altering the flow parameters did not appear to improve model prediction accuracy may indicate errors either in measurements or in model development. As noted previously, certain model assumptions such as the volume of supply ductwork can have significant impacts on the prediction capability of the model. Also, since HVAC airflows have been found to be so significant, any measurement errors or uncertainties in the measurement devices can also have significant impacts on the prediction accuracy of the model. Also, an always present source of error is the "well-mixed" assumptions. During $CO_2$ testing, the placement of the CO2 sensor may not properly capture the room average concentration depending on the how well the room air is actually mixed.

The reoccurring theme throughout this research has been that the airflow dynamics of these types of buildings are HVAC dominated. Thus, if altering the

flow parameters does not yield any improved results beyond measuring all HVAC flows, one may be tempted to alter the HVAC flows in the model to improve accuracy. However, this must not be done arbitrarily. One option would be to more accurately model the ductwork system to account for duct leakage, accurate duct volume, concentration peak delays due to ductwork distances, more realistic contaminant distribution based on the nature of the ductwork distribution, etc. The HVAC flows could then be altered from the measured values to account for the impact of these factors.

Table 5.8 showed that the identified macro-zones were directly related to the air changes in each room. Considering this along with the evidence of HVAC dominance, it is concluded that the tracer gas behavior of a room is driven by the air change rate. The attempt at calibration of flow parameters and the subsequent analyses of Figure 5.36 and Figure 5.37 revealed that the room air change rate is significantly more sensitive to factors such as room volume and outside air percentage than to room "leakiness", i.e. flow coefficients and exponents. This stresses the importance of accurately measuring factors impacting room air changes.

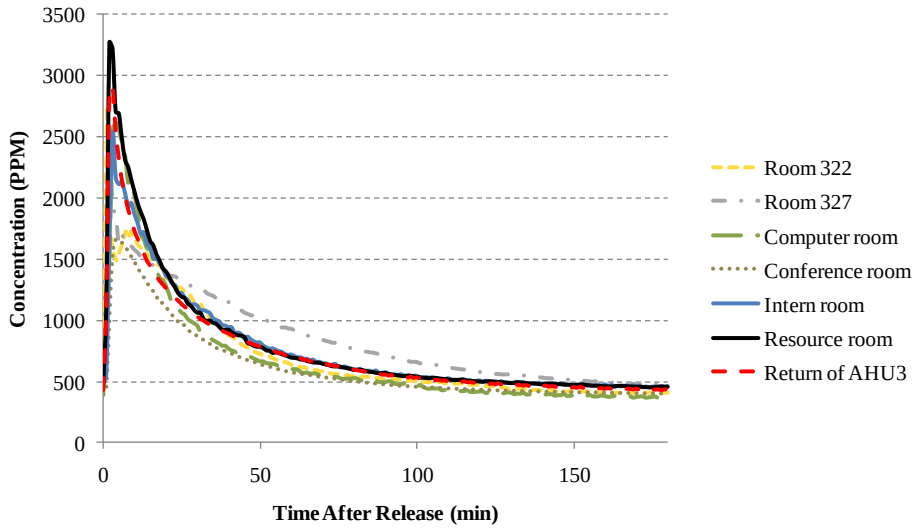


*Figure 5.26*: Measured $CO_2$ Concentration Curves for AHU3 Release 1 (Sae Kow, 2010)

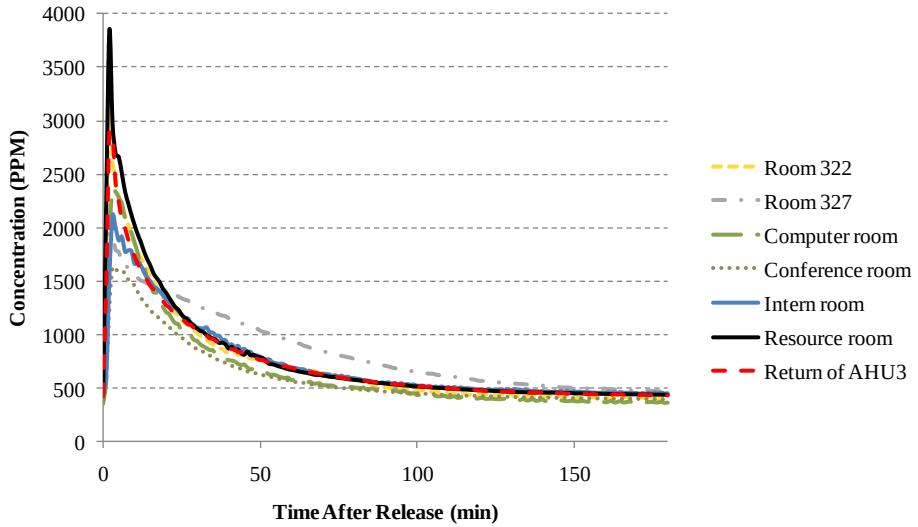


*Figure 5.27*: Measured $CO_2$ Concentration Curves for AHU3 Release 2 (Sae Kow, 2010)

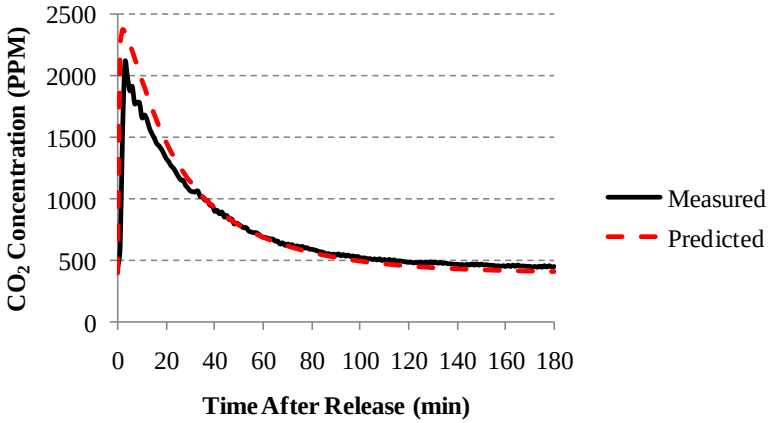


*Figure 5.28*: Intern Measured vs. Predicted $CO_2$ Concentration Curves

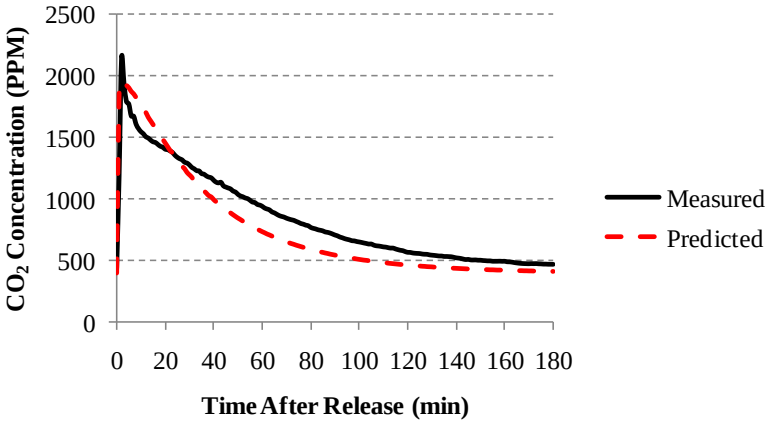


*Figure 5.30*: Room 327 Measured vs. Predicted $CO_2$ Concentration Curves

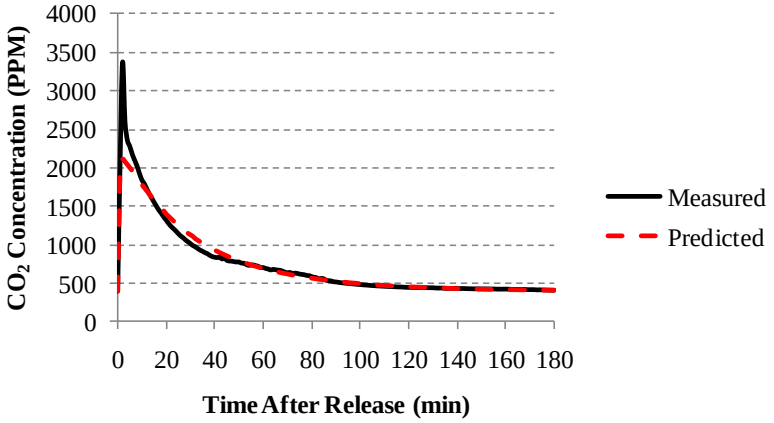


*Figure 5.29*: Room 322 Measured vs. Predicted $CO_2$ Concentration Curves

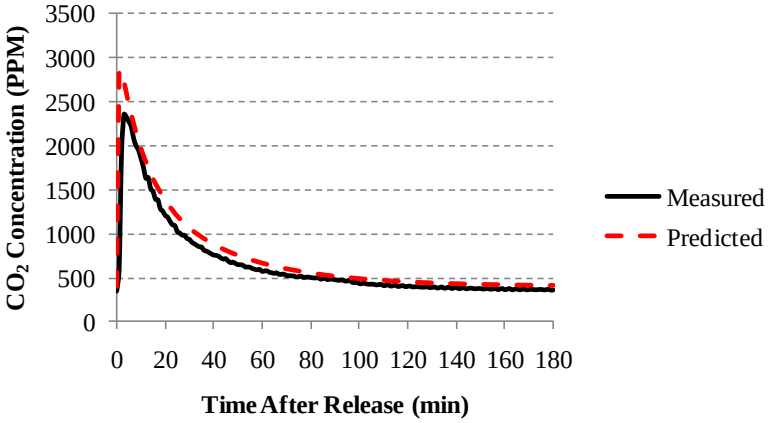


*Figure 5.31*: Computer Measured vs. Predicted $CO_2$ Concentration Curves

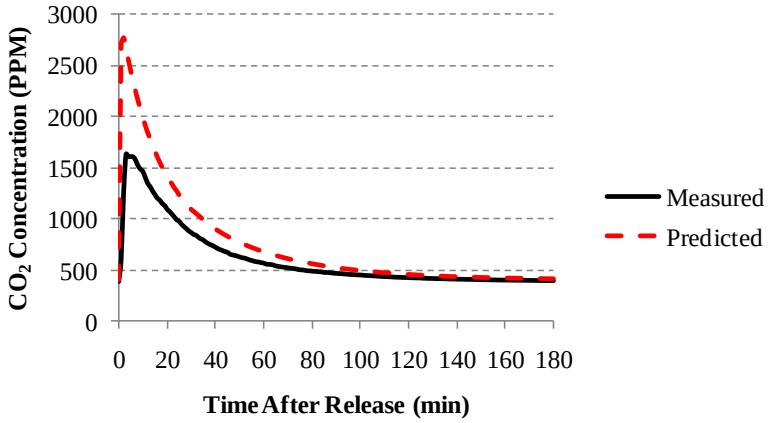


*Figure 5.32*: Conference Measured vs. Predicted $CO_2$ Concentration Curves

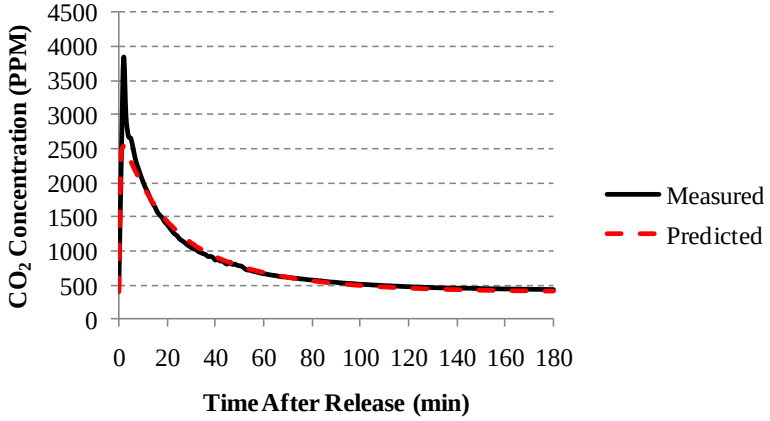


*Figure 5.33*: Resource Measured vs. Predicted $CO_2$ Concentration Curves

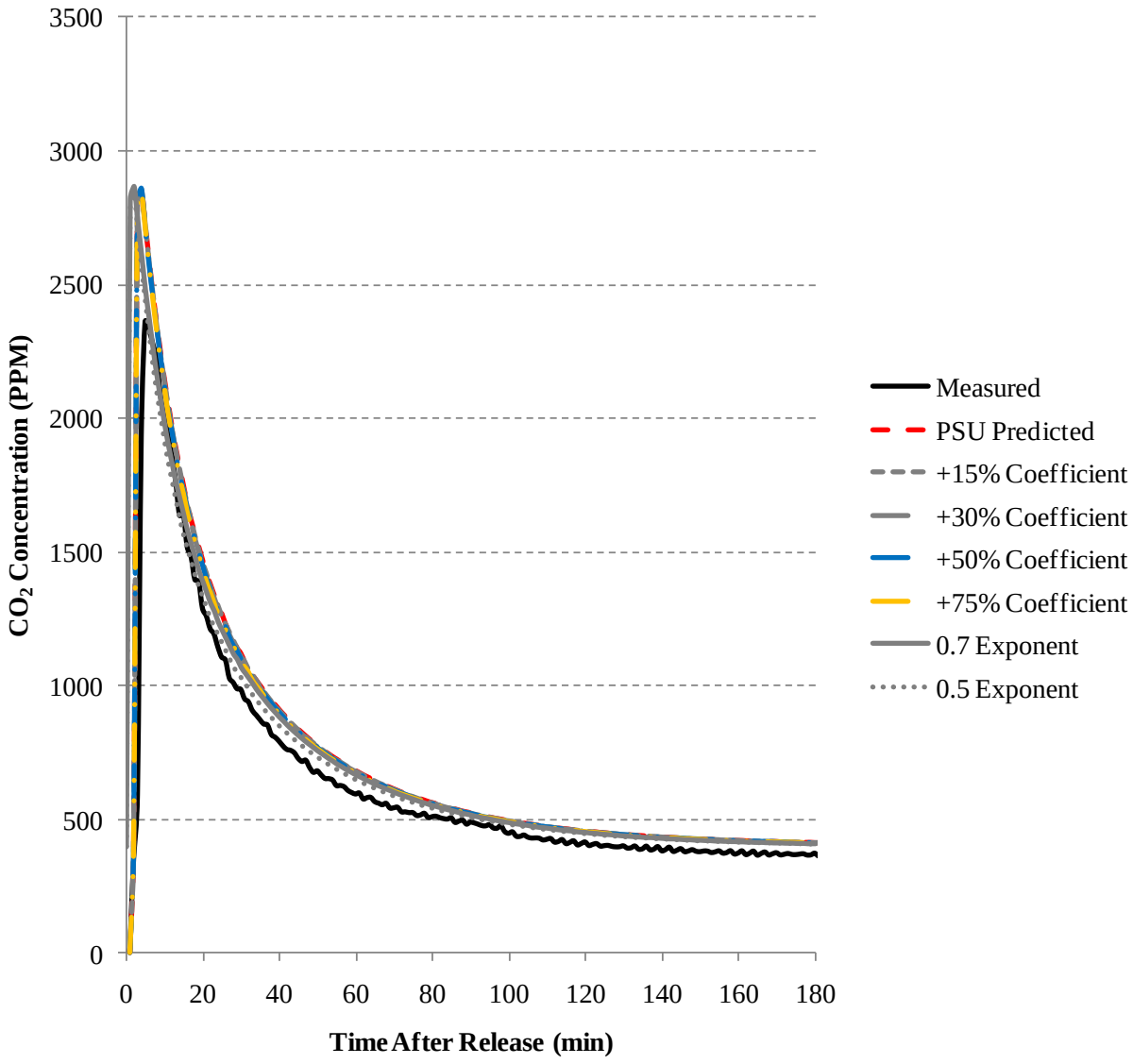


*Figure 5.34*: The Effect of Altering Airflow Parameters on Predicted $CO_2$ Behavior for Macro-Zone 3

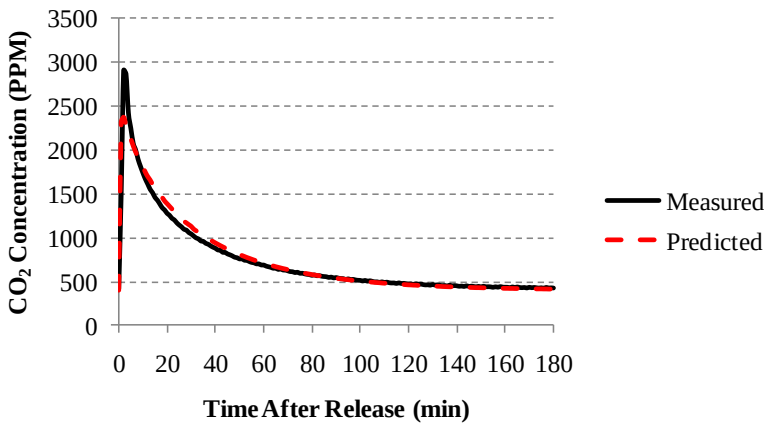


*Figure 5.35*: AHU3 Return Measured vs. Predicted $CO_2$ Concentration Curves

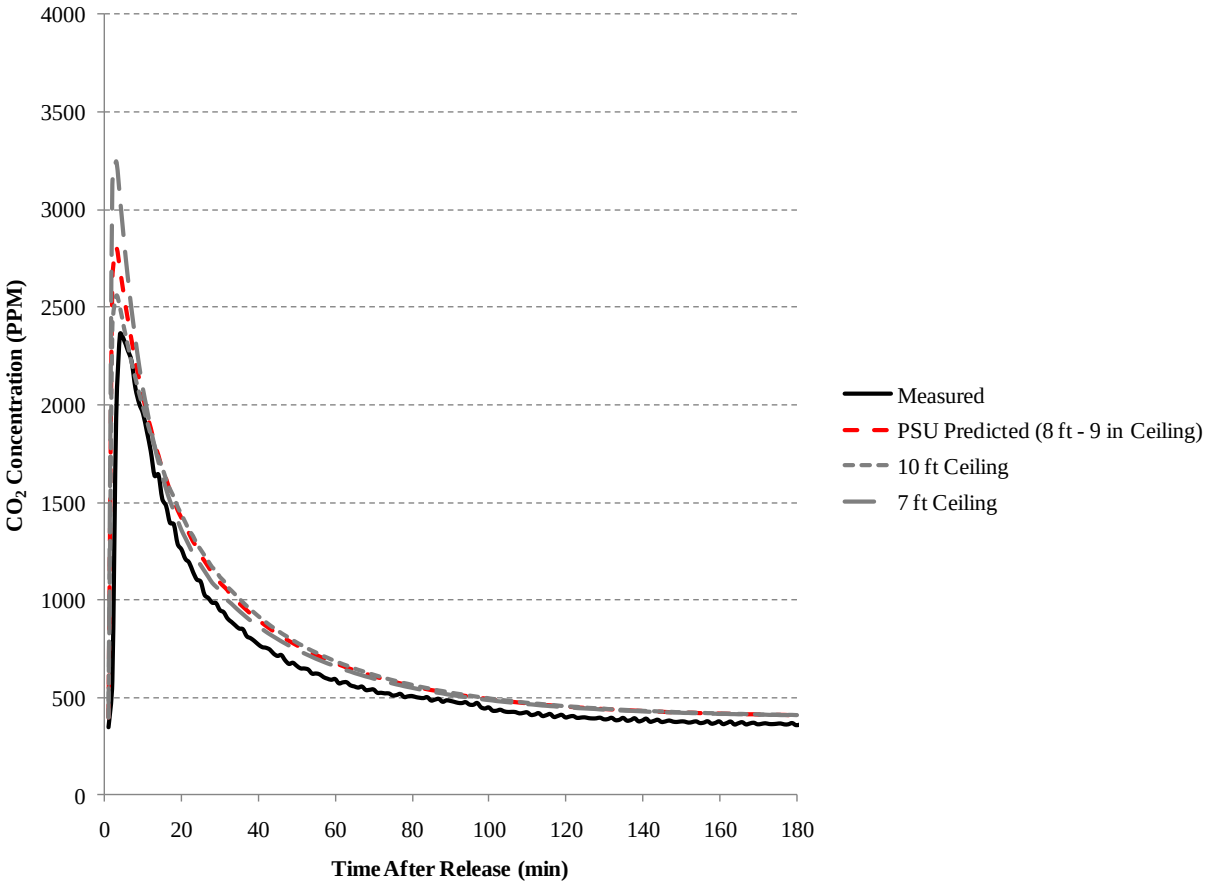


*Figure 5.36*: The Effect of Altering Room Volume on Predicted $CO_2$ Behavior for Macro-Zone 3

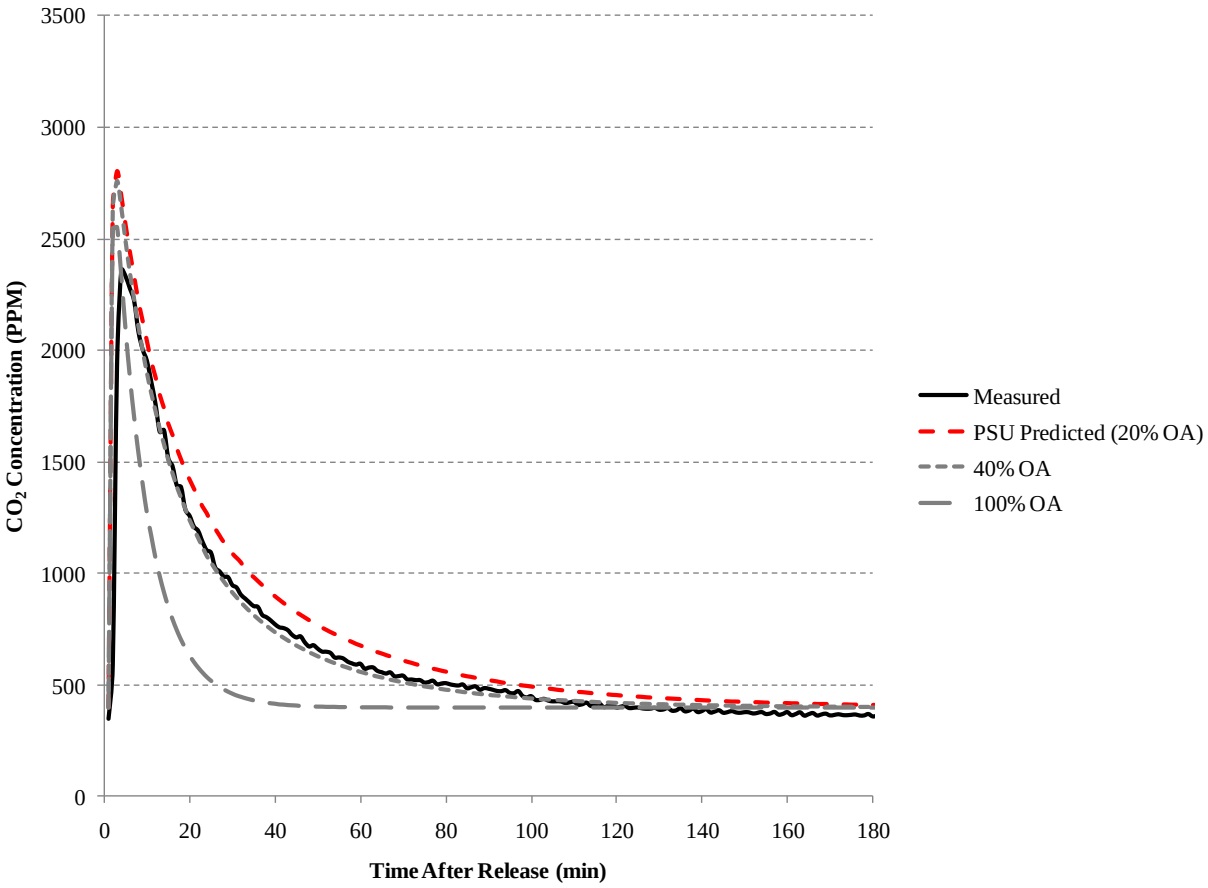


*Figure 5.37*: The Effect of Altering Outside Air Percentage on Predicted $CO_2$ Behavior for Macro-Zone 3

# CHAPTER 6: SUMMARY AND CONCLUSIONS

## 6.1 Research Objectives

The intent of this research was to develop a candidate calibration methodology that explicitly incorporates $CO_2$ tracer gas tests starting with methods that complement and do not fundamentally alter the basic approach currently implemented in PCW. The methodology was to be evaluated and refined using data from two buildings, one synthetic building and one actual building, which were studied in the framework of previous research. Extensions of this methodology which could potentially be investigated in future research efforts were to be outlined.

## 6.2 Summary of Synthetic Building Analysis

The initial development and evaluation of the proposed calibration methodology was conducted using a synthetic building. It was noted that previous work by Firrantello (2007) and Sae Kow (2010) both involved constant weather and operating conditions as well constant leakage parameters. The impacts that these factors could have on calibrating the PCW model was not investigated. Therefore, the proposed calibration methodology began by exploring these effects.

First, an airflow-based sensitivity analysis was proposed to identify the sensitivity of the building's airflow dynamics to changes in climate conditions and leakage parameter assumptions. The airflow-based sensitivity analysis, which evaluated the effects of wind speed, wind direction, ambient air temperature, and

leakage severity, originated as a $3^k$ factorial analysis. However, the analysis revealed that the relationship between the effects and the factor levels were approximately linear. Therefore, the analysis was simplified to a $2^k$ factorial. Also, a full factorial analysis may not be necessary and could possibly be substituted with a fractional factorial since there were little interaction effects. The interaction between wind and leakage severity is the exception. Scatter plots were found to be the most efficient way of displaying the results of this sensitivity analysis. The flow magnitudes and directions of air through individual airflow paths were plotted with varying scenarios on each axis to show the effect of changing one condition. Wind direction and wind speed were found to be the most significant variables, i.e. they were the most likely to significantly change airflow magnitudes and airflow directions within the building. The significance of wind, however, seemed to depend on whether or not the building was "leaky" in terms of leakage severity. Overall, the synthetic building's airflow dynamics seemed to be dominated by HVAC airflows. This airflow-based sensitivity analysis provided useful information on the influential drivers of the airflow dynamics. However, it did not help with identifying macro-zones for model reduction. Therefore, a move to a tracer gas-based ($CO_2$) analysis was deemed the most appropriate next step.

The tracer gas-based analysis step proposed using tracer gas data to determine macro-zones which will reduce the complexity of the model. The concept of model reduction was adopted because the calibration of multi-zone airflow models is an over-parameterized problem. Macro-zones are groups of

rooms whose dynamic airflow behavior are similar under varying conditions. Since macro-zone identification via airflow-based sensitivity analysis was deemed too problematic, tracer gas simulations were utilized. Along with HVAC zoning and floor plan geometry, it was proposed to use tracer gas histories to group rooms into macro-zones for model reduction. It was found that the best way to visualize the results of tracer gas release simulations was to use individual $CO_2$ concentration curves for each room. After performing various releases under different conditions, it was again found that the airflow dynamics of the building are dominated by HVAC airflows. In other words, the tracer gas histories and the macro-zones identified by these curves did not change significantly with varying conditions. Different conditions did result in slight variations in the decay rates of individual rooms. However, the significance of these variations is dependent on the situation, the purpose of the calibration, and the contaminant being analyzed. Similarly, with multiple air handling units, the significance of any cross-contamination between zones will be situation dependant.

An alternative method of visualizing the results of the tracer gas simulations was to calculate the decay coefficient for each room by performing a linear regression of the natural log transformation of the $CO_2$ concentration curves. This method would help characterize the entire concentration curve and better differentiate the slight variations found in the decay rates. Unfortunately, the $CO_2$ decay was found to follow a higher order exponential model. Therefore, a simplifying assumption was made to determine the decay coefficient from a small portion of the natural log transformed plot which was approximately linear.

Scatter plots of the decay coefficients were used to visualize how they change under varying conditions. These plots allowed for the interpretation of any clustering or trends in decay coefficients. Although these plots provided some insight into how the building reacts to changes in ambient temperature, wind, and leakage severity, it was again concluded that the airflow dynamics were HVAC dominated. As concluded from the tracer gas concentration plots, the significance of the scatter among decay coefficients is dependent on the calibration purpose and the contaminant type. These scatter plots also assisted with identifying macro-zones.

Once the macro-zones are identified, aggregate leakage parameters can be determined for each macro-zone based on tracer gas data. These new leakage parameters can then be used to update the model. However, since model calibration for a synthetic building is an arbitrary process, it was concluded that the remaining steps of the methodology should be performed on a model of a real building for which real data had been collected.

### 6.3 Summary of Real Building Analysis

Next, the proposed methodology was refined using a model of a real building for which measured data was available from previous research efforts. The airflow-based sensitivity analysis consisted of four factors (ambient air temperature, wind speed, wind direction, and leakage severity) at two factor levels each. The scatter plots generated from this analysis revealed mostly a "y = x" relationship indicating HVAC dominance of the airflow dynamics for the building. Similar to the synthetic building results, wind speed and wind direction

seemed to have some significant effects but only under the "leaky" condition. Also, the significance of any airflow magnitude or direction change is a function of the calibration purpose, the contaminant type, and the nature of the release. Similar to the synthetic building, the airflow-based sensitivity analysis plots did not help with identifying macro-zones. However, they provided some useful insights on how the building's airflow dynamics are impacted by the varying conditions.

Next a tracer gas-based sensitivity analysis was performed on the real building. A $CO_2$ release in the air handling unit was simulated under varying two factor levels of wind speed, wind direction, and leakage severity. At this point, careful attention was paid to the nature of the $CO_2$ release and the assumptions used in PCW to mimic an actual release which can significantly impact the resulting $CO_2$ concentration curves. For each release scenario, the concentration curves for each room were plotted on the same graph. The complexity of these graphs, due to the large number of rooms, led to a need to find other ways to investigate this data. Therefore, the concentration curves for individual rooms for each scenario were isolated on one plot. These graphs showed how the tracer gas behavior of each room responded to varying conditions. Similar to the airflow-based analysis, it was found that wind speed and wind direction appeared to have a significant effect only when the leakage severity is "leaky". Also, for rooms with exterior walls, wind appears to result in slightly faster $CO_2$ decay under almost any condition due to wind induced infiltration. These graphs also revealed some interesting impacts of leakage severity on rooms with mechanical

ventilation as compared to rooms without mechanical ventilation. As with the synthetic building, the significance of the slight variations in these concentration curves within a room under varying conditions is dependent on the situation.

In an attempt to better visualize these slight variations, the next step was to determine decay coefficients for each room under the various simulation conditions. However, due to the nature of the release and the fact that the decay follows a higher order exponential, it was too difficult to make the assumption used for the synthetic building. There was no part of the natural log transformation plot where each curve could be assumed linear for the calculation of decay coefficients. Therefore, the release assumption used for the synthetic building was also used for the real building model. Although this allowed for the calculation of decay coefficients, the simplified release assumption ignored peak concentrations which are also important. It was concluded that both decay coefficients and peak concentrations should be considered for macro-zone identification since both will impact occupant exposure.

Next, the $CO_2$ concentration curves were used to identify macro-zones. First, macro-zones were assumed based on floor plan geometry. The $CO_2$ concentration curves for each assumed macro-zone were plotted. Separating the concentration curves into several plots helped to relieve some of the confusion from plotting them all together. It was immediately realized that the assumed macro-zones based on floor plan geometry alone did not create groups of rooms with similar tracer gas behavior. Variations in decay rates and peak concentrations by visual comparison led to a second iteration of macro-zones. This second

iteration showed improved matches within each macro-zone. These plots were generated for each simulation scenario from the tracer gas-based sensitivity analysis. It was revealed that the macro-zone groupings did not change under varying conditions. Since all previous results have indicated HVAC domination of the airflow dynamics, these macro-zones were compared to the measured HVAC flow rates. It was found that the identified macro-zones were directly related to the air change rates in the rooms. A similar conclusion was drawn from the synthetic building analysis. Therefore, the tracer gas-based sensitivity analysis may not be necessary and macro-zones could possibly be identified by room air change rates alone. However, the tracer gas-based sensitivity analysis does have its use in that it provides the confidence to make such a conclusion.

With the macro-zones identified, the final step was to calibrate the model. It was proposed that the flow parameters, i.e. coefficient and exponent, in each airflow path in each macro-zone be tuned to improve the match between the predicted and the measured $CO_2$ concentration curves for at least one room of each macro-zone. Then, the resulting flow parameters determined for each macro-zone would then be used to update the multi-zone model by becoming the new flow parameters for all the airflow paths in each respective macro-zone. A formal factorial analysis can be set up to organize the simulations needed to vary the flow parameters. It was noted that this process only provides a method for calibrating one macro-zone at a time.

For the real building investigated in this research, it was found that altering the flow parameters in the flow paths of macro-zones did not seem to

significantly improve the match between measured and predicted tracer gas curves. It was hypothesized that after all of the HVAC flows had been measured and entered into the model, the remaining discrepancies between predicted and measured curves would be the result of incorrect flow parameters in the mathematical relationships describing the airflow through the building envelope and between internal zones in the multi-zone model. However, altering the flow parameters did not significantly rectify the differences between predicted and measured concentration curves. It is possible that these discrepancies are a result of measurement errors or modeling errors. One possibility that involves both model assumptions and measurement is the "well-mixed" problem. The multi-zone model assumed that the room is "well-mixed" and that the contaminant concentration is uniform throughout the room volume at each time step. However, in reality the room may be poorly mixed and the $CO_2$ sensor may be in a location with a high concentration or low concentration of $CO_2$ with respect to the rest of the room. Sae Kow (2010) notes encountering this problem.

Since most of the analyses performed in this research indicate that the airflow dynamics of the building are HVAC dominated, it is recommended that more attention be paid to accurate modeling of the mechanical ventilation system. Future research could utilize tracer gas testing to determine the significant HVAC airflows.

Finally, because it was identified that the macro-zones were directly related to the air changes in each room, and considering this along with the evidence of HVAC dominance, it was concluded that the tracer gas behavior of a

room is driven by the air change rate. Attempted calibration revealed that the tracer gas behavior in a room is significantly more sensitive to factors such as room volume and outside air percentage than to room "leakiness", i.e. flow parameter assumptions. This stresses the importance of accurately measuring factors which have significant impacts on room air change rates. After accurately modeling room air change rates, further discrepancies between predicted and measured behavior can be rectified by altering flow parameters in the multi-zone model.

It has been noted that this study only considered releases in an air handling unit. This simplification is considerable since the building's response to a release could be quite different for other release locations. If the building's airflow dynamics are dominated by climatic conditions (e.g. a naturally ventilated building) or if after a release has occurred operations personnel decide to shut down the HVAC system, then the building's leakage paths will become more important in how they impact interior airflow dynamics. Under these situations, the methodology for tuning flow parameters would become more significant. However, since most "non-critical" buildings will not have advanced sensing and alarm equipment, it is very likely that a significant amount of time will pass before a release is noticed and any control measures can be performed. Therefore, the HVAC system would be running during the most critical time, i.e. 10-30 min after the release. Therefore, the significance of parameters affecting air change rates versus leakage parameters in the calibration will vary depending on the situation.

The advantages and insights provided by the proposed calibration methodology are listed below:

1. The concept of macro-zone identification provides a robust manner of calibrating a complex and over-parameterized model consistent with experimental data. Macro-zones reduce the number of individual flow parameters that need to be tuned during calibration.
2. Provides a scientific means of identifying sets of rooms or "macro-zones" which have similar airflow dynamics and tracer gas behavior. Therefore, occupants in these rooms are likely to be exposed in the same manner when a contaminant release occurs.
3. Identification of these "macro-zones" takes into account the effect of different climatic conditions and building flow characteristics (as against previous work which only considered one set of conditions).
4. Suggests rooms where it would be advantageous to monitor $CO_2$ decay, i.e. where one should locate $CO_2$ sensors during field testing.
5. Allows calibrating flow parameters for different macro-zones based on measured $CO_2$ concentration tests.
6. Facilitates the understanding of building airflow behavior and tracer gas behavior under varying conditions via experimental design techniques.

## 6.4 Summary of Proposed Calibration Methodology

The specific intent of the proposed calibration methodology was to improve upon the PSU tuning algorithm by explicitly using $CO_2$ tracer gas data

during the calibration process of multi-zone airflow models. The entire methodology is summarized below:

1. Preliminary Model Tuning: Develop a "somewhat" realistic multi-zone model of the building by calibrating based on the PSU tuning algorithm (Firrantello, 2007). This step is necessary for enhancing the robustness of the entire calibration.
2. Airflow-Based Sensitivity Analysis: Use experimental design techniques such as factorial analysis to evaluate whether the building airflow dynamics are climate or HVAC system dominated; and if so, by how much. Also, this sensitivity is meant to identify the significant or important drivers of the airflow dynamics. This step is needed in order to verify that the calibration performed under one set of operating and climatic factors still applies for other conditions.
3. Identify Macro-Zones for Model Reduction: Calibrating multi-zone airflow models is a highly over-parameterized problem. Model reduction is warranted which is achieved by grouping rooms into macro-zones according to HVAC zoning, building geometry, and a tracer gas-based sensitivity analysis. Each room within a macro-zone will have similar airflow dynamics. A preliminary observation (yet to be tested against more case study examples) is that the great effort of performing factorial sensitivity tests with tracer gas releases could be avoided by simply selecting the macro-zones based on room air change rates.

4. Perform tracer gas release tests in the building being analyzed and place sensors in at least one room of each identified macro-zone. Some amount of replication is strongly advised.
5. Model Tuning and Calibration: Tune the flow parameters of the multi-zone model to improve the match between measured and predicted tracer gas concentration dynamics in each macro-zone. If flow parameter tuning is unsuccessful, investigate possible errors in measurements of factors that directly influence the room air changes (i.e., HVAC flow rates, room volumes, outside air intake, etc.), as well as possible $CO_2$ measurement errors (i.e., deviations from the well-mixed assumption).
6. Evaluate Model Adequacy: Evaluate the adequacy of the updated model based on some metric. Since a robust metric for model adequacy has yet to be determined, and since previous research has questioned the confidence in conclusions from any one metric, the evaluation of the model can be based on several metrics such as: (a) percentage of correctly predicted airflow directions or (b) percentage of satisfactory ASTM Standard D5157 statistical metrics or some modified from thereof involving predicted vs. measured $CO_2$ data.

# CHAPTER 7: RECOMMENDATIONS FOR FUTURE WORK

The proposed calibration methodology was evaluated and refined using data from two buildings, one synthetic building and one actual building, which were studied in the framework of previous research. Extensions of this methodology which could potentially be investigated in future research efforts are outlined below.

1. Explore in more detail different release scenarios since this research focused mainly on calibrating PCW with releases in air handling units. Analyze how other release scenarios impact the calibration procedure. Investigate important conclusions from simulating and testing releases in other critical areas of a particular building (e.g. main lobby, mailroom, etc.). Examine where to perform tracer gas releases if there is no duct distribution system.
2. Develop candidate calibration methodologies to handle transient airflow situations. The assumption in this research was a quasi-static state of airflows. The HVAC systems were forced to operate at constant air volume conditions while $CO_2$ testing was being performed. It is more common to encounter buildings with systems that involve some sort of variable air volume flow. While increasing the complexity of the calibration procedure, variably flows are more representative of realistic operation.

3. Develop candidate calibration methodologies for buildings that are climate dominated, i.e., buildings whose airflow dynamics change significantly under varying weather conditions. This could apply to tall buildings or naturally ventilated buildings, for example. Since this research found buildings to be HVAC dominated and since the tuning of flow parameters seemed to have little impact, the applications of such a tuning methodology may be more appropriate for naturally ventilated buildings. The changes to the methodology for these types of buildings may also be applied to mechanically ventilated buildings whose systems are shut off after a release has occurred.
4. Develop a method of identifying and tuning the flow parameters of individual airflow paths in any room that may be causing a problem in the match between model predictions and measured data.
5. The methodology in this research assumes calibration for one macro-zone at a time. Research and evaluate methodologies for calibrating all macro-zones simultaneously.
6. Consider how more detailed modeling will impact tracer gas-based calibration. For example, the use of CONTAM rather than PCW to account for duct leakage, specific duct routing through the building, controls, etc.
7. Research other metrics for evaluating model adequacy. Firrantello (2007) and Sae Kow (2010) both noted issues with the currently used metrics: (a) percentage of correctly predicted airflow directions and (b) ASTM

Standard D5157 statistical metrics. Consider streamlining ASTM Standard D5157 so as to have fewer metrics for comparing measured and modeled indoor air quality behavior. Evaluate the use of using the root mean square error (RSME), or similar statistics, between predicted and measured $CO_2$ concentration data as a metric for model quality.

8. Develop automated procedures for extracting macro-zones from a model. For example, statically based categorization techniques could be integrated into the PCW software program.
9. Use more case studies to verify the conclusions that in mechanically ventilated buildings, macro-zones can be identified strictly by HVAC zoning and room air change rates.
10. Research and analyze in more depth the use of compartmental modeling/inverse methods for calculating flow parameters to update the model. Mathematically develop equations for various possible compartmental model situations and solve for flow parameters. Evaluate the utility of using matrix notation and determine how this notation can reveal useful information without having to solve any equations. This is similar to the work presented by Evans (1996).
11. Investigate other applications for multi-zone model calibration methodologies. These applications could include quantifying building indoor air quality for the purposes of green building design or for improving the design of health care facilities, naturally ventilated

buildings, or certain industrial facilities, all of which require careful consideration of building airflow dynamics.

## REFERENCES


Awbi, H.B., 1991. *Ventilation of Buildings*. London, UK: E&FN Spon, Chapman and Hall.

Axley, J., 1988. Progress Toward a General Analytical Method for Predicting Indoor Air Pollution in Buildings: Indoor Air Quality Modeling Phase III Report. National Bureau of Standards, Gaithersburg, MD.

ASHRAE, 2003. Risk Management Guidance for Health, Safety, and Environmental Security Under Extraordinary Incidents. American Society of Heating, Refrigerating, and Air-Conditioning Engineers, Atlanta, GA.

ASHRAE, 2009. *ASHRAE Handbook: Fundamentals*, IP Edition. American Society of Heating, Refrigerating, and Air-Conditioning Engineers, Atlanta, GA.

ASTM, 2003. D5157-97: Standard Guide for Statistical Evaluation of Indoor Air Quality Models. The American Society for Testing and Materials, Philadelphia, PA.

Bahnfleth, W.P., 2004. Reducing Building Vulnerability: Recent Guideline Documents. *Homeland Security for Buildings*. Supplement to *HPAC Engineering* Magazine.

Bahnfleth, W.P., Freihaut, J., Bem, J., and Reddy, T.A., 2008. Development of Assessment Protocols For Security Measures - A Scoping Study, Subtask 06-11.1: Literature Review. Report submitted to National Center for Energy Management and Building Technologies, prepared for U.S. Department of Energy.

Bahnfleth, W.P., Freihaut, J., Bem, J., Reddy, T.A., and Snyder, S., 2009. Development Of Assessment Protocols For Security Measures – Final Report 06-11.2: Identification and Evaluation of Existing Tools. Report submitted to the National Center for Energy Management and Building Technologies, prepared for U.S. Department of Energy.

Bem, J.S., 2008. Development of a Security Design Anlaysis Procedure for the Protection of Low-Risk Buildings from Chemical and Biological Attacks. Master of Science Thesis, Department of Architectural Engineering, The Pennsylvania State University.

Box, G.E.P., Hunter, W.G., and Hunter, J.S., 1978. *Statistics for Experimenters*. New York: John Wiley & Sons.

Etheridge, D. and Sandberg, M., 1996. *Building Ventilation – Theory and Measurements*. Chichester, U.K.: John Wiley & Sons.

Evans, W.C., 1996. Linear Systems, Compartmental Modeling, and Estimability Issues in IAQ Studies. *Characterizing Sources of Indoor Air Pollution and Related Sink Effects, ASTM STP 1287*, Bruce A. Tichenor, Ed., American Society for Testing and Materials, pp.239-262.

Feustel, H.E., and Kendon, V.M., 1985. Infiltration Models for Multicellular Structures: A Literature Review. *Energy and Buildings*, vol. 8, pp. 123-136.

Feustel, H.E., and Dieris, J., 1992. A Survey of Airflow Models for Multizone Structures. *Energy and Buildings*, vol. 18. pp. 79-100.

Firrantello, J., Bahnfleth, W., Musser, A., Freihaut, J., and Jeong, J.W., 2005. Application of Sensitivity Analysis to Multizone Airflow Model Tuning. *Proceedings of Clima 2005* (8th REHVA World Congress). Paper 289, 6 pages.

Firrantello, J., Bahnfleth, W., Jeong, J.W., Musser, A., and Freihaut, J., 2007. Field Testing of a Data Driven Multizone Model Calibration Procedure. Department of Architectural Engineering, The Pennsylvania State University.

Firrantello, J., 2007. Development of a Rapid, Data Driven Method for Tuning Multizone Airflow Models. Master of Science Thesis, Department of Architectural Engineering, The Pennsylvania State University.

Heinsohn, R. and Cimbala, J., 2003. *Indoor Air Quality Engineering – Environmental Health and Control of Indoor Pollutants*. New York: Marcel Dekker.

Hou, D., Jones, J.W., Hunn, B.D., and Banks, J.A., 1996. Development of HVAC System Performance Criteria Using Factorial Design and DOE-2 Simulation. *Proceedings of the Tenth Symposium on Improving Building Systems in Hot and Humid Climates* (Fort Worth, TX, May 13-14, 1996).

Janus, M., Fenton, G., and Blewett, W., 2005. Protection of Buildings from Chemical and Biological Threats. *The WIT Transactions on the Built Environment*, vol. 82, pp. 785-794.

Sae Kow, P., 2010. Field Verification of a Semi-Empirical Multizone Airflow Modeling Calibration Method. Master of Science Thesis, Department of Architectural Engineering, The Pennsylvania State University.

Kowalski, W.J., 2003. Immune Building Systems Technology. New York: McGraw-Hill.

Kowalski, W.J., Bahnfleth, W., and Musser, A., 2003. Modeling Immune Building Systems for Bioterrorism Defense. *Journal of Architectural Engineering*, June 2003, pp. 86-86. American Society of Civil Engineers.

Kreider, J.F., Curtiss, P.S., Rabl, A., 2005. *Heating and Cooling of Buildings – Design for Efficiency*, 2nd ed. Boulder: Kreider and Associates, LLC.

Lawrence, T. and Braun, J., 2005. Evaluation of Simplified Models for Predicting $CO_2$ Concentrations in Small Commercial Buildings. *Building and Environment*, vol. 41. pp. 184-194.

LBNL, 1989. COMIS (Conjunction of Multizone Infiltration Specialists). Lawrence Berkeley National Laboratory, Berkeley, CA.

Montgomery, D.C., 2009. *Design and Analysis of Experiments*, 7th ed. New Jersey: John Wiley & Sons.

Musser, A. and Persily, A.K., 2002. Multizone Modeling Approaches to Contaminant-Based Design. *ASHRAE Transactions*, vol. 108(2), June. American Society of Heating, Refrigerating, and Air-Conditioning Engineers, Atlanta, GA.

Nakano, V.M., Croisant Jr., W.J., and Abraham, D.M., 2007. A Design Assessment System to Protect Buildings From Internal Chemical and Biological Threats. *Proceedings of the 2007 ASCE International Worskhop on Computing in Civil Engineering* (Pittsburgh, PA, July 24-27, 2007).

NIST, 2008. Multizone Modeling Website. National Institute of Standards and Technology. http://www.bfrl.nist.gov/IAQanalysis/

Persily, A.K., 1998. Airtightness of Commercial and Institutional Buildings: Blowing Holes in the Myth of Tight Buildings. *DOE/ASHRAE/ORNL/BETEC/NRCC/CIBSE Conference Thermal Performance of the Exterior Envelopes of Buildings VII*, pp.829-837.

Price, P.N., Chang, S.C., and Sohn, M.D., 2004. Characterizing Buildings for Airflow Models: What Should We Measure. Indoor Environment Department, Lawrence Berkeley National Laboratory, Berkeley, CA.

Reddy, T.A., 2006. Literature Review on Calibration of Building Energy Simulation Programs: Uses, Problems, Procedures, Uncertainty, and Tools. *ASHRAE Transactions*, vol. 112(1), January. American Society of Heating, Refrigerating, and Air-Conditioning Engineers, Atlanta, GA.

Reddy, T.A. and Bahnfleth, W.P., 2006. Requirements for a Probabilistic Quantitative Relative Risk-Based Decision Methodology for Reducing Vulnerability of Building Occupants to Extreme IAQ Events. *ASHRAE Transactions*, vol. 113(1), DA-07-031, January. American Society of Heating Refrigerating, and Air-Conditioning Engineers, Atlanta, GA.

Reddy, T.A., Maor, I., and Panjapornpon, C., 2007. Calibrating Detailed Building Energy Simulation Programs with Measured Data. *HVAC&R Research*, vol. 13, no. 2. American Society of Heating, Refrigerating, and Air-Conditioning Engineers, Atlanta, GA.

Spengler, J.D., Samet, J.M., and McCarthy, J.F., 2001. *Indoor Air Quality Handbook*. New York: McGraw-Hill.

Stoecker, W.F., 1989. *Design of Thermal Systems*, 3rd ed. New York McGraw-Hill.

Street, R.L., Watters, G.Z., and Vennard, J.K., 1996. *Elementary Fluid Mechanics*, 7th ed. New Jersey: John Wiley & Sons.

USGBC, 2010. Leadership in Energy and Environmental Design Rating System. United States Green Building Council. www.usgbc.org

Vandemusser Design LLC, 2007. PCW 1.0 Software User Manual. Vandemusser Design LLC under subcontract to The Pennsylvania State University.

Walton, G.N., 1995. CONTAM94: A Multizone Airflow and Contaminant Dispersal Model with a Graphic User Interface. *Proceedings of the Fourth international IBPSA Conference* (Madison, Wisconsin, August 14-16, 1995).

Walton, G.N., and Dols, W.S., 2005. CONTAM 2.4 User Guide and Program Documentation. Building Environment Division, Building and Fire Research Laboratory, National Institute of Standards and Technology, Gaithersburg, MD.

# APPENDIX A

# ANCILLARY ANALYSIS PLOTS

## A.1 Synthetic Building Analysis Plots

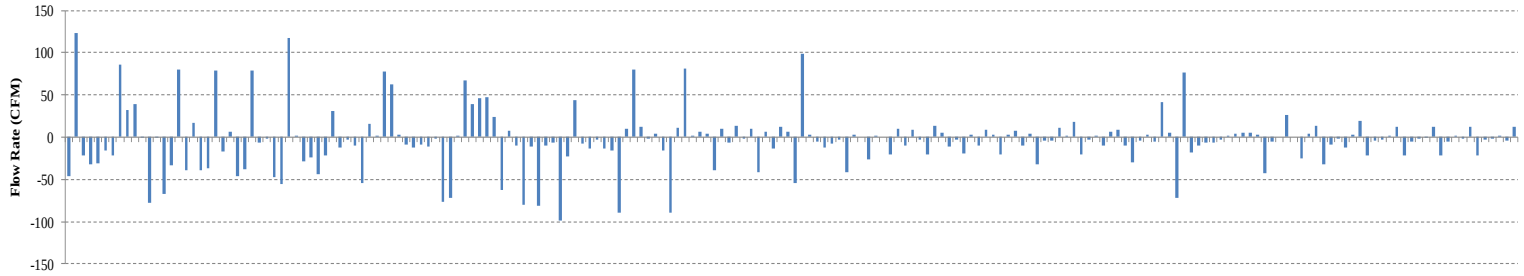


*Figure A1.1*: Bar Graph of Airflow Magnitudes and Directions for the 70°F, 10 mph, Leaky Scenario

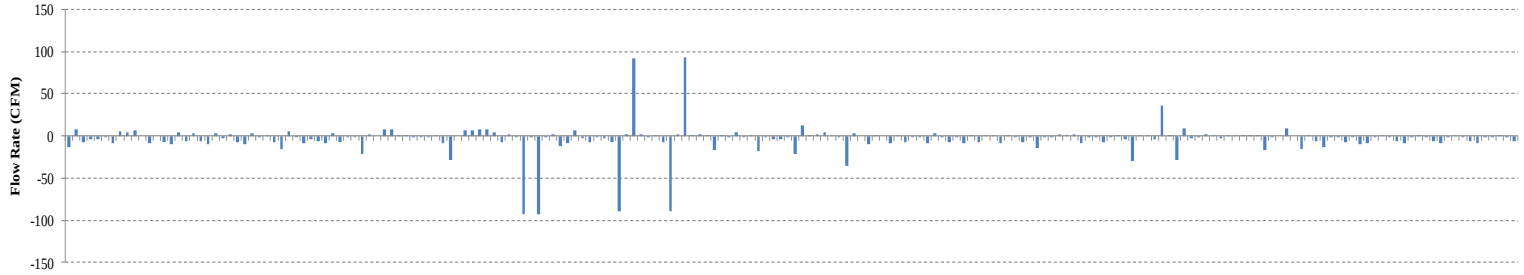


*Figure A1.2*: Bar Graph of Airflow Magnitudes and Directions for the 70°F, 10 mph, Tight Scenario

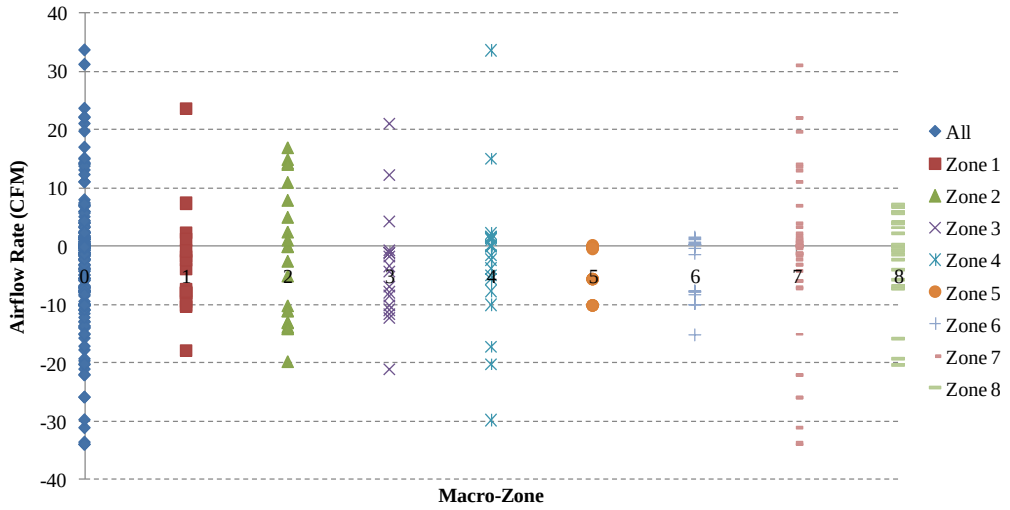


*Figure A1.3*: Airflow Rates for Each Airflow Path Separated by Assumed Macro-Zones (70°F, 5 mph, "Average")

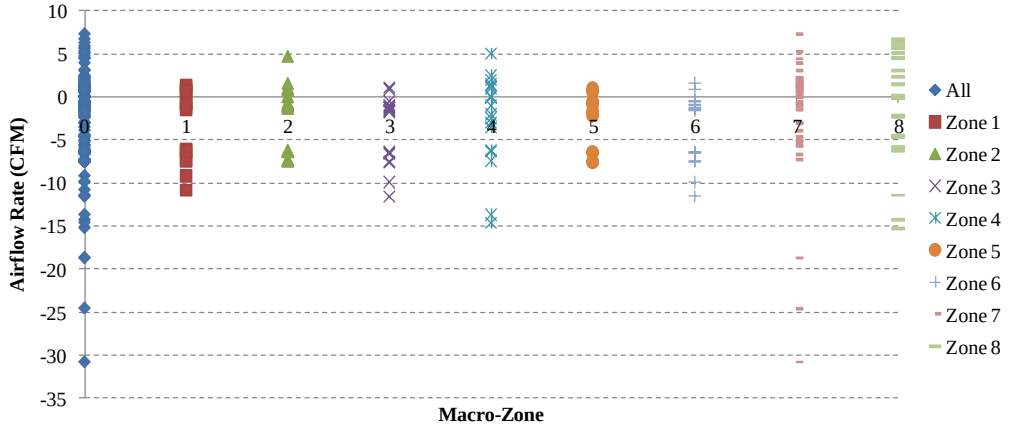


*Figure A1.4*: Airflow Rates for Each Airflow Path Separated by Assumed Macro-Zones (70°F, 0 mph, "Average")


*Figure A1.5*: Tracer Gas Release in All Zones (0 min)

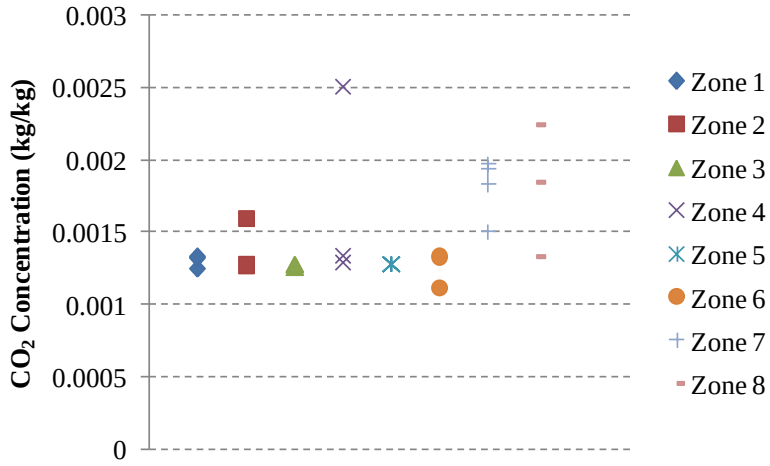


*Figure A1.7*: Tracer Gas Release in All Zones (10 min)

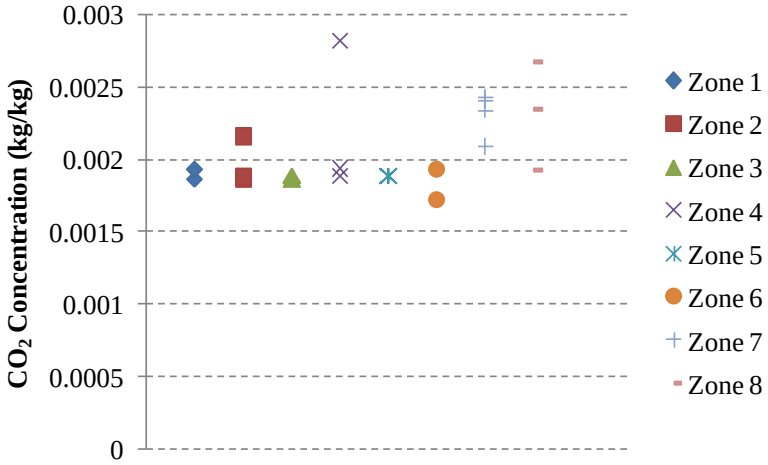


*Figure A1.6*: Tracer Gas Release in All Zones (5 min)

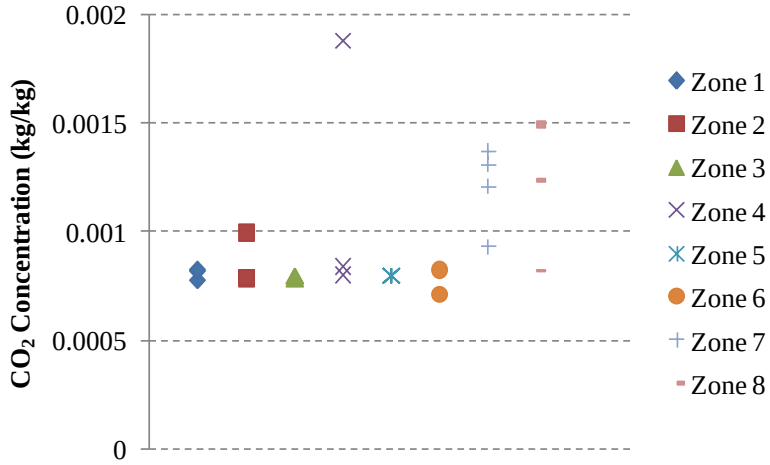


*Figure A1.8*: Tracer Gas Release in All Zones (15 min)

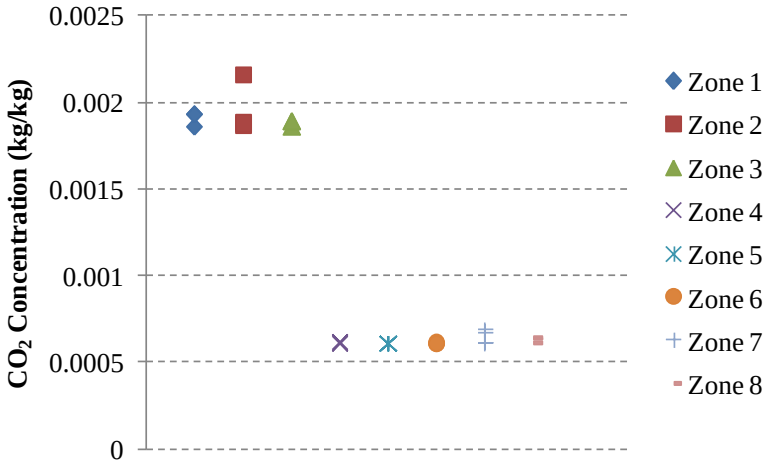


*Figure A1.9*: Tracer Gas Release in North AHU (5 min)

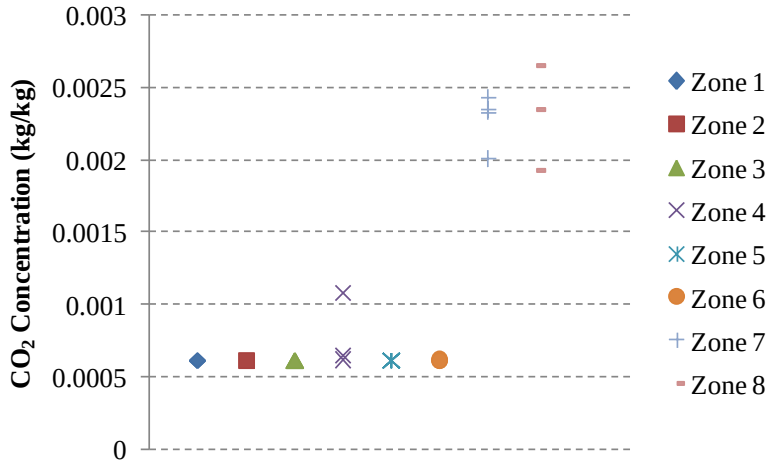


*Figure A1.11*: Tracer Gas Release in Core AHU (5 min)

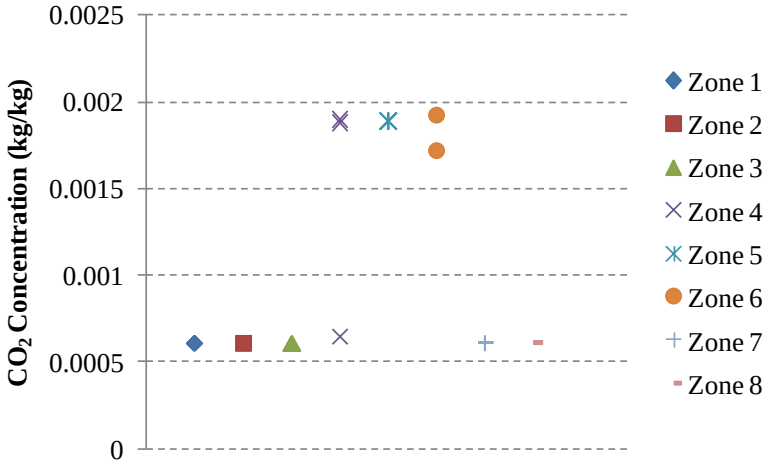


*Figure A1.10*: Tracer Gas Release in South AHU (5 min)

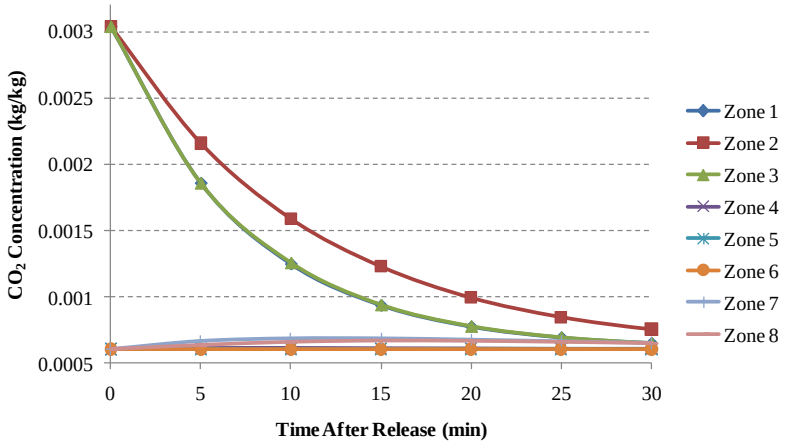


*Figure A1.12*: Tracer Gas Release in North AHU

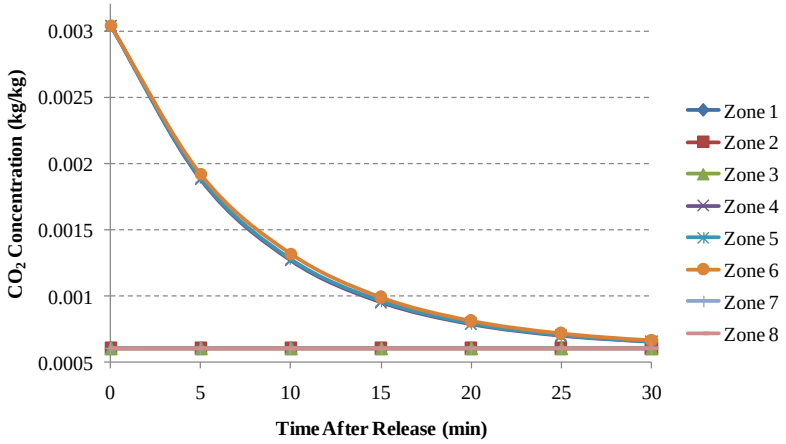


*Figure A1.13*: Tracer Gas Release in South AHU

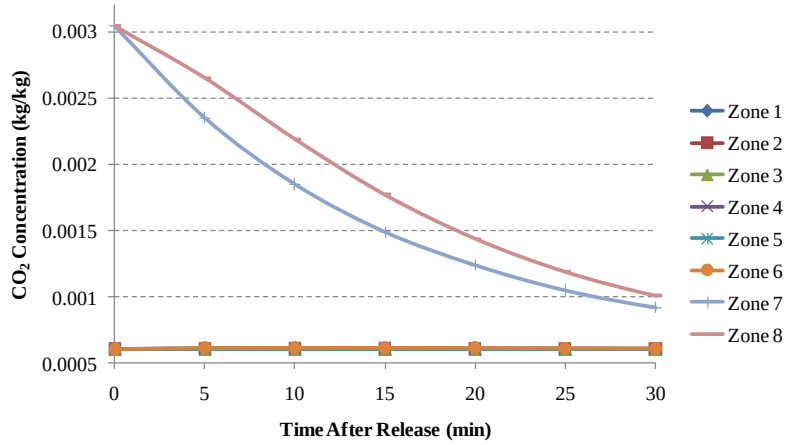


*Figure A1.14*: Tracer Gas Release in Core AHU

## A.2 Real Building Analysis Plots

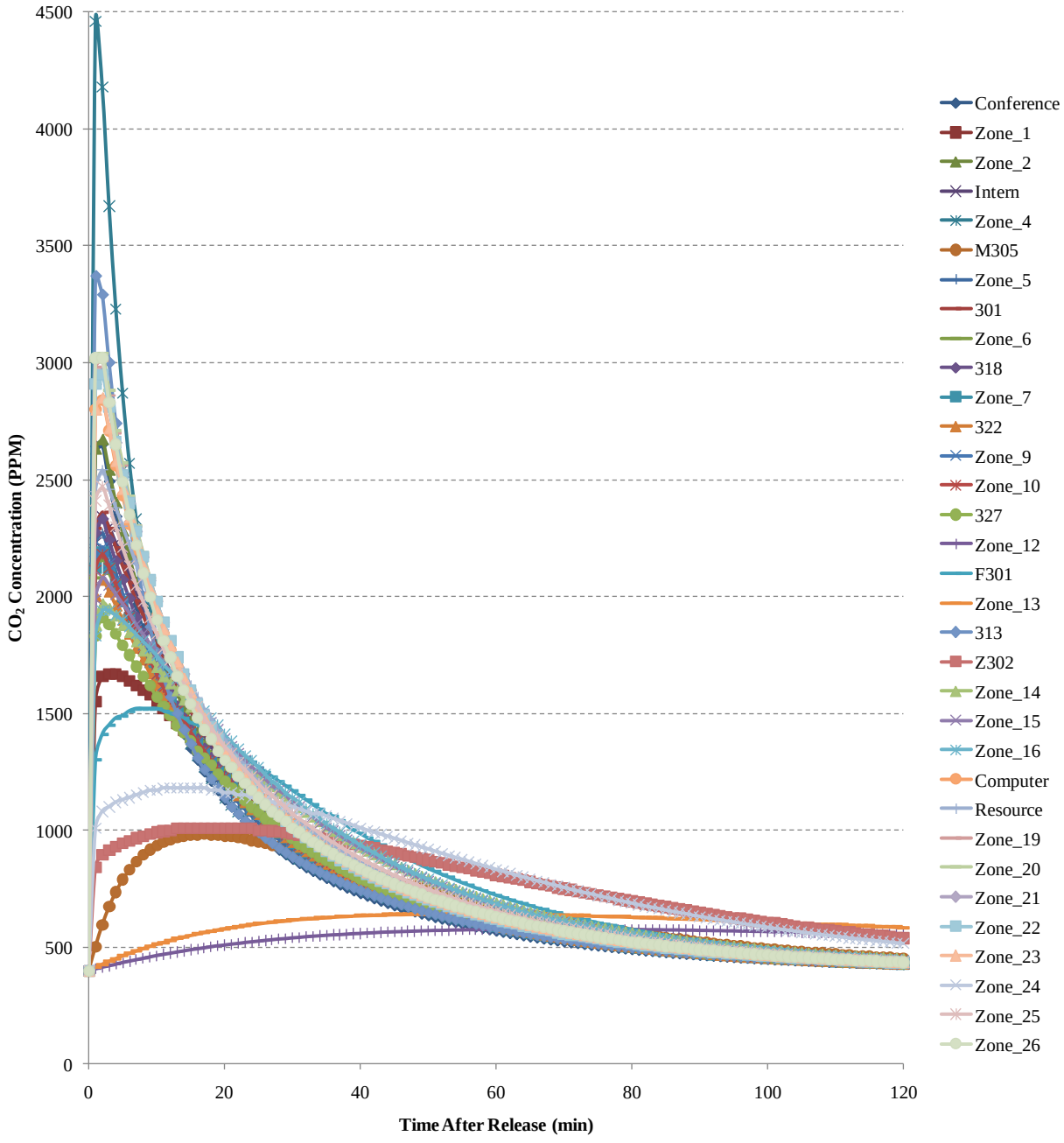


*Figure A2.1*: $CO_2$ Concentration Curves for Individual Rooms (67°F, NW Wind at 10 mph, "Leaky")

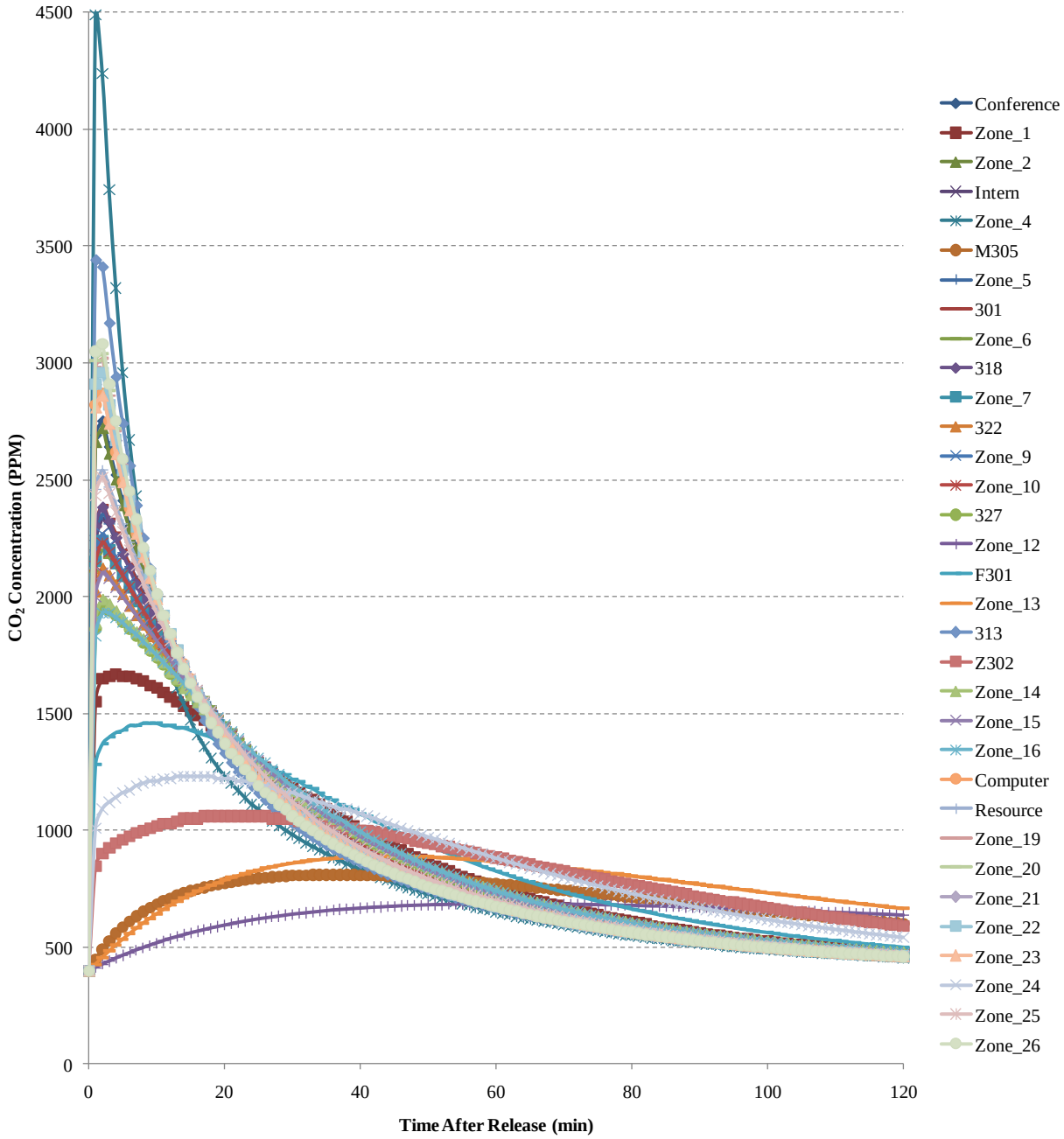


*Figure A2.2*: $CO_2$ Concentration Curves for Individual Rooms (67°F, N Wind at 10 mph, "Tight")

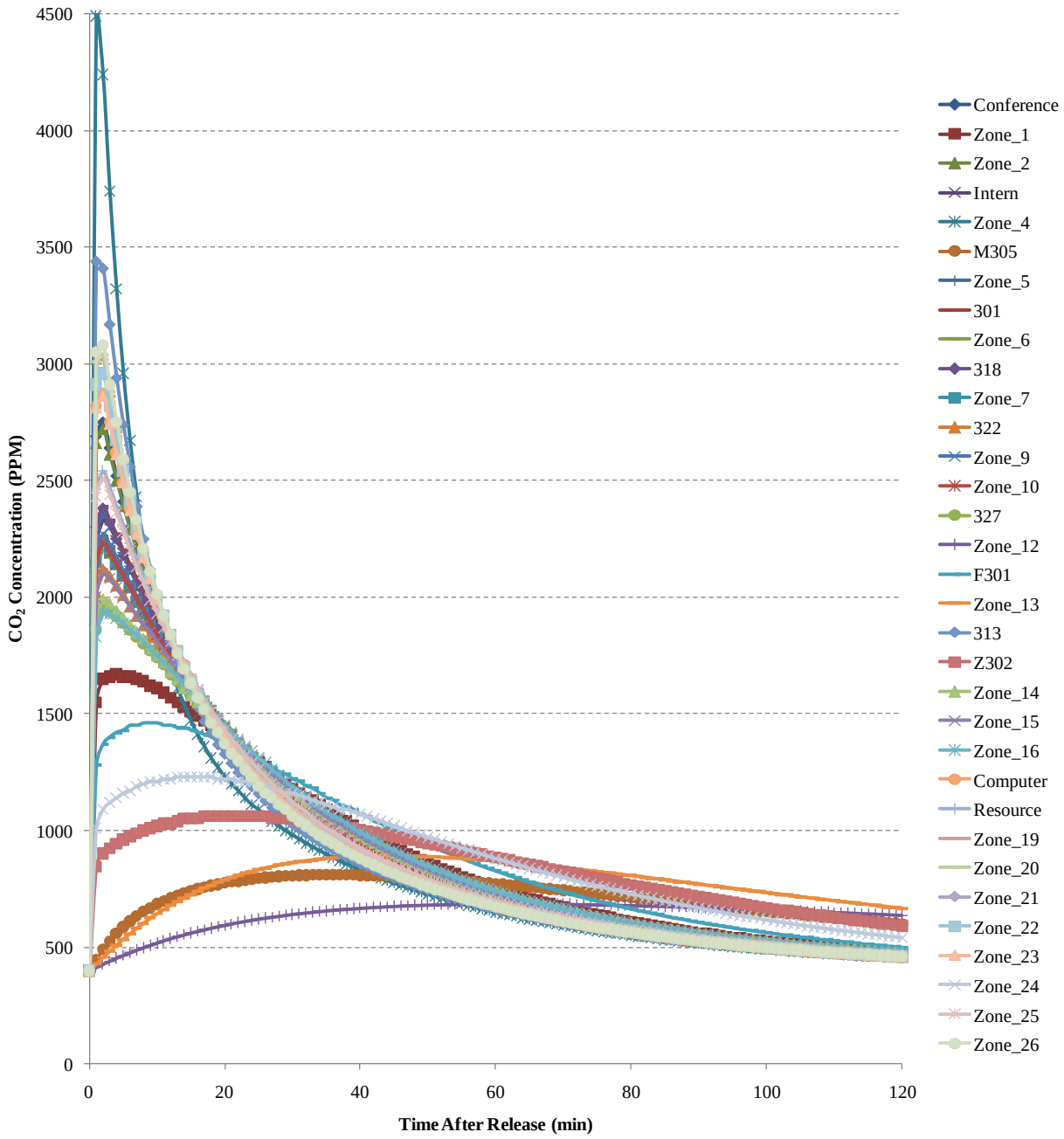


*Figure A2.3*: $CO_2$ Concentration Curves for Individual Rooms (67°F, NW Wind at 10 mph, "Tight")

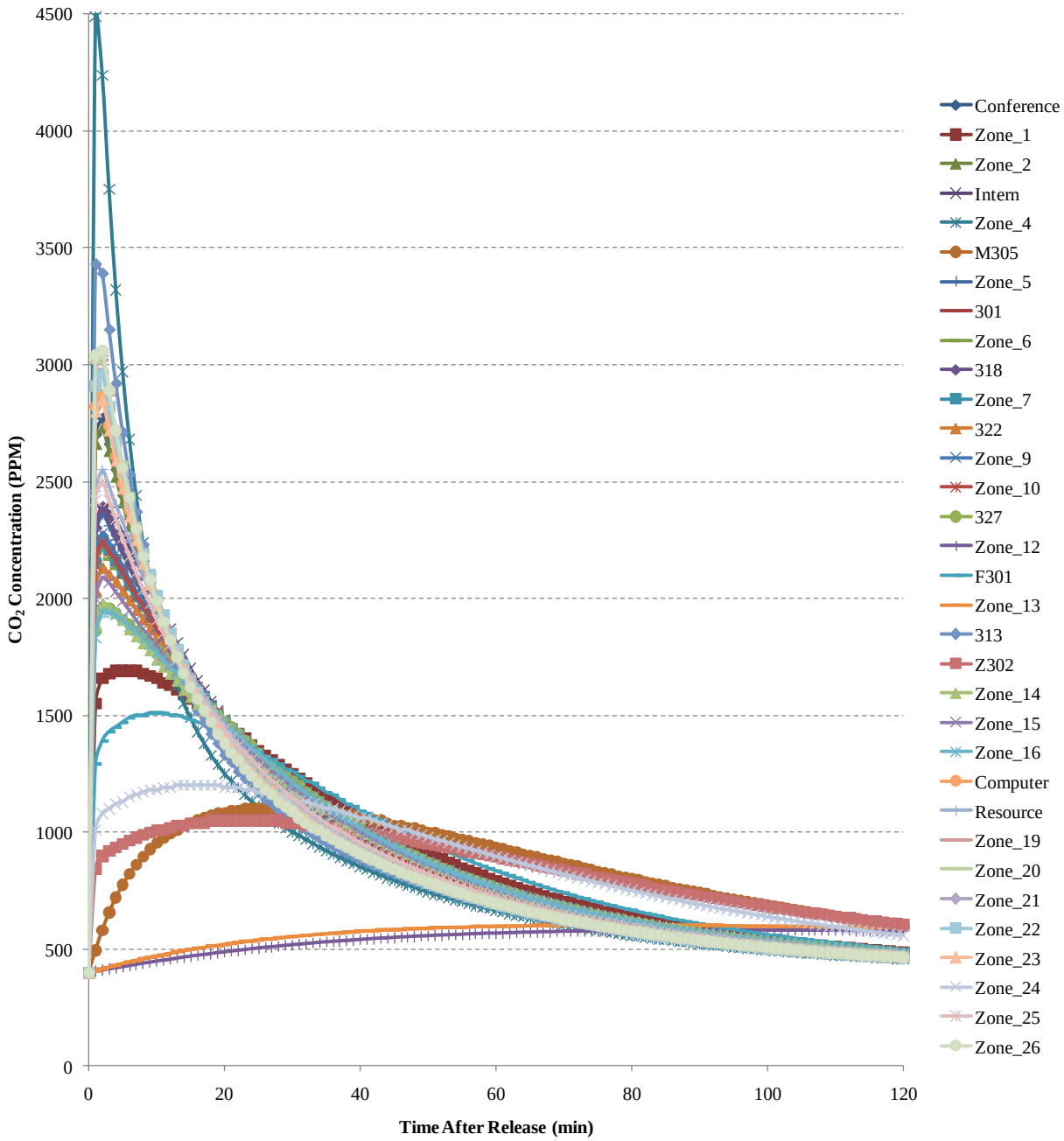


*Figure A2.4*: $CO_2$ Concentration Curves for Individual Rooms (67°F, N Wind at 0 mph, "Leaky")

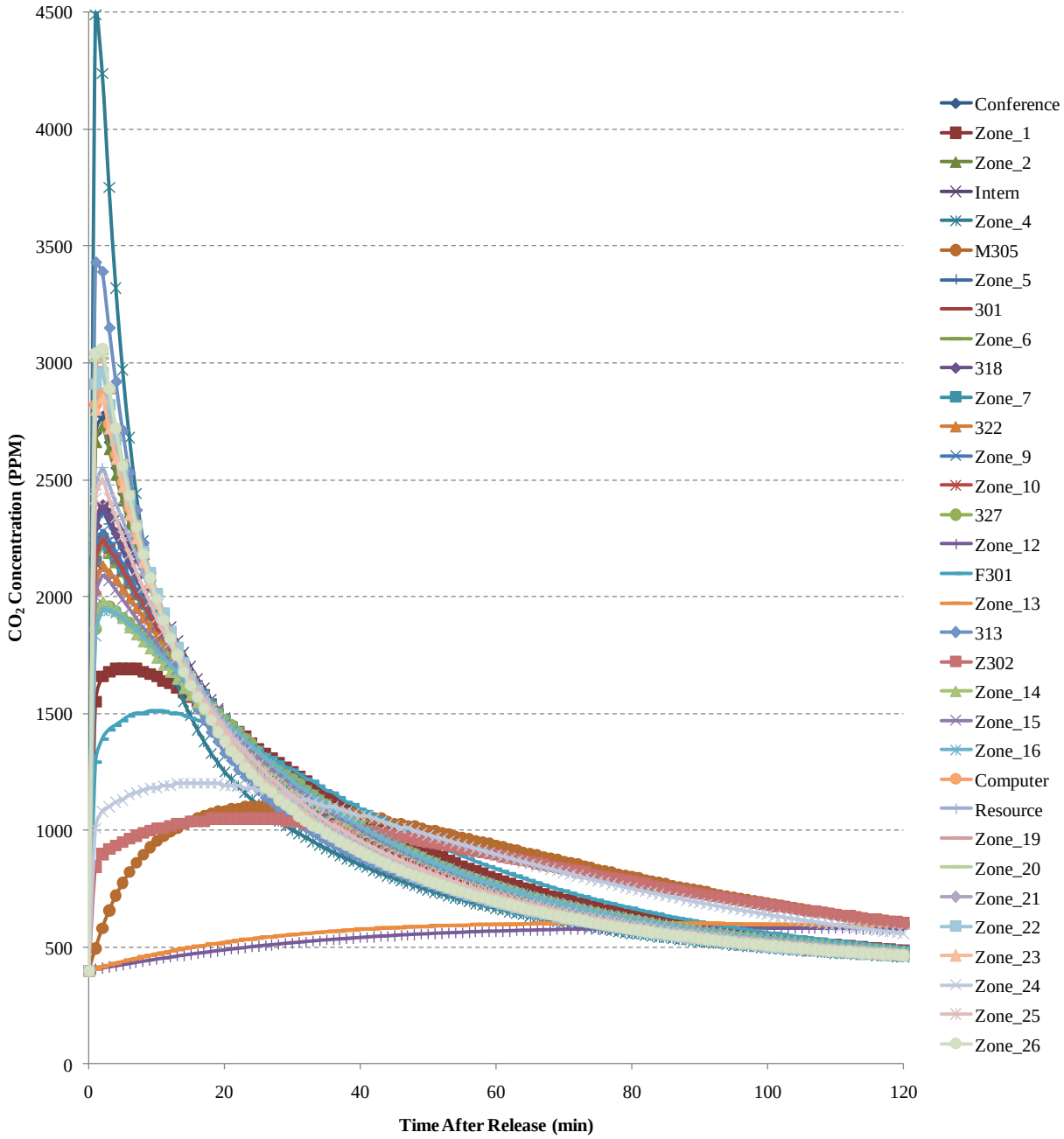


*Figure A2.5*: $CO_2$ Concentration Curves for Individual Rooms (67°F, NW Wind at 0 mph, "Leaky")

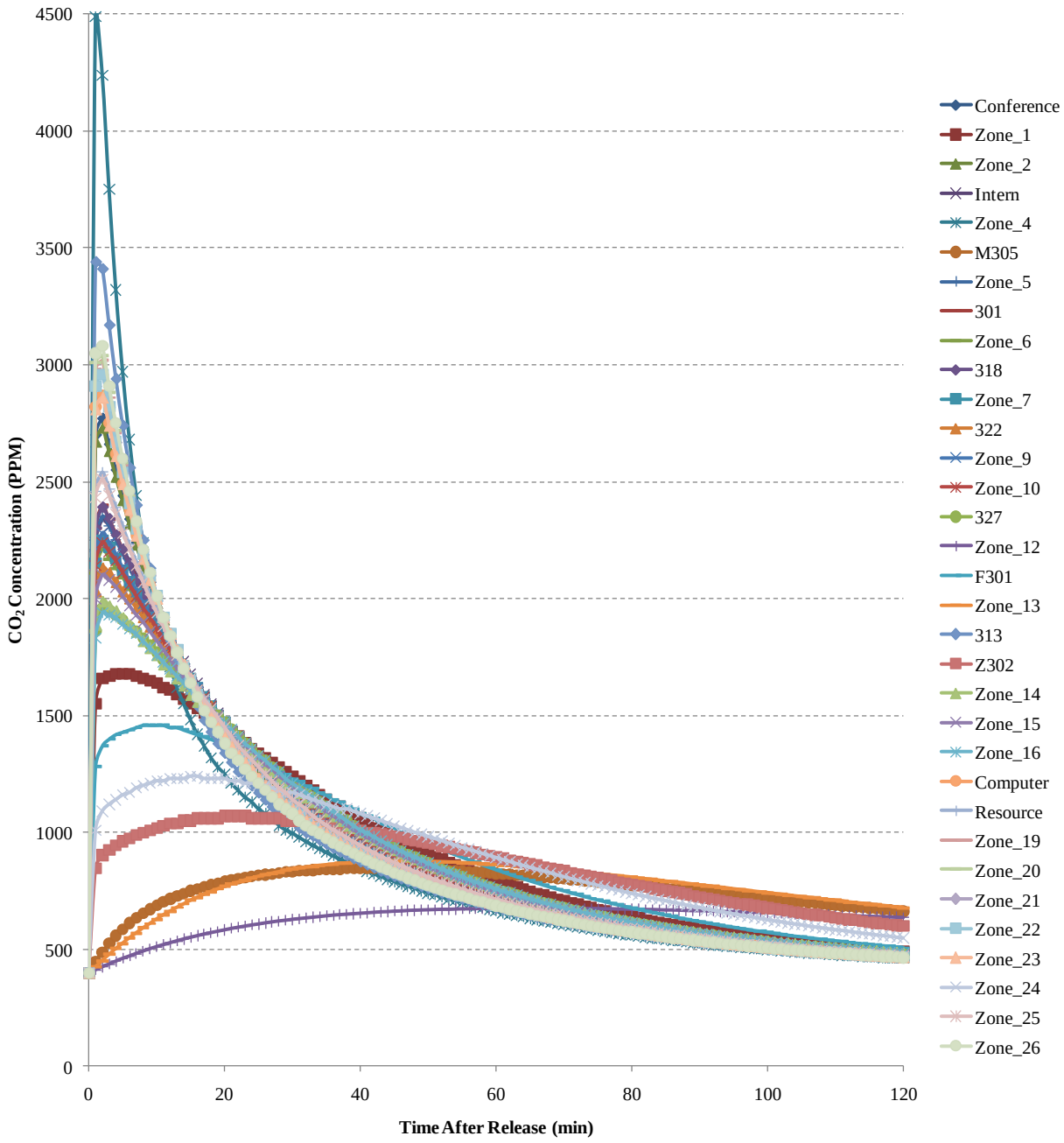


*Figure A2.6*: $CO_2$ Concentration Curves for Individual Rooms (67°F, N Wind at 0 mph, "Tight")

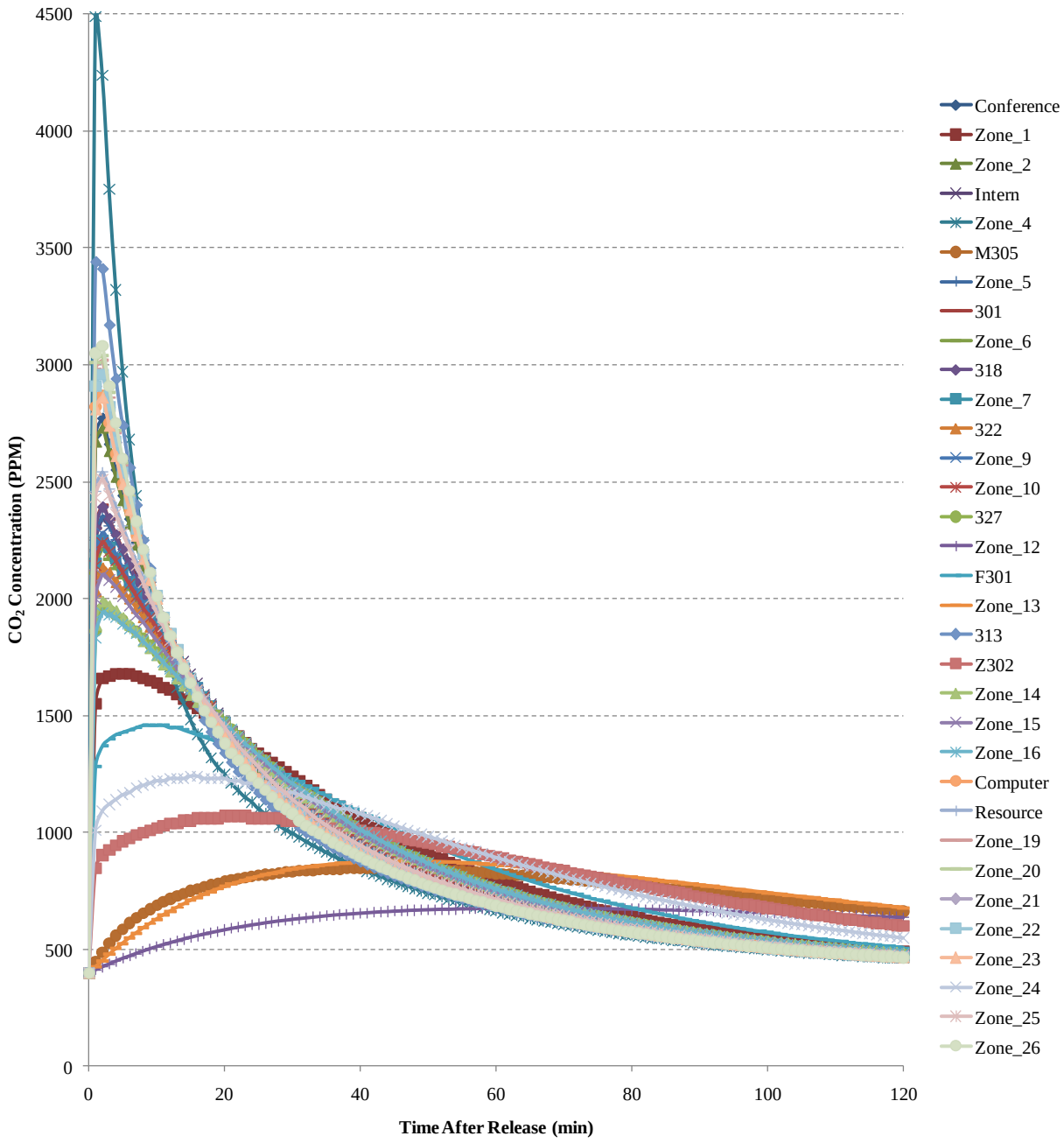


*Figure A2.7*: $CO_2$ Concentration Curves for Individual Rooms (67°F, NW Wind at 0 mph, "Tight")

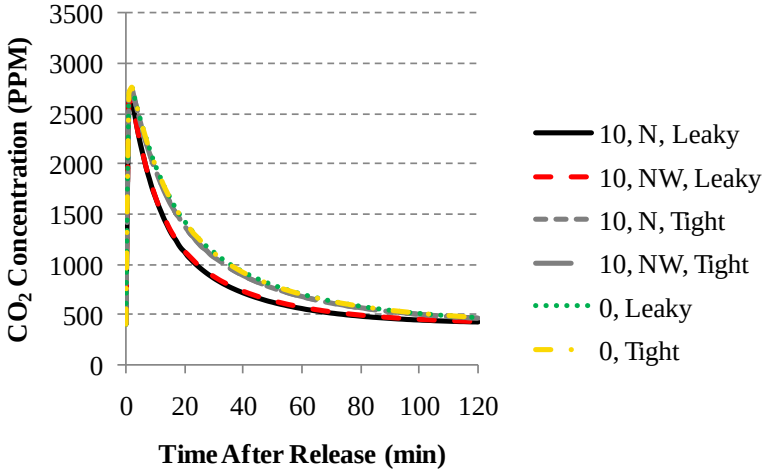


*Figure A2.8*: Conference Sensitivity Analysis

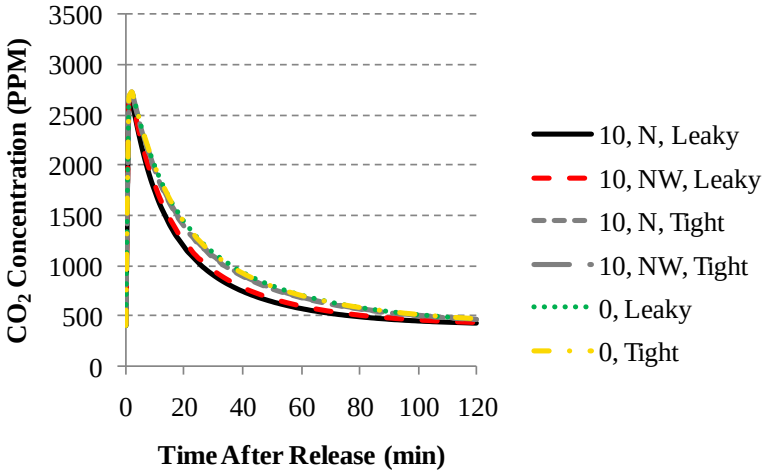


*Figure A2.9*: Zone_2 Sensitivity Analysis

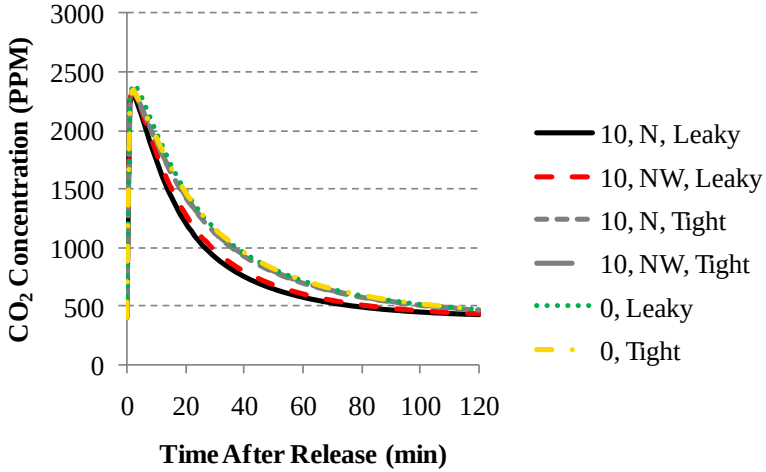


*Figure A2.10*: Intern Sensitivity Analysis

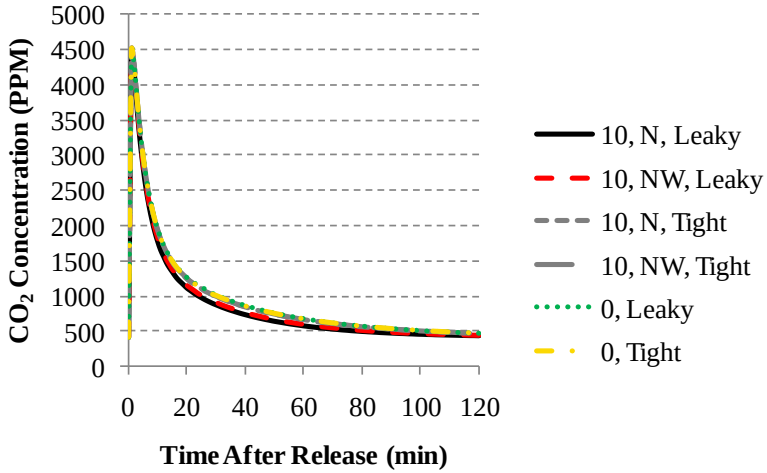


*Figure A2.11*: Zone_4 Sensitivity Analysis

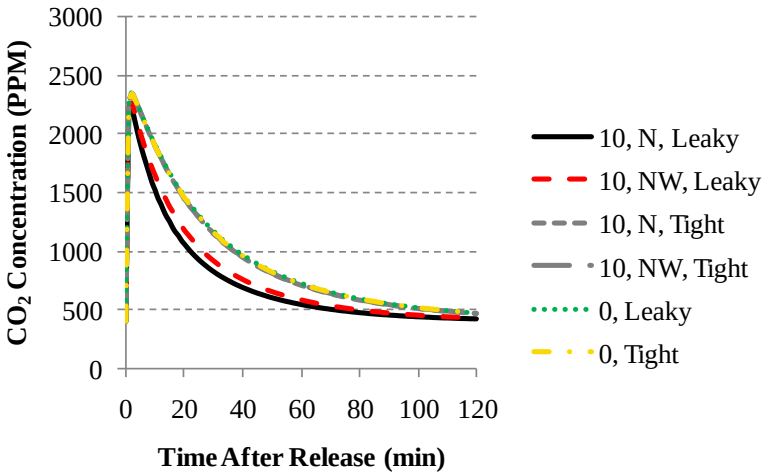


*Figure A2.12*: Zone_5 Sensitivity Analysis

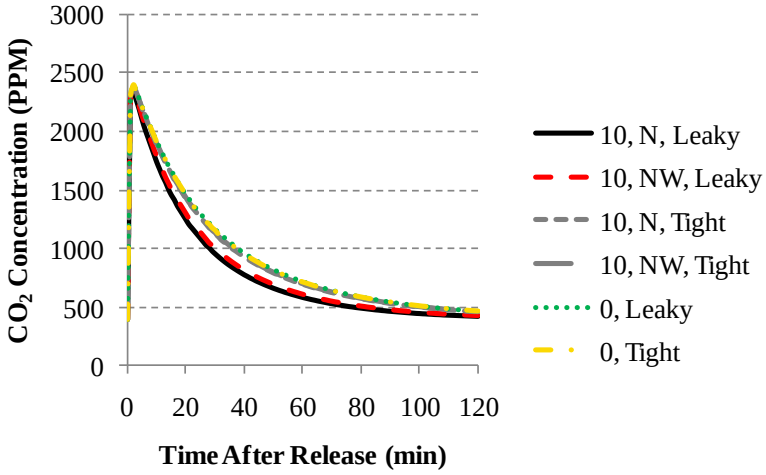


*Figure A2.13*: 301 Sensitivity Analysis

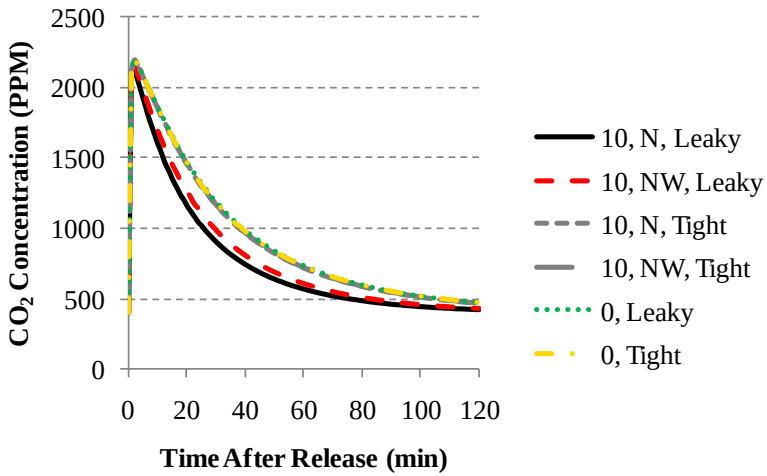


*Figure A2.14*: Zone_6 Sensitivity Analysis

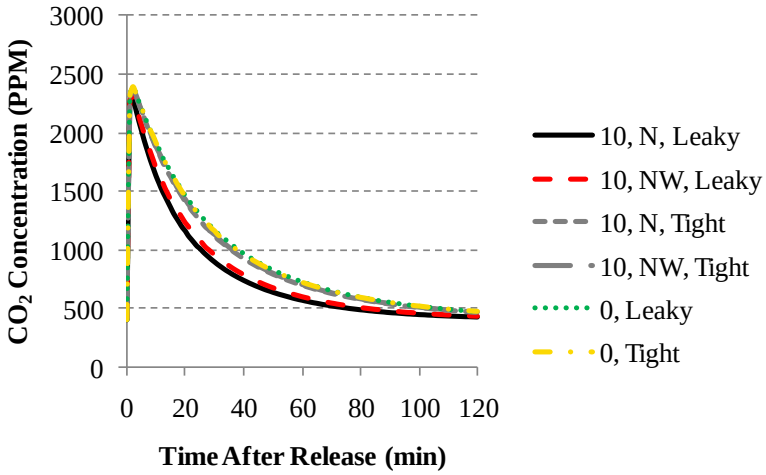


*Figure A2.15*: 318 Sensitivity Analysis

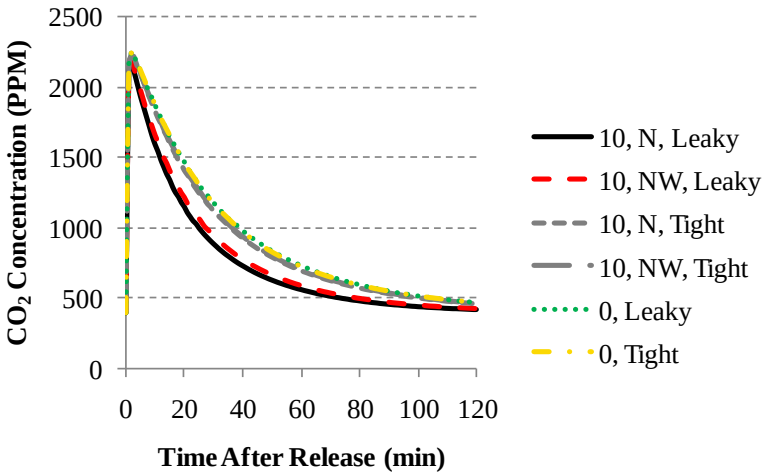


*Figure A2.16*: Zone_7 Sensitivity Analysis

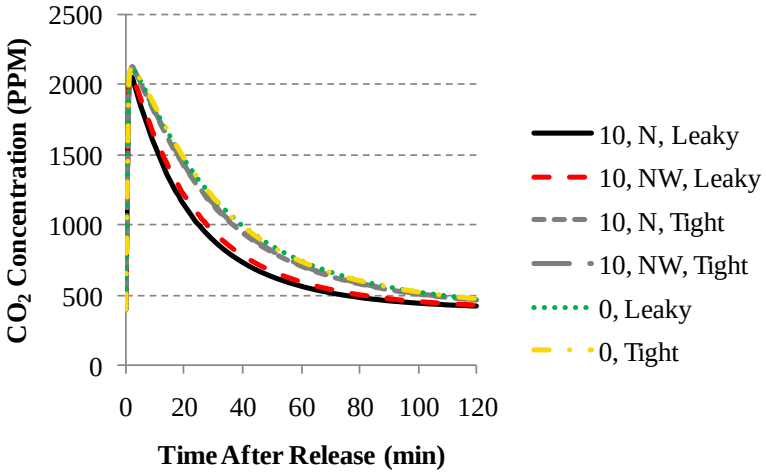


*Figure A2.17*: 322 Sensitivity Analysis

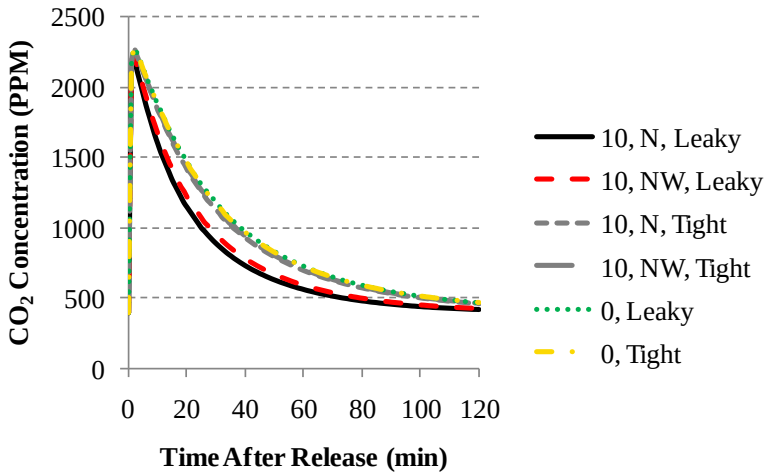


*Figure A2.18*: Zone_9 Sensitivity Analysis

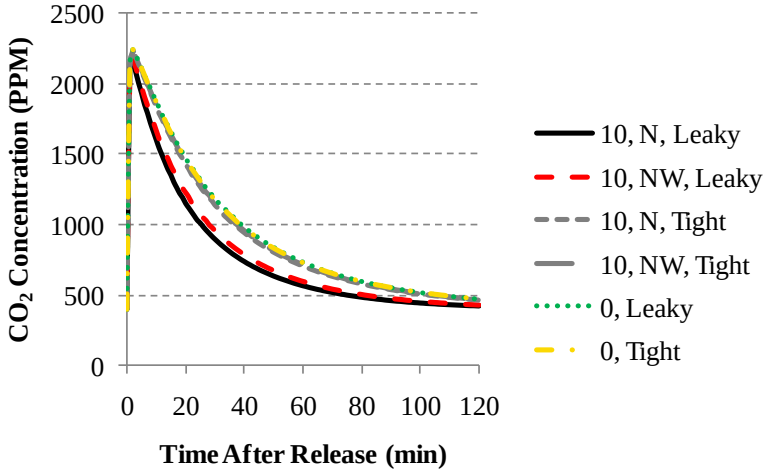


*Figure A2.19*: Zone_10 Sensitivity Analysis

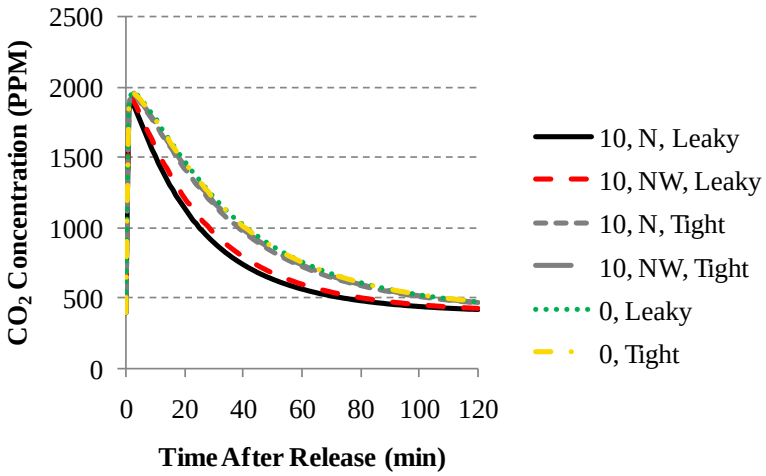


*Figure A2.20*: 327 Sensitivity Analysis

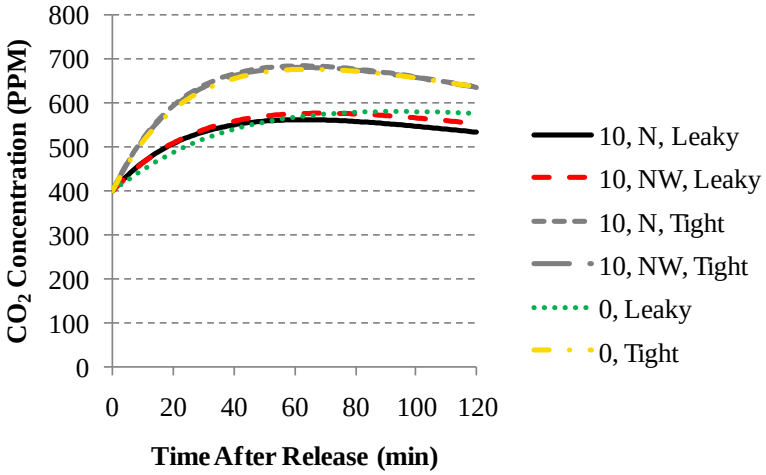


*Figure A2.21*: Zone_12 Sensitivity Analysis

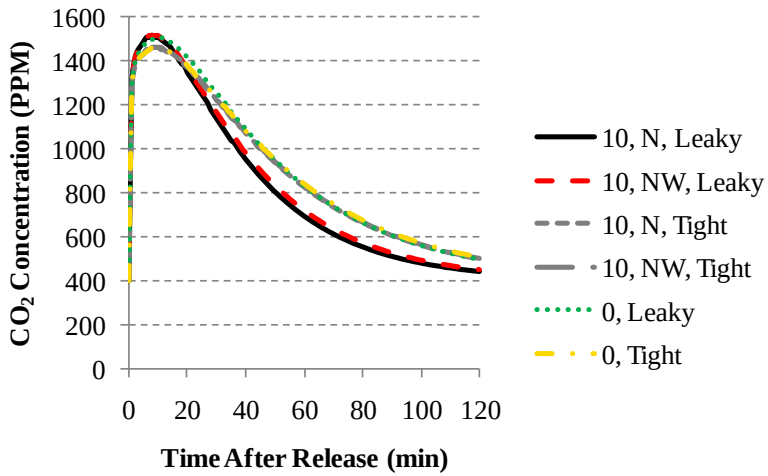


*Figure A2.22*: F301 Sensitivity Analysis

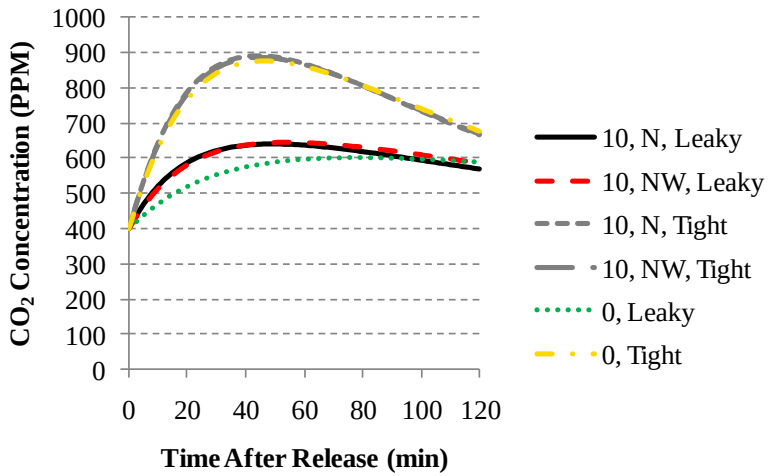


*Figure A2.23*: Zone_13 Sensitivity Analysis

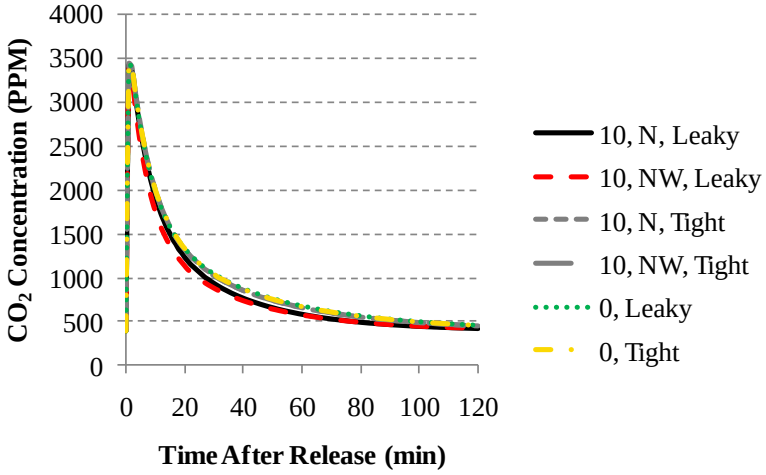


*Figure A2.24*: 313 Sensitivity Analysis

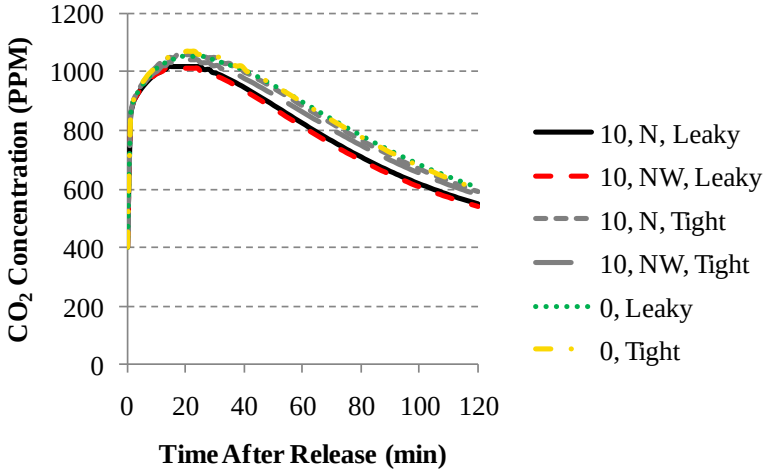


*Figure A2.25*: Z302 Sensitivity Analysis

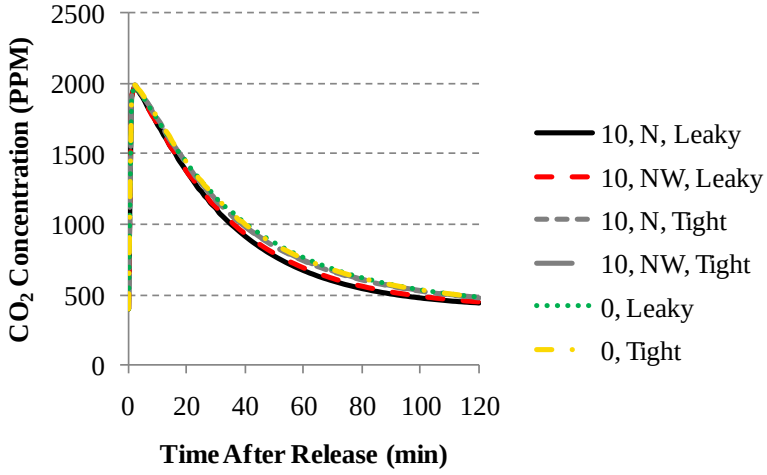


*Figure A2.26*: Zone_14 Sensitivity Analysis

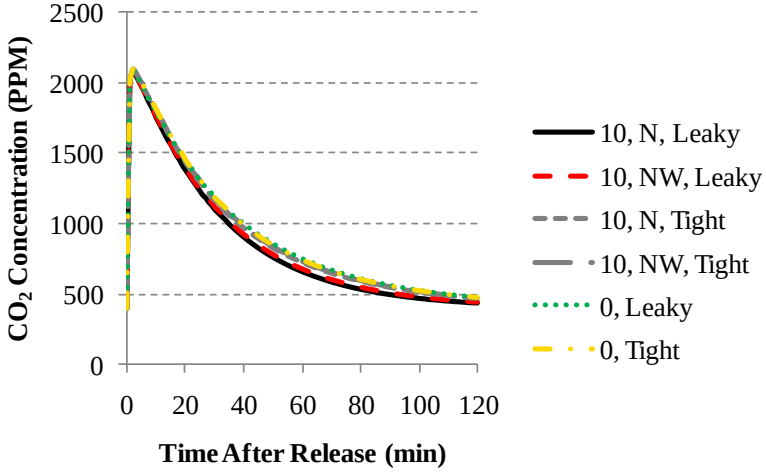


*Figure A2.27*: Zone_15 Sensitivity Analysis

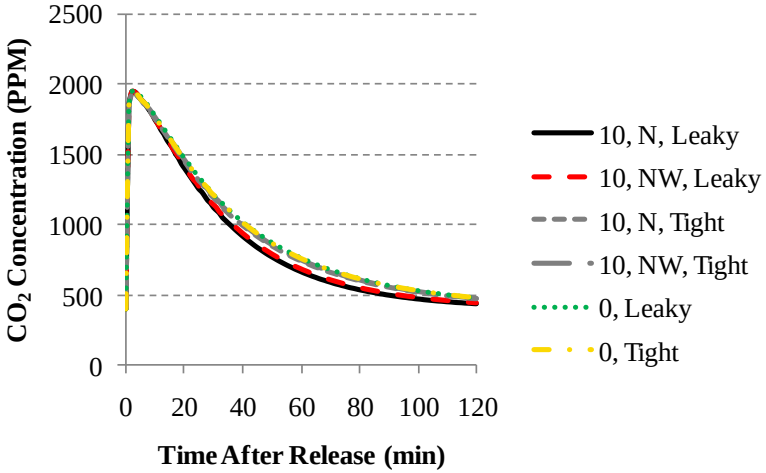


*Figure A2.28*: Zone_16 Sensitivity Analysis

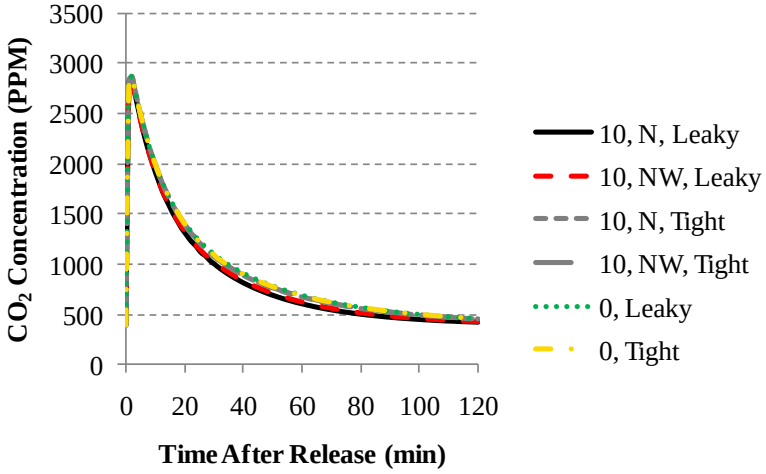


*Figure A2.29*: Computer Sensitivity Analysis

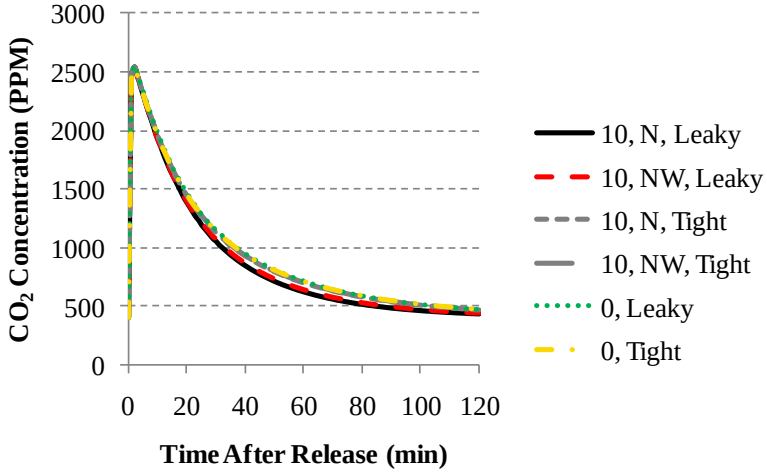


*Figure A2.30*: Resource Sensitivity Analysis

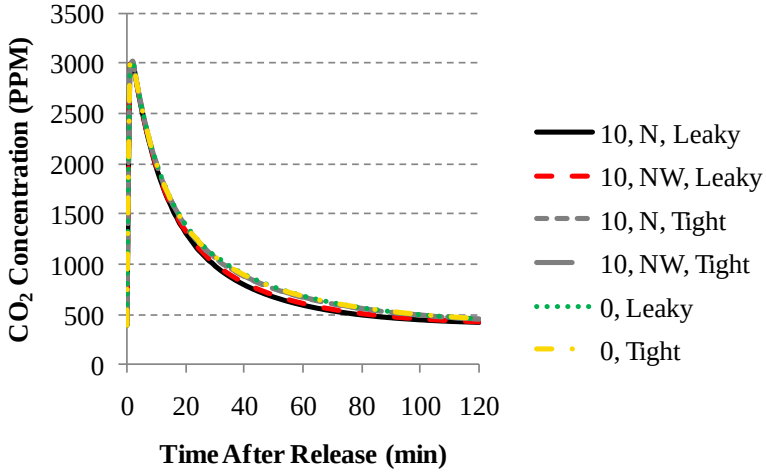


*Figure A2.31*: Zone_19 Sensitivity Analysis

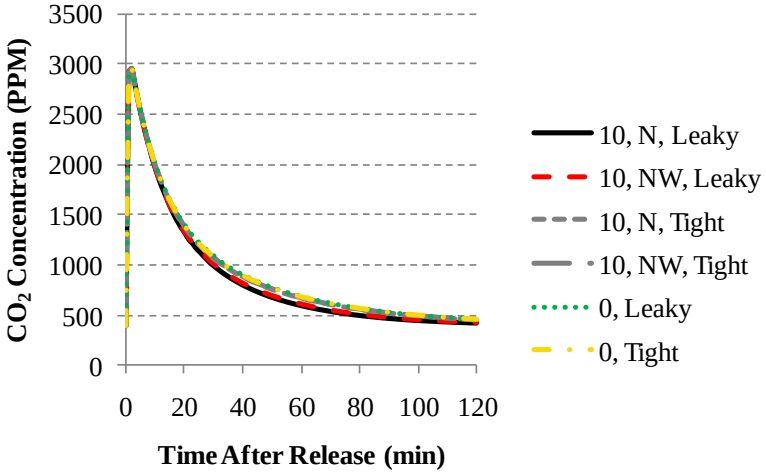


*Figure A2.32*: Zone_21 Sensitivity Analysis

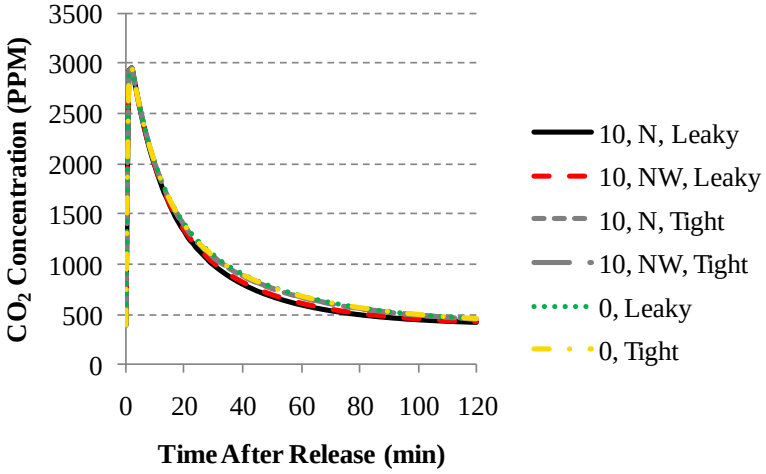


*Figure A2.33*: Zone_22 Sensitivity Analysis

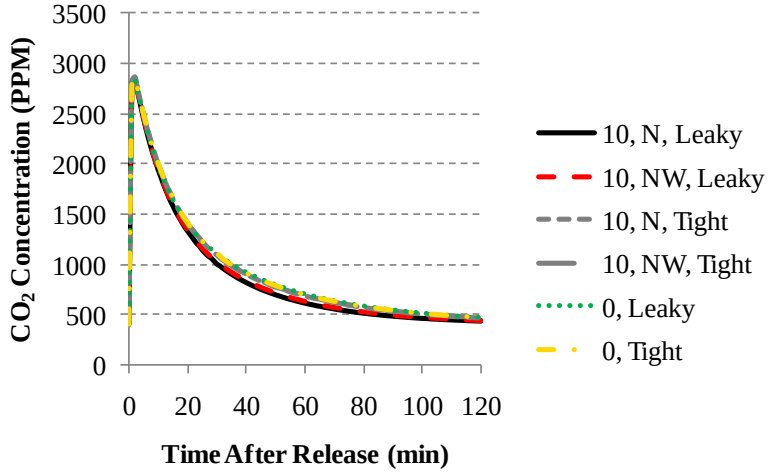


*Figure A2.34*: Zone_23 Sensitivity Analysis

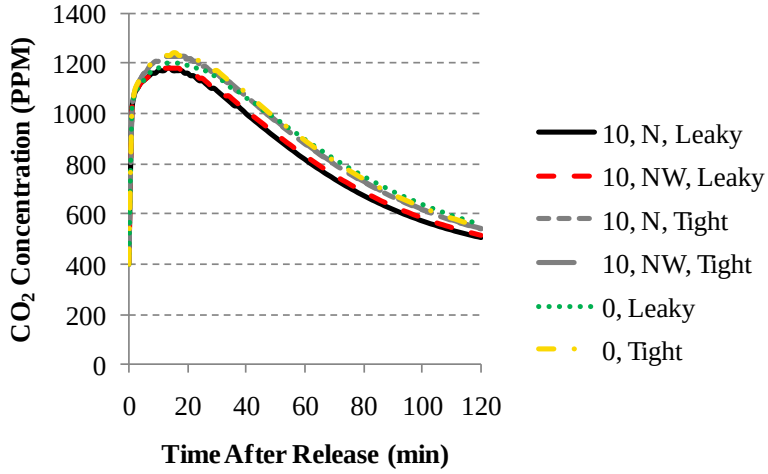


*Figure A2.35*: Zone_24 Sensitivity Analysis

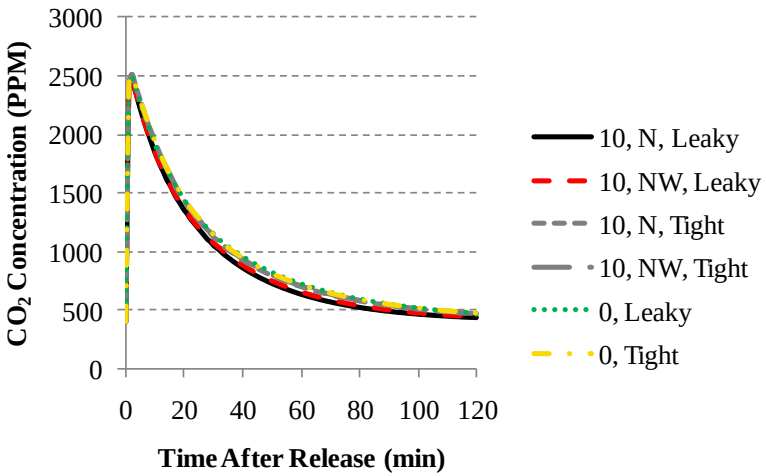


*Figure A2.36*: Zone_25 Sensitivity Analysis

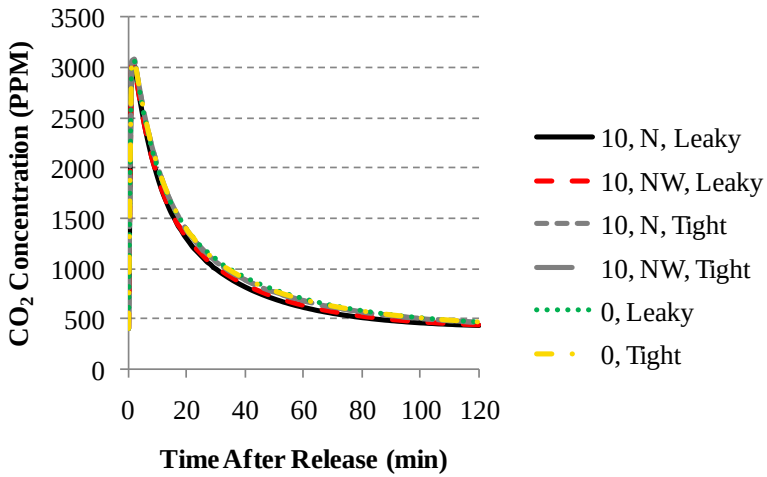


*Figure A2.37*: Zone_26 Sensitivity Analysis

*Figure A2.38*: $CO_2$ Concentration Curves for Second Iteration of Macro-Zones (10 mph Northwest Wind and "Leaky")

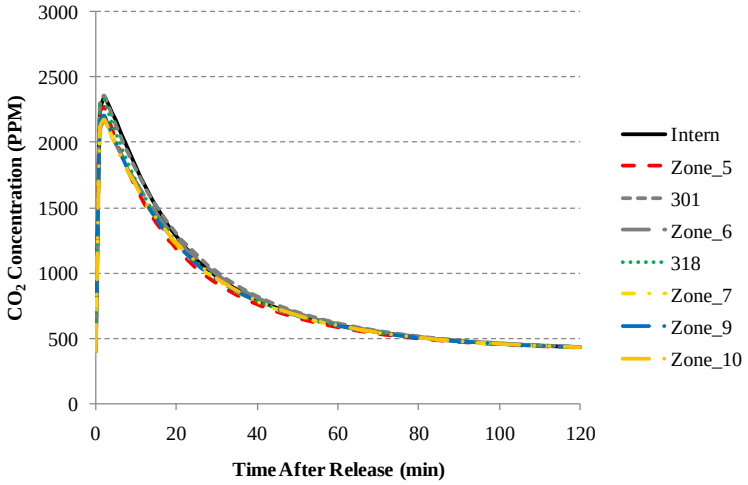


(a) Macro-Zone 1

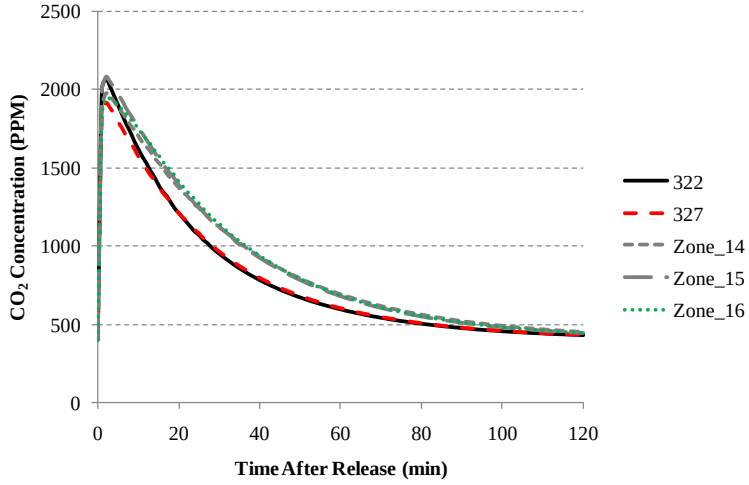


(b) Macro-Zone 2

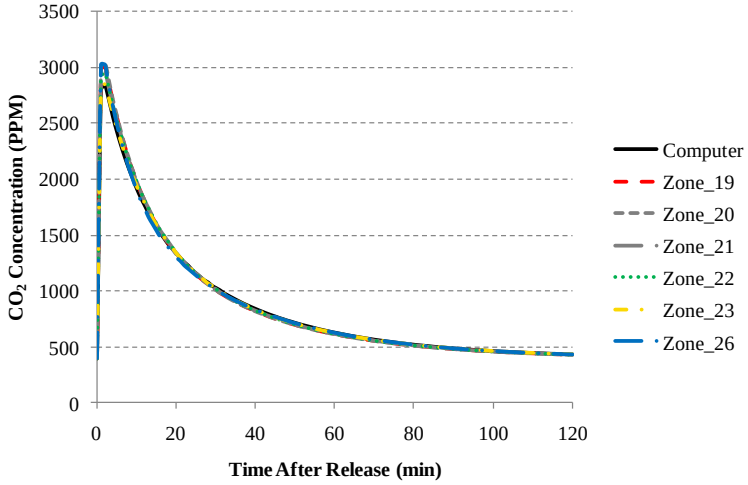


(c) Macro-Zone 3

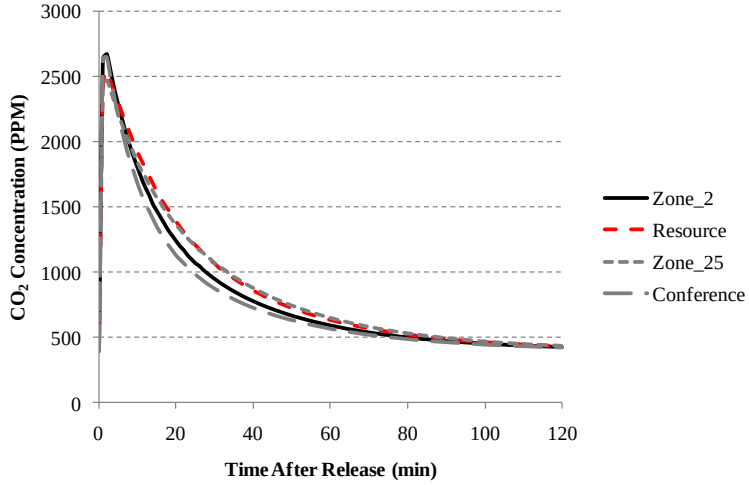


(d) Macro-Zone 4

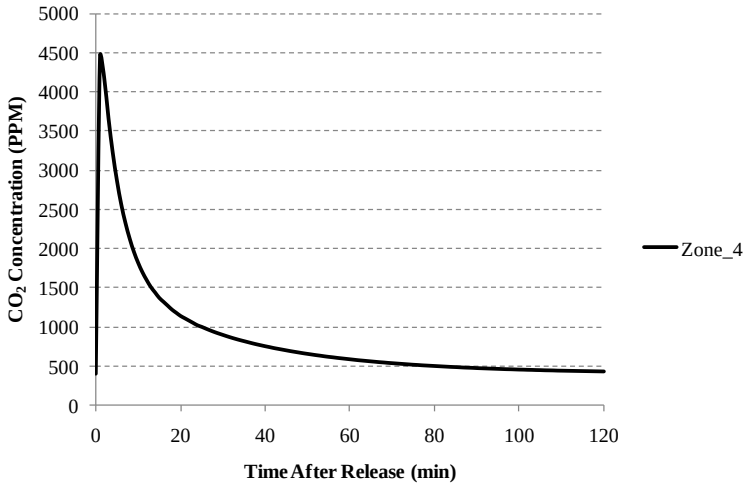


(e) Macro-Zone 5

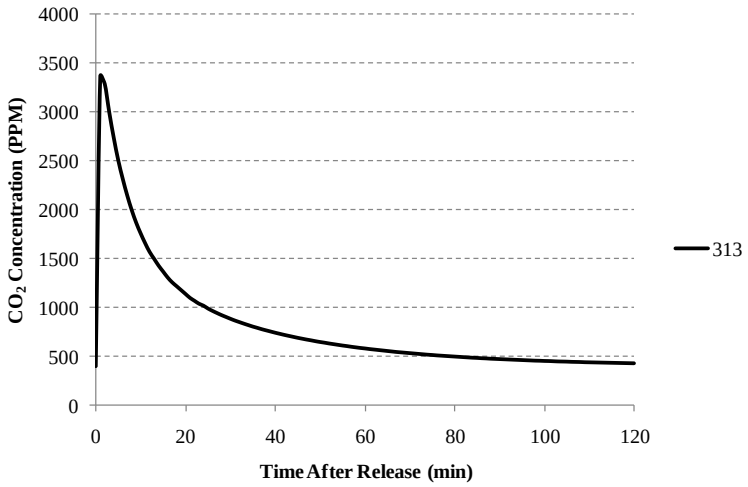


(f) Macro-Zone 6

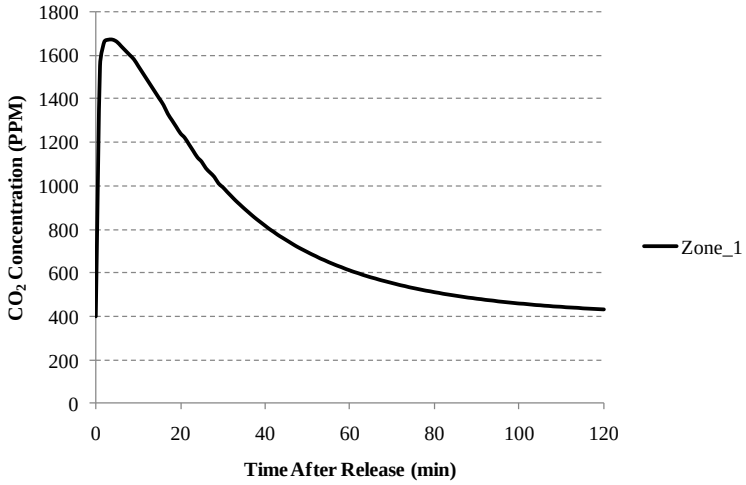


(g) Macro-Zone 7

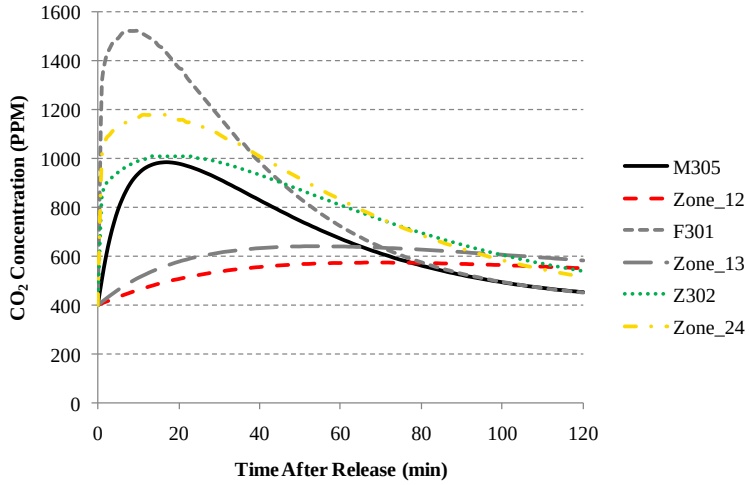


(h) Macro-Zone 8

*Figure A2.39*: $CO_2$ Concentration Curves for Second Iteration of Macro-Zones (10 mph North Wind and "Tight")

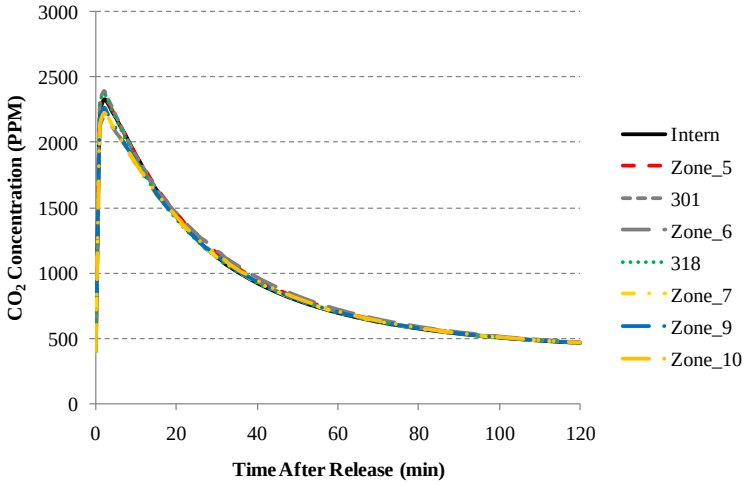


(a) Macro-Zone 1

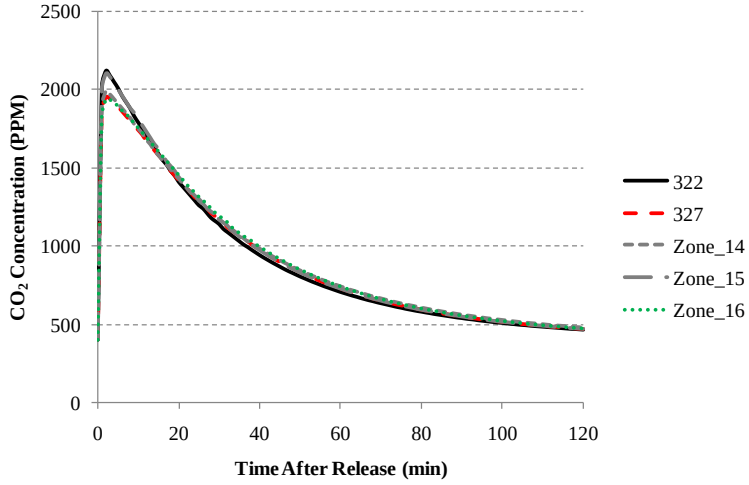


(b) Macro-Zone 2

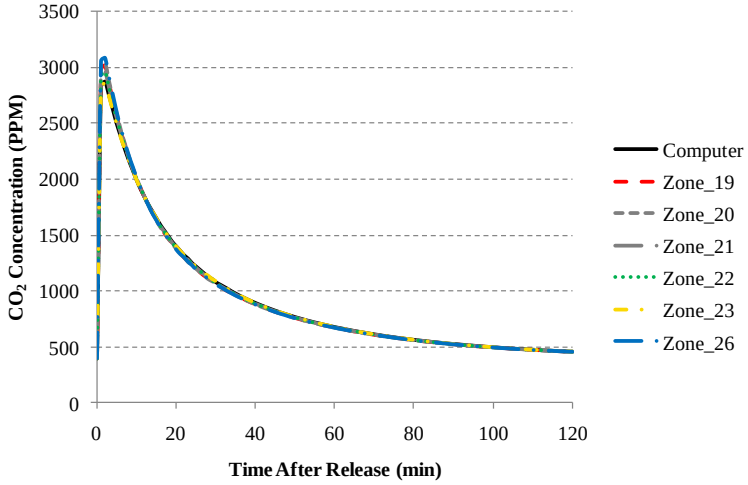


(c) Macro-Zone 3

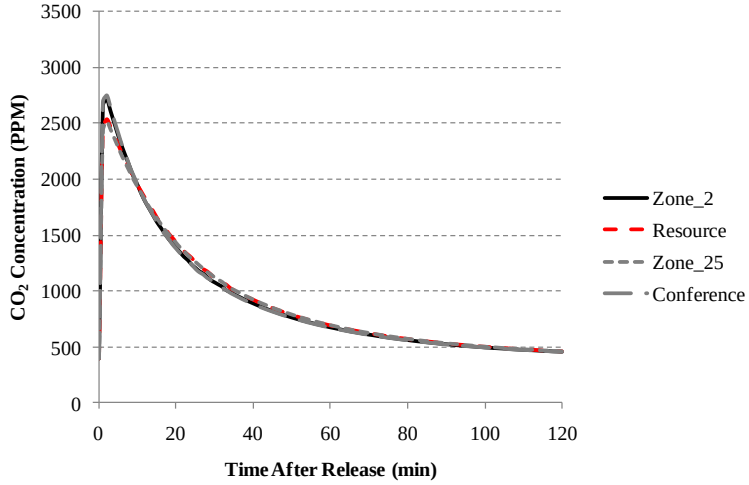


(d) Macro-Zone 4

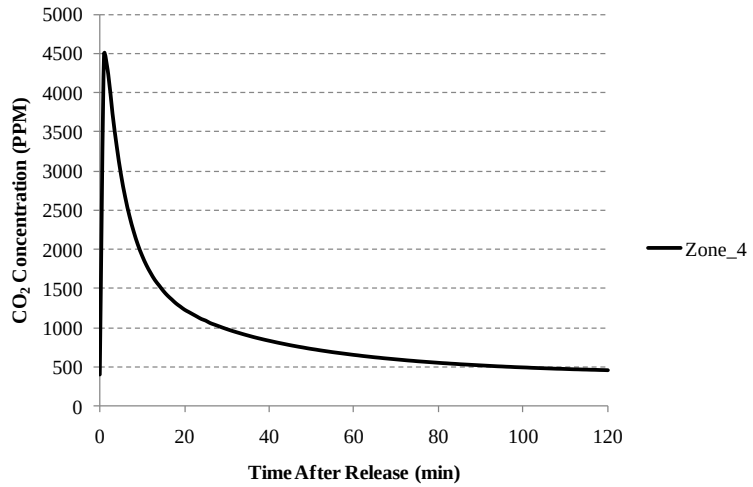


(e) Macro-Zone 5

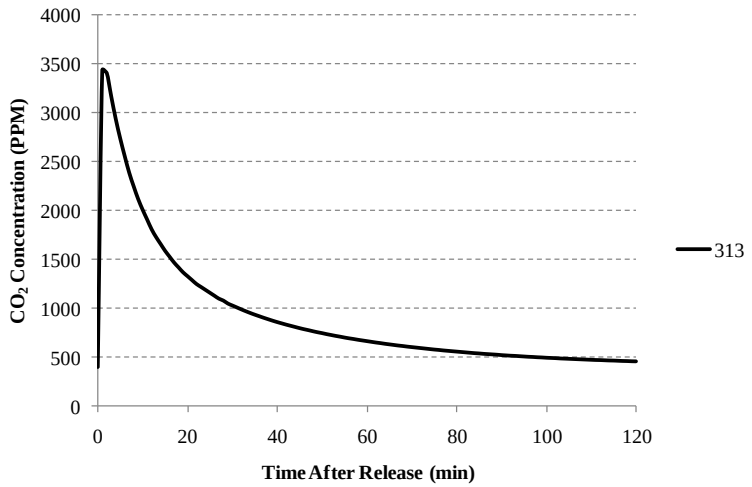


(f) Macro-Zone 6

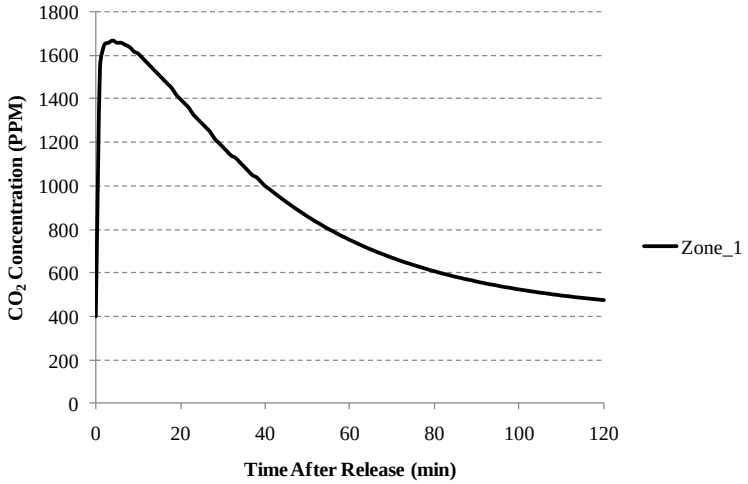


(g) Macro-Zone 7

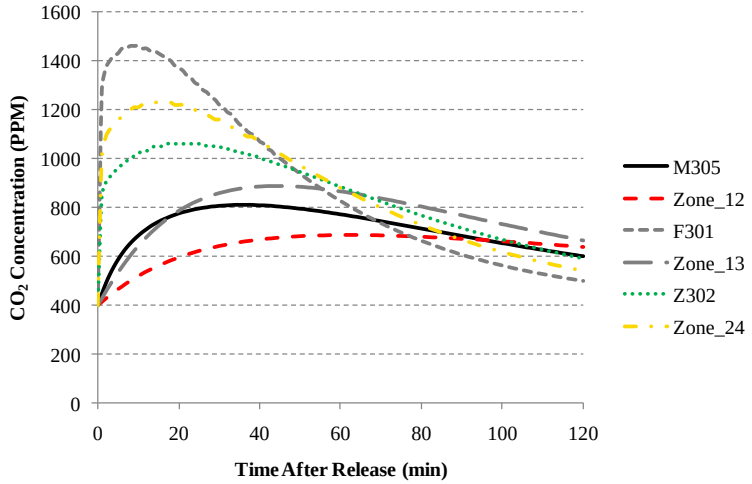


(h) Macro-Zone 8

*Figure A2.40*: $CO_2$ Concentration Curves for Second Iteration of Macro-Zones (10 mph Northwest Wind and "Tight")

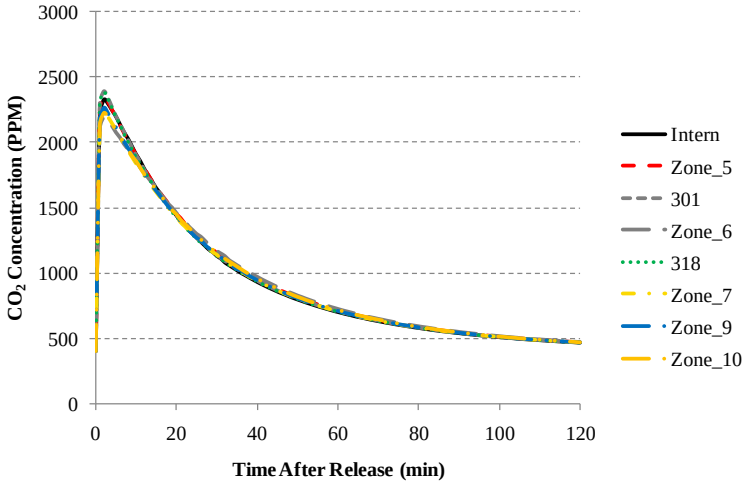


(a) Macro-Zone 1

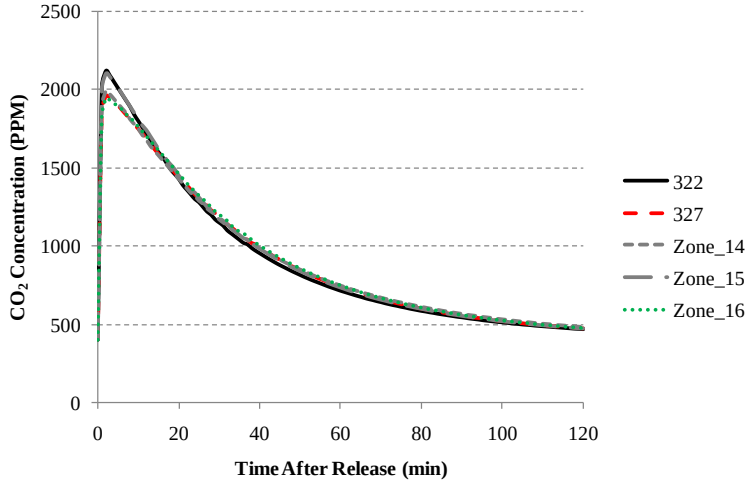


(b) Macro-Zone 2

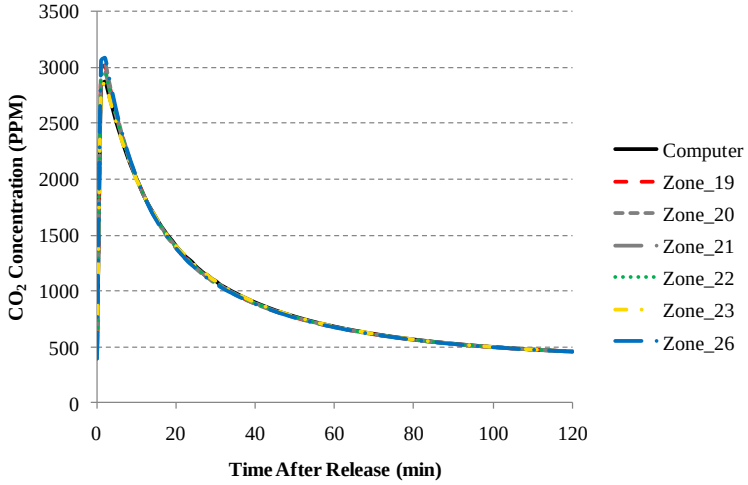


(c) Macro-Zone 3

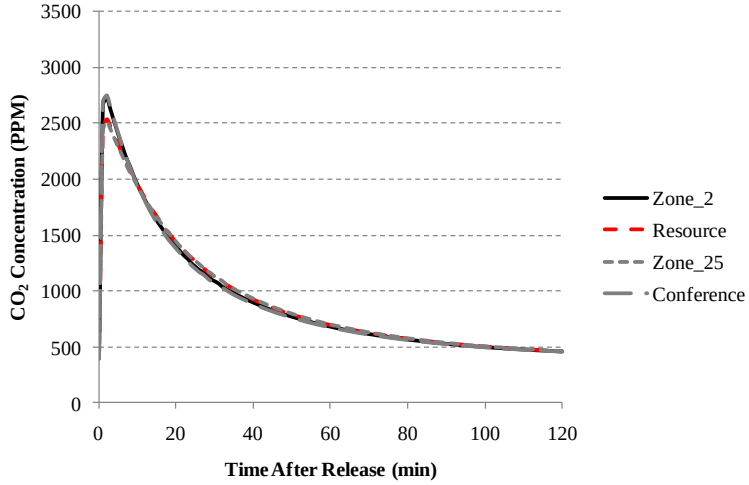


(d) Macro-Zone 4

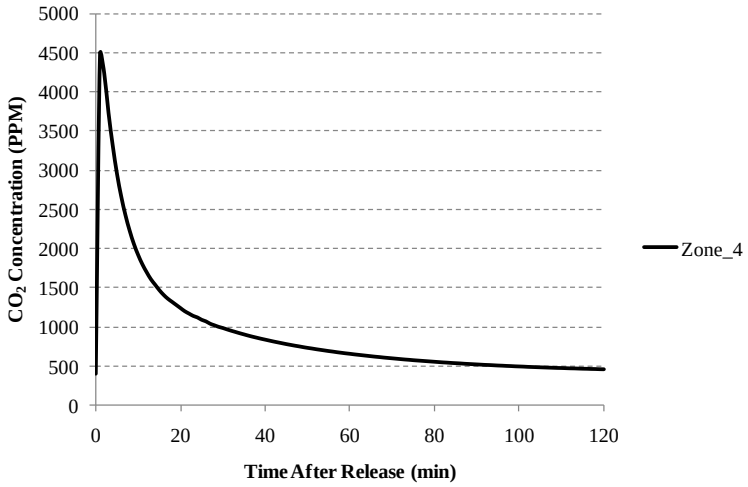


(e) Macro-Zone 5

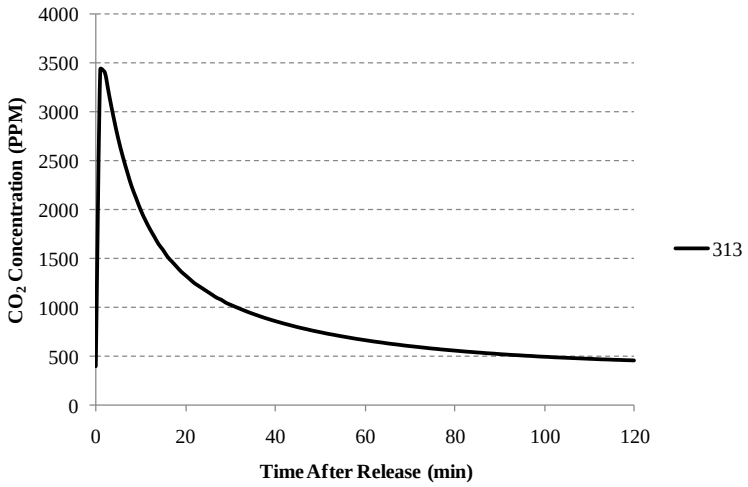


(f) Macro-Zone 6

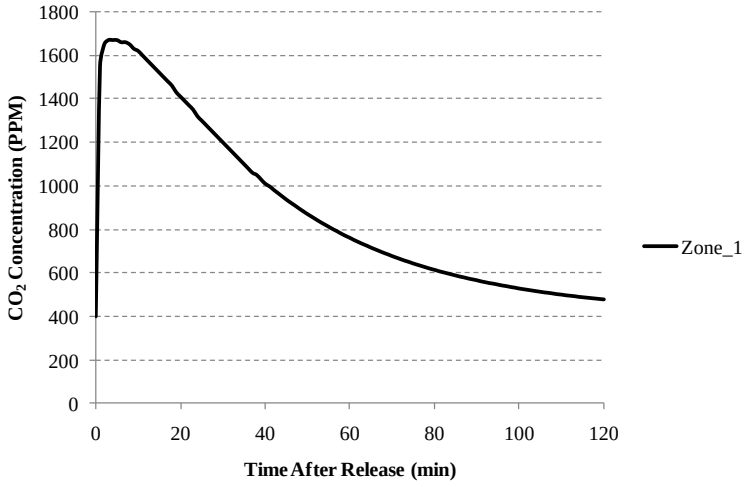


(g) Macro-Zone 7

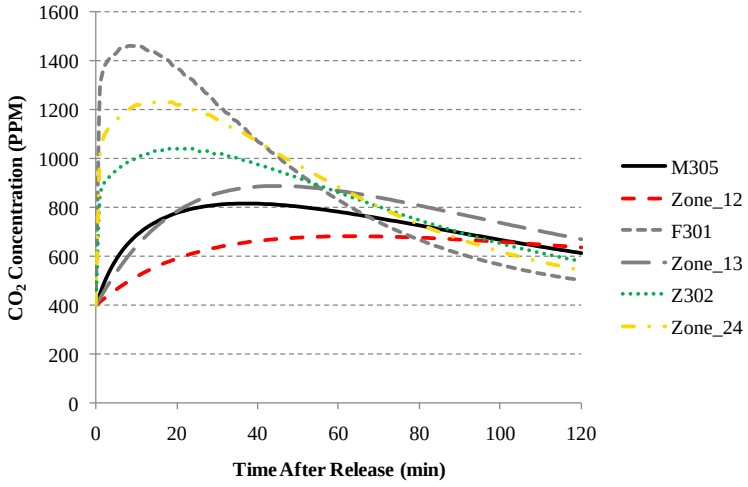


(h) Macro-Zone 8

*Figure A2.41*: $CO_2$ Concentration Curves for Second Iteration of Macro-Zones (No Wind and "Leaky")

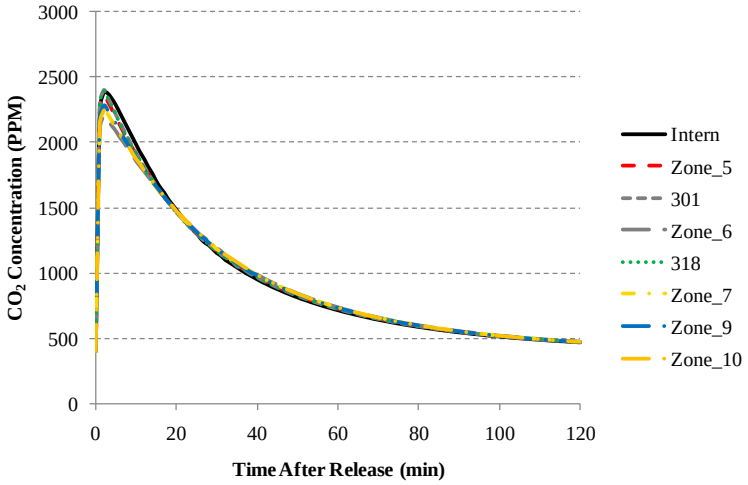


(a) Macro-Zone 1

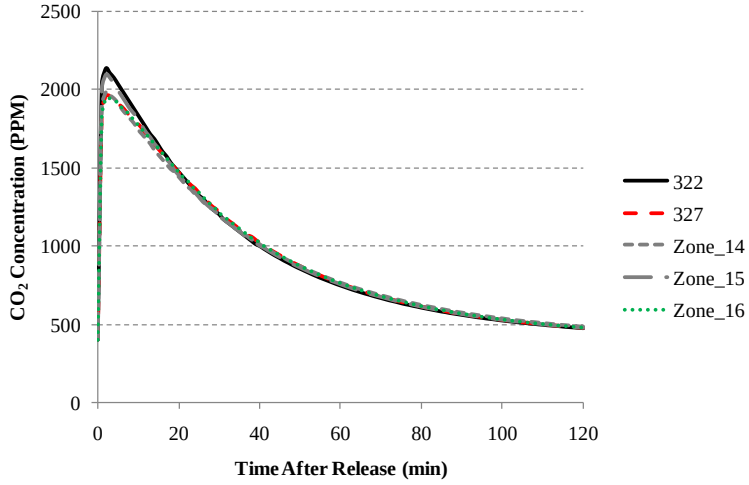


(b) Macro-Zone 2

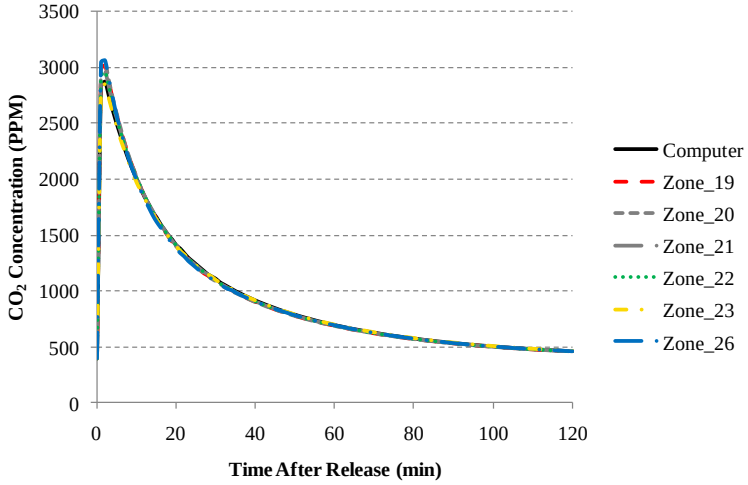


(c) Macro-Zone 3

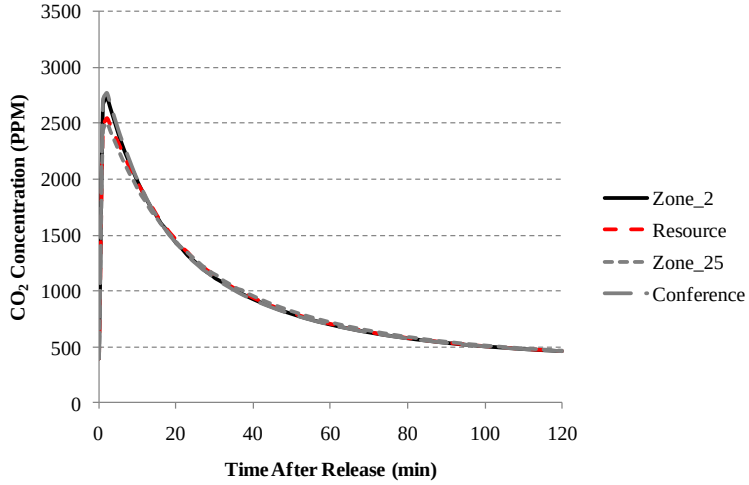


(d) Macro-Zone 4

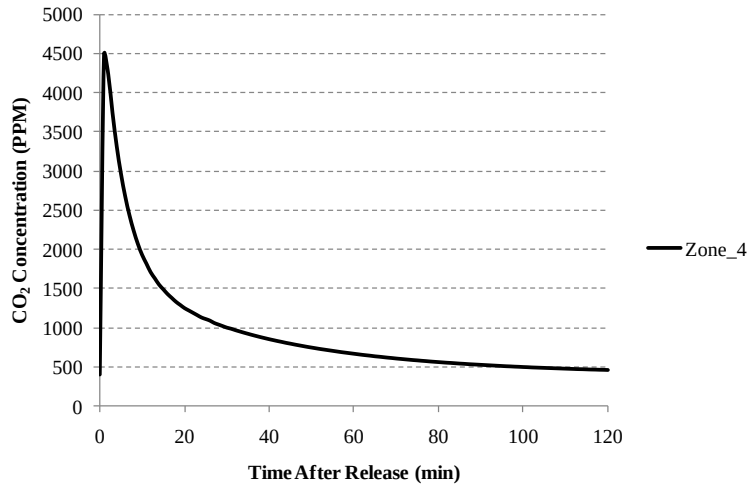


(e) Macro-Zone 5

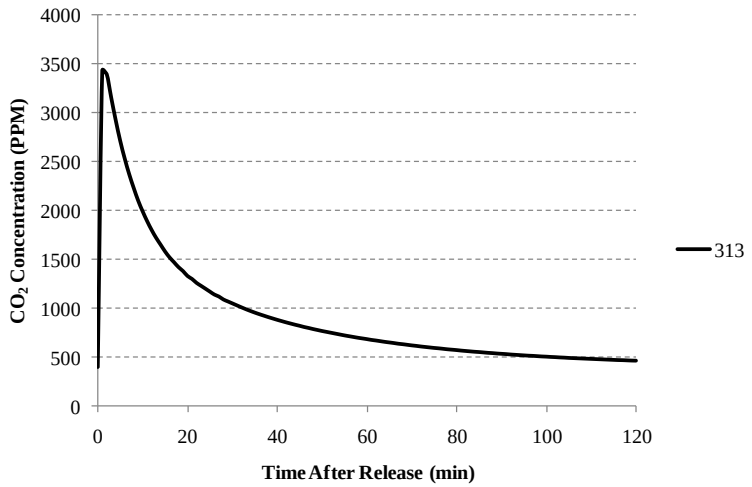


(f) Macro-Zone 6

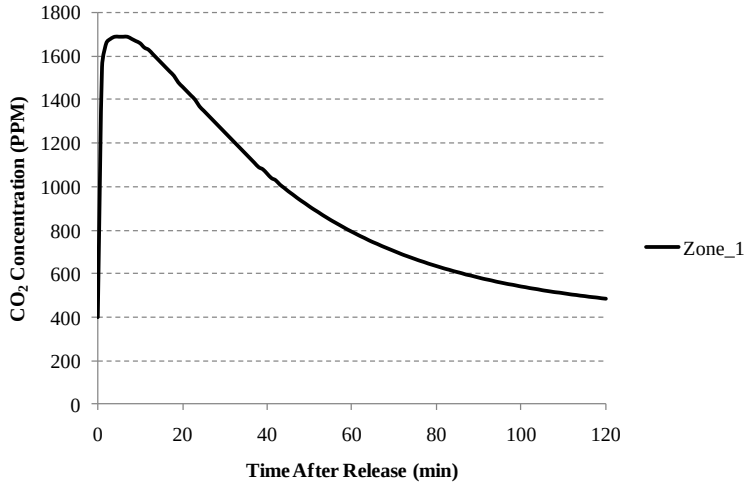


(g) Macro-Zone 7

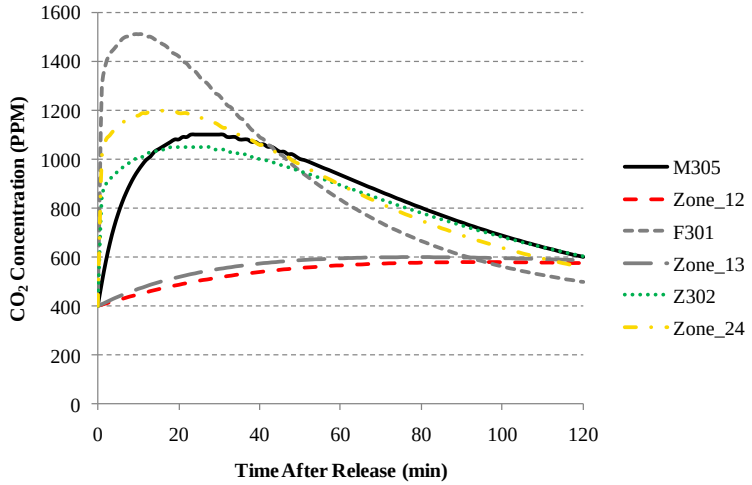


(h) Macro-Zone 8

*Figure A2.42*: $CO_2$ Concentration Curves for Second Iteration of Macro-Zones (No Wind and "Tight")

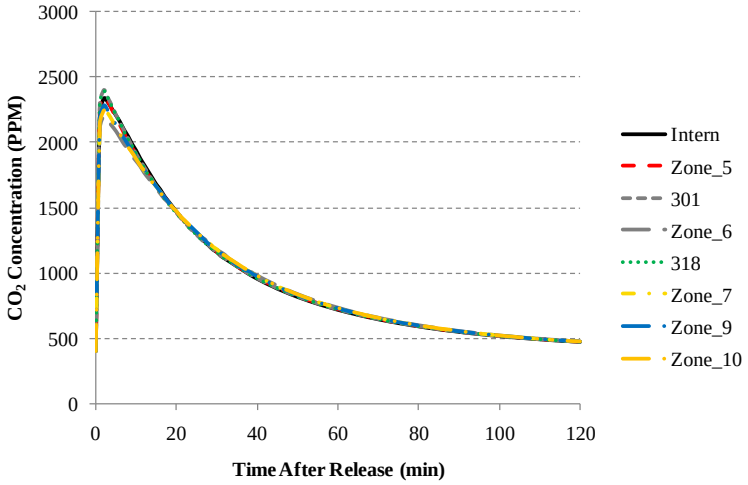


(a) Macro-Zone 1

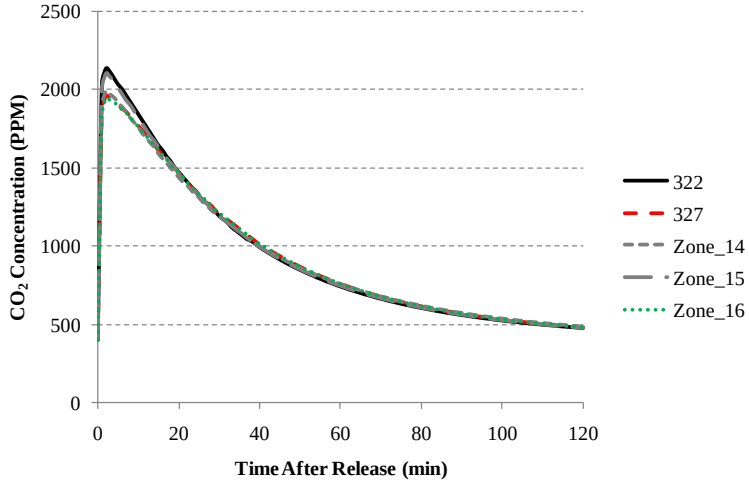


(b) Macro-Zone 2

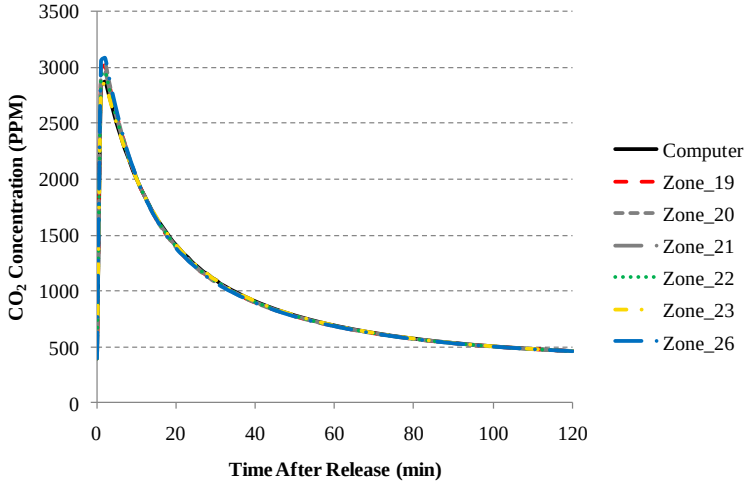


(c) Macro-Zone 3

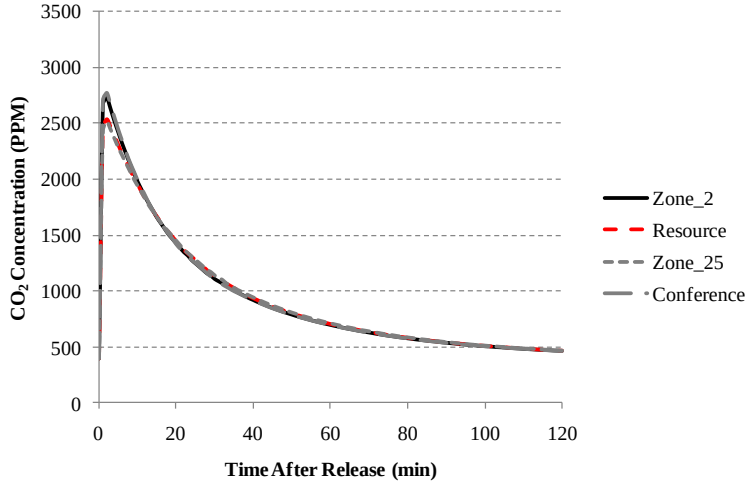


(d) Macro-Zone 4

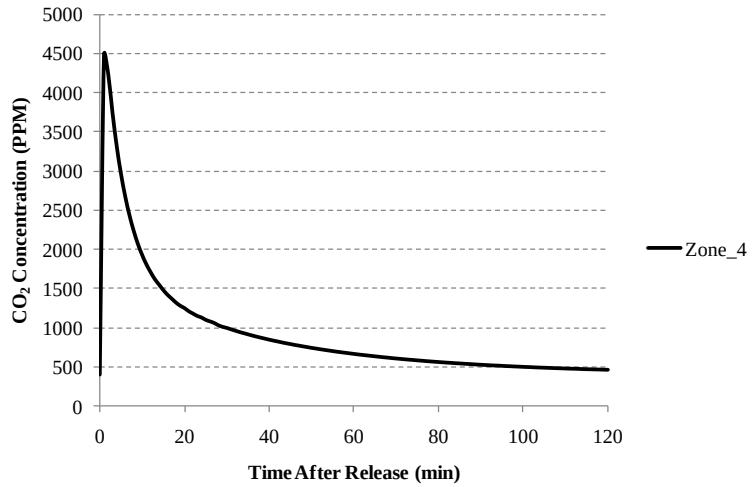


(e) Macro-Zone 5

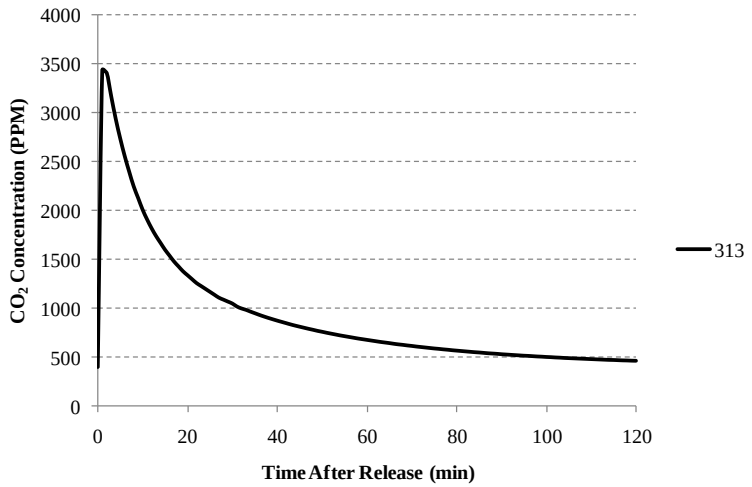


(f) Macro-Zone 6

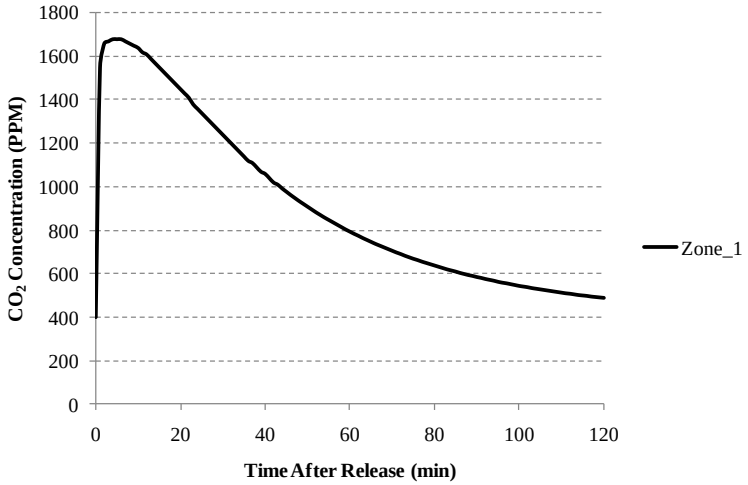


(g) Macro-Zone 7

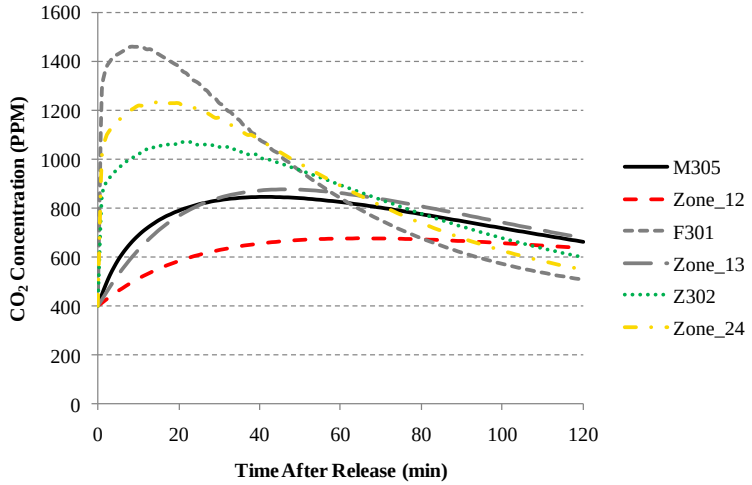


(h) Macro-Zone 8

# APPENDIX B

# EXPERIMENTAL DESIGN AND FACTORIAL ANALYSIS

## B.1 Introduction

Throughout this research, the method of setting up airflow model simulations for either an airflow-based or a tracer gas-based sensitivity analysis was based on "Design of Experiments" (DOE) techniques. DOE is the terminology used to describe a large body of methods used for designing experiments and statistically analyzing the results. DOE techniques are applied to a wide range of industries and are particularly essential in Industrial Engineering practices. Montgomery (2009) provides an excellent up-to-date source for DOE techniques, focusing on science and engineering examples, and was the main source used for this research. A more historical source is Box et. al (1978).

DOE techniques are used to set up or plan experiments and analyze experimental results for some system or process. They provide a methodology for altering input independent variables and analyzing the behavior of the system quantified by some output or response variable. DOE techniques also extend to the topic of model building. For example, many DOE methods allow one to develop empirical models of the system being analyzed based on the results of the designed experiment. "It is also usually very helpful to present the results of many experiments in terms of an empirical model, that is, an equation derived from the data that express the relationship between the response and the important design factors" (Montgomery, 2009). In other words, DOE methods allow one to identify a subset of influential variables from a list of candidate variables that most impact the system and build a mathematical relationship between those influential variables and the system response. The most common goal of DOE

methodologies is to design the experiment in such a way that minimizes the amount of time and effort needed, minimizes the cost of experimentation, minimizes sources of variability or error, and produces the most robust data set for evaluation of the system. Using the statistical DOE methods to analyze a system not only provides credibility to the results but also allows one to draw objective conclusions about system behavior. This is an important concept because the conclusions an analyst might draw regarding a certain process can be influenced by how the experiment was carried out.

Understanding the behavior of a system or process through experimentation involves identifying independent input variables (x's) to be analyzed, observing a system response variable (y), and accounting for controllable and uncontrollable nuisance factors. According to Montgomery (2009), the objectives of the experimentation may include the following:

1. Determining which variables are most influential on the response y.
2. Determining where to set the influential x's so that y is almost always near the desired nominal value.
3. Determining where to set the influential x's so that variability in y is small.
4. Determining where to set the influential x's so that the effects of the uncontrollable variables are minimized.

There are various terms used for the independent variables being analyzed in experimental design including "factors" or "treatments". From here on, they will be referred to as "factors". Thus, as outlined by Montgomery (2009) above,

DOE techniques can be used to determine which factors or factor interactions are most influential on the response variable of the system. DOE can also be used to find values of the factors or "factor levels" which either optimize some process or reduce the variability in the process. Another major goal of DOE techniques is to isolate the effects of specific factors of interest while simultaneously eliminating the effects of various possible nuisance factors, both controllable and uncontrollable. It should be noted that statistical methods do not prove that any factors or any factor interactions actually have an effect "but they do allow us to measure the likely error in a conclusion or to attach a level of confidence to a statement" (Montgomery, 2009). Therefore, as mentioned previously, DOE methods provide credibility and objectivity to conclusions drawn regarding a certain system or process. "The primary advantage of statistical methods is that they add objectivity to the decision-making process. Statistical techniques coupled with good engineering or process knowledge and common sense will usually lead to sound conclusions" (Montgomery, 2009).

Montgomery (2009) outlines the steps of designing an experiment as follows: (1) recognize the problem statement, (2) select the response variable, (3) chose the factors to be analyzed and their levels, (3) chose the type of experimental design, (4) perform the experiment, (5) statistically analyze the data, and (6) draw conclusions and make recommendations. Experimental designs usually follow some sort of sequential approach and are therefore iterative processes. The initial choice of the type of experimental design may not capture enough of the system behavior and thus design augmentations may be warranted.

One common use of DOE techniques is called "factor screening" (Montgomery, 2009). This is where one "screens" a large number of possible variables and identifies which ones are most influential on the system or process response variable. In performing a regression analysis, this would involve identifying the significant regressor variables. Therefore, factor screening is an important part of model building. Factor screening is also similar to sensitivity analysis. The purpose of sensitivity analysis is to observe the behavior of the response variable(s) as certain input variables or factors are altered. Therefore, sensitivity analysis aims at identifying influential factors to understand system behavior but does not necessarily result in identifying an empirical model. Other possible reasons for using DOE techniques include system or process optimization, confirmation, discovery, etc. (Montgomery, 2009).

In this research, the system or process being analyzed was the multi-zone model in PCW/CONTAM. The goal of the various sensitivity analyses was to determine which input variables (e.g. wind speed, wind direction, leakage severity, etc.) had significant effects on the model output or response variables (e.g. $CO_2$ concentrations, airflow magnitudes, and airflow directions).

**B.2 Basic Concepts of Experimental Design**

Montgomery (2009) specifies that the three basic principles of experimental design are "randomization", "replication", and "blocking". Randomization is a fundamental feature for all DOE methods. By randomly selecting the individual runs of the experiment, one ensures that the random errors are normally and independently distributed random variables with a mean zero

and constant but unknown variance. This is a fundamental requirement of statistical methods. Experimental error or random error or pure error incorporates "sources of variability in the experiment including measurement, variability arising from uncontrolled factors, differences between the experimental units (such as test material, etc.) to which the [factors] are applied, and the general background noise in the process (such as variability over time, effects of environmental variables, and so forth)" (Montgomery, 2009). Randomization in the experimental design usually guarantees that the effects of random errors are negligible. Analyzing the residuals allows one to determine if the randomized design has accomplished this goal. There should be no observable structure in the residuals if plotted versus run order or versus the predicted response, for example (Montgomery, 2009). The residual of a data point is the difference between that data point and the average value for that factor level combination. Randomization therefore, guarantees that the effects of any "extraneous factors" or unknown sources of error on the response variable are not confused with the effects of the factors specifically being analyzed in the experiment.

Replication involves replicating each factor combination for the purpose of generating a more robust data set and for providing a measure of experimental error. "This estimate of error becomes a basic unit of measurement for determining whether observed differences in the data are really statistically different" (Montgomery, 2009). For this research, replication is meaningless since multi-zone airflow models are deterministic simulation models. This means that each replication of the same input parameters will yield exactly the same response

or output. Therefore, no estimate of error can be obtained. Without an estimate of error, one cannot perform the statistical tests necessary to determine if the effects of each factor or each factor interaction are significant. "One approach to the analysis of an unreplicated factorial is to assume that certain high-order interactions are negligible and combine their mean squares to estimate the error" (Montgomery, 2009). Another method is to construct a normal probability plot of the effects. "The effects that are negligible are normally distributed, with mean zero and variance $\sigma^2$ and will tend to fall along a straight line on this plot, whereas significant effects will have nonzero means and will not lie along the straight line" (Montgomery, 2009). Then the effects that are graphically deemed to be negligible are combined into an estimate of error. The inability to have an estimate of error is one reason why in this research only graphical methods (i.e. effect scatter plots and $CO_2$ concentration curves) were used to evaluate effects of airflow model parameters on the various model outputs. In order to obtain an estimate of error, a stochastic model would have to be used. Stochastic models account for natural variability in the system and therefore the output responses are random variables (Montgomery, 2009). This issue of deterministic versus stochastic modeling is beyond the scope of this discussion.

Blocking is a form of controlled randomization or a restriction on randomization. "Often blocking is used to reduce or eliminate the variability transmitted from nuisance factors – that is, factors that may influence the experimental response but in which we are not directly interested" (Montgomery, 2009). Therefore, where randomization protects against the effects of unknown

nuisance factors that are uncontrollable, blocking protects against the effects of known and controllable nuisance factors. If a nuisance factor is known and uncontrollable and its value can be measured during each experiment, "analysis of covariance" can be used to determine its effect (Montgomery, 2009).

### B.3 Design of Experiments Techniques

Montgomery (2009) begins by explaining basic statistical concepts which are involved in DOE methods including experimental or statistical error, variability, random variables, probability distributions, expected values, random samples, sampling distributions, confidence intervals, and tests of hypotheses. Employing these basic concepts, the first level of DOE techniques involve comparative experiments which aim to determine if there is a statistical difference between two sets of data from two different conditions or factor levels. More specifically, these experiments involve one factor at two different factor levels. Comparative experiments can compare the means of two sample data sets to determine if they are equal or if one is greater than or less than the other. Comparative tests can also determine if the sample mean is greater than or less than a specific value. Tests on means of normal distributions with unknown variance are referred to as "two-sample t-tests" and test on means with known variance are referred to as "two-sample Z-test". Refer to Montgomery (2009) for a complete discussion on these comparative designs.

The next level in DOE techniques is the analysis of variance or ANOVA test which involves one factor at any number of factor levels for any number of replications at each factor level. The runs which compose the ANOVA

experiment are completely randomized. “The name analysis of variance is derived from the partitioning of total variability into is component parts” (Montgomery, 2009). The variability in experimental data is typically quantified by the “sum of squares”. The sum of squares is the sum of the squared difference between the value of each response observation and the overall mean response observation. This sum of squares is a measure of the total variability in the response data. The ANOVA test begins by decomposing the total sum of squares into the sum of squares associated with the factor levels and the sum of squares associated with random error. Therefore, the ANOVA determines how much of the total variability in the data is due to the difference in factor levels and how much is due to random error. Hypothesis testing can then be used to determine if the factor level means are statistically different or not. If they are, one can conclude that changing the factor level has a statistically significant impact on the response. However, ANOVA fails to determine exactly which means differ. Subsequent analysis methods are therefore necessary. One can also form an empirical regression model from the results of the ANOVA test.

Blocking can be applied to ANOVA tests to eliminate a known nuisance factor. These designs are called “Randomized Complete Block Designs” (RCBD) (Montgomery, 2009). For the decomposition of the total sum of squares, there is another term now for the sum of squares associated with the blocking. Therefore, the variability due to the nuisance factor is separated from the variability due to the factor levels. When performing the ANOVA, one can now determine if the factor levels are significant and if the nuisance factor involved in blocking is

significant. “Latin Square” designs provide two restrictions on randomization or blocking in two directions which eliminates the variability due to two nuisance factors. Refer to Montgomery (2009) for a complete discussion of ANOVA techniques.

The next level of DOE techniques are the full factorial and various fractional factorial designs. The majority of the text by Montgomery (2009) covers factorial designs and their numerous augmentations. The remainder of this discussion will focus on factorial designs. Montgomery (2009) also covers fitting regression models, response surface methods, experiments with random factors, and other advanced DOE techniques which are beyond the scope of this research.

### *B.3.1 Factorial Analysis*

For the analysis of two or more factors at various factor levels, “factorial designs” are the most efficient method of performing such experiments. “By a factorial design, we mean that in each complete trial or replication of the experiment all possible combinations of the levels of the factors are investigated” (Montgomery, 2009). Factors can be quantitative or qualitative and the factor levels can therefore represent a numerical value or some qualitative value (e.g. material type, operator name, equipment type, etc.). Factorial analysis methods are one of the most common and widely used types of DOE techniques. They provide an improvement to the common “one-factor-at-a-time” analysis methods which fail to capture any interaction effects between variables. Factorial designs make the most efficient use of the experimental data, i.e. one can capture all the significant effects from the least amount of experimentation. “The effect of a

factor is defined to be the change in response produced by a change in the level of the factor" (Montgomery, 2009). This is referred to as a "main effect" and is distinguished from "interaction effects" which correspond to when the "difference in response between the levels of one factor is not the same at all levels of the other factors" (Montgomery, 2009). If a response surface is generated graphically showing the change in response due to two different factors, interaction effects between these two factors would be represented as curvature in the surface.

In general a full factorial design is designated as $X^k$ where "X" is the number of factor levels and "k" is the number of factors. Therefore a $2^3$ factorial analysis involves analyzing three factors at two levels each for a total of 8 experimental runs. In this research one experimental run is equivalent to one multi-zone airflow model simulation. The most common type of factorial designs are the $2^k$ designs which consider only two factor levels of each factor. These designs assume that the response is linear over the range of factor levels chosen. The $2^3$ design will be used as an example here to elucidate how a factorial design is performed.

### *B.3.2 The $2^3$ Full Factorial Design*

For a $2^3$ design, one is evaluating the effects of three variables or factors on some response "y" of a certain system or process. Two levels of each of the three factors are used for the analysis. Since there are only two levels of each factor, they can be referred to as "high" and "low" or "+" and "-". For the sake of this example the three factors will be termed "A", "B", and "C". The notation used in Montgomery (2009) will also be adopted here. For each factor level

combination, the lowercase letters “a”, “b”, and “c” will be used to denote which factors are at their “high” level. Therefore, the eight experimental runs of the $2^3$ include the following factor level combinations: a, b, c, ab, bc, ac, abc, and (1). The (1) notation refers to the response variable value resulting from the run where all three factors are at their “low” level. The “a” notation refers to the response variable value resulting from the run where factor A is at its high value and factors B and C are at their low value. The same reasoning applies to the other six factor level combinations. The main effect of any factor is defined as the difference in the average response when the factor is at its high level and the average response when the factor is at its low level. Therefore, the effect of factor A would be calculated using Equation B.1.

$$\begin{aligned} Effect\ of\ A &= \frac{a + ab + ac + abc}{4n} - \frac{(1) + b + c + bc}{4n} \\ &= \frac{1}{4n}[-(1) + a - b + ab - c + ac - bc + abc] \end{aligned} \tag{B.1}$$

In this equation, “n” is the number of replicates of the design. Similar calculations can be done for the effect of B and the effect of C or any of the factor interaction effects. The sum of the factor level combinations is referred to as the “contrast” of the factor. The contrast of Factor A, for example, can be identified from Equation B.1 and is shown in Equation B.2 below.

$$Contrast_A = [-(1) + a - b + ab - c + ac - bc + abc] \tag{B.2}$$

Therefore,

$$Effect\ of\ A = \frac{Contrast_A}{4n} \tag{B.3}$$

For the general $2^k$ design, the effect of any factor can be calculated using Equation B.4 below (Montgomery, 2009).

$$Effect\ of\ AB\ldots K = \frac{2}{n2^k}(Contrast_{AB\ldots K}) \tag{B.4}$$

To display the experimental runs, it is common to set up a design matrix or "D-matrix" following the "standard order" or "Yate's order" (Montgomery, 2009). For this $2^3$ design, the standard order design matrix is shown in Table B.1 below. Notice that the columns in Table B.1 under each factor list the contrast coefficients for that factor. Therefore, one can easily determine the contrasts for each factor by looking at the design matrix. Note that the standard order is not necessarily the actual run order of the experiments. Since factorial designs, as with all DOE designs, should be randomized, the run order of the eight runs in Table B.1 should be randomly generated during experimentation.

Table B.1

*Standard Order Design Matrix*

| **Run Number** | **Factor Level Combination** | **Factor** | | |
|---|---|---|---|---|
| | | A | B | C |
| 1 | (1) | - | - | - |
| 2 | a | + | - | - |
| 3 | b | - | + | - |
| 4 | ab | + | + | - |
| 5 | c | - | - | + |
| 6 | ac | + | - | + |
| 7 | bc | - | + | + |
| 8 | abc | + | + | + |

After running all 8 experimental runs, the value of the response variable is recorded for each factor level combination. Table B.2 shows a design where three replicates were performed and thus, three values of the response variable are recorded for each factor level combination. Therefore, a total of 24 experimental runs were performed. When calculating the effects as in Equations B.1 through B.4 above, the average response value of the replicates is used for each factor level combination.

Table B.2

*Standard Order Design Matrix with Recorded Responses*

| **Run Number** | **Factor Level Combination** | **Factor** | | | **Response** | | |
|---|---|---|---|---|---|---|---|
| | | A | B | C | 1 | 2 | 3 |
| 1 | (1) | - | - | - | $y_{11}$ | $y_{12}$ | $y_{13}$ |
| 2 | a | + | - | - | $y_{21}$ | $y_{22}$ | $y_{23}$ |
| 3 | b | - | + | - | $y_{31}$ | $y_{32}$ | $y_{33}$ |
| 4 | ab | + | + | - | $y_{41}$ | $y_{42}$ | $y_{43}$ |
| 5 | c | - | - | + | $y_{51}$ | $y_{52}$ | $y_{53}$ |
| 6 | ac | + | - | + | $y_{61}$ | $y_{62}$ | $y_{63}$ |
| 7 | bc | - | + | + | $y_{71}$ | $y_{72}$ | $y_{73}$ |
| 8 | abc | + | + | + | $y_{81}$ | $y_{82}$ | $y_{83}$ |

To determine the various interaction effects, the D-matrix in Table B.1 above can be expanded to the "X-matrix" (Montgomery, 2009). Here, the contrast coefficients are simply multiplied to obtain the contrast coefficient for each interaction. For example, for the AB interaction and factor level combination "a", the contrast coefficient for "AB" will be equal to the positive under "A" times the negative under "B" yielding a negative under "AB". See Table B.3 below for the complete expanded matrix for this $2^3$ design.

Table B.3

*Standard Order Expanded Matrix*

| **Run Number** | **Factor Level Combination** | **Factor** | | | | | | |
|---|---|---|---|---|---|---|---|---|
| | | A | B | C | AB | AC | BC | ABC |
| 1 | (1) | - | - | - | + | + | + | - |
| 2 | a | + | - | - | - | - | + | + |
| 3 | b | - | + | - | - | + | - | + |
| 4 | ab | + | + | - | + | - | - | - |
| 5 | c | - | - | + | + | - | - | + |
| 6 | ac | + | - | + | - | + | - | - |
| 7 | bc | - | + | + | - | - | + | - |
| 8 | abc | + | + | + | + | + | + | + |

As mentioned above with the ANOVA test, the total variability in the data, as quantified by the total sum of squares, is decomposed into the sum of squares of individual parts. For the $2^3$ factorial design, the sum of squares decomposition is expressed as in Equation B.5 (Montgomery, 2009).

$$SS_{TOTAL} = SS_A + SS_B + SS_C + SS_{AB} + SS_{AC} + SS_{BC} + SS_{ABC} + SS_{ERROR} \tag{B.5}$$

The sum of squares for each factor and interaction can be calculated using Equation B.6 (Montgomery, 2009).

$$SS = \frac{(Contrast)^2}{8n} \tag{B.6}$$

In Equation B.6, "n" is again the number of replicates. For the general $2^k$ design, the sum of squares for any factor or interaction can be calculated using Equation B.7 below (Montgomery, 2009).

$$SS_{AB\ldots K} = \frac{1}{n2^k}(Contrast_{AB\ldots K})^2 \tag{B.7}$$

Refer to Montgomery (2009) for a derivation of this sum of squares expression. The total sum of squares can be calculated as the sum of each data

point squared minus the grand average of all data points squared divided by the total number of data points. For a $2^3$ factorial analysis the total sum of squares can be calculated using Equation B.8 below.

$$SS_{TOTAL} = \sum_{i=1}^{2}\sum_{j=1}^{2}\sum_{k=1}^{2}\sum_{l=1}^{n} y_{ijkl}^2 - \frac{y_{total,avg.}^2}{8n} \tag{B.8}$$

In Equation B.8 above, "i" represents the number of levels of factor A, "j" represents the number of levels of factor B, "k" represents the number of levels of factor C, and "l" represents the number of replicates. Refer to Montgomery (2009) for a derivation of this type of expression for the total sum of squares. Once the total sum of squares is known and the sum of squares for each factor and each factor interaction is know, the sum of squares error can be calculated by subtracting all the other sum of squares from the total. This is simply a manipulation of Equation B.5 above.

It is advantageous to use some type of model to describe the observations of an experiment. One common model used is the linear statistical model known as the "effects model". For the $2^3$ factorial design, the effects model would take the form of Equation B.9 below (Montgomery, 2009).

$$y_{ijkl} = \mu + \tau_i + \beta_j + \gamma_k + (\tau\beta)_{ij} + (\tau\gamma)_{ik} + (\beta\gamma)_{jk} + (\tau\beta\gamma)_{ijk} + \epsilon_{ijkl} \tag{B.9}$$

In this model, "$y_{ijkl}$" is the ijkl$^{th}$ response observation, "$\mu$" is the overall mean of all observations, "$\tau_i$" is the effect of factor A, "$\beta_j$" is the effect of factor B, "$\gamma_k$" is the effect of factor C, $\epsilon_{ijkl}$ is the random error, and the remaining four terms are the various factor interaction effects. According to this effects model,

each observed response value is equal to the mean value plus the effects of each factor and factor interaction plus random error. Therefore, if all factor and interaction effects are statistically insignificant, the expected value of each response will be the mean value plus random error. Next, the sum of squares for all of the factors and factor interactions can be expressed in variant forms of the effects model. Refer to Montgomery (2009) for examples of these conversions. Then, if the total sum of squares is divided by the total degrees of freedom, one obtains the mean square or the sample variance which is the standard measure of variability. Similarly, the mean square can be calculated for each factor and each factor interaction using Equation B.10 below.

$$Mean\ Square = MS = \frac{Sum\ of\ Squares}{degrees\ of\ freedom} \tag{B.10}$$

"The degrees of freedom of a sum of squares is equal to the number of independent elements in that sum of squares" (Montgomery, 2009). For a $2^3$ factorial analysis, the total degrees of freedom will be equal to (8n – 1) where "n" is the number of replicates. The degrees of freedom for each factor or factor interaction will be equal to (# of factor levels – 1) or 1 since there are only two factor levels of each factor. The degrees of freedom for error will then be equal to the total degrees of freedom minus the degrees of freedom for each factor and factor interaction. Finally, using the effects model and the definitions for the mean squares, one can evaluate the expected value of each of the mean squares. Refer to Montgomery (2009) for the derivations of these expected values. What one finds is that the expected value of the mean square error or $E(MS_E)$ is an estimator of

the sample variance or $\sigma^2$. The expected value of mean square of the factors or factor interactions yield different results. For example, the expected value of the mean square for factor A or E($MS_A$) is an estimator of the sample variance $\sigma^2$ only if the effect of that factor is zero. This can be seen by the expressions for the expected values in Equations B.11, B.12, and B.13 below (Montgomery, 2009).

$$E(MS_E) = \frac{SS_E}{df} = \sigma^2 \tag{B.11}$$

$$E(MS_A) = \frac{SS_A}{df} = \sigma^2 + \frac{f(\tau_i^2)}{df} \tag{B.12}$$

$$E(MS_{AB}) = \frac{SS_{AB}}{df} = \sigma^2 + \frac{f\left((\tau\beta)_{ij}^2\right)}{df} \tag{B.13}$$

Therefore, if any of the factors or factor interactions have a significant effect on the response variable, then their mean square will be greater than the mean square error. If they have no effects then they will be estimators of $\sigma^2$ and their expected mean square values will equal the mean square error.

Finally, the "F-test" is the statistical test used to evaluate whether or not each factor or factor interaction is statistically significant. Montgomery (2009) shows that each mean square, or each sum of squares divided by the appropriate degrees of freedom, follows a chi-squared distribution. This is assuming that the random errors are normally and independently distributed with mean zero and variance $\sigma^2$. Dividing the mean square for each factor or factor interaction by the mean square error (Equation B.14 below) yields a ratio of two chi-squared distributed random variables which follows the "F" distribution.

$$F_A = \frac{\frac{SS_A}{df_A}}{\frac{SS_E}{df_E}} = \frac{MS_A}{MS_E} \quad \text{(B.14)}$$

If the factor A is significant, for example, then by observing the expressions for the expected values in Equations B.11 and B.12, the numerator of Equation B.14 will be greater than the dominator. In hypothesis testing, this represents an "upper-tail" or "one-tail" critical region. Tables of the F distribution values, provided in any statistics or DOE text, list the F-value for various levels of significance or "α" for the degrees of freedom of the numerator mean square and the degrees of freedom for the denominator mean square in Equation B.14. To be 95% confident the user would need to look up the F-value on the table for α = 0.05. If the calculated F-value is greater than the "critical" F-value obtained for the desired level of significance, then that factor is statistically significant at the selected level of significance. In equation form, the factor A is significant if Equation B.15 below is true.

$$F_A > F_{\alpha, \frac{df\ MS_A}{df\ MS_E}} \quad \text{(B.15)}$$

From this analysis one can identify which factors or factor interactions have statistically significant impacts on the response variable of the process or system being analyzed.

### *B.3.3 Additions to the Factorial Analysis*

Once the analysis has determined which factors are significant, one can build regression models and fit response surfaces for the system. For example, if factor A, factor C, and factor AC, from the above example, were found to be

statistically significant, the resulting regression model may take the form of Equation B.16 (assuming no quadratic terms are significant).

$$y = \beta_0 + \beta_1 x_1 + \beta_3 x_3 + \beta_{13} x_1 x_3 \quad \text{(B.16)}$$

In Equation B.16, the β's represent the regression coefficients and the x's represent the independent variables. The subscripts 1 and 3 refer to factor A and factor C, respectively. It turns out that the β's are equal to half of the factor effects calculated from the factorial analysis and $\beta_0$ is the average of all of the responses observed from the designed experiment. These parameter estimates for the two level factorial turn out to be the least squares estimates (Montgomery, 2009). This means that these parameters result in a regression model that minimizes the sum of square error between model predicted values and actual values.

Montgomery (2009) also covers a wide range of "fractional factorial" designs which help to reduce the number of experimental runs needed. For full factorial designs, the number of experimental runs needed for analysis can quickly become impractical. For example, a $2^{10}$ for analyzing ten variables would require 1,024 experimental runs. It is quite common to have processes and systems that involve a large number of variables. Fractional factorial designs analyze a subset of the full factorial design experimental runs. The reduction in experimental runs needed comes at a price, however, since the resulting data set is less robust. In other words, the "aliasing" of effects occurs where the effects of certain factors or factor interactions cannot be distinguished individually. Well designed fractional factorials only alias high factor interaction terms which are most likely insignificant. Poor fractional factorial designs begin to alias two factor

interactions and even main effects which may be statistically significant. If an aliased factor is found to be significant, without further experimentation there is no way of knowing if that factor is actually significant or if the factor it is aliased with is the significant factor. Plackett-Burman designs involve experiments with only one more experimental run than there are variables. These designs are heavily aliased with main effects partially aliased with two factor interactions. Refer to Montgomery (2009) for a full discussion on the various types of fractional factorial designs.

**B.4 Conclusions**

The range of possible applications for DOE techniques is too broad to cover here. They are utilized by many industries and especially in industrial engineering practices. Hou et al. (1996) provide an example of the application of a $2^k$ factorial design integrated with a detailed building energy simulation program. The authors use the factorial design to set up energy simulation runs to analyze the effects of various factors on the energy performance of a building's heating, ventilation, and air-conditioning (HVAC) system. This example is similar to the application of factorial design techniques used in this research because detailed energy simulation programs are also deterministic models like the multi-zone airflow program PCW/CONTAM. Therefore, Hou et al. (1996) could not calculate statistical significance since there is no estimate of random error (i.e., replicates of a deterministic program are identical). Rather, they simply observed the energy use behavior predicted by the program as the input factors were altered. Similarly, in this research, factorial design techniques were used for

sensitivity analysis to determine response trends in the multi-zone airflow model as input factors were altered. Due to the lack of a single quantitative metric (like total building energy use for energy simulations) and the deterministic nature of multi-zone simulation programs, which limits the ability to perform statistical significance tests, graphical methods were used to observe the effects of input factors on building airflow dynamics and tracer gas behavior.

# APPENDIX C

# CONTAM/PCW MULTI-ZONE AIRFLOW MODELS

## C.1 Introduction to CONTAM/PCW Multi-Zone Models

Multi-zone modeling has been discussed in Section 1.3 and Section 4.1.2. This purpose of this appendix is to provide a little more detail into multi-zone modeling. Refer to Walton and Dols (2005) or Vandemusser (2007) for complete discussions on the CONTAM and PCW user interfaces, simulation engines, mathematical theory, etc. The notation used in this appendix is consistent with that used by Walton and Dols (2005).

As mentioned previously, multi-zone models employ the "well-mixed" assumption. "The fundamental assumption in CONTAM is that the building can be modeled by some number of zones of well-mixed air. Therefore, the program stands as a compromise of accuracy, complexity, and speed between a single-zone model and a CFD (computation fluid dynamics) model of the entire building" (Walton, 1995). CONTAM/PCW is mainly used for either airflow analysis or contaminant dispersion analysis both of which are based on the conservation of mass. The program offers a variety of simulation options as discussed by Walton and Dols (2005) and Vandemusser (2007). As mentioned in Section 4.1.2, this research focuses on steady-state airflow simulation and transient contaminant simulation. For contaminant dispersion analysis, CONTAM/PCW can model both trace and non-trace contaminants. Trace contaminants are those which do not alter the density of air. This research uses $CO_2$ as a tracer gas. One note of caution is that when specifying a tracer gas in CONTAM/PCW, the program will consider it to be a trace contaminant even if its concentration reaches a level that would change air density.

CONTAM/PCW does not model any heat transfer phenomenon. User specified zone and ambient temperatures (either constant or varied by a schedule) are used to account for buoyancy induced airflows from temperature differences. Zone pressures in CONTAM/PCW can be either constant or variable. With variable, the zone pressure is calculated during the simulation. Constant pressures are specified by the user and can be used to simulate a fan pressurization test, for example.

The sketchpad graphical user interface for CONTAM is used to build the systems of equations needed to perform the airflow analysis or the contaminant dispersion analysis. It is not meant to provide drawing or visualization capabilities similar to computer aided design (CAD) or three dimensional modeling tools. Rather, the sketch pad icons represent the information/inputs needed to build a system of equations for the simulation engine to solve. User assumptions and expertise are needed to translate the actual building into multi-zone representation. This is referred to "building idealization" as was shown in Figure 1.1.

**C.2 Airflow Analysis Mathematical Theory**

Feustal and Kendon (1985) provided a literature review that identified 15 multi-chamber infiltration models developed between 1966 and 1983. Many differed in the number of cells that can be modeled but most had similar flow equations. Only a few of the 15 could simulate ventilation systems and the interrelation of mechanical and natural ventilation. A later report by Feustal and Dieris (1992) discusses 50 different computer programs for multi-zone airflow

analysis. It is quite obvious that the mathematics behind multi-zone models has been in development for some time and has taken various forms. This discussion focuses on the mathematics behind NIST's CONTAM/PCW.

Multi-zone models are comprised of a network of nodes representing zone volumes connected by mathematical relationships representing airflow paths. In CONTAM/PCW, these mathematical relationships are referred to as "airflow elements". The volumetric airflow rate through an airflow path from zone "j" to zone "i" or "$F_{j,i}$" is given by some function of the pressure difference between those two zones as shown in Equation C.1 (Walton and Dols, 2005).

$$F_{j,i} = f(P_j - P_i) \tag{C.1}$$

In Equation C.1, "$P_j$" and "$P_i$" are the pressures in zones "j" and "i", respectively. The volumetric airflow rate sign convention is positive for flows from "j" to "i" negative for flows from "i" to "j". This relationship is often non-linear. The most commonly used relationship is the empirical power-law relationship as given in Equation C.2.

$$F_{j,i} = k(\Delta P)^n \tag{C.2}$$

In Equation C.2, "k" is a flow coefficient and "n" is a flow exponent. This power-law empirical model is based on engineering equations for orifice flow (ASHRAE, 2009 and Street et al., 1996).

Refer to Walton and Dols (2005) or Vandemusser (2007) for complete details of all the possible airflow elements offered by CONTAM/PCW which include the following:

1. One-Way Flow Power-Law Models

2. One-Way Flow Quadratic Models
3. Two-Way Flow Models
4. Backdraft Damper Flow Models
5. Fan and Forced Flow Models
6. Cubic Spline Flow Models

This research focuses on the general power-law relationship in Equation C.2 which is also the default airflow element used in PCW. Walton and Dols (2005) give recommendations for the flow exponent in this equation and appropriate values for the flow coefficient are recommended in the literature (e.g., Persily, 1998). Optional airflow path properties that are available in CONTAM/PCW include contaminant filtration, schedules, and wind pressure profiles. The user specified elevation of the airflow path determines how it responds/influences building stack effect. For transient airflow analysis, schedules can be set to govern the flow through an airflow path representing fan or damper operation for example.

The pressure differences across these airflow paths are influenced by temperature changes and thus air density changes (stack effect), wind induced pressures, and mechanically induced pressures (i.e., from ventilation and exhaust fans). “Flow within each airflow element is assumed to be governed by Bernoulli’s equation” (Walton and Dols, 2005). Bernoulli’s equation, which is derived from Euler’s equation of motion, as given in Equation C.3 (Street et al., 1996), allows one to relate and predict pressures and velocities in a flow field. Equation C.3 is the one-dimensional Bernoulli equation for an incompressible

(constant density) and ideal (no viscous forces) fluid which are practical simplifications for many engineering applications (Street et al., 1996).

$$\frac{p_1}{\gamma} + \frac{V_1^2}{2g_n} + z_1 = \frac{p_2}{\gamma} + \frac{V_2^2}{2g_n} + z_2 = H \qquad \text{(C.3)}$$

In Equation C.3, "p" is pressure, "V" is velocity, "$g_n$" is the acceleration due to gravity, "z" is the elevation, "γ" is the specific weight, and "H" is a constant. The "1" and "2" subscripts represent the points on either side of the airflow path. The specific weight of the fluid is equal to the density multiplied by the acceleration due to gravity. Bernoulli's equation says that the total head (units of length) is constant at all points along a streamline. However, there can be changes in pressure head "$p/\gamma$", changes in velocity head "$V^2/2g_n$", or changes in elevation "z". Changes in the total head such as energy added by a fan or energy lost by friction can be accounted for by adding additional terms to Equation C.3. The static pressures, "$p_1$" and "$p_2$" on either side of the flow path correspond to the zone pressures. "Where a flow connects to the building façade, the pressure also may depend on pressure imposed by wind" (ASHRAE, 2009). Hyrdostatic pressure can also be accounted for in CONTAM/PCW. "The hydrostatic equation is used to relate the pressure difference across the flow element to the elevations of the element ends and the zone elevations, assuming the air in the room is at constant temperature" (Walton and Dols, 2005). Therefore, the total pressure difference is equal to the difference in the zone total pressures plus pressure due to density and elevation difference ("$P_s$") plus pressure due to wind ("$P_w$") as shown in Equation C.4 (Walton and Dols, 2005).

$$\Delta P = P_j - P_i + P_s + P_w \quad \text{(C.4)}$$

The contribution to the overall pressure difference from each varies for each airflow path. Due to nonlinearity, as expressed in Equation C.2, one cannot calculate the airflow due to each and simply add them together (Kreider et al., 2005). Rather, the individual pressure differences must be calculated and summed as in Equation C.4 and then the airflow through the path can be determined from Equation C.1.

For calculating wind pressure influence on an airflow path, CONTAM/PCW has three options: none, constant, or pressure dependant on wind speed and direction. For steady-state calculations wind speed and wind direction are held constant. For transient simulations, a user developed weather file can be uploaded to vary wind conditions during the simulation period. NIST also provides a weather file development software (NIST, 2008). Wind pressure is the main driving force in infiltration airflow and is a function of wind speed, wind direction relative to the wall surface, and the surrounding local terrain. The wind pressure on an external wall is given by Equation C.5 (Walton and Dols, 2005).

$$\begin{aligned} &Wind\ Pressure \\ &= (Dynamic\ pressure\ of\ wind\ at\ reference\ height) \\ &* (wind\ pressure\ modifier) * (wind\ pressure\ profile) \end{aligned} \quad \text{(C.5)}$$

In Equation C.5, the dynamic pressure of wind at reference height is determined from constant wind conditions in a steady-state simulation or from wind data from a user uploaded weather file. The wind pressure modifier is a coefficient accounting for local terrain effects which account for the difference in the wind velocity profile between the building and the wind velocity measurement location

(e.g., an airport). The wind pressure profile is a pressure coefficient accounting for relative wind direction. "CONTAM refers to the function relating the average wind pressure coefficient for the face of a building to the angle of incidence of the wind on the face of the building as the wind pressure profile or "f(θ)" (Walton and Dols, 2005). Wind pressure profiles can be generated in CONTAM by imputing up to 16 angle and pressure coefficient pairs and then selecting one of three different curve fit options. PCW has built-in wind pressure profiles for various building shapes (i.e., high rise and low rise at different aspect ratios) which can also be manually modified if desired.

From Bernoulli's equation, the wind pressure on a building surface is proportional to the difference between the square of the approaching wind velocity and the square of the final wind velocity at the building boundary. However, since the final wind velocity is difficult to determine, it is assumed to be zero and the incoming wind velocity is instead multiplied by a coefficient (Kreider et al., 2005). The wind pressure "$P_w$" on a building surface can be calculated using Equation C.6 (Walton and Dols, 2005).

$$P_w = \frac{\rho V_H^2}{2} C_p \tag{C.6}$$

In Equation C.6, "ρ" is the air density, "$V_H^2$" is the approach wind speed at the height of the building, and "$C_p$" is the wind pressure coefficient. Refer to ASHRAE (2009) for details on the wind pressure coefficient. The same wind pressure on the building surface can also be calculated by Equation C.7 (Walton and Dols, 2005).

$$P_w = \frac{\rho V_{met}^2}{2} C_h f(\theta) \tag{C.7}$$

In Equation C.7, "$V_{met}^2$" is the wind velocity at the meteorological station where it is typically measured, "$C_h$" is the wind speed modifier coefficient which accounts for terrain and elevation effects, and "f(θ)" is the wind pressure profile coefficient which is a function of the relative wind direction as shown in Equation C.8. Walton and Dols (2005) provides a method for calculating "$C_h$".

$$\theta = \theta_w - \theta_s \tag{C.8}$$

In Equation C.8, "$\theta_w$" is the wind azimuth and "$\theta_s$" is the surface azimuth angle. The azimuth is relative to north (i.e., N = 0°). For a more detailed discussion on airflow around buildings, refer to Chapter 24 of ASHRAE (2009).

Continuing with the airflow analysis, the mass of air in zone "i" is given by Equation C.9 (Walton and Dols, 2005) which is the ideal gas equation of state.

$$m_i = \rho_i V_i = \frac{P_i V_i}{R T_i} \tag{C.9}$$

In Equation C.9, "$\rho_i$" is the air density in zone "i", "$V_i$" is the zone volume, "R" is the gas constant of air, and "$T_i$" is the zone air temperature. For transient simulations, the change in mass of the air in zone "i" with respect to time is given by Equation C.10 (Walton and Dols,2005) after using the product rule of differentiation on Equation C.9.

$$\frac{\partial m_i}{\partial t} = \rho_i \frac{\partial V_i}{\partial t} + V_i \frac{\partial \rho_i}{\partial t} = \sum\nolimits_j F_{j,i} + F_i \approx \frac{1}{\Delta t}\left[\left(\frac{P_i V_i}{R T_i}\right) - (m_i)_{t-\Delta t}\right] \tag{C.10}$$

Therefore, the change in zone air mass is equal to the sum of all the airflows between zone "i" and the surrounding zones through the various airflow paths

plus the term "$F_i$" which accounts for all "non-flow processes that could add or remove significant quantities of air from the zone" (Walton, 1995). These non-flow processes can be accounted for in CONTAM/PCW but are not considered in this study. In terms of airflow elements, the change in zone air mass is the sum of all of the non-linear power-law equations for all the airflow paths connected to the zone being analyzed. For steady-state airflow analysis, the airflows in CONTAM/PCW are evaluated by assuming quasi-steady conditions. In other words, the sum of all volumetric airflows into and out of a zone is equal to zero as expressed in Equation C.11 (Walton and Dols, 2005). The steady-state assumption is considered to be reasonable since most of the driving forces for airflows change slowly as compared to the rate at which the airflow system reestablishes steady state (ASHRAE, 2009). Therefore, multi-zone models account for the conservation of mass but not the conservation of momentum. CFD analysis is required for such detail.

$$\sum_j F_{j,i} = 0 \qquad \text{(C.11)}$$

"The steady-state airflow analysis for multiple zones requires the simultaneous solution of [Equation C.11] for all zones" (Walton and Dols, 2005). The relationship between the volumetric airflow rate and the pressure difference as given by the various airflow elements in CONTAM/PCW are usually non-linear (e.g., Equation C.2). Therefore, the simultaneous solution of Equation C.11 for all zones requires a method for the simultaneous solution of nonlinear algebraic equations. CONTAM/PCW uses the "Newton-Raphson" (N-R) method for this.

The N-R method, which is based on the Taylor-series expansion of a function, is an iterative method that can be used to solve a set of continuous and differentiable nonlinear equations (Stoecker, 1989). An initial guess of the values are needed in this method and guesses too far from the correct values could lead to convergence problems.

Using matrix relationships, the N-R method calculates a new estimate of the vector of all zone pressures, $\{P\}^*$, from the current vector estimate of pressures, {P}, using Equation C.12 (Walton and Dols, 1995).

$$\{P^*\} = \{P\} - \{C\} \tag{C.12}$$

In Equation C.12, the correction vector, {C}, is computed by the matrix relationship given in Equation C.13 (Walton and Dols, 2005).

$$[J]\{C\} = \{B\} \tag{C.13}$$

In Equation C.13, {B} is a column vector with each element given by Equation C.14 (Walton and Dols, 2005). The [J] matrix is the square (i.e., N by N matrix for a multi-zone model of N zones) known as the Jacobian matrix whose elements are given by Equation C.15 (Walton and Dols, 2005).

$$B_i = \sum_j F_{j,i} \tag{C.14}$$

$$J_{i,j} = \sum \frac{\partial F_{j,i}}{\partial P_i} \tag{C.15}$$

"In [Equations C.14 and C.15] $F_{j,i}$ and $\partial F_{j,i}/\partial P$ are evaluated using the current estimate of pressure {P}. The [CONTAM/PCW simulation engine] contains subroutines for each airflow element which return the mass flow rates and the

partial derivative values for a given pressure difference input" (Walton and Dols, 2005). Since Equation C.13 represents a system of linear equations which must be solved for each iteration until a solution is converged upon, the CONTAM/PCW simulation engine utilizes two solution methods: "Skyline" and "Pre-conditioned Conjugate Gradient" (PCG). Refer to Walton and Dols (2005) or for a more detailed discussion on these solution methods.

In CONTAM the ambient zone is assumed to be a constant pressure zone. "The ambient zone is set to zero causing the computed zone pressures to be values relative to the true ambient pressure and helping to maintain numerical significance in calculating ΔP" (Walton, 1995). By default the ambient zone surrounds the building.

"Conservation of mass at each zone provides the convergence criterion for the N-R iterations" (Walton and Dols, 2005). If Equation C.10 (or Equation C.11 for steady-state) is satisfied for all zones for the current system pressure estimate then the solution has converged. Walton and Dols (2005) discuss a convergence test for evaluating accuracy. Also, the authors note some instances of slow convergence or oscillations between two values. Refer to Walton and Dols (2005) for a discussion on the use of relaxation coefficients and other methods for solving convergence issues.

The N-R method requires an initial guess of the zone pressure values which may be obtained by including a linear approximation of the airflow and pressure drop relationship for each airflow path as given in Equation C.16 (Walton and Dols, 2005).

$$F_{j,i} = c_{j,i} + b_{j,i}\left(P_j - P_i\right) \tag{C.16}$$

Similar to the procedure described above, conservation of mass at each zone leads to a set of linear equations of the form in Equation C.17 (Walton and Dols, 2005).

$$[A]\{P\} = \{B\} \tag{C.17}$$

"Matrix [A] in [Equation C.17] has the same sparsity pattern as [J] in [Equation C.13] allowing use of the same sparse matrix solution process for both equations. This initialization handles stack effects very well and tends to establish the proper directions for the flows. The linear approximation is conveniently provided by the laminar regime of the element models used by CONTAM" (Walton and Dols, 2005). For similar problems, the solution of previous problems can be used as the initial guess pressure values of the new problem.

As mentioned previously, the default airflow element used in PCW is the one-way power-law empirical model given in Equation C.2. Walton and Dols (2005) note that the main advantage of the power-law relationship is that its partial derivatives which comprise the Jacobian matrix are easily calculated. Equation C.18 (Walton and Dols, 2005) provides the partial derivative.

$$\frac{\partial F_{j,i}}{\partial P_j} = \frac{nF_{j,i}}{\Delta P} \tag{C.18}$$

From Equation C.18 it is clear that as the pressure drop approaches zero, the derivative becomes undefined. Thus Equation C.18 is appropriate for turbulent flow. For laminar flow as ΔP approaches zero, the Equation C.2 is replaced with Equation C.19 (Walton and Dols, 2005).

$$F_{j,i} = \frac{c_k \rho \Delta P}{\mu} \quad \text{(C.19)}$$

In Equation C.19, "$c_k$" is a laminar flow coefficient and "μ" is the viscosity. The viscocity is calculated by CONTAM/PCW from the pressure and temperature. Therefore, the partial derivatives become simple constants as shown in Equation C.20.

$$\frac{\partial F_{j,i}}{\partial P_j} = \frac{c_k \rho}{\mu} \quad \text{(C.20)}$$

Refer to Walton and Dols (2005) or Vandemusser (2007) for similar theoretical analysis of the other airflow element types, how to find coefficients and exponents based on measured pressure and flow data points, a discussion on airflow in ductwork, polynomial fan performance curves, etc.

**C.3 Contaminant Dispersal Mathematical Theory**

The CONTAM/PCW contaminant dispersal model is based on the methods developed by Axley (1988). The analysis is based on the conservation of mass for all contaminants in the simulation. CONTAM/PCW has the following options for mathematical contaminant source/sink models:

1. Coefficient Model
2. Pressure Driven Model
3. Cutoff Concentration Model
4. Decaying Source Model
5. Boundary Layer Diffusion Model
6. Burst Source Model
7. Deposition Velocity Sink Model

8. Deposition Rate Sink Model

Refer to Walton and Dols (2005) or Vandemusser (2007) for a more detailed discussion on these various source and sink models. As demonstrated in this research, the program user can also simulate contaminant releases by defining initial contaminant concentrations at the release location.

Contaminant dispersal analysis is the application of conservation of mass for all species in a control volume. The gas constant of species "α" can be calculated by dividing the universal gas constant by the molar mass, "$MM_\alpha$" of the contaminant as shown in Equation C.21.

$$R_\alpha = \frac{R_{universal}}{MM_\alpha} \tag{C.21}$$

For a mixture of gases in the zone volume, the overall gas constant of the mixture is the sum of the product of each individual gas constant and each individual concentration. As for other air properties, in this research only trace contaminants were considered which do not impact the properties of air (i.e., density). For trace contaminant simulations, CONTAM uses dry air as defined by ASHRAE (2009) for its calculations.

The well-mixed assumption extends to the contaminant analysis in that the concentration of a contaminant is uniform throughout the volume of a zone at each time step. The mass of a contaminant, say "α", in zone "i" is equal to the mass of the zone air, "$m_i$" multiplied by the concentration of the contaminant, "$C_{\alpha,i}$" as shown in Equation C.22.

$$m_{\alpha,i} = m_i C_{\alpha,i} \tag{C.22}$$

Walton and Dols (2005) discuss three modes in which a contaminant is removed from a zone air volume.

1. Air with a certain contaminant concentration flowing out through various airflow paths (Equation C.23).

$$\sum_j F_{j,i}\, C_{\alpha,i} \tag{C.23}$$

2. Removal (i.e., by filtration) at a rate given by Equation C.24 where "$R_{\alpha,i}$" is a removal coefficient.

$$C_{\alpha,i} R_{\alpha,i} \tag{C.24}$$

3. First-order chemical reactions with other contaminants, say "β", at the rate given in Equation C.25 where "$\kappa_{\alpha,\beta}$" is the kinetic reaction coefficient between the two contaminant species.

$$m_i \sum_\beta \kappa_{\alpha,\beta}\, C_{\beta,i} \tag{C.25}$$

Similarly, Walton and Dols (2005) discuss two modes in which a contaminant can be added to a zone air volume.

1. Air with a certain contaminant concentration flowing in through various airflow paths as given by Equation C.26 where "$\eta_{\alpha,j,i}$" is the filter efficiency of the airflow path.

$$\sum_j (1 - \eta_{\alpha,j,i})\, F_{j,i} C_{\alpha,j} \tag{C.26}$$

2. Contaminant generation from some source at the rate "$G_{\alpha,i}$".

Trace contaminants are those who's mass is significantly less than the zone air mass and thus the contaminant does not impact the zone air density. For

a trace contaminant "α", the transient contaminant mass balance on the zone is given by Equation C.27 (Walton and Dols, 2005).

$$\frac{dm_{\alpha,i}}{dt} = \sum_j F_{j,i}\left(1-\eta_{\alpha,j,i}\right)C_{\alpha,j} + G_{\alpha,i} + m_i \sum_\beta \kappa_{\alpha,\beta} C_{\beta,i} - \sum_j F_{j,i} C_{\alpha,i} - R_{\alpha,i} C_{\alpha,i} \tag{C.27}$$

"This differential equation is approximated by an implicit difference equation. There is one such equation for every contaminant in every zone. These equations must be solved simultaneously for all zones and contaminants" (Walton, 1995). In other words, the transient conservation of mass of species in a control volume (c.v.) is explained by Equation C.28 and expressed formally in Equation C.29 (Walton and Dols, 2005).

$$\begin{aligned}(mass\ of\ contaminant\ \alpha\ in\ c.v.\ at\ time\ t+\Delta t) \\ = (mass\ of\ contaminant\ \alpha\ at\ time\ t) \\ +\ \Delta t(rate\ gain\ of\ contamint\ \alpha \\ - rate\ loss\ of\ contaminant\ \alpha)\end{aligned} \tag{C.28}$$

$$\begin{aligned}\rho_i V_i C_{\alpha,i}\big|_{t+\Delta t} \approx \rho_i V_i C_{\alpha,i}\big|_t \\ + \Delta t\left[\sum_j F_{j,i}\left(1-\eta_{\alpha,j,i}\right)C_{\alpha,j} + G_{\alpha,i} + m_i \sum_\beta \kappa_{\alpha,\beta} C_{\beta,i}\right. \\ \left. - \sum_j F_{j,i} C_{\alpha,i} - R_{\alpha,i} C_{\alpha,i}\right]_{t+\delta t}\end{aligned} \tag{C.29}$$

The solution of Equation C.29 depends on the choice of "δt". The number of equations to be solved is equal to the number of contaminants multiplied by the number of zones or control volumes. The CONTAM/PCW engine has three solutions methods for the matrix of equations which must be solved

simultaneously. These methods include the "skyline" algorithm, an "iterative biconjugate gradient" algorithm, and an "iterative successive over-relaxation" algorithm. Refer to Walton and Dols (2005) for a more detailed discussion on these various solution options and stability/convergence issues.

The CONTAM simulation engine also has the ability to model one-dimensional convection-diffusion flow in ductwork or in a zone rather than using the "well-mixed" assumption. This allows one to model the stratification of a contaminant in one direction. This is one step closer to the detail provided by CFD programs. Refer to Walton and Dols (2005) and Vandemusser (2007) for a discussion on this capability. This one-dimensional analysis was not used in this research. However, it may provide an opportunity for more detailed calibration in a single zone if multiple tracer gas sensors are used during real building releases to measure contaminant stratification in that zone after a release.

Finally, CONTAM provides the opportunity to predict occupant exposure "E" to a contaminant release. The exposure is the integral of the concentration as a function of time over the time in which the occupant is exposed as given by Equation C.30 (Walton and Dols, 2005).

$$E = \int_{t_1}^{t_2} C(t)dt \tag{C.30}$$

**C.4 The Modeling and Simulation Process in PCW**

The following is a brief summary of the process used to perform simulations and subsequent model calibration using the PCW user interface. PCW

has three phases: “Input”, “Measurement”, and “Results”. For complete modeling and simulation instructions refer to Vandemusser (2007).

Input Phase:

1. Define project settings and defaults (i.e., units, sketchpad setup, default zone temperatures, etc.)
2. Set default level height (i.e., the floor-to-floor height of the building).
3. Define weather and wind parameters (i.e., ambient temperature, absolute pressure, altitude, wind speed, wind direction, relative humidity, local terrain condition) for steady-state weather simulations. Upload a user generated weather file for transient weather simulations.
4. Define contaminants that will be used in the contaminant dispersion analysis. PCW already has $CO_2$ and SF6 loaded into the program.
5. Start drawing (diagrammatically) the zones of the building in the sketchpad, adding levels as necessary. This requires idealizing the actual building as a multi-zone model with zones connected by airflow paths.
6. Change level heights as necessary.
7. Enter into the program the length of each wall. With these dimensions and the level height, PCW calculates the wall areas. Zone volumes are automatically calculated only for square and rectangular rooms.
8. Automatically assign zones. This is an automated feature which helps to reduce simulation time in PCW as compared to CONTAM.

9. Name zones so that one can track which zone corresponds to which room(s). Enter in zone areas and volumes for irregularly shaped zones and check automatically calculated areas.
10. Add elevator shaft or stairwell zones as necessary. This tells PCW that these zones require specialized leakage parameters.
11. Define leakage severity as either “normal”, “tight”, or “leaky”. The PCW user is encouraged to use “normal” unless they have reason to believe that their building is leakier or tighter than average.
12. Set building type as either low rise or high rise with different options for aspect ratio. This sets the default terrain-related parameters and wind pressure profiles used to calculate air leakage through exterior flow paths.
13. Add a roof to the model.
14. Automatically assign leakage. This is an automated feature which helps to reduce simulation time in PCW as compared to CONTAM. PCW automatically defines all exterior and inter-zonal airflow paths and populates them with default airflow elements (i.e., one-way flow power-law) and parameters. Add filters or change wind pressure settings as necessary. Manually add user defined airflow paths and airflow elements as necessary. For example, this step does not automatically define mechanical airflow paths such as fans or transfer grills.
15. Add simple AHU’s to the model. Add supply diffusers and return registers to the model. Define volumetric flow rates for each supply and return

based on mechanical design documents and assign that flow to the appropriate AHU.

16. Define filters in airflow paths as necessary.
17. Add contaminant sources if necessary or assign initial concentrations to simulate a release.
18. Check input phase and run simulation. This is a test simulation which checks for any errors in the model set up. If successful, one can move to the "Measurement" phase.

Measurement Phase:

1. Measure actual flow directions in the building under constant airflow conditions using whatever measurement method is available. Input the measured flow directions into PCW.
2. Define branch duct systems by linking supply diffusers and return registers which belong to the same branch ductwork.
3. Measure diffuser airflows using a flow hood for example. Update any diffuser flow or branch flow in PCW based on measurements taken.
4. PCW will automatically compare the model predicted flow directions with the user measured flow directions.
5. Next PCW performs a parametric analysis which attempts to tune model parameters to improve the number of airflow directions that are correctly predicted. This $2^7$ factorial analysis calculates the main effects of seven variables (terrain factors, interior wall leakage, exterior wall leakage, shaft wall leakage, wind direction, wind velocity, and outdoor temperature) and

the five most significant interaction effects on the percentage of correctly predicted airflow directions.

6. Next, PCW will allow the user to enter measurements for variables identified as being significant.
7. Some of the parameters may be difficult to measure so PCW next performs a regression analysis to optimize the factors that the user did not enter measured values for.
8. PCW will then automatically tune the model with the entered measurements and the optimized factors from the regression analysis in an attempt to improve the number of predicted airflow directions that match with the measured direction.

Results Phase:

1. Set the simulation parameters (i.e., the date and time, time step, steady-state vs. transient, etc.).
2. Simulate the model.
3. PCW has a “Scenario Manager” which allows the user to manage files that have different simulation scenarios.
4. Initialize the results viewer for contaminant decay curves or a color coded display of contaminant concentration dispersion over each time step.
5. Export airflow simulation or contaminant dispersion results to a text file.

# APPENDIX D

## COPYRIGHT PERMISSION

623 Elmwood Street, State College, PA 16801

Steve Snyder

03/21/11

**Subject: Copyright Permission**

Steve,

I give you permission to use material from my Master's thesis and research with proper citation.

Joseph Firrantello

1

Re: COPYRIGHT PERMISSION

Hello Steve Snyder,

I give you a permission to reproduce my CO2 test data for the MBNA building as well as CO2 test data for the third floor of MBNA building.

Bests,

Ponpeera Saekow

April 25, 2011